UNIVERSIDADE FEDERAL DE PERNAMBUCO
CENTRO DE TECNOLOGIA E GEOCIÊNCIAS
DEPARTAMENTO DE OCEANOGRAFIA
PROGRAMA DE PÓS-GRADUAÇÃO EM OCEANOGRAFIA

GABRIEL BITTENCOURT FARIAS

INFLUENCES OF PHYSICAL FORCES ON THE DISTRIBUTION OF BIOMASS AND DIVERSITY OF BACTERIOPLANKTON AND PHYTOPLANKTON IN NORTHEASTERN BRAZIL

Recife
2023

GABRIEL BITTENCOURT FARIAS

INFLUENCES OF PHYSICAL FORCES ON THE DISTRIBUTION OF BIOMASS AND DIVERSITY OF BACTERIOPLANKTON AND PHYTOPLANKTON IN NORTHEASTERN BRAZIL

Thesis presented to the Postgraduate Program in Oceanography at the Federal University of Pernambuco, as a partial requirement for obtaining a PhD in Oceanography.

Area of concentration: Biological Oceanography.

Advisor: Prof. Dr. Pedro Augusto Mendes de Castro Melo.

Co-Advisor: Prof. Dr. Juan Carlos Molinero Vargas.

Recife

2023

Catalogação na fonte
Bibliotecária Margareth Malta, CRB-4 / 1198

F224i Farias, Gabriel Bittencourt.
Influences of physical forces on the distribution of biomass and diversity of bacterioplankton and phytoplankton in Northeastern Brazil / Gabriel Bittencourt Farias. – 2023.
174 f.: il., fig. e tab.

Orientador: Prof. Dr. Pedro Augusto Mendes de Castro Melo.
Coorientador: Prof. Dr. Juan Carlos Molinero Vargas.
Tese (Doutorado) – Universidade Federal de Pernambuco. CTG. Programa de Pós-Graduação em Oceanografia, 2023.
Inclui referências e Apêndices.
Texto em inglês.

1. Oceanografia. 2. Sistemas planctônicos oligotróficos. 3. Teias tróficas planctônicas. 4. HPLC. 5. Citometria de fluxo. I. Melo, Pedro Augusto Mendes de Castro (Orientador). II. Molinero Vargas, Juan Carlos (Coorientador). III. Título.

UFPE

551.46 CDD (22. ed.) BCTG/2023-232

GABRIEL BITTENCOURT FARIAS

INFLUENCES OF PHYSICAL FORCES ON THE DISTRIBUTION OF BIOMASS AND DIVERSITY OF BACTERIOPLANKTON AND PHYTOPLANKTON IN NORTHEASTERN BRAZIL

Thesis presented to the Postgraduate Program in Oceanography at the Federal University of Pernambuco, Center for Technology and Geosciences, as a partial requirement for the degree of Doctor of Oceanography. Area of concentration: Biological Oceanography.

Approved in: 04/09/2023.

COMMITTEE

_____

Prof. Dr. Pedro Augusto Mendes de Castro Melo (Advisor)
Universidade Federal de Pernambuco

_____

Prof. Dr. Fernando Antonio do Nascimento Feitosa (External Examiner)
Universidade Federal de Pernambuco

_____

Drª María Celeste López-Abbate (External Examiner)
Instituto Argentino de Oceanografia

_____

Prof. Dr. Frederico Pereira Brandini (External Examiner)
Universidade de São Paulo

_____

Prof. Dr. Emilio Marañón (External Examiner)
Universidade de Vigo

ACKNOWLEDGEMENTS

This document represents the end of a cycle of more than 10 years in my academic life, a great challenge both professionally and personally. I would like to thank all the people who have been with me throughout this process.

First of all, I would like to thank my family immensely, especially my late grandmother, Lindinalva, and my mother, Genalva, who always invested in and sacrificed for my education. I wouldn't have achieved anything or gotten anywhere if it hadn't been for their example, patience and partnership over the years. Even though they often didn't understand what I was doing (after all, this boy never stops studying?), they were always by my side.

To my wife Simone, the greatest blessing in my life over the last few years, for her understanding, patience, affection and love. Thank you for being by my side, encouraging me and putting up with me.

To Professor Pedro Melo, for all the trust you've shown me since I was an undergraduate and for becoming more than just an advisor and partner over the years.

To my co-supervisor Juan-Carlos Molinero for agreeing to accompany me during this period, for all his teachings, encouragement, patience and collaboration in carrying out this thesis. It definitely wouldn't have existed in this form if it hadn't been for you.

I would also like to say a huge thank you to Professor Sigrid for all her teaching, both scientific and personal, since I arrived in Recife.

Claire Carré for all the help she gave me both in Brazil and in France and Professor Beatrice Béc for all the teachings during my time in Montpellier.

The University of Montpellier and MARBEC for providing the infrastructure and all the support offered for the development of this study. I would like to extend my sincere thanks to all the members of the "MARBEC" Joint Research Unit at the University of Montpellier (UM).

To the National Council for Scientific and Technological Development (CNPq) for awarding me a PhD scholarship (88882.379302/2019-01).

To the IMAGO laboratory that carried out the HPLC and nutrient analyses. To the French oceanographic fleet for funding the ABRACOS survey and to the officers, crew and scientific team of the R/V Antea for their contribution to the success of the operations. This work is a contribution to the LMI TAPIOCA (www.tapioca.ird.fr), the CAPES/COFECUB program (88881.142689/2017-01), the European Union's Horizon 2020 projects PADDLE (grant agreement no. 73427) and TRIATLAS (grant agreement no. 817578).

To the UFPE Oceanography Department and the UFPE Oceanography Museum for

providing the infrastructure and all the support offered for the development of this study.

To the UFPE Postgraduate Program in Oceanography (PPGO) and all the staff and professors who are part of the UFPE Department of Oceanography, who were important in my education.

To the friends I made at the Zooplankton and Phytoplankton Laboratory at UFPE and will carry with me throughout my life (Claudeilton Santana, Ralf Cordeiro, Renata, Angélica, Pedro, Kaio, Yago, Erick, Denise Costa, Nathalia, Gabriela Figueiredo, Morgana Lolaia, Simone Lira, among others) for the time we spent together and for the countless moments of joy and anxiety we shared, making the journey since my master's degree so fulfilling. It has been and always will be a great pleasure to work with each and every one of you. Thank you for every moment spent with me, for the conversations and teachings.

And to all those who have contributed directly or indirectly to the realization of this work; my sincere thanks.

If education alone doesn't transform society, without it society won't change either (FREIRE, 2001).

ABSTRACT

The energy flux in marine plankton food webs heavily relies on phytoplankton and bacterioplankton. Despite their ecological significance, tropical plankton communities, particularly in the Southwestern Tropical Atlantic, are not fully understood. This Ph.D. thesis aims to improve our understanding of tropical phytoplankton and bacterioplankton communities in the Southwestern Tropical Atlantic, their potential impact on the metabolic structure and trophic pathways of plankton food webs, and the underlying environmental processes regulating their dynamics. The thesis was structured in three main manuscripts that explored (i) the influence of the thermohaline configuration on coarse scale patterns of phytoplankton communities' structure and main groups driving the total phytoplankton biomass, (ii) changes in autotrophic:heterotrophic ratios and their use as indicators of trophic pathways, and (iii) bottom-up and top-down processes driven the structure of microbial communities. The data used here were obtained from a research program composed of two oceanographic campaigns (ABRACOS 1 and 2), which extended to around 300 km^2, and were performed during contrasting environmental settings (austral spring and fall). In the first manuscript, this data was used to examine how thermohaline stratification influence phytoplankton biomass and structure (i.e., size) along a coastal-offshore gradient. The results highlighted the role played by thermohaline structure as the main regulator of community dynamics. During fall, shallower thermocline and nutricline led to a threefold increase in biomass in the upper layers of the oceanic region. Despite this seasonal increase, we observed a dominance of recycled production, along with an uncoupled dynamics between biomass and size structure were observed. Picophytoplankton and nanophytoplankton accounted for about 80% of the community in both seasons, likely due to nitrogen limitation. Subsequently, in the manuscript 2 we then investigated how changes in thermohaline structure affect the autotrophic and heterotrophic biomass proportions of picophytoplankton and nanoplankton. To do so, we used cytometry data from fall campaign (ABRACOS 2). We explored their potential as indicators of trophic pathways within the plankton food web and identified environmental and biotic factors shaping their distribution. Nitrogen-limited environments led to the dominance of heterotrophic bacterial biomass over autotrophic growth. However, in the oceanic region, at the deep chlorophyll maximum, increased nutrient availability favored an increase in picoeukaryote biomass. Overall, these results emphasize the importance of heterotrophic biomass in planktonic microbial communities, providing insights on carbon fluxes in oligotrophic marine ecosystems. In the third manuscript, we investigated whether the community structure of

picoplankton and nanoplankton influences the distribution of planktonic microorganism biomass and explored the role of bottom-up and top-down controls in food web formation. Our results suggest a predominant bottom-up control in regulating microphytoplankton biomass through changes in silicate availability and subsequent impact on diatoms. In contrast, mixotrophic and autotrophic microphytoplankton exhibited contrasting relationships with silicate, thriving at low concentrations and dominating in nutrient-rich environments, respectively. We also found that the Tintinnins play a predominant top-down control on autotrophic phytoplankton distribution. These results highlight the role of thermohaline structure controlling the structure (i.e., size, richness) and productivity of microbial communities. Finally, this thesis represents an important initial step toward modeling microbial networks in the Southwestern Tropical Atlantic.

Keywords: oligotrophic plankton systems; planktonic trophic webs; HPLC; flow cytometry.

RESUMO

O fluxo de energia nas teias alimentares planctônicas marinhas depende em grande parte do fitoplâncton e do bacterioplâncton. Apesar de sua relevância ecológica, as comunidades de plâncton tropical, especialmente no Atlântico Sudoeste Tropical, não são totalmente compreendidas. Essa tese de doutorado teve como objetivo ampliar a compreensão acerca das comunidades de fitoplâncton e bacterioplâncton no Atlântico Sudoeste Tropical, seu potencial impacto na estrutura metabólica e nas vias tróficas das teias alimentares do plâncton, e os processos ambientais subjacentes que regulam suas dinâmicas. A tese foi estruturada em três principais manuscritos que exploraram (i) a influência da configuração termohalina nos padrões de estrutura das comunidades de fitoplâncton em larga escala e nos principais grupos que impulsionam a biomassa total do fitoplâncton, (ii) mudanças no equilíbrio dinâmico entre processos autotróficas:heterotróficas e seu uso como indicadores de vias tróficas e (iii) processos de regulação ascendentes e descendentes que determinam a estrutura das comunidades microbianas. Os dados aqui utilizados foram obtidos por um programa de pesquisa composto por duas campanhas oceanográficas (ABRACOS 1 e 2), que se estenderam por cerca de 300 km^2 e foram realizadas durante configurações ambientais contrastantes (primavera e outono austral). No primeiro manuscrito esses dados foram utilizados para examinar como a estratificação termohalina influencia a biomassa e a estrutura (i.e. tamanho) do fitoplâncton ao longo de um gradiente espacial (costa-oceano) e temporal (primavera e outono). Os resultados destacaram o papel desempenhado pela estrutura termohalina como o principal regulador das dinâmicas da comunidade. Durante o outono, a termoclina e a nutriclina menos profundas levaram a um aumento três vezes maior na biomassa na região oceânica superficial. Apesar desse aumento sazonal, observamos uma predominância de produção reciclada, juntamente com dinâmicas desvinculadas entre biomassa e estrutura de tamanho. Picofitoplâncton e nanofitoplâncton representaram cerca de 80% da comunidade em ambas as estações, provavelmente devido à limitação de nitrogênio. Em seguida, no segundo manuscrito, investigamos como as mudanças na estrutura termohalina afetam as proporções de biomassa autotrófica e heterotrófica de picofitoplâncton e nanoplâncton. Para isso, utilizamos dados de citometria da campanha de outono (ABRACOS 2). Exploramos o potencial dessas proporções como indicadores de vias tróficas na teia alimentar do plâncton e identificamos fatores ambientais e bióticos que moldam sua distribuição. Ambientes limitados por nitrogênio levaram à predominância da biomassa bacteriana heterotrófica sobre o crescimento autotrófico. No entanto, na região oceânica, na máxima clorofila profunda, o aumento da disponibilidade de

nutrientes favoreceu um aumento na biomassa de picoeucariotos. No geral, esses resultados enfatizam a importância da biomassa heterotrófica nas comunidades microbianas planctônicas, fornecendo informações sobre fluxos de carbono em ecossistemas marinhos oligotróficos. No terceiro manuscrito, investigamos se a estrutura da comunidade de picoplâncton e nanoplâncton influencia a distribuição da biomassa de microorganismos planctônicos e exploramos o papel de controles ascendentes e descendentes na formação da teia alimentar. Nossos resultados sugerem um controle predominante ascendente na regulação da biomassa de microfitoplâncton por meio de mudanças na disponibilidade de silicato e impacto subsequente em diatomáceas. Em contraste, microfitoplâncton mixotrófico e autotrófico apresentaram relações contrastantes com o silicato, prosperando em baixas concentrações e dominando em ambientes ricos em nutrientes, respectivamente. Também constatamos que os tintínidos exercem um controle predominante descendente na distribuição do fitoplâncton autotrófico. Esses resultados destacam o papel da estrutura termohalina no controle da estrutura (i.e. tamanho, riqueza) e produtividade das comunidades microbianas. Finalmente, esta tese representa um importante passo inicial para a modelagem de redes microbianas no Atlântico Sudoeste Tropical.

Palavras-chave: sistemas planctônicos oligotróficos; teias tróficas planctônicas; HPLC; citometria de fluxo.

FIGURES LIST

1. General Introduction

2. Phytoplankton Spatiotemporal Variability

3. Nutritional environment driving the heterotrophic and autotrophic biomass

4. Bottom-up and top-down drivers of the microplankton community

TABLE LIST

2. Phytoplankton Spatiotemporal Variability

3. Nutritional environment driving the heterotrophic and autotrophic biomass

4. Bottom-up and top-down drivers of the microplankton community

SUMMARY

1 GENERAL INTRODUCTION

1.1 PLANKTON IN MARINE ECOSYSTEMS

The pelagic ecosystem encompasses great diversity, of planktonic communities from different evolutionary branches divided into a wide range of functional groups: virioplankton, bacterioplankton, phytoplankton, zooplankton, and ichthyoplankton (Bassani, 2002). A size-based classification is also used: picoplankton (<2 μm), nanoplankton (from 2 to 20 μm), microplankton (from 20 to 200 μm), mesoplankton (from 0.2 to 20 mm), macroplankton (from 20 to 200 mm), and megaplankton (> 200mm) (Figure 1) (Reynolds, 2006; Sieburth; Smetacek; Lenz, 1978). This large size spectrum also makes the use of different sampling methods (and mesh sizes in the case of zooplankton) needed in their research (Figure 1), increasing the complexity in the study of the entire plankton compartment. In addition to this taxonomic and size diversity, the large plankton abundance represents approximately 98% of the biomass in the global ocean (Sardet, 2015; Suthers; Rissik; Richardson, 2019). Hence, plankton plays a central role in transferring matter and energy in ocean food webs, thus influencing biogeochemical cycling and feedback to climate (Figure 2). For example, bacterioplankton encompasses relevant primary producers, i.e. Cyanobacteria, and decomposers in marine trophic webs (Cabral; Andrade; Paranhos, 2017). Bacterioplankton represents a compartment of prokaryotic cells with a large range of ecological functions in marine ecosystems from the remineralization of organic matter to the fixation of nitrogen. Although cell size constraints the dimension of molecules bacteria can assimilate (mainly monomers and oligomers), their complex extracellular enzyme system enables an efficient utilization and remineralization of both dissolved and particulate organic matter (Grossart, 2010). Therefore, these cells may embody more than 90% of producers and decomposers biomass in tropical environments (Moreira, 2017).

Figure 1. Plankton size classes from picoplankton to megaplankton. Note the wide range of sizes. The left column shows plankton functional groups classified according to their size. The right column displays Niskin bottle and all plankton nets and mesh sizes used for each plankton size group.

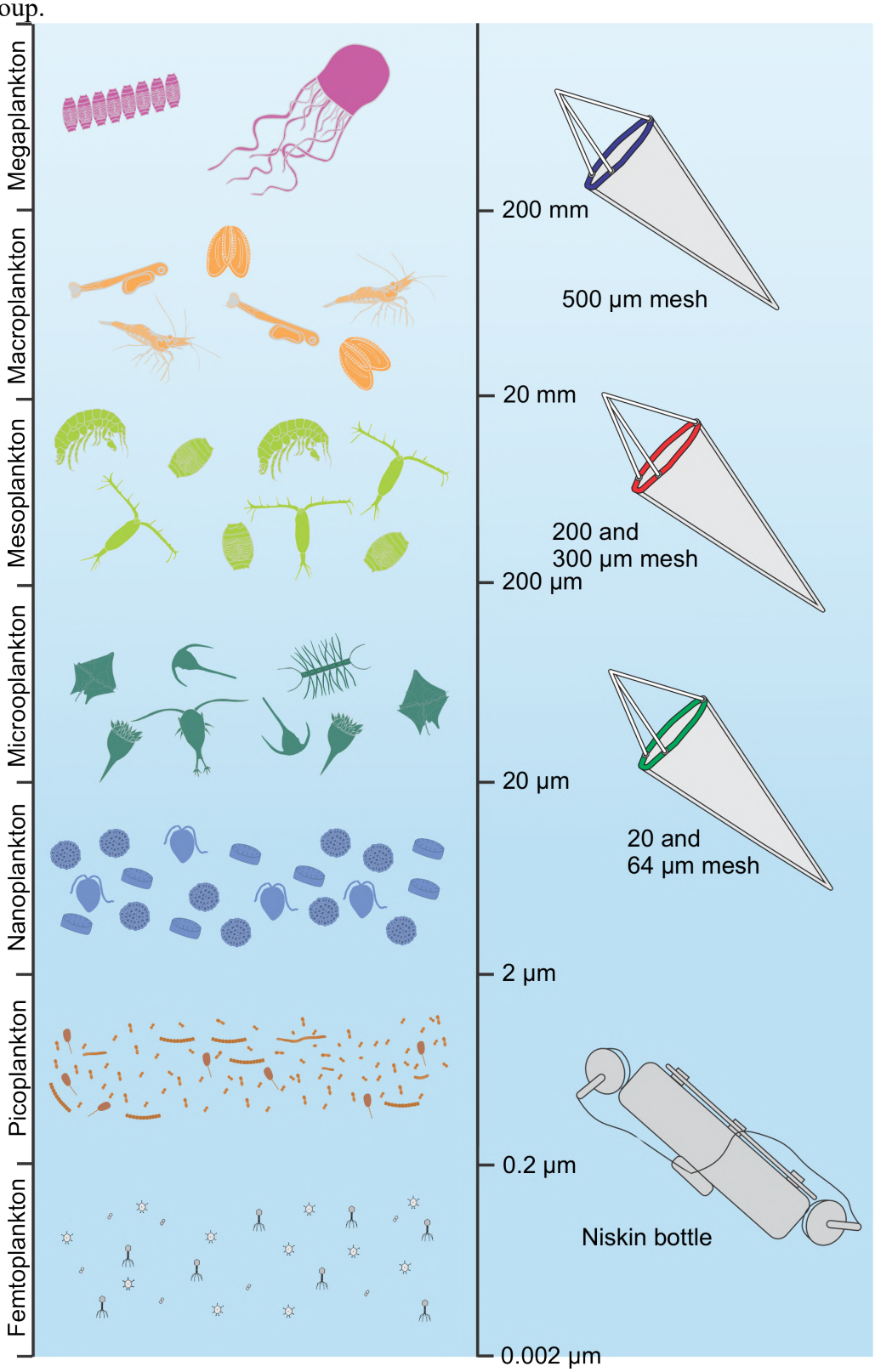

FONTE: AUTOR

Marine Cyanobacteria, also called blue-green algae, contribute to *ca.* 25% of global marine primary productivity, featuring two of the most abundant genera of photosynthetic organisms on the planet, *Synechococcus* and *Prochlorococcus*, that can reach abundances of up to 10^5-10^6 cells per mL (Larkin; Mackey; Martiny, 2019). Cyanobacteria also include marine diazotrophs, mainly represented by the genus *Trichodesmium*, which fix atmospheric nitrogen (N_2) into available nutrients, such as ammonia (NH_3) and nitrate (NO_3^-) that are then used by photoautotrophs (Figure 2a) (Capone et al., 2005). Heterotrophic bacteria further play a major role in marine biogeochemical cycles, primarily responsible for the attenuation of net particulate organic matter production in the euphotic zone and the remineralization of nutrients, such as nitrogen and phosphorus (Azam et al., 1983; Azam; Malfatti, 2007).

Figure 2. The central role of the plankton in marine biogeochemical cycles. (A) In the nitrogen cycle, cyanobacteria convert dissolved nitrogen into ammonium, which can be used by some phytoplankton groups, but most of it is converted by bacteria into nitrite or nitrate. Ammonium, nitrate, and nitrite can undergo denitrification by bacteria and get converted back into N_2, which is either reincorporated into the cycle or released into the atmosphere. In comparison to the nitrogen cycle, the phosphorus cycle (B) is much shorter and slower. Rivers and dust deposition are the primary sources of mineral phosphorus delivered into the ocean. In the marine environment, the phosphate is consumed by phytoplankton and then transferred through grazing to higher trophic levels and returned to the ocean through decomposition; (C) The marine carbon cycle involves the transfer of carbon between the atmosphere, ocean, and marine organisms. Phytoplankton converts carbon dioxide into organic matter through photosynthesis. Zooplankton feeds on phytoplankton and transfers carbon to upper trophic levels and contributes to the RDOC pool by the sinking of unconsumed dying/dead organisms and prey detritus produced by sloppy feeding. In addition, bacterioplankton plays a crucial role in the cycling of carbon by breaking down organic matter and recycling nutrients. RDOC stands for "refractory dissolved organic carbon", the process refers to the production of a dissolved compounds that cannot be further degraded in the short term and becomes part of the ocean's dissolved C reservoir (i.e. the microbial carbon pump, Jiao et al. 2010).

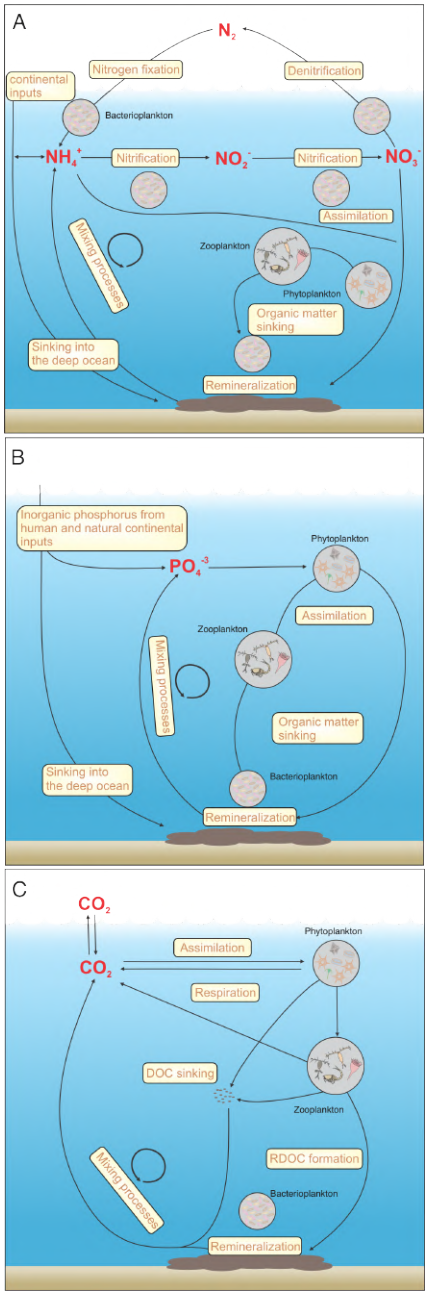

FONTE: AUTOR

Another compartment of plankton communities, the eukaryotic phytoplankton is responsible for about 50% of the global marine primary productivity and production of O_2 (Edwards, 2017; Field et al., 1998). Their photosynthetic activity removes a large amount of carbon from the atmosphere, which is converted into organic matter available for upper trophic levels, such as the diverse members of the zooplankton, or sinks to the deep ocean through the biological carbon pump (Ducklow; Steinberg; Buesseler, 2001; Karlusich; Ibarbalz; Bowler, 2020). In addition, dinoflagellates and coccolithophores assist in cloud formation through the production of dimethylsulfoniopropionate and other volatile organic substances (Bullock; Luo;

Whitman, 2017; Nunes-Neto; Do Carmo; El-Hani, 2009). It is worth noticing that, although phytoplankton present photoautotrophy as a fundamental characteristic, a large portion of phytoplankton organisms are mixotrophs. These mixotrophic phytoplankton consume suspended organic matter, and in some cases are active predators of picophytoplankton and heterotrophic bacteria. As representative of the mixotrophic phytoplankton, there are many dinoflagellates and other small Nanoflagellates (Flynn et al., 2013; Raven; Beardall, 2022; Stoecker et al., 2017).

1.2 Plankton functional traits

Understanding ecological traits in marine organisms is essential for deciphering how populations and communities' function and respond to environmental changes. In ecology, traits are defined as characteristics that predict a taxa's fitness in response to an environmental variable or their contribution to ecosystem function (Litchman; Klausmeier, 2008; Litchman; Ohman; Kiorboe, 2013). Trait-based studies in plankton ecology are far from being a new concept. Since the paradox of plankton (Hutchinson, 1961), much research on attributes of plankton organisms was aimed at understanding community's structure in marine ecosystems. This nurtured new ecological theories, such as the Margalef mandala, which explains the complexity of pelagic ecosystems based on their functional and structural characteristics. The mandala linked phytoplankton biodiversity to ecosystem functioning, turbidity, and nutrient concentrations (Margalef, 1978). The investigation of such ecological traits can be used not only to depict the main environmental variables driving the dynamics of plankton communities but also to model and predict future changes (Litchman et al., 2015).

In the last decade, trait-based models have grown in complexity encompassing detailed traits of marine plankton community structure and biogeography (Glibert, 2016), such as preference for nutrient uptake, motility, nutritional modes, and the propensity to produce toxic compounds (Figure 3) (Glibert, 2016). Among these functional traits, probably the most prominent is body size, as it influences community structure, carbon fixation rates, respiration, stability, and food web trophodynamics (Hillebrand et al., 2022; Litchman; Klausmeier, 2008). Size is a highly predictive trait for phytoplankton metabolism, and a highly suitable indicator of plankton responses to climate change, as will be discussed further in the text. Body size is a pivotal functional trait, especially for plankton, which varies in several orders of magnitude (Figure 1). Small cells dominate under oligotrophic and warm conditions, except when other environmental and biotic factors, i.e. changes in nutrient concentration, and competition with

other taxa come into play, highlighting the complexity of factors influencing plankton structure (Hillebrand et al., 2022). Size further shapes interspecific interactions, especially predator-prey relationships, which structure food webs length and the role of the plankton in pelagic trophodynamics.

Figure 3. A simplified version of the updated Margalef Mandala proposed by Glibert (2016). The axes include: the gradient of N forms preferentially used by the phytoplankton, from NH4+ to NO3 (1); the gradient of dissolved inorganic N:P available to the phytoplankton (2); motility of the cells, ranging from no motility to swimming (flagellated) to cells with sink/float vertical migration strategy (3); adaptation to high vs low light and the tendency to be autotrophic vs mixotrophic (herein generally meaning phagotrophic) (4); tolerance to temperature variability (5); turbulence from low to high (6); cell size, from small to large (7); ecological strategy along the k to r spectrum (8); the propensity of the cells to be toxic or to produce other bioactive compounds such as reactive oxygen (9); growth rate from low to high (10); and propensity for the resulting production to cycle through either the microbial food web (regenerated production, 11) or to constitute new production (12).

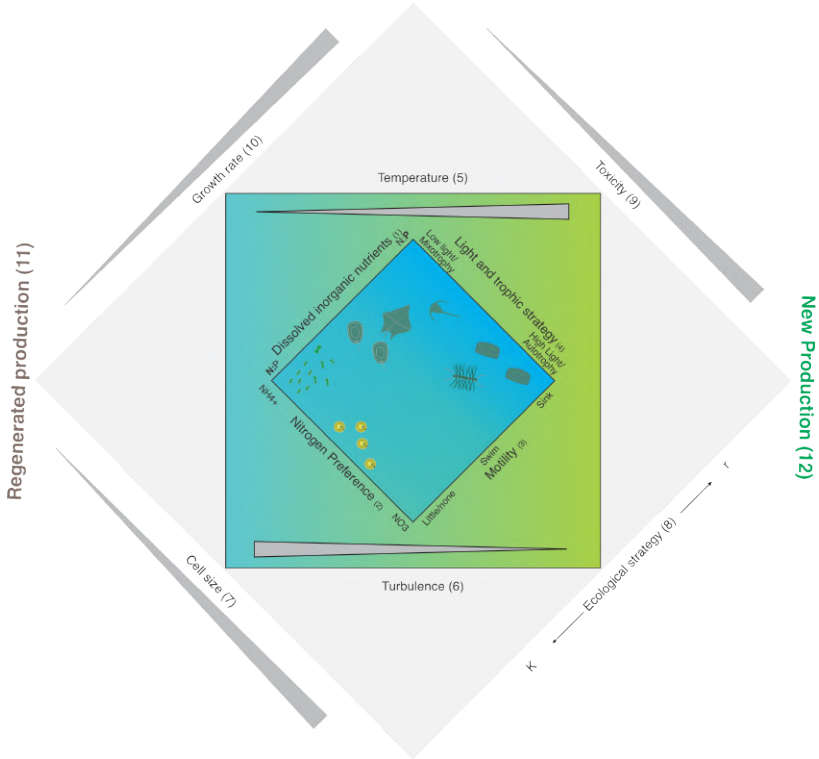

FONTE: AUTOR

1.3 The phytoplankton and bacterioplankton in marine pelagic trophic webs

Due to their fundamental functional role and diversity, phytoplankton and bacterioplankton are crucial for the maintenance of pelagic trophic webs. These plankton cells form the base of marine food webs, with their size classes contributing to distinct trophic pathways and food web length (Chisholm, 1992). The smaller fractions of phytoplankton (pico- and

nanophytoplankton), and the dissolved organic matter they release, have a trophic link with tiny heterotrophs, which assimilate labile dissolved carbon produced during their growth, i.e., heterotrophic bacteria, or directly prey on them, i.e., heterotrophic, mixotrophic protists and ciliates. This promotes a microbial path of pelagic food webs (Safran, 2009) (Figure 4), which is an important pathway of primary productivity in oligotrophic systems (Fenchel, 2008). In addition, microphytoplankton sustain a short and relatively efficient chain where they are grazed by micro- and mesozooplankton, sustaining higher consumers (Armengol et al., 2019). This simple, direct transfer of matter and energy is called the herbivorous-metazoan, or classical food web (Giorgio; Williams, 2005; Schmoker; Hernández-León; Calbet, 2013) (Figure 4).

The balance between these two trophic pathways (microbial and classic) determines the energy transfer efficiency and the overall productivity and structure of marine ecosystems. The trophic efficiency among marine compartments changes in concomitance with the length of the trophic web, the nutritional value of the prey, physical processes, and latitudinal gradients (Garvey; Whiles, 2016). For instance, the trophic efficiency is estimated to be 5%, 10%, and 15% in upwelling, temperate, and tropical ecosystems, respectively (Bachiller et al., 2020; Eddy et al., 2021; Young et al., 2015). Consequently, as the assimilated fraction of the carbon moves up the food chain, the matter and energy provided by primary producers are progressively reduced to a fraction of the initially available (Eddy et al., 2021). Thus, the production of consumers at a specific trophic level is not only influenced by the rate primary producers synthesize new organic matter, but also by the length of the trophic web, metabolic processes, and the influence of energy pathways, including the microbial food web (Eddy et al., 2021, Hanley; Pierre, 2015). Hence, the size structure of phytoplankton and bacterioplankton is key to understand the trophic dynamics of marine ecosystems. Size composition, however, is highly variable, as it is also influenced by biochemical, ecological, and spatial variables, as shown in Figure 5.

Figure 4. The microbial and classical plankton food webs. The microbial marine food web involves the transfer of energy and nutrients from small phytoplankton to heterotrophic bacteria and other nano- and microzooplankton, which are then consumed by larger organisms, forming a longer trophic web common in tropical oligotrophic ecosystems. This web plays a crucial role in the cycling of nutrients in the ocean. In turn, the classical food web involves larger organisms, such as the microphytoplankton that is grazed by micro- and mesozooplankton which then sustain fish and mammal's biomass. This configuration predominates in temperate ecosystems and resurgence zones. Both food webs are interconnected and play important roles in maintaining the carbon flux of marine ecosystem.

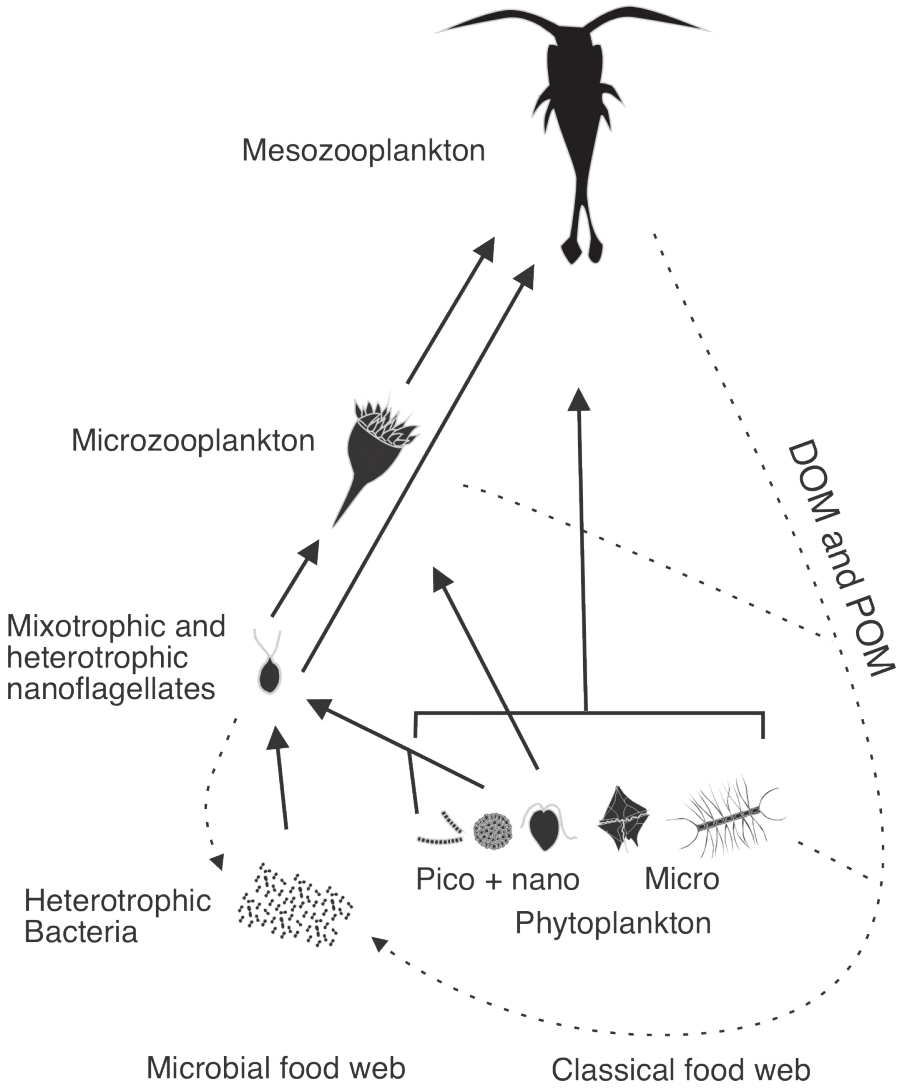

FONTE: AUTOR

1.4 Factors that regulate marine phytoplankton and bacterioplankton distribution and production

Phyto- and bacterioplankton communities, functional traits, and structure are shaped by multiple environmental and biological forces (Figure 5). These forces act over a wide range of scales. At the geological scale (millions of years) processes such as the break of supercontinents allowed the diversification of marine phytoplankton. In the long-term, large-scale factors, deep-water mass cycles, and ocean basin processes influence the distribution of communities and the large-scale transport of nutrients. Lastly, short-term, local forces, i.e., seasonal variabilities in thermohaline structure temperature, light availability, and grazing, locally regulates the diversity, nutritional modes, and biomass of populations (Jardine et al., 2017; Katz; Fennel; Falkowski, 2007; Ryabov; Rudolf; Blasius, 2010; Toseland et al., 2013; Vernet et al., 2019). In the short-term, bottom-up drivers, such as nutrients availability, i.e., nitrogen, phosphorus, and some trace elements such as iron, as well as light penetration, are among the main shaping drivers (Andersson; Haecky; Hagström, 1994; Pan; Zhang; Zhang, 2007). The predominance of microbial or herbivorous trophic pathways is conditioned, among other factors, by the availability of resoures in the water column (Berglund et al., 2007). For instance, small Cyanophyceae thrive in low nitrogen-to-phosphorus waters over large Bacillariophyta which are less efficient phosphorus competitors (Vrede et al., 2009). Resource availability also influences nutritional strategies in the plankton community, i.e., the proportion between mixotrophy and autotrophy (Paczkowska et al., 2019). In conditions of both low prey and nutrient concentrations, such as in oligotrophic oceans, mixotrophic flagellates might prosper over their specialized autotrophic (strictly photosynthetic) and heterotrophic counterparts by balancing the lack of resources (Katechakis; Stibor, 2006; Ptacnik et al., 2004; Tsai; Mukhanov, 2021). Under these conditions, nanoflagellates may use photosynthesis to fulfill their energy demands and use phagotrophy of bacteria as main source of N and P (Ptacnik et al., 2016).

Figure 5. Multiple factors affect water properties and consequently the ecology of plankton, i.e., life cycle, taxa interactions, and cell size, from the global scale to local changes in the water column structure.

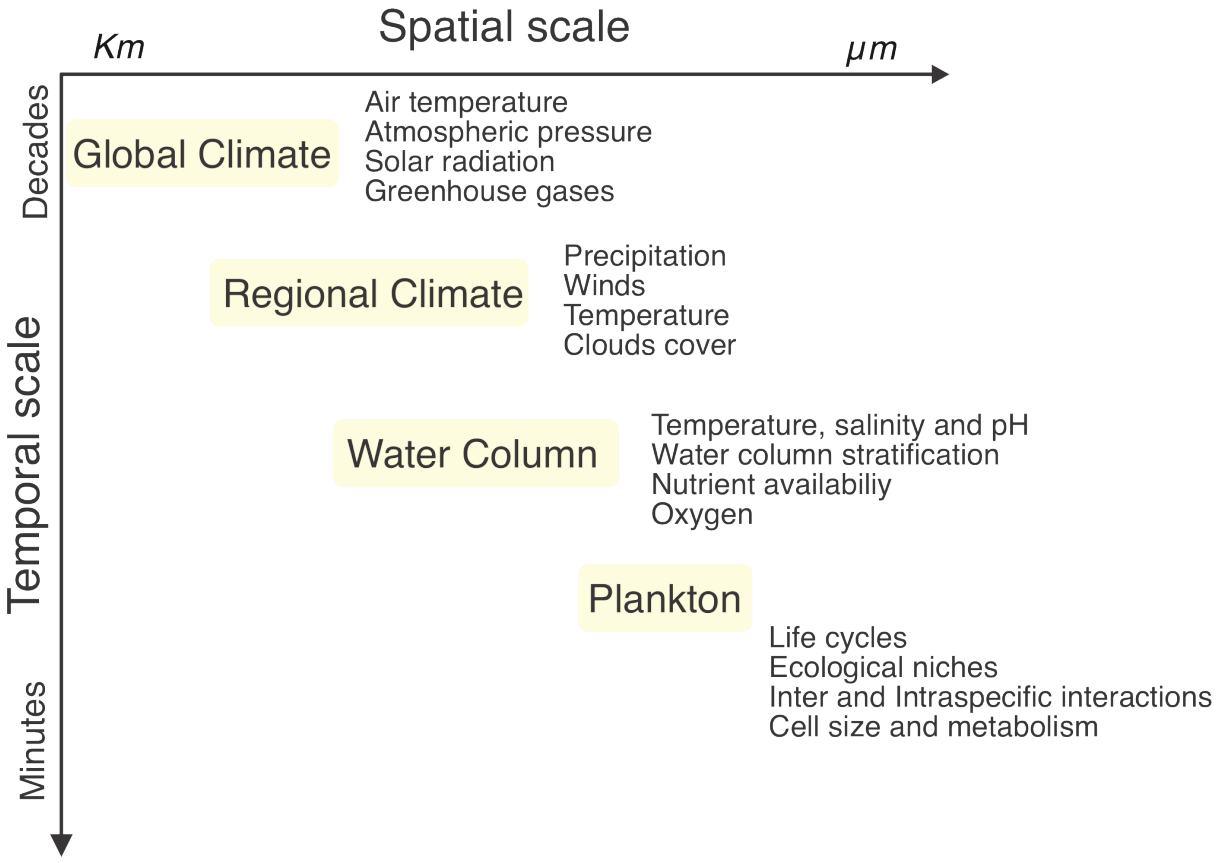

FONTE: AUTOR

Temperature universally has a pivotal control on the metabolism of ectotherms, as in the case of most planktonic taxa, with increasing metabolic rates in higher temperatures (Grimaud et al., 2017; Staehr; Birkeland, 2006). Moreover, temperature shapes the thermohaline structure of the water column, thus regulating the availability of nutrients in the euphotic layer (Boyle; Keigwin, 1987). Thermohaline stratification is a major force that vertically shapes the distribution of plankton (Figure 6) (Hickman et al., 2012). The barrier created by the pycnocline, which encompasses both the thermocline and halocline, generates a layer of high nutrient concentration near its upper base, the Deep Chlorophyll Maximum (DCM). The DCM is a permanent feature in many tropical and subtropical oceans, with depth and thickness seasonal variations.

Latitudinal gradients in these physical forces result in contrasting vertical zonation of the water column, from the poles to the tropics (Figure 6), which is controlled by seasonal regimes of rainfall, trade winds, continental runoffs, and water temperature, caused by unequal distribution of solar radiation (Feucher; Maze; Mercier, 2019; Serrano; Valle-Levinson, 2021;

Thurman, 2019). These variables influence the water column density and regulate the depth and structure of stratification and pycnocline. In the tropics, the pycnocline is relatively shallow, while in high latitudes, it is deeper and stronger. This results from differences in solar radiation, higher in the tropics and therefore warmer, leading to a steeper temperature gradient and a stronger pycnocline (Knauss; Garfield, 2016). In contrast, in high latitudes, lower water temperature leads to a more uniform temperature profile and a weaker pycnocline. Additionally, the pycnocline is affected by ocean currents and the presence of sea ice (Chen et al., 2021; Cheng et al., 2022; Tanimoto; Ouellette; Koseff, 2020). For example, in regions where there is a strong ocean current that flows parallel to the coastline, such as the western boundary currents, the pycnocline is often deeper due to the advection of denser water from the deeper ocean. Similarly, in regions with sea ice, the formation of ice can increase the salinity of the water below the ice line, resulting in the formation of a stronger pycnocline.

Figure 6. Meridional section of the world ocean illustrating the surface and deep layers of the water column separated by the pycnocline. The pycnocline is the line that connects maximum density gradient caused by differences in temperature (thermocline) or salinity (halocline) and defines the limit of the mixing depth. This vertical gradient changes with latitude and seasonal variabilities (dashed line) in the water column temperature and salinity. Light availability has a negative relationship with depth, with three main zones observed. The euphotic zone is the sunlit upper layer of the ocean where photosynthesis occurs, in the first 200 m, under this, the mesophotic zone is the middle layer with reduced light, and the oligophotic or midnight zone is the deepest and darkest layer of the ocean with life adapted to extreme conditions. On the other hand, nutrient concentration has a positive correlation with depth. The dynamic between the mixed layer, euphotic zone depth, and nutrient concentrations shape seasonal productivity patterns.

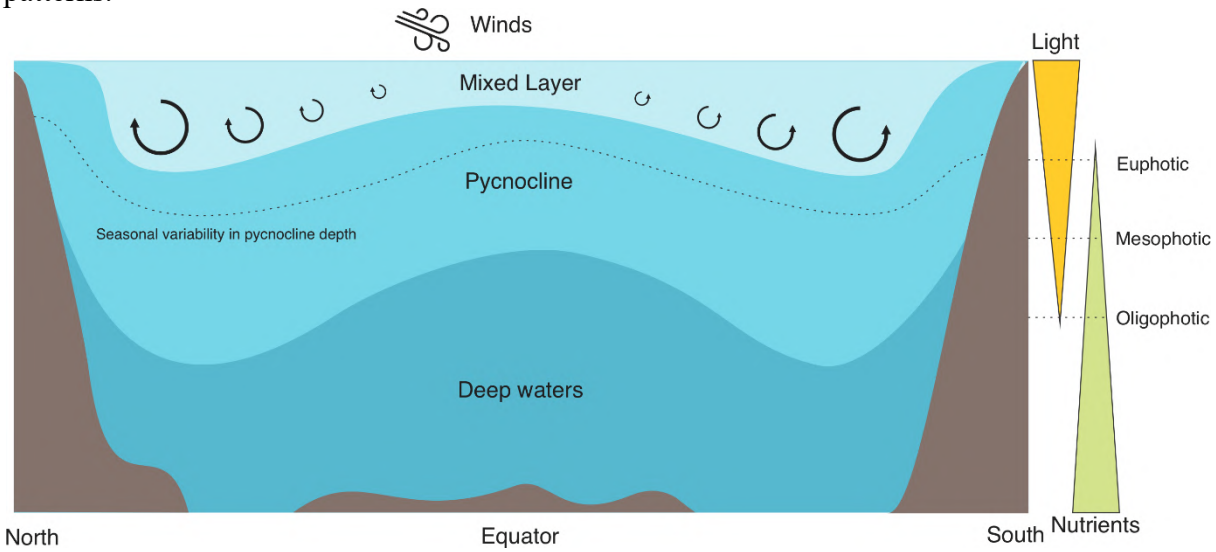

FONTE: AUTOR

Changes in thermohaline structure, and consequently in nutrients upward flux, together with seasonal patterns of light availability, shape seasonal patterns of bacterioplankton and

phytoplankton biomass and productivity (Speight; Henderson, 2013). Temperate regions experience a large variation in the depth and intensity of the thermocline, with a shallower and stronger thermocline in summer and a deeper and weaker one in winter, producing increased mixing during winter months. However light limitation makes that primary productivity only peaks during spring, with a later small bloom in autumn. Polar waters are consistently cold, allowing for year-round mixing and distribution of nutrients. However, seasonal productivity fluctuates due to changes in light levels. Winter months have abundant nutrients but no light, resulting in low productivity, peaking with the increase in light intensity during spring and summer. On the other hand, in tropical regions, light does not limit the growth of primary producers. However, the sustained warmer temperatures enhance vertical stratification and thermocline thickness, preventing nutrient-rich bottom water from reaching the surface. As a result, productivity in tropical water is usually nutrient-regulated, and dominated by small cells, leading to low productivity levels year-round (Reynolds, 2006; Suthers; Rissik; Richardson, 2019) (Figure 7).

Figure 7. Seasonal patterns of phytoplankton productivity influenced by nutrient and light limitation (bottom-up control), and the grazing by zooplankton (top-down control) in (a) temperate, (b) polar and (c) tropical regions. Redraw from Castro and Huber (2012) and Sommer et al., (2012).

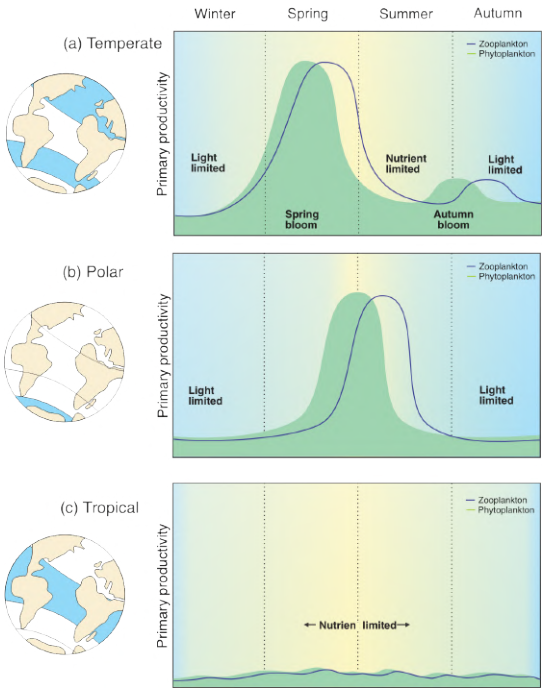

FONTE: AUTOR

1.5. Plankton trophic webs in the changing ocean

Global anthropogenic change dramatically transforms marine trophic webs. Ocean warming modifies the distribution of marine species, phenology, and community functional traits, thus disrupting their intricate food web relationships (Gissi et al., 2021; Maureaud et al., 2017). Warming changes the physical structure of the water column, which influences phytoplankton productivity and their associated trophic pathways (Höfer et al., 2019; Jiang et al., 2019; Šolić et al., 2020). Additionally, ocean acidification caused by the increasing levels of atmospheric carbon dioxide absorbed by the ocean is hindering the ability of calcium carbonate shell-forming organisms, such as coccolithophores, to form and maintain their shells, thereby having a cascading effect on the entire food web (Alma et al., 2020; Fitzer et al., 2015). Although this same ocean acidification can have no negative effect or even be benefic for other microalgae such as diatoms (Kroeker et al., 2013). Climate change further modifies precipitation patterns and the timing of seasonal events, leading to imbalances in nutrient levels and disrupting the food web (Brierley; Kingsford, 2009; Danovaro et al., 2011; Gissi et al., 2021).

In plankton communities, these effects have faster and more acute responses in comparison to other pelagic compartments, as they are tightly coupled with environmental variability (Raven; Beardall, 2021). Due to their short life cycle, these communities rapidly respond to changes in temperature, salinity, and water column structure (Edwards, 2017). Therefore, climate-driven changes, i.e., warming, modification of ocean currents, and nutrient regimes, disturb plankton communities. Additionally, by restructuring large-scale patterns of primary producers, warming also impact local diversity (i.e., an range expansion of warmer affinity taxa into temperate and cold systems). These biogeographical changes further percolate the average body size of plankton communities, food web structure, and predator-prey interactions (Richardson, 2008). In coastal waters, warming, eutrophication, and overfishing yield to an increase of opportunistic phytoplankton groups and more frequent harmful algal blooms, which affect seafood production and human health (Grattan; Holobaugh; Morris, 2016).

Warming also shifts the dominance of the main nutrition modes of pelagic food webs. That is, enhanced temperature favors respiration over primary productivity, not only decreasing autotrophic carbon fixation, but fostering biomass of small heterotrophs and enhancing the mixotrophy on phytoplankton taxa to maintain their nutritional demands (Allen; Gillooly; Brown, 2005; Wilken et al., 2013). However, although some studies point-out that the overall biomass and productivity decrease along with global ocean warming (Signorini; Franz; Mcclain, 2015), following the temperature-size rule, we can expect a reduction in body size of populations of the same species (James' rule) or closely related species (Bermanns' rule)

(Atkinson; Ciotti; Montagnes, 2003; Meiri, 2011; Verberk et al., 2021). The relative contribution of smaller fractions of plankton groups is expected to increase, with a gradual shift toward a smaller average size of dominant organisms in plankton communities (Morán et al., 2010). The Metabolic theory predicts that mixotrophy tends to gain prevalence with ocean warming, with recent findings pointing out a rapid adaptation of mixotrophic Nanoflagellates to a more heterotrophic behavior with increasing temperatures (Lepori-Bui et al., 2022; Novak et al., 2019). Indeed, large-scale models have suggested a dominance of mixotrophic over purely autotrophic or heterotrophic protists in the global ocean (Mitra et al., 2016). Consequently, the current research focus in plankton ecology has shifted towards the smaller taxa and the understanding of their alternative nutrition modes, such as mixotrophy, as well as their relationship to climate change (Edwards, 2019; Flynn et al., 2013; Henson et al., 2021; Livanou et al., 2021; Pang et al., 2019). It is crucial to comprehend the mechanisms driving small-size plankton taxa to unravel the dominant trophic pathways in hydrographic provinces of oligotrophic regions.

1.6 Motivation and Structure

Tropical plankton and microbial communities form the basis of wide diversity networks, energy fluxes and biogeochemical cycles, yet the impact of global ocean threats (warming, deoxygenation, acidification) on such communities are poorly understood, particularly if compared with temperate regions. To assess and potentially predict how tropical plankton communities might respond to future Global Change scenarios, and to which extent this will affect global marine productivity, quantifying processes regulating plankton structure and dynamics is fundamental. Most of our current understanding of how climate change affects plankton communities arises from long-term surveys and historical datasets (Beaugrand, 2013; Jonkers; Hillebrand; Kucera, 2019). However, such large-scale sustained observations are rare in tropical regions from the Global South, with most of the available evidence of climate effect on plankton coming from the north Atlantic and north Pacific where extensive biological datasets are more prolific (Batten et al., 2019). Additionally, as suggested by the results of global scale expeditions i.e., Tara Ocean, the advance to more holistic views in marine ecology studies, with the use not only of new methodologies but also the link with different compartments in marine ecosystems, is essential to understand the impact of climate and environmental change (Sunagawa et al., 2020). Predicting the effects of multiple global change

stressors on microbial communities is a challenging endeavor due to the complex interactions among driving factors.

Plankton research in tropical areas, such as the tropical South Atlantic still has several gaps that need to be addressed. Some of these include:

1. Lack of comprehensive data: Despite decades of research, the vast majority of the tropical areas remain poorly sampled on the small and large time-scale (i.e. seasonal, year, and decadal variability), making it difficult to fully recognize distribution and diversity patterns of planktonic organisms in this region.
2. Lack of understanding of the microbial community in the tropical South Atlantic: although there are several studies in the temperate regions of the South Atlantic, including genetic diversity surveys, our understanding of the microbial community abundance, biomass and variability in the tropical Atlantic, especially in the southwestern portion, is limited to punctual studies, and in the case of the heterotrophic bacteria only one general published data is available (Moreira, 2017).
3. Physical-biological interactions: The relationships between the physical and biological processes and how they shape the distribution and diversity of planktonic communities are not yet fully understood in the tropical South Atlantic.

Furthermore, in the Ocean Decade, the advance to a throughout comprehension of marine ecosystems functioning is essential to create concrete management and conservation strategies in the changing ocean. Therefore, this thesis aims to provide an assessment of environmental and biological drivers of the pico- and nanoplankton biomass and community structure in the Southwestern Tropical Atlantic, and to investigate their impact on the metabolic structure and trophic pathways of plankton food webs. To do so, beside this General Introduction, the document is divided into three main manuscripts (Chapter 2, 3 and 4) (Figure 8), and a General Discussion which are structured as follows:

In the second chapter, using data from two oceanographic surveys performed during austral spring and fall in the Southwestern Tropical Atlantic, we analyzed the space-time variability of phytoplankton biomass and size structure along a coast-offshore gradient and quantified the influence of thermohaline stratification on the phytoplankton community. We further tested the extent of coupling between phytoplankton biomass and size structure (i.e., whether high biomass is driven by large, coupled production, or small phytoplankton cells, uncoupled production). In the third chapter, looking at the smaller fraction of the community (picoplankton and nanoplankton) we tested the hypothesis that the observed changes in

thermohaline structure from the shelf to the oceanic islands shift biomass ratios of plankton microbial groups from the dominance of autotrophic to heterotrophic biomass. Specifically, we examine spatial patterns of pico- and nanoplankton biomass ratios, their potential use as a proxy of trophic pathways within the plankton food web, and depict environmental and biotic drivers of their distribution. In the fourth chapter, we use our comprehensive study of the pico- and nanoplankton in the first two manuscripts to investigate how this microbial community structure influences the biomass distribution of microplankton or if other bottom-up or top-down controls have a stronger effect. In this chapter, we search for insights into the ecological processes shaping the food web. Lastly, we ensemble the results and their implications in a general discussion addressing their role on the trophic web and how this may change in the near future.

Figure 8. Schematic representation of the structure of the thesis in the plankton size and time scale of each chapter.

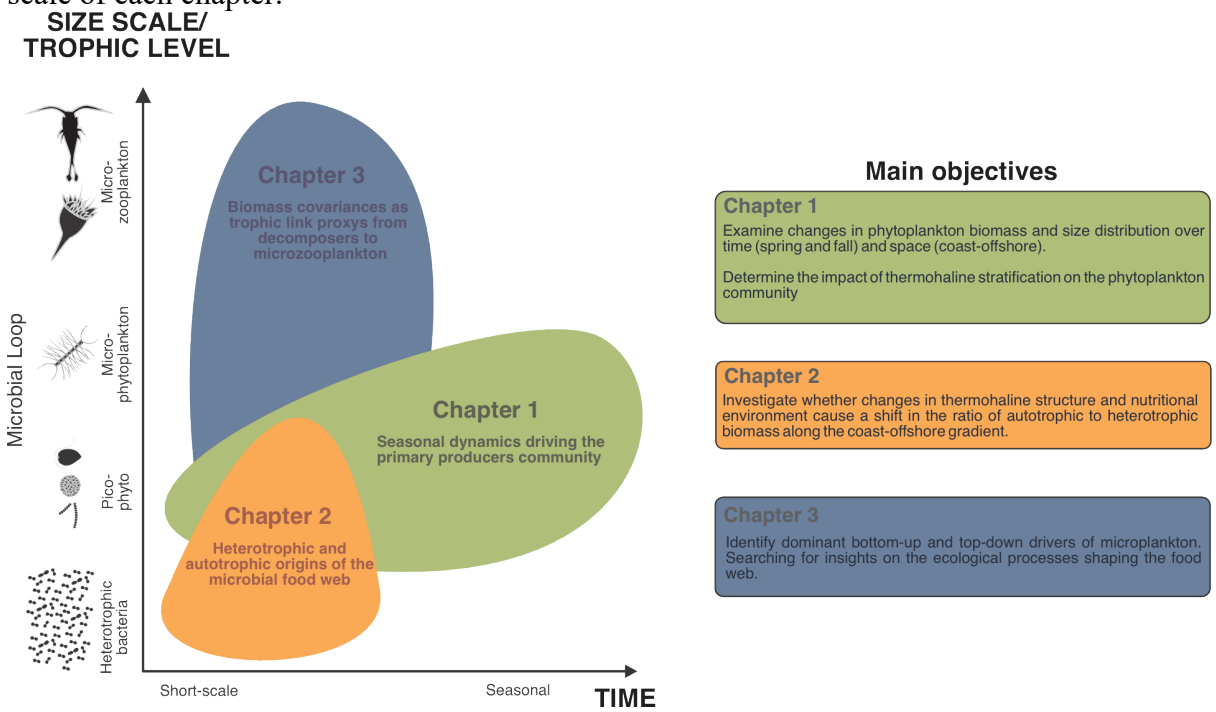

FONTE: AUTOR

2 UNCOUPLED CHANGES IN PHYTOPLANKTON BIOMASS AND SIZE STRUCTURE IN THE WESTERN TROPICAL ATLANTIC

Published – Journal of Marine Systems

doi: https://doi.org/10.1016/j.jmarsys.2021.103696

Abstract

Structural changes in phytoplankton communities have large influence on marine elemental cycling, food web dynamics and carbon export. Here we used data from two field expeditions, performed in spring and fall, over a coast-offshore gradient to investigate phytoplankton structure and dynamics in the Southwestern Tropical Atlantic (SWTA). Results revealed a predominant role of the thermohaline structure as the main driver of phytoplankton dynamics regardless the season. In fall, the thermocline and nutricline shallowing promoted a biomass increase, which was 3-fold higher around the oceanic islands. The structure of phytoplankton community mainly varied vertically, with *Prochlorococcus* pigments contributing greatly to the higher nutrient Deep Chlorophyll Maximum, whereas other Cyanophyceae predominated in nutrient poor surface layers during the two seasons. In addition, a clear coast-offshore variability in the new production (*Fp*) was observed, with the shelf region displaying higher values (up to 0.21), promoted by larger Bacillariophyceae pigments concentration, thus suggesting a coastal influence on shelf production. Although the phytoplankton biomass increased seasonally, our results highlighted a predominance of recycled production (*Fp*) and uncoupled dynamics between biomass and size of phytoplankton structure, with pico- and nanophytoplankton dominating the relative biomass, i.e., ca. 80% of the community in both seasons. We hypothesize that these patterns may result from a strong nitrogen limitation (N:P of around 3:1), which likely constrain a pronounced growth of the microphytoplankton.

Key Words: Primary producers dynamics; pigment composition; tropical thermohaline structure; nutrient ratios

Introduction

Phytoplankton communities are essential components in marine ecosystems functioning and key players in the global carbon cycling, contributing to about half of Earth primary productivity (Litchman et al., 2015). They encompass a variety of taxonomic and functional entities associated to diverse biogeochemical cycles, and therefore their structural changes alter marine elemental cycling (Finkel et al., 2010; Litchman et al., 2015). Understanding how phytoplankton respond to the environmental variability is thus critical to assess not only changes in biogeochemical cycles, but also their implications in food webs functioning under global change scenarios.

Phytoplankton structure, biomass and growth are shaped by multiscale interlinked environmental forces, from long-term, large-scale factors, i.e., climate, deep circulation/geostrophic currents, to short term, local ones, i.e., temperature, light, turbulence and nutrients concentration (Jardine et al., 2017; Ryabov et al., 2010; Toseland et al., 2013). The relative importance of these forces however, greatly varies among phytoplankton functional groups due to the diversity of life history traits and ecophysiological requirements (Falkowski and Oliver, 2007; Litchman and Klausmeier, 2008). For instance, nutrient competition favors niche partitioning and shapes phytoplankton distribution, with Cyanophyceae thriving in low nitrogen-to-phosphorus waters over Bacillariophyta that are less efficient phosphorus competitors (Egge, 1998; Vrede et al., 2009). Moreover, empirical evidence on competition theory has shown that light intensity and temperature further influence the minimum nutrient requirements of phytoplankton taxa (Burson et al., 2018; Lewington-Pearce et al., 2019). Hence, a thorough assessment of phytoplankton dynamics requires an integrative multi-scale, multi-stressor approach to effectively quantify, and eventually model, phytoplankton responses under changing ocean conditions.

In the last decade, growing interest has focused on plankton functional traits. Probably the most prominent is body size, as it influences community structure, stability, and food webs trophodynamics (Litchman and Klausmeier, 2008). In oligotrophic systems, smaller phytoplankton groups (picophytoplankton, < 2 μm and nanophytoplankton, 2-20 μm) are known to absorb nutrients more efficiently than large phytoplankton cells due to their higher surface-volume ratio (Chisholm, 1992; Flombaum et al., 2013; Lange et al., 2018). In contrast, larger cells (microphytoplankton, > 20 μm) are generally dominant under turbulent conditions with higher nutrient concentration (Falkowski and Oliver, 2007). Hence, the contribution of pico- and nanophytoplankton to phytoplankton biomass change along with nutrient gradients

and primary productivity (Bell and Kalff, 2001). However, empirical evidence has shown that in oligotrophic ecosystems the increase of phytoplankton biomass may be decoupled from significant variations in the size structure, with a predominance of smaller cells during high productivity events (Dandonneau et al., 2004; Marañón et al., 2003, 2000; Rii et al., 2016).

The southwestern tropical Atlantic (SWTA) is an oligotrophic area characterized by the intrusion of subtropical underwater channeled by the North Brazil Undercurrent - North Brazil Current system (Dossa et al., 2021; Stramma and England, 1999). The thermohaline structure of the region is characterized by the existence of different provinces portrayed by specific thermocline structure and stratification strength (Araujo et al., 2011; Assunção et al., 2020). How such environmental configuration shapes the structure of primary producers remains unclear, although their understanding might shed light on the dynamics of primary producers in oligotrophic ocean regions.

Here, using data from two oceanographic surveys performed during austral spring and fall in the SWTA, we analyzed the space-time variability of phytoplankton biomass and size structure along a coast-offshore gradient, and quantified the influence of thermohaline stratification on the phytoplankton community. We further tested the extent of coupling between phytoplankton biomass and size structure (i.e., whether high biomass is driven by large, coupled production, or small phytoplankton cells, uncoupled production).

Material and Methods

Study area

The SWTA has a narrow continental shelf not exceeding 40 km with a shelf break varying between 40 and 80 meters and a continental slope between 1600 and 3600 m (Knoppers et al., 1999). The region is governed by the western boundary current system, which is dominated by the North Brazilian undercurrent and the North Brazilian current (Fig. 1b) (da Silveira et al. 2000; Dossa et al., 2021). Offshore, the geomorphology is characterized by a chain of seamounts (between 20 and 250 meters high), the Fernando de Noronha ridge that includes the oceanic island of Rocas Atoll and the Fernando de Noronha Archipelago (Fig. 1b) (Castello, 2010; Kikuchi, 2002; Mabesoone and Coutinho, 1970). This area is further influenced by the central and southern branch of the South Equatorial current and the South Equatorial Undercurrent, which form the South Equatorial Current System (Dossa et al., 2021).

Two thermohaline provinces have been defined from the continental slope to the oceanic islands (Fig. 1b) (Assunção et al., 2020). The first area located along the continental slope corresponds to the western boundary current system, which is characterized by a low thermal stratification, the presence of frequent and thick barrier layer and an average mixed layer depth of 53 and 39 m in spring and fall, respectively. The second area encompasses the Rocas Atoll and part of Fernando de Noronha ridge seamounts and corresponds to the South Equatorial Current System. This area is characterized by a deeper mixed layer (~90 and 46 m in spring and fall, respectively), a sharp thermocline, a strong static stability and weak surface current (~0.34 $m.s^{-1}$). Between these two thermohaline provinces lies a transitional area, with an intermediate stratification and moderate static stability (Fig. 1b).

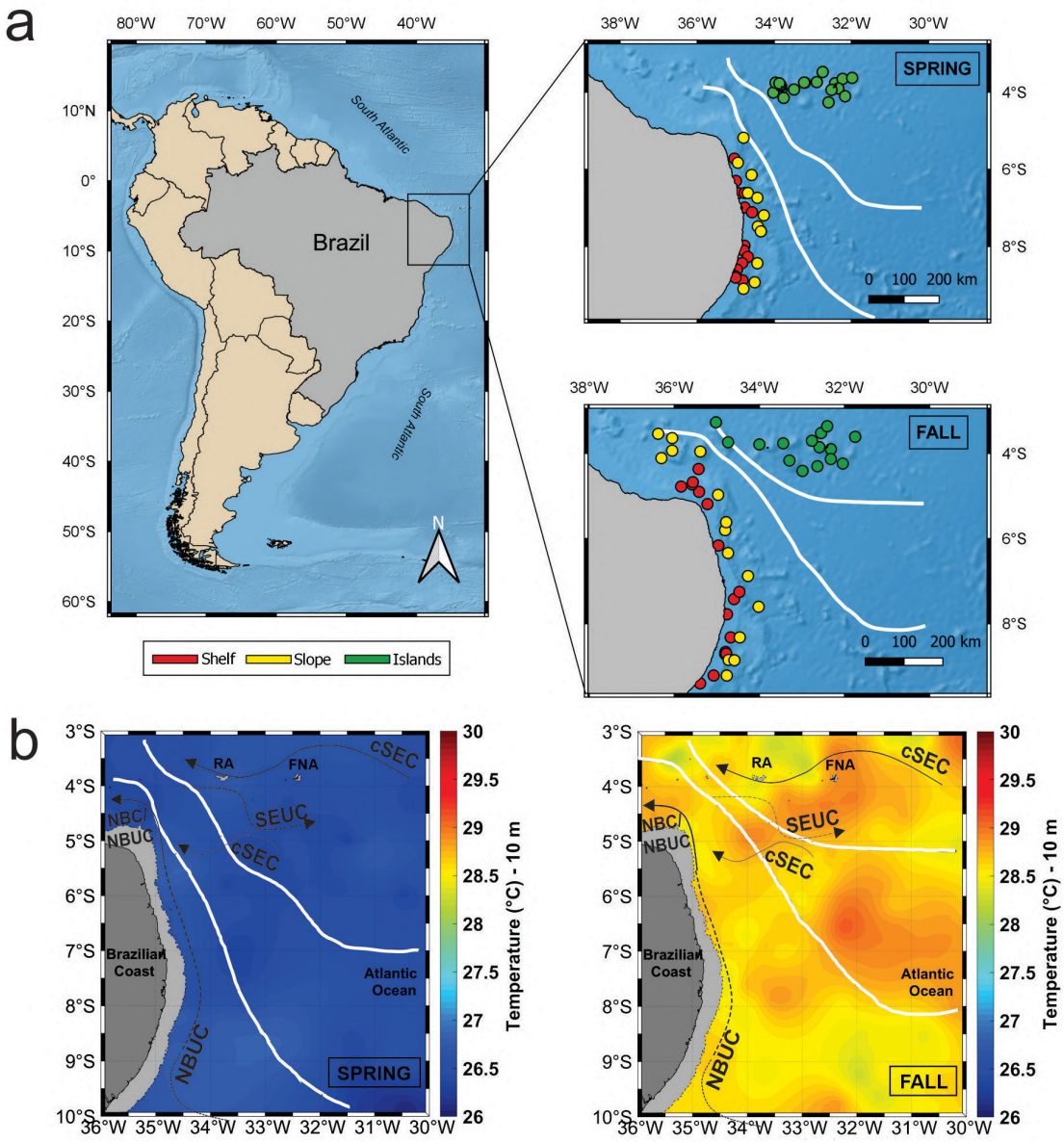

Figure 1 - (a) Study area with the position of sampling stations surveyed during austral spring and fall in the three regions, Shelf: red; Slope: yellow; Islands: green. White solid lines delimit themohaline areas defined by Assunção et al., 2020. (b) 10 m depth temperature field in spring a and fall. White solid lines delimit thermohaline areas. The continental shelf limited by the isobaths of 60 m is represented in light grey. RA: Rocas Atoll; FNA: Fernando de Noronha archipelago. The main currents are represented. cSEC: central branch of the South Equatorial Current; SEUC: South Equatorial Undercurrent; NBUC: North Brazil Undercurrent; NBC: North Brazil Current. Redrawn from Assunção et al. (2020).

Field Collection

Samples were collected during the "Acoustics along the BRAzilian COaSt (ABRACOS)" oceanographic campaigns, carried out in Austral spring (30 August - 20 September of 2015 - ABRAÇOS 1; Bertrand, 2015) and fall (9 April - 9 May of 2017 - ABRAÇOS 2; Bertrand,

2017) on board the French R/V ANTEA. Spring 2015 and fall 2017 are representative of canonical spring and fall conditions in terms of thermohaline structure and currents dynamics (Assunção et al., 2020; Dossa et al., 2021). Hence, hereafter we will only use spring and fall to identify the oceanographic campaigns. ABRACOS 1 comprehended 54 stations encompassing the shelf, the continental slope and oceanic islands (Fig. 1a), while ABRACOS 2 extended the study area towards the western part of the Fernando de Noronha ridge and totaled 61 stations (Fig. 1a). In all stations, vertical profiles of conductivity, temperature, depth and fluorescence were acquired from the surface to 1000 m depth (or 10 m above the sea bottom) using a CTD Seabird SBE911+.

Water sampling for pigments and nutrients were carried out using a rosette at four depths defined by CTD profiles: Surface, Mixed Layer, Deep Chlorophyll Maximum (DCM) (which showed a mean depth of 100 m in spring and 80 m in fall) and at 200 m. In shelf shallow stations (< 50 m depth), where no peak of fluorescence was observed, the DCM and 200 m samplings were replaced by a Shallow Bottom, sampling at ~10 m above the bottom. For each station and sampled depth, 500 ml of water were filtered in Whatman GF/F glass fiber for the estimation of pigment concentrations of the total phytoplankton community. Size fractionation of water samples was done using a 20 µm filter meshes to estimate the biomass of pico- and nanophytoplankton (< 20 µm) and microphytoplankton (> 20 µm, by the difference between total and < 20 µm fractions). Filters were stored at -80ºC for subsequent HPLC pigment analysis.

Water samples for nutrient concentrations estimation (NOx [NO_2^- + NO_3^-], PO_4^{3-} and SiO_4^{4-}) were collected in 30 ml falcon tubes, pasteurized (heated at 80°C for 2.5 hours in an oven) and frozen to ensure stability until the laboratory analysis. Nutrient analyses were achieved using classical colorimetric methods (Grasshoff; Ehrhardt; Kremling, 1983).

HPLC analyses

Chemotaxonomic analysis was carried out on an Agilent Technology 1200 series HPLC following the LOV Method described in Hooker et al. (2000), to assess phytoplankton biomass and diversity. Pigments were extracted in 100% methanol in the dark for 5 minutes at 4ºC. Samples were then sonicated and filtered on cellulose acetate filters to remove cell debris. A 600 µl aliquot was diluted with 150 µl Milli-Q water. For the analysis, 125 µl of this solution was taken and diluted in an injection loop with 125 µl of a 28 mM solution of Tetrabutyl ammonium acetate. The pigments were then separated on a ZORBAX Eclipse XDB-C8 column

from Agilent Technology, with 3 mm in diameter, 150 mm in length and 3.5 µm in porosity. The column temperature was maintained at 60°C and the flow rate at 0.55 ml min^{-1}. The separation was based on a linear gradient between a solution of methanol/Tetrabutyl ammonium acetate 28 mM, 70:30 (v/v), and a 100% solution of methanol. Chlorophyll-a + Divinyl Chlorophyll-a were used to determine total phytoplankton biomass (TChl-a), while all other pigment markers allowed identifying major algal groups (Table 1). The HPLC system was calibrated with external standards (DHI Water and Environment, Horsholm, Denmark).

Taxa	Pigments	Acronym
Dictyochophyceae	19′Butanoyloxyfucoxanthin	19BF
Bacillariophyceae	$Chlorophyll_{C3}$,$Chlorophyll_{C2}$, Diatoxanthin, Fucoxanthin	Chl_{C2}, Chl_{C3}, dia, fuco
Prymnesiophyceae	19′Hexanoyloxyfucoxanthin	19HF
Cryptophyceae	Alloxanthin	allo
Dinophyceae	Diatoxanthin, Peridin	dia, peri
Chlorophyceae	Chlorophyll-*b*, Neoxanthin, Violaxanthin	Chl-*b*, neo, vio
Prochlorococcus	Divinyl Chlorophyll-*b*	div Chl-*b*
Cyanophyceae	Zeaxanthin	zea
All community (TChl-a)	Chlorophyll-*a*, Divinyl Chlorophyll-*a*	Chl-*a*, div Chl-*a*

Table 1 - Pigment biomarkers in major phytoplankton groups. Selected following Roy et al. (2021)

Data analysis

The overall methodological approach is described in Figure 2. Average stations values of biological and environmental variables for each region and depth were calculated to generate mean vertical profiles (Fig. 3). The biological (TChl-a, see Table 1) and environmental (nutrients, temperature and salinity) data were tested for normality (Kolmogorov-Smirnov) and homoscedasticity (Levene). Subsequently, these data were used for comparison among seasons (spring and fall) and diel periods (day and night) using t-test or Mann-Whitney (MW), and by depth (Surface, Mixed Layer, Shallow Bottom, DCM and 200 m) and region (shelf, continental slope and islands) using parametric (one-way ANOVA) or non-parametric (Kruskal-Wallis, KW) analysis of variance (Fig. 2), depending on the normality of the data. Day and night samples were aggregated since no significant differences were found among them (see Supplementary Figure 1).

To examine the variability in phytoplankton communities, we applied a PERMANOVA in log-transformed biological data using a Bray Curtis similarity matrix with the software *PRIMER 6* (Clarke and Gorley, 2006) (Fig. 2). Additionally, to evaluate nonlinear interactions

between environmental factors and phytoplankton biomass, we used Generalized Additive Models (GAMs) (Fig. 2). GAMs allow one response variable to be fitted by several predictors in additive models and have the advantage of not requiring an *a priori* specification of functional relationships, which is suitable for describing complex ecological interactions. The model assumes that the effects of each predictor on the response variable can be described by smooth functions (Hastie and Tibshirani 1986; Wood 2006). Here, we modeled the response of phytoplankton taxa and TChl-a, as a proxy for phytoplankton community, to the effect of nutrients, physical (salinity, mixed layer depth and barrier layer thickness) and spatial (depth and regions) factors, using the function 'gam' in the R package 'mgcv' (Wood, 2011). Models did not include outliers and we used the Generalized cross-validation (GCV) score for model selection.

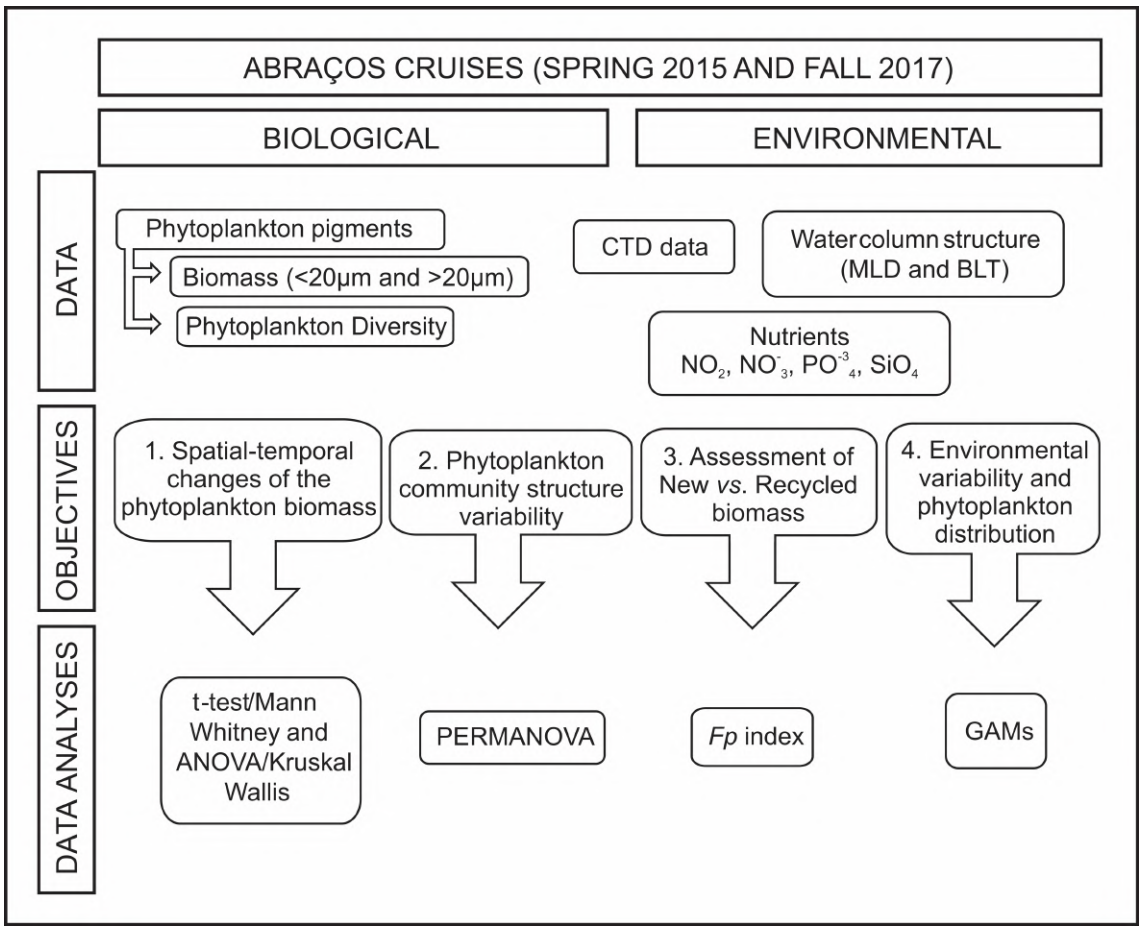

Figure 2 - Flow diagram of the research procedure of data collection and analysis. MLD: mixed layer depth; BLT: barrier layer thickness.

The phytoplankton size structure can also be inferred from the trophic status of producer communities. This was assessed by the quantification of the *Fp* index *sensu* Claustre (1994) (Fig. 2). The *Fp* index denotes the biomass ratio of the phytoplankton involved in the new production over the total phytoplankton:

$$Fp = \frac{\sum \text{fuco} + \sum \text{peri}}{\sum \text{fuco} + \sum \text{peri} + \sum \text{19'-HF} + \sum \text{19'-BF} + \sum \text{zea} + \sum \text{Chl b} + \sum \text{allo}}$$

where the numerator corresponds to the new production composed by Dinophyceae and Bacillariophyceae, and the denominator corresponds to the total biomass of the main groups of the phytoplankton community. To search for seasonal variabilities in the *Fp* values we used t-test or Mann-Whitney, depending on the normality of the data. For all analysis, p values < 0.05 were considered significant.

Results

Environmental seascape

Sea surface temperature was higher in fall than in spring (28.9 ºC vs. 26ºC; t-test, $p < 0.001$) regardless the region (Fig 1b). In the shelf region, temperature was homogeneous along the water column (~26ºC and 28ºC in spring and fall, respectively), while in the continental slope and islands stations the thermal vertical structure showed a general decrease with depth, with temperature values at DCM varying between seasons (~23ºC and ~25ºC in spring and fall, respectively). Likewise, in the 200 m depth temperature was higher (from ~18ºC to 15ºC in spring and fall, respectively) in the continental slope (MW test, $p < 0.001$) than in the islands stations, where it remained constant among seasons (~12.5ºC) (Fig. 3a; Supplementary Table 1).

Salinity varied between 35 and 37 and showed a slight surface coast-offshore gradient with lower values observed in islands stations (ANOVA, $p < 0.001$), with an average of 36.2, in spring, and 35.9 in fall. The vertical profiles showed that DCM and 200 m depth were characterized by higher salinities over the continental slope in both seasons (t-test, $p < 0.001$), with average values of 37.02 at the DCM and 36.06 at 200 m depth in spring, and 37.17 at the DCM and 35.57 at 200m in fall (Fig. 3a; Supplementary Table 1).

Regardless of the season, shelf stations showed a slight vertical increase of nutrients concentration, whereas stations of the continental slope and islands displayed an increased gradient of PO_4^{3}, SiO_4^{-4}, and NO_3^{-} , with a depleted surface layer (Surface and Mixed Layer) separated from a richer deeper layer (DCM and 200 m depth) (Fig. 3b and c; Supplementary Table 1). Overall, the average nutrient concentration was higher in fall (Supplementary Table 1), except for the average NO_3^{-} (3.58 *vs.* 0.71 μmol l^{-1}) and SiO_4^{-4} (1.59 *vs.* 1.26 μmol l^{-1})

concentrations at the DCM (Fig. 3c; Supplementary Table 1). In spring, SiO_4^{-4} surface concentrations were higher in the shelf than in offshore stations (KW test, p= 0.003; ~0.84 µmol l^{-1}), with some stations reaching ~1.5 µmol l^{-1}, whereas the islands stations showed higher surface PO_4^{3-} (ANOVA, p= 0.002; ~0.10 µmol l^{-1}) (Fig. 3c; Supplementary Table 1). The continental slope showed slightly higher surface NO_3^- in both seasons (Surface and Mixed Layer; ~ 0.07 and 0.32 µmol l^{-1} in spring and fall respectively), although no statistical difference was found between regions. At the DCM, nutrients concentration was higher in the islands stations at both seasons (MW test, p< 0.05) (Fig 3b and c; Supplementary Table 1).

An evident increase with depth in NO_2^- concentration was observed during fall in the shelf, with a NO_2^- depleted surface (0.006 µmol l^{-1}) and a richer layer in Shallow Bottom (0.021 µmol l^{-1}) (Fig. 3b; Supplementary Table 1). This feature was conspicuous in the continental slope and islands showing a well-defined primary nitrite maximum with a NO_2^- enrichment near the DCM. This was more evident in fall (0.02 µmol l^{-1} *vs.* 0.08 µmol l^{-1} in the continental slope and 0.05 µmol l^{-1} *vs.* 0.07 µmol l^{-1} in the islands), although the NO_2^- concentrations were statistically different only in the continental slope (MW, p= 0.008).

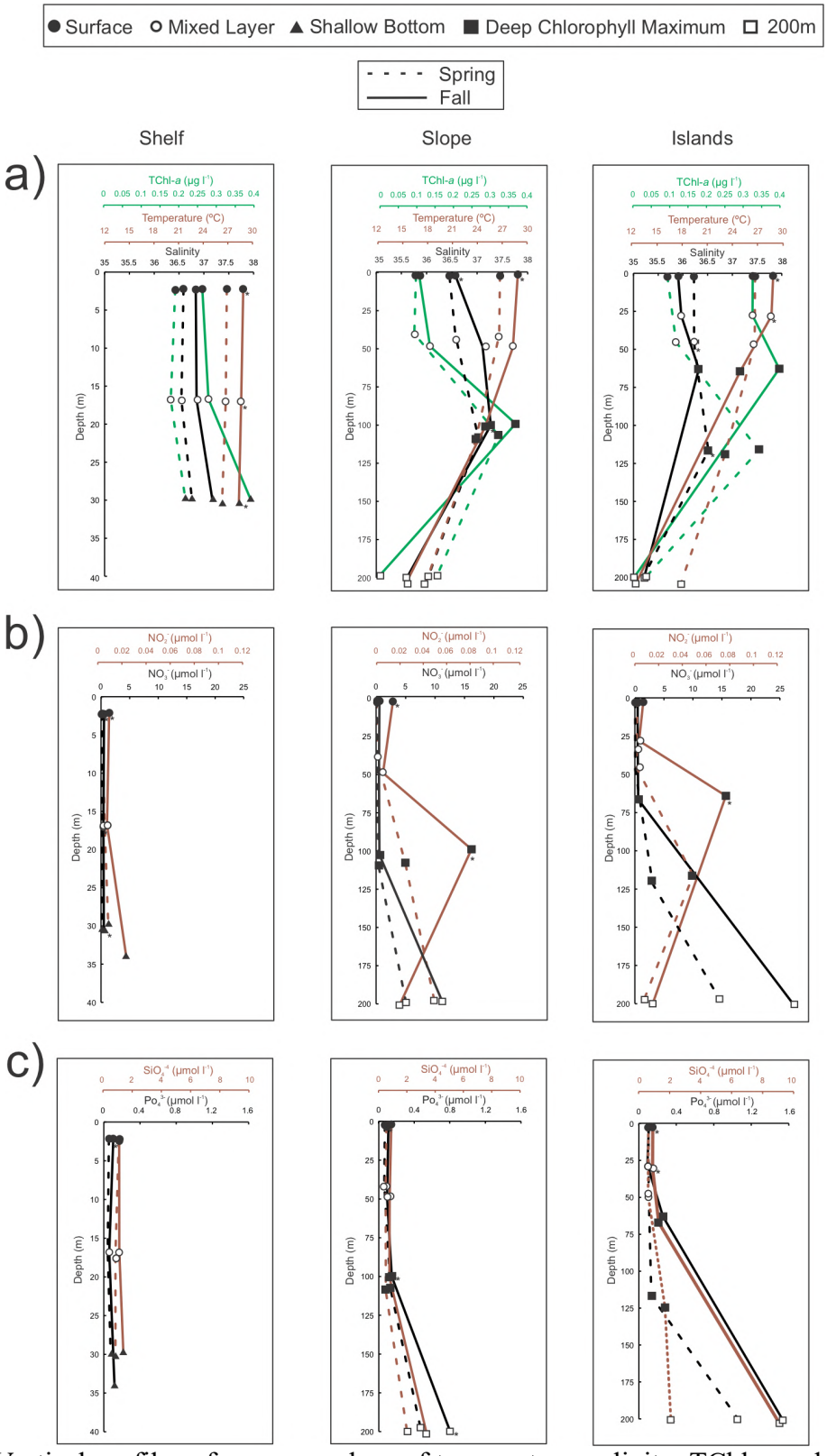

Figure 3 - Vertical profiles of average values of temperature, salinity, TChl-a and nutrients at the depths sampled by the rosette in spring (dotted line) and fall (continuous line). The symbol * denotes depths at which the concentrations were statistically different between seasons. Notice different depth scales in the shelf. (a) average TChl-a, temperature and salinity; (b) average concentrations of NO_2 and NO_3^-; (c) average concentrations PO_4^{3-} and SiO_4^{4-}.

Phytoplankton biomass

The total Chl-a (TChl-a: Chl-a + divinyl Chl-a) concentration ranged from 0.01 to 0.49 (μg l^{-1}) in spring, and 0.003 to 1.7 μg l^{-1} in fall. Overall, TChl-a was higher in fall, but this difference was only significant around the islands (MW test; $p < 0.05$), where it displayed a threefold increase in biomass on the surface layer (Fig 4; Supplementary Table 1). In spring, the shelf stations showed higher TChl-a in the surface layer (Surface and Mixed Layer; KW test, $p < 0.5$; ~ 0.18 μg l^{-1}), while the continental slope and islands stations showed similar concentrations (Surface and Mixed Layer, ~ 0.10 μg l^{-1}). In the shelf region, Shallow Bottom TChl-a values were 0.22 and 0.39 μg l^{-1} in spring and fall, respectively, with some stations showing concentrations similar to the DCM. During fall, islands stations displayed higher TChl-a than the other regions in the surface layer (Surface and Mixed Layer; KW test, $p < 0.001$; ~0.32 μg l^{-1}), whereas in DCM islands and continental slope showed similar TChl-a in both seasons (~0.34 and ~0.39 μg l^{-1} in spring and fall respectively) (Fig. 4; Supplementary Table 1). The lower TChl-a was observed in the 200 m depth stations in both seasons (<0.03 μg l^{-1}). The lack of samples at 200 m depth during spring impaired comparison between seasons.

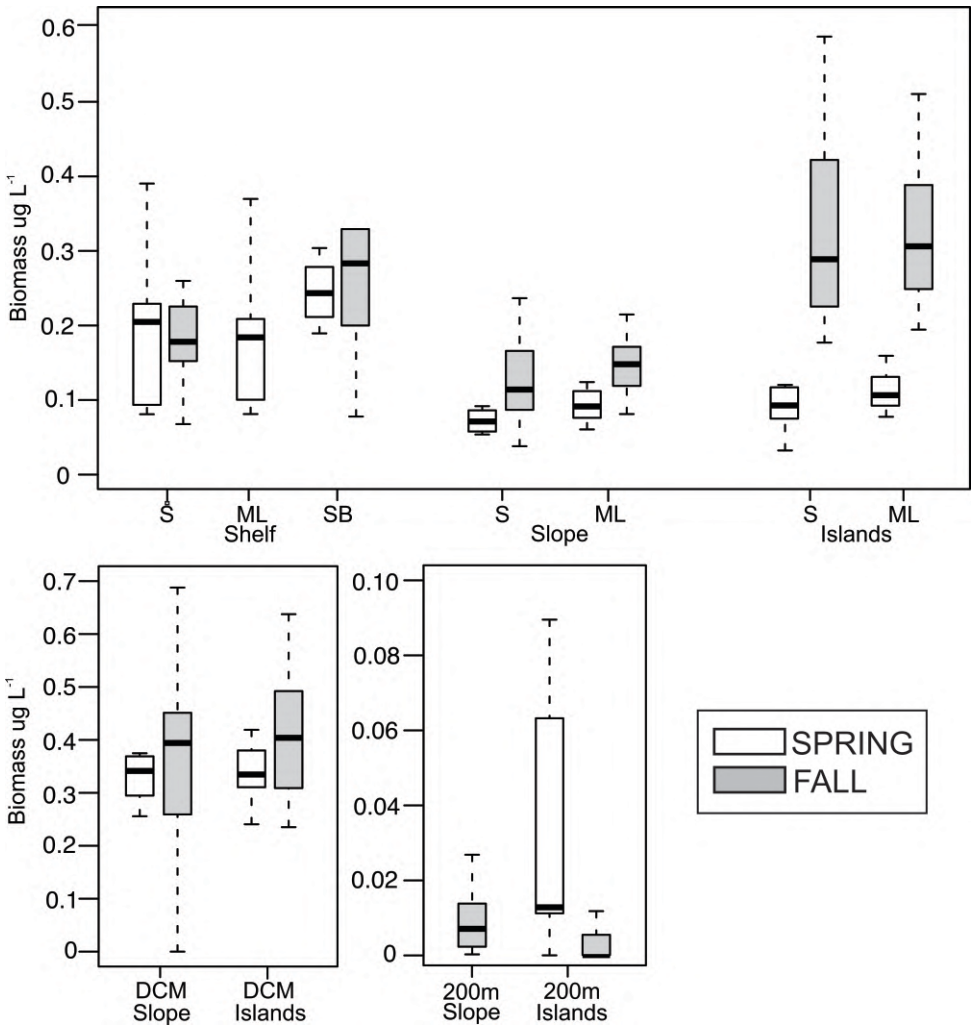

Figure 4 - Total phytoplankton biomass (TChl-a concentrations, see Table 1) in the SWTA during spring and fall. S: surface, ML: mixed layer; SB: shallow bottom, DCM: deep chlorophyll maximum. Outliers were removed from the analysis. Notice different y axis scales between plots.

Pico- and nanophytoplankton vs. microphytoplankton contribution

The Figure 5 represents the pattern in pico- and nanophytoplankton and microphytoplankton contribution for all regions. The pico- and nanophytoplankton (< 20 μm fraction) strongly dominated (>80%) the community regardless the season and depth (Fig. 5). In the Mixed Layer, this fraction accounted for 90% and 80% of the TChl-*a* in spring and fall, respectively (Fig. 5). In fall (no data in spring), at the more productive depths (Shallow Bottom and DCM), the contribution of microphytoplankton was reduced in comparison with the Mixed Layer, not exceeding 10% of the total biomass. The higher contribution of the microphytoplankton in fall was related to the increase of Dinophyceae (peri) and Bacillariophyceae (fuco) at all depths (Fig. 7).

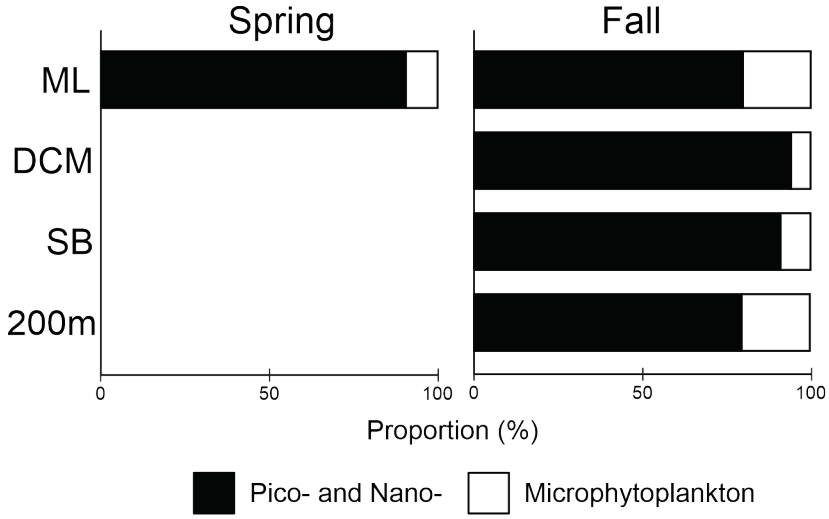

Figure 5 - Average relative contribution of pico- and nanophytoplankton, and microphytoplankton to the total biomass (TChl-a concentrations) for all sampling areas. S: surface, ML: mixed layer; SB: shallow bottom, DCM: deep chlorophyll maximum.

Phytoplankton community structure and distribution

A total of 15 pigments were analyzed: Chl-*a*, Chl-*b*, Chl_{C2}, Chl_{C3}, Peri, 19BF, 19HF, Fuco, Neo, Vio, Dia, Allo, Zea, Div Chl-*a* and Div Chl-*b*. These pigments were used to characterize the dominant taxonomic groups among the phytoplankton community (see Table 1).

Factor	df	MS	Pseudo-F	*p* (MC)
Region	2	2291.1	4.40	0.009
Water Layer	4	33786	65.95	<0.001
Season	1	6888.9	13.24	<0.001

Table 2 - Results of PERMANOVA main tests comparing phytoplankton communities among the factors season (spring and fall), region (shelf, continental slope and islands) and water layer (Surface, Mixed Layer, Shallow Bottom, Deep Chlorophyll Maximum and 200 m). MC: Monte Carlo.

The horizontal and vertical patterns of pigments distribution (Fig. 6) showed higher Cyanophyceae (zea) concentration in the surface layer regardless the region and season, although their relative contribution declined in fall, i.e., ~58% and ~40% in spring and fall, respectively (Figs. 6 and 7). An increase of accessory pigments of three phytoplankton groups, Bacillariophyceae (fuco), Dinophyceae (peri) and Chlorophyceae (Chl-*b*, neo, vio) was observed in fall in all regions (Figs. 6 and 7). These differences in community structure were confirmed by the PERMANOVA (Table 2), which pointed out structural community changes among seasons. The Bacillariophyceae pigment increase was more evident over the shelf, going from 20 to 40% of the total accessory pigments in fall (Figs. 6 and 7).

The overall pattern of phytoplankton community was shaped mainly by the pico- and nanophytoplankton (Fig. 5). Microphytoplankton pigments showed a clear dominance of the Bacillariophyceae pigments in the shelf stations, representing up to 80% of the total pigments concentration, whereas offshore a similar vertical and horizontal pattern with the pico- and nanophytoplankton was perceived (see Supplementary Figure 2).

Factor Regions		
Groups	t	*p* (MC)
Shelf, Continental Slope	3.498	<0.001
Shelf, Islands	1.157	0.22
Continental Slope, Islands	2.255	<0.001
Factor Depths		
Groups	t	*p* (MC)
200 m, DCM	5.844	<0.001
200 m, ML	5.984	<0.001
200 m, S	5.632	<0.001
SB, ML	0.974	0.41
SB, S	0.806	0.59
DCM, ML	16.111	<0.001
DCM, S	15.343	<0.001
ML, S	2.693	<0.001

Table 3 - Pairwise PERMANOVA results showing comparisons of phytoplankton communities among the factors region (shelf, continental slope and islands) and water layer (S: surface; ML: mixed layer; SB: shallow bottom; DCM; 200 m).

In contrast to surface layers, the pigment concentrations of all groups increased in both seasons in the DCM, especially *Prochlorococcus* (Div Chl-*b*) reaching up to 30% of the community pigment concentrations over the continental slope, which was reflected in the PERMANOVA results, that indicated different communities between the surface layers and DCM (Table 3). The 200 m depth, also showed a contrasting community from the other depths (Table 3), with an increase in the Prymnesiophyceae (19HF) and Dictyochophyceae (19BF) pigments concentration (Fig. 7).

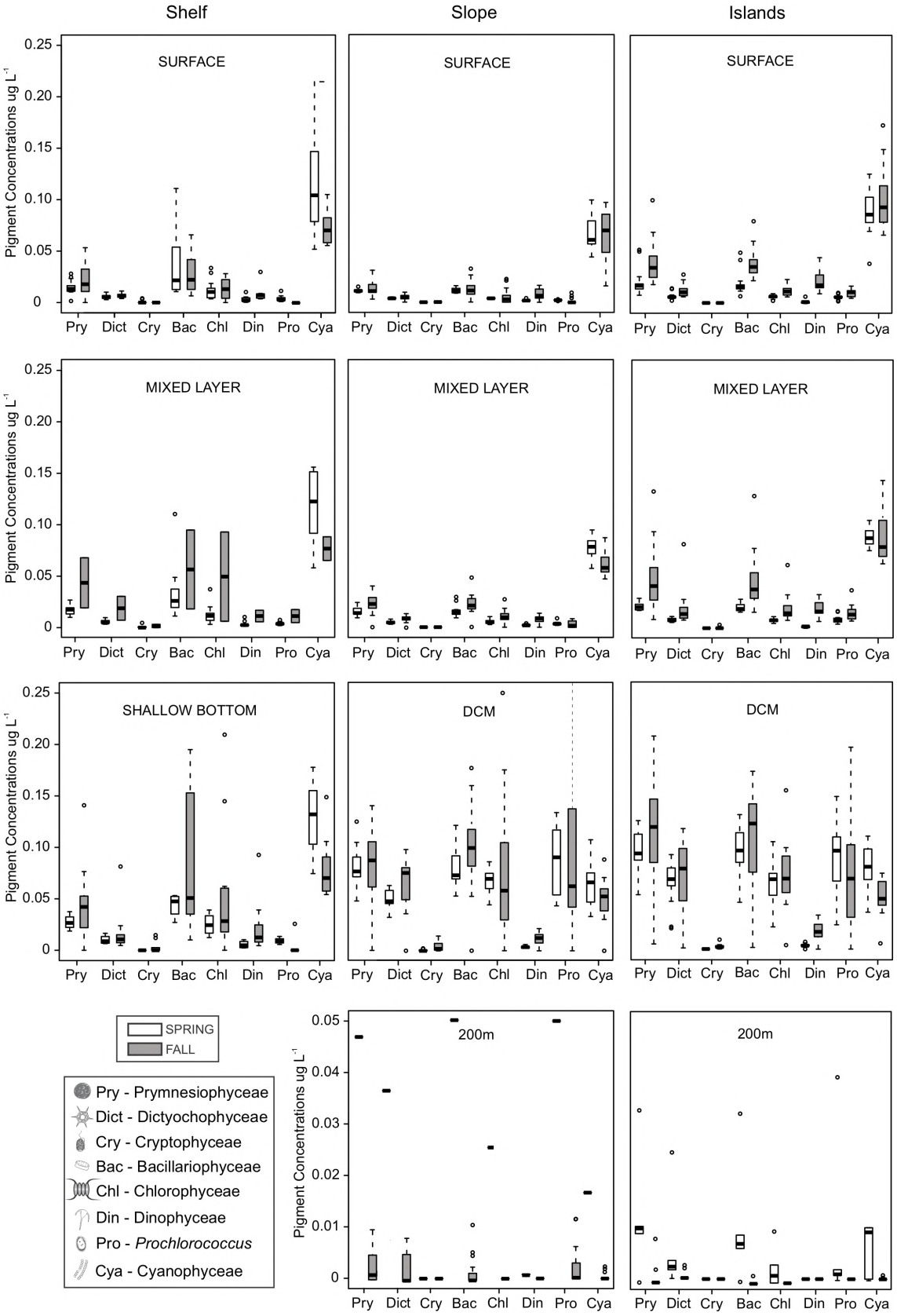

Figure 6 - Concentrations of phytoplankton taxa pigment biomarkers (as indicated in Table 1) in the SWTA during spring and fall for all regions and depths. Notice the different scale in the 200 m plots. DCM: deep chlorophyll maximum.

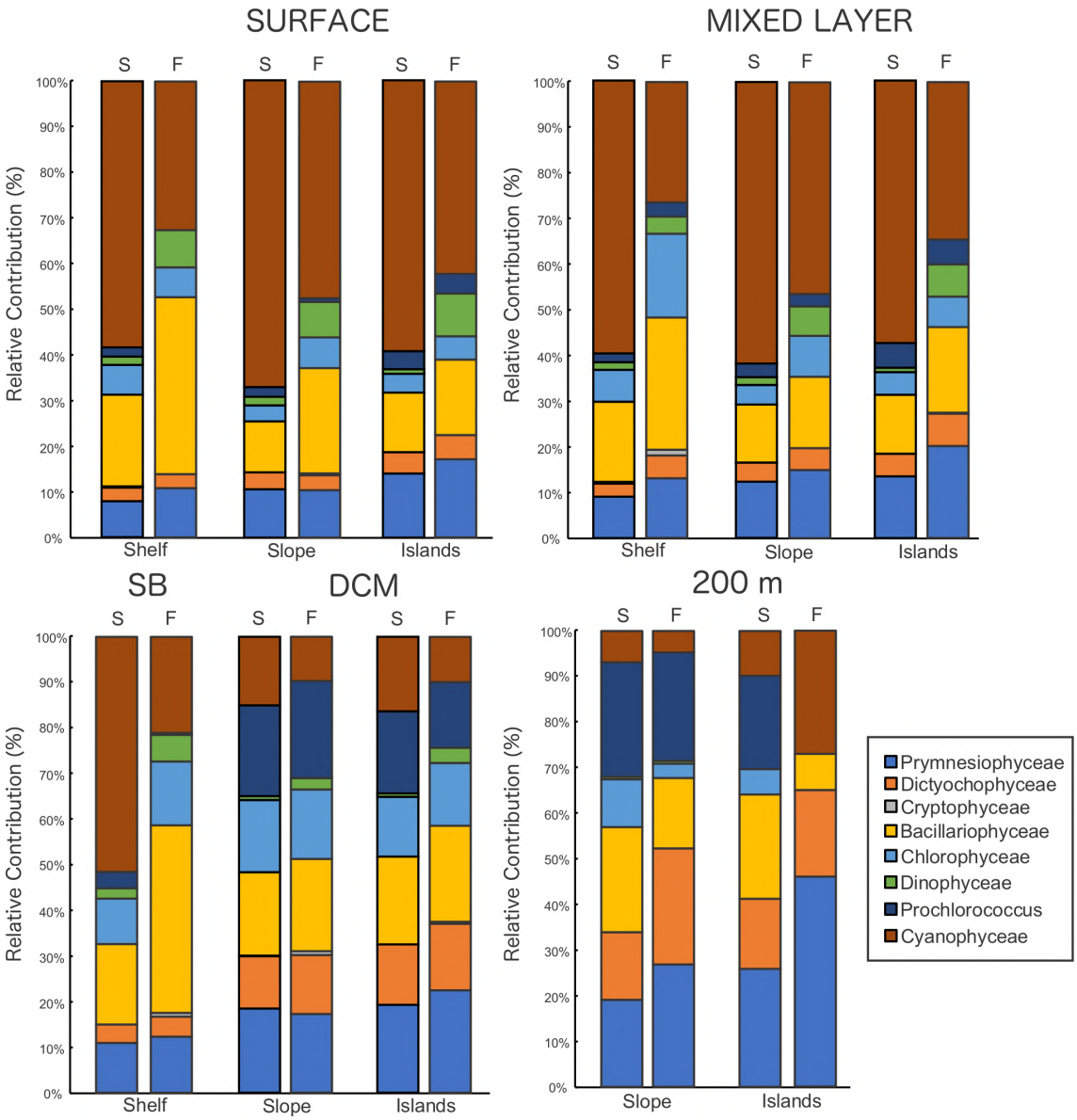

Figure 7 - Relative contribution of phytoplankton taxa pigment biomarkers (as indicated in Table 1) to the total pigments concentrations in the SWTA during spring and fall as a proxy of each taxa contribution to total biomass. S: spring; F: fall; SB: shallow Bottom; DCM: deep chlorophyll Maximum.

Environmental variability and phytoplankton community

GAM models assessing the influence of environmental parameters on the total (TChl-a) or individual taxa explained at least 40% of the total variance (Table 4). Depth was the main predictor of the TChl-a in both seasons with the higher biomass in 50 m (spring) and 125 m (fall), which represented the main DCM depth in both seasons. Depth was also the main predictor for Prymnesiophyceae (19HF), Dictyochophyceae (19BF) and *Prochlorococcus* (Div Chl-*b*), which displayed their higher accessory pigment concentrations near the DCM in both seasons, although the later presented small variability in spring (Fig. 8b). Cyanophyceae (zea)

displayed a decrease in concentration with depth (Fig 8b), highlighting their association with the shallow layer. Besides depth, salinity and SiO_4^{-4} were significant predictors for the whole community distribution, with an increase in biomass associated to salinity 37, in spring, and an inverse relation between salinity and TChl-a, in fall. In both seasons, SiO_4^{-4} values above 1 µmol l^{-1} were also associated to a phytoplankton biomass increase (Fig 8a). This pattern was observed for Bacillariophyceae (fuco; both seasons), Cryptophyceae (allo; spring) and Chlorophyceae (Chl-*b*, neo, vio; fall), that showed SiO_4^{-4} as their main predictor (Fig 8b). In spring, NOx was the main predictor for Chlorophyceae (Chl-*b*, neo, vio) distribution, with the higher importance of this phytoplankton group between concentrations of 1 and 2 µmol l^{-1} (Fig. 8b). Considering the spatial variability, only the continental slope was significant and associated to the lower biomass (Fig. 8a).

	Model	Season	R^2	GCV
Pry	*pry* = ***s(Depth)*** + *s(Sal)* + *s(NOx)* + *regions*	Spring	0.93	0.9×10^{-4}
	pry = ***s(Depth)*** + *s(Sal)* + *regions*	Fall	0.69	0.6×10^{-3}
Dict	*dict* = ***s(Depth)*** + *s(NOx)* + *regions*	Spring	0.95	0.4×10^{-4}
	dict = ***s(Depth)*** + *s(Sal)* + *regions*	Fall	0.76	0.3×10^{-3}
Cry	*cry* = *s(Sal)* + ***s(SiO₄)*** + *s(PO_4^{3-})* + *regions*	Spring	0.40	0.2×10^{-6}
	cry = ***s(Depth)*** + *s(Sal)* + *regions*	Fall	0.60	0.4×10^{-5}
Bac	*bac* = ***s(Depth)*** + *s(Sal)* + ***s(SiO₄)*** + *s(PO_4^{3-})* + *regions*	Spring	0.94	0.1×10^{-3}
	bac = ***s(Depth)*** + *s(Sal)* + ***s(SiO₄)*** + *s(PO_4^{3-})* + *regions*	Fall	0.84	0.2×10^{-3}
Chl	*chl* = ***s(Depth)*** + *s(Sal)* + ***s(NOx)+*** *s(SiO)* + *s(PO_4^{3-})* + *regions*	Spring	0.95	0.3×10^{-4}
	chl = ***s(Depth)*** + *s(Sal)* + ***s(SiO₄)*** + *regions*	Fall	0.73	0.6×10^{-3}
Din	*din* = ***s(Sal)*** + *regions*	Spring	0.51	0.3×10^{-5}
	din = ***s(Depth)*** + *s(Sal)* + *s(BLT)* + *regions*	Fall	0.67	0.3×10^{-4}
Cya	*cya* = ***s(Depth)*** + *s(Sal)* + *s(MLD)* + *regions*	Spring	0.70	0.1×10^{-2}
	cya = ***s(Depth)*** + *s(Sal)* + *s(MLD)* + *regions*	Fall	0.82	0.03×10^{-2}
Pro	*pro* = ***s(Depth)*** + *s(NOx)* + *s(PO_4^{3-})* + *regions*	Spring	0.92	0.6×10^{-4}
	pro = ***s(Depth)***	Fall	0.73	0.3×10^{-3}
TChl-a	*tchl-a* = ***s(Depth)*** + *s(Sal)* + *s(SiO_4)* + *regions*	Spring	0.89	0.2×10^{-2}
	tchl-a = ***s(Depth)*** + *s(Sal)* + *s(SiO_4)* + *regions*	Fall	0.71	0.2×10^{-2}

Table 4 - Statistical summary of generalized additive models between the biomass of the different taxa and the environmental parameters. R2 is the adjusted proportion of total variability explained by the model. GCV: generalized cross validation score; NOx: NO3- + NO_2; Depth; Sal: salinity; TChl-a: total biomass; MLD: mixed layer depth; BLT: barrier layer thickness Pry: Prymnesiophyceae; Dict: Dictyochophyceae; Cry: Cryptophyceae; Bac: Bacillariophyceae; Chl: Chlorophyceae; Din: Dinophyceae; Pro: *Prochlorococcus*; Cya: Cyanophyceae; n = 101 (spring) and 160 (fall). In bold are the main predictors of the taxa in each model.

New Biomass vs. Recycled Biomass

The phytoplankton trophic status was studied based on the *Fp* index representing the biomass ratio of the phytoplankton involved in the new production (Bacillariophyceae and Dinophyceae) over the total phytoplankton (Table 5). Overall, the average new production associated to Bacillariophyceae (fuco) and Dinophyceae (peri) was low, not surpassing 0.21 (Table 5). In both seasons, the new biomass was higher over the shelf (average *Fp* in the Shallow Bottom ranging from 0.10 to 0.21 in spring and fall, respectively). The continental slope and islands stations showed similar *Fp* in the Mixed Layer and DCM, with an average *Fp* of 0.09 (Table 5). An increase in the *Fp* value of all regions in fall was noticed, although it was only significant in the islands surface layer (Surface and Mixed Layer) (t-test, $p < 0.001$).

		Shelf	Slope	Islands			Shelf	Slope	Islands
	S	0.13	0.06	0.04		S	0.18	0.06	**0.09**
	ML	0.11	0.07	0.04		ML		0.09	**0.09**
Spring	SB	0.10			Fall	SB	0.21		
	DCM		0.05	0.06		DCM		0.07	0.06
	200m			0.04		200m			
Average		0.11	0.06	0.045			0.19	0.07	0.08

Table 4 - Fp index value for all regions and depths in both seasons in the SWTA. In bold values that were significantly higher in that season. S: surface; ML: mixed layer; SB: shallow bottom; DCM: deep chlorophyll maximum.

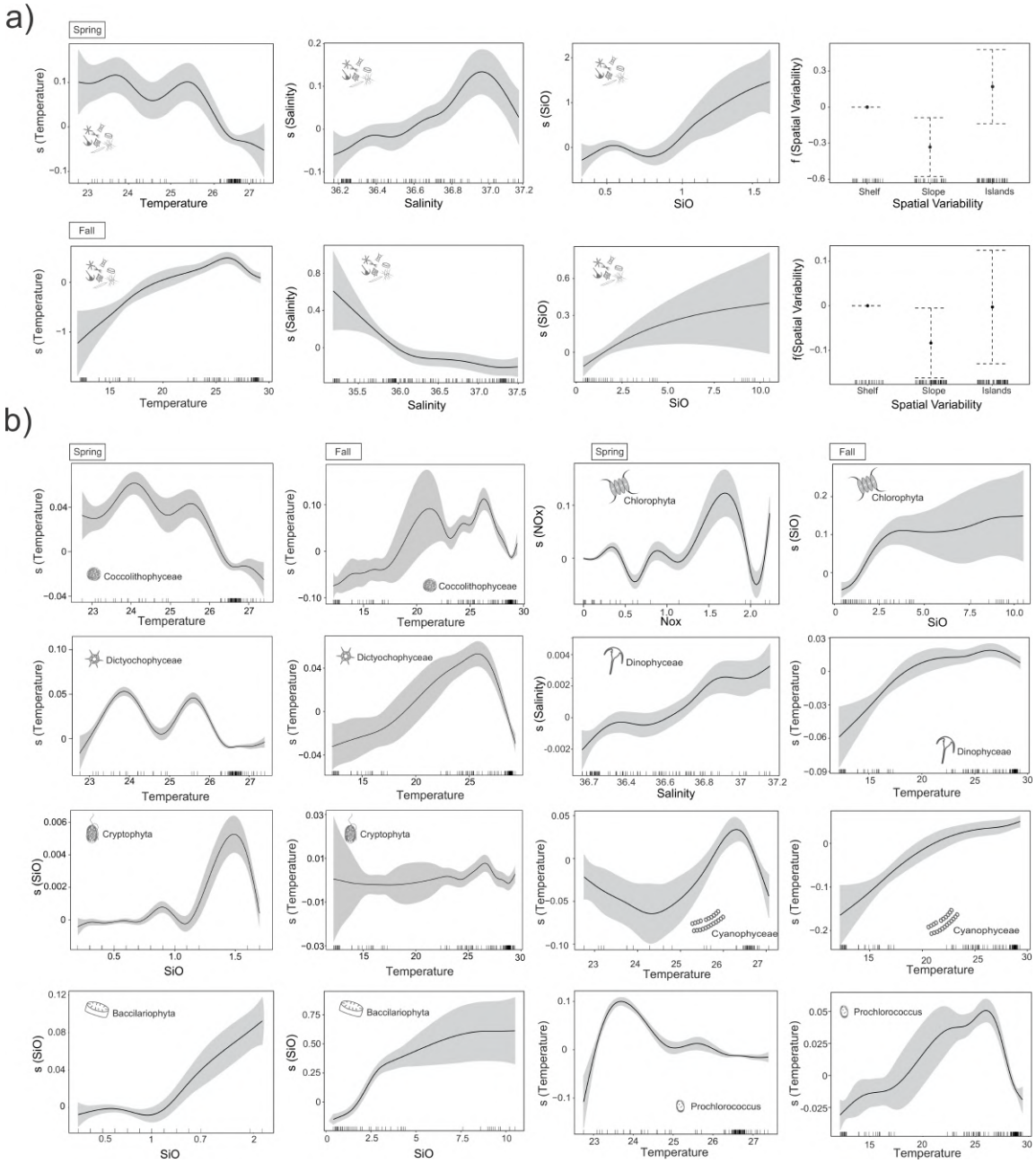

Figure 8 - Generalized Additive Models (GAMs) results describing the main factors that influenced the phytoplankton, for the entire community (a) and for the identified groups in both seasons (b). Solid lines represent smoothed mean relationships from GAM's and shaded areas are 95% confidence intervals.

Discussion

Our results pointed out a mosaic-like phytoplankton distribution mainly shaped by the thermohaline structure governing the SWTA, which during fall promoted a shallower depth of mixed layer and nutricline, thereby favoring a higher phytoplankton biomass. Along with such environmental configuration, and in spite of being enclosed in a tropical regime, the phytoplankton biomass displayed clear seasonal differences, although the contribution of pico- and nanophytoplankton to total phytoplankton biomass was similar regardless the season, suggesting an uncoupled dynamics between phytoplankton size structure and biomass standing stock.

Influence of physical oceanographic structures on nutrients and biomass distribution

The nutrients concentration showed a general increase with depth, excepting NO_2^-, which formed a primary nitrite maximum near the DCM in the continental slope (fall) and oceanic islands (spring and fall). Such feature has been previously reported from field records in oligotrophic stratified waters (Lomas and Lipschultz, 2006; Mackey et al., 2011), including in the SWTA (Paulo, 2016; Souza et al., 2013). The primary nitrite maximum may be related with both the excretion of NO_2^- by phytoplankton, i.e., due to incomplete nitrate reduction, and with the nitrification of bacteria (Al-Qutob et al. 2002; Meeder et al. 2012), although this should be confirmed with further field experiments. In addition, it is worth noticing the observed dominance of *Prochlorococcus* in the primary nitrite maximum. Indeed, this Genus has been formerly linked to the accumulation of nitrite in the water column due to the incomplete nitrate reduction of low light adapted ecotypes (Berube et al., 2016).

In fall, the depth of thermocline favored a shallower nutricline, thus increasing nutrients availability in upper layers. However, in spring, some stations near Fernando de Noronha Archipelago and Rocas Atoll displayed an increase of nutrients at DCM similar to the concentration recorded at 200 m depth. In addition, the interaction of oceanic islands and seamounts with the dynamics of water masses promotes an Island Mass Effect that foster productivity in the open ocean (Doty and Oguri 1956; Boden 1988; Hasegawa et al. 2008). In the SWTA, such island mass effect has been observed in both nutrients concentration and plankton productivity (Chaves et al., 2006; Macedo et al., 1988; Melo et al., 2012; Souza et al., 2013). This phenomenon exhibits a marked seasonality, mainly occurring in the western region of the oceanic islands between March and July, concurrently with the enhancement of the South Equatorial Current (Tchamabi et al., 2017; Travassos et al., 1997). Also, during spring strong

vertical shear, topographically induced, was observed between the surface South Equatorial Current and the subsurface South Equatorial Under Current, forming mesoscale meanders and a subsurface eddy-like structure, which likely contributed to the observed nutrients increase (Reference?). However, such feature was not reflected in phytoplankton biomass, probably due to a lag in phytoplankton response. An alternative explanation may be linked to a phosphate limitation during the upwelling event, as suggested by the observed Redfield Ratio of N:P=24:1.

In all other stations, the observed nutrients concentration is in line with previous reports in the area that showed similar seasonal patterns (Hazin, 2009; Souza et al., 2013). Likewise, surface nitrogen concentrations, under 1 μmol l^{-1}, were similar to values reported for other stratified oligotrophic waters (Islabão et al., 2017; Mena et al., 2019). However, compared with other regions it is worth noticing that the N:P ratio of about 3:1, was markedly lower than the ratio observed in the Tropical Eastern Pacific (7-10:1) and in the Mediterranean Sea (5:1) (Mena et al., 2019; Yasunaka et al., 2019). Overall, our records pointed out a nitrogen limitation with a N:P local ratio lower than the Redfield Ratio (16:1).

Nutrients availability in the SWTA are closely connected to seasonal patterns of dominant physical structures. For instance, the continental slope DCM showed lower nutrients concentration than the oceanic islands, regardless the season. The continental slope further showed the thickest thermocline and larger barrier layer, although the latter was not evenly distributed throughout the region (Assunção et al., 2020). Such physical barrier shape productivity of surface waters preventing upward transport from deep cold nutrient-rich waters. (Cabrera et al., 2011; Qu and Meyers, 2005). Nevertheless, over the continental slope, surface layers showed higher NO_3^- concentrations than around the islands, likely due to the activity of diazotrophic Cyanophyceae, which is the main group responsible for nitrogen fixation in the tropical ocean (LaRoche and Breitbarth, 2005) and was more abundant in this region.

Phytoplankton biomass was generally low, with maxima lower than 1.8 μg l^{-1}, although a seasonal increase was observed in surface layers of islands stations. Souza et al. (2013) also noticed an increase in chl-a concentration from late summer to fall around the oceanic islands, although with higher biomass (~ 0.47 μg l^{-1} in the mixed layer). In addition, these authors observed a higher nitrogen availability than the observed in this study, which also exhibited a similar low N:P ratio (5:1), thus suggesting a nitrogen limitation to primary production, as observed here. It is worth noticing that in fall higher nitrate concentrations in surface waters of the continental slope were uncoupled from phytoplankton biomass, which was almost three times lower than shelf and oceanic islands stations, possibly due to zooplankton grazing, as

suggested by maximum zooplankton abundance recorded in the continental slope (Figueiredo et al., 2020).

In this region, the variability of phytoplankton biomass has been previously ascribed to the seasonality of riverine nutrient inputs and upwelling events promoted by the Island Mass Effect and Taylor column effect (Ekau and Knoppers, 1999; Otsuka et al., 2018; Souza et al., 2013). Furthermore, TChl-a concentration in oligotrophic oceans is characterized by seasonal changes that follow the intensity of the mixed layer, thus increasing when the mixed layer is deeper and reaching the nutricline (Mignot et al., 2014; Signorini et al., 2015). In our study, we found a different pattern with a biomass increase in the shallower mixed layer and nutricline that was linked to the shallower thermocline. Our results suggest a pivotal role played by the vertical thermohaline structure in the seasonal variability of phytoplankton.

Phytoplankton community dynamics associated with environmental variability

Phytoplankton dynamics was shaped by water column vertical stratification, displaying marked changes in the distribution of phytoplankton, particularly between surface (Surface and Mixed Layer) and deep waters (DCM and 200 m depth), with a more diverse community in the latter. In surface layers, Cyanophyceae were dominant. This group is known to flourish in oligotrophic communities worldwide (Karlusich et al., 2020; Queiroz et al., 2015), contributing to ~25% of the ocean net primary productivity (Lange et al., 2018) and having an essential role in the oceanic nitrogen cycle, due to their ability to use atmospheric nitrogen. Indeed, this feature allows the group dominating low nitrogen-to-phosphorus environments, such as the SWTA (Vrede et al., 2009). With depth increase and the overall decrease of other Cyanophyceae, *Prochlorococcus* flourished. *Prochlorococcus* inhabits a wide range of depths from the surface waters to the base of the euphotic zone, due to their variable genetic ecotypes adapted to growth at high or low-light intensities (Moore et al., 1998). In communities dominated by the low-light adapted ecotypes, higher biomasses near the DCM are likely to be reached, as observed in oligotrophic oceans (Berube et al., 2016; Hawco et al., 2021). These ecotypes display a prochlorophyte chlorophyll-binding protein, which together with divinyl chlorophyll-*b* allows low-light adapted ecotypes a higher absorption of the blue light presented in deeper layers (Islabão et al., 2017). Although we did not distinguish ecotypes, *Prochlorococcus* biomass increased near the DCM, and the known relation with the nitrite primary maximum formation may indicate the dominance of low-light adapted *Prochlorococcus* in the SWTA phytoplankton community.

The observed higher biomass of Chlorophyceae over the shelf, near the surface, and the biomass increase during fall may be indicative of riverine discharges, as this group is mostly composed by freshwater species (Mishra et al., 2009). Similarly, Bacillariophyceae were also abundant near the shelf, favored by the higher silicate concentrations. This trend was evident in the microphytoplankton pigments, that despite displaying low biomass, were dominated by Bacillariophyceae. In oligotrophic regions, diatoms are commonly more abundant in the inner shelf than in oceanic regions, due to higher silicate availability and a weaker thermocline stratification (Falkowski and Oliver, 2007; Mishra et al., 2020). On the other hand, Dinophyceae relative biomass was low at both seasons, with a slight increase in fall. This is likely underestimated by our pigment analysis, as this group is composed by a variety of trophic strategies, i.e., autotrophic, mixotrophic and heterotrophic, that may represent ca. 50% of the dinoflagellate's community (Hansen, 2011; Jeong et al., 2010; Sherr and Sherr, 2007). In addition, other dinoflagellates can be characterized by different pigments, such as fucoxanthin or chlorophyll-*b*, which suggest a possible underestimation of this groups (Zapata et al., 2012).

Prymnesiophyceae and Dictyochophyceae were more frequent in the light-limited and nutrient rich deep layers. Prymnesiophyceae show low light and nitrate saturation of growth (Araujo et al., 2017), thus, this group can thrive in regions constraining the growth of other groups such as Bacillariophyceae and Chlorophyceae, as seem to be the case here (Araujo et al., 2017; Gregg and Casey, 2007). On the other hand, Dictyochophyceae are widespread components of the microphytoplankton in the size range of 20-100 μm (Lemonnier et al., 2016), especially in subtropical and temperate marine regions (Andersen, 2004) . In the HPLC analysis, this group is represented by the large silicoflagellate *Dictyocha* sp., and small picoflagellates and picoeukaryotes. Therefore, due to the dominance of the pico- and nanophytoplankton in the SWTA phytoplankton community, Dictyochophyceae is likely composed by small cells, although more specific analyses are needed to unveil the composition of this group.

Size structure and trophic status

Cell size is an ecological trait that affect all aspects of phytoplankton ecology, such as diversity, production, competition, and biomass transference to the higher trophic levels (Barton et al., 2013; Marañón, 2015). We observed a dominance of pico- and nanophytoplankton in both seasons, in agreement with reported observations in many oligotrophic regions (Dai et al., 2020; Mena et al., 2019; Pérez et al., 2005). These small sized communities are usually associated

with recycling trophic webs. The *Fp* index is derived from the assumption that global new production is mainly related to diatoms and dinoflagellate growth, although dinoflagellates growth is less relevant (Claustre, 1994). This qualitative tool allows comparing trophic status of some oceanographic regimes and inferring about the size dynamics of a community. In the southernmost area of the tropical Atlantic, a preeminence of recycled productivity was previously reported, with the new production representing between 16 and 30% of the total phytoplankton production (Metzler et al., 1997). Our results pointed out a predominance of recycled production, with a conspicuous coast-offshore gradient evidenced by the observed higher *Fp* in the shelf, which doubled that in other regions, likely due to the influence of the riverine runoff on the coast productivity (Ekau and Knoppers, 1999; Otsuka et al., 2018). In addition, a significant seasonal increase in the new production was observed in oceanic islands, although, the values remained low and did not surpass 0.09, suggesting a dominance of small cells also in discrete productivity peaks.

The overall increase in nutrients concentration usually results in an enhancement of large phytoplankton cells and a change in the trophic balance to a more classic food web instead of a microbial one (Chisholm, 1992; Falkowski and Oliver, 2007; Landry, 2002; Vargas et al., 2007). However, in oligotrophic regions of the Atlantic Ocean, the dominance of small cells does not necessarily couples to lower relative biomass, since small cells dominated over most of the stations and seasons, regardless of the biomass standing stock. Indeed, even during enhanced production and biomass, the dominance of pico- and nanophytoplankton remains (Marañón et al., 2003, 2000). Our observations support the hypothesis of the dominance of smaller cells (<20 μm) in tropical environments, with a change in the trophic status only in a few shelf stations that showed high *Fp* (<0.5). The pico- and nanophytoplankton predominance is probably linked to the low N:P (<5), which appears insufficient to trigger the growth of larger cells. Nitrogen has been previously observed as a limiting nutrient for the phytoplankton growth in the SWTA (Hazin, 2009), with a N:P ratio in the euphotic zone lower than 5:1 throughout the year.

Large phytoplankton cells (i.e., diatoms and dinoflagellates) play an important role in carbon sequestration, due to their higher sinking rate in contrast to smaller phytoplankton cells (Guidi et al., 2016). In the oligotrophic ocean however, their role in the carbon pump is partially replaced by small phytoplankton cells, which may form colloids and aggregates in the water column enhancing their rates of sedimentation. In a global change scenario, the expansion of oligotrophic regions and enhanced stratification are expected, along with a predominance of microbial food webs. Understanding the role of such small phytoplankton groups in the carbon

pump is therefore crucial to assess not only changes in biogeochemical cycling, but also changes in food quality for pelagic food webs.

Conclusions

In the SWTA phytoplankton community, an uncoupling between the biomass increase and size was observed, with the phytoplankton being dominated by the small celled community and a recycled production (*Fp*) during the entire study time. Here we hypothesize that this may be caused by a nitrogen limitation that constrain population growth of larger phytoplankton taxa. In the SWTA this was the first study to analyze the contribution of the phytoplankton different size classes offshore. The domination of the pico- and nanophytoplankton presented here, highlights their importance to the global oligotrophic oceans. In the scenario of global ocean changes, in which water column stratification is expected to intensify, the abundance of this small phytoplankton and the recycling production will probably rise. Thus, the understanding of their distribution and role in the biogeochemical cycles is of pivotal importance to forecast the health of the pelagic food webs in the near future.

Acknowledgements

We wish to express our thanks to the Coordenação de Aperfeiçoamento de Pessoal de Nível Superior – Brasil (CAPES) for the concession of the first author's scholarship, and the IMAGO lab who realized the HPLC and nutrients analysis. We acknowledge the French oceanographic fleet for funding the survey ABRACOS and the officers, crew and scientific team of the R/V Antea for their contribution to the success of the operations. This work is a contribution to the LMI TAPIOCA (www.tapioca.ird.fr), CAPES/COFECUB program (88881.142689/2017-01), the European Union's Horizon 2020 projects PADDLE (grant agreement No. 73427) and TRIATLAS (grant agreement No. 817578).

3 NUTRITIONAL ENVIRONMENT CONTROL ON THE SPATIAL DISTRIBUTION AND STRUCTURE OF PLANKTON MICROBIAL BIOMASS IN AN OLIGOTROPHIC SEA

Submitted – Hydrobiologia

Abstract

In oligotrophic oceans, trophic transfer at the base of pelagic food webs is driven by shifts in biomass ratios of plankton microbial groups, which determine dominant nutrition modes, i.e., autotrophy and heterotrophy. Understanding how the physical environment impacts transient spatial patterns of these communities is essential to quantify productivity of plankton food webs. Using data from a coast-offshore field expedition in the Southwestern Tropical Atlantic, we assessed the influence of nutrient limitation and contrasting hydrological settings on spatial patterns and biomass ratios of pico- and nanoplankton. The results showed an overall nitrogen-limited nutritional environment that lessen autotrophic growth while favoring the dominance of heterotrophic bacteria biomass. Offshore, this configuration is however altered in the deep chlorophyll maximum due to an enhanced nutrient availability promoted by a shallower nutricline, which favors an increase picoeukaryotes biomass. Autotrophic cells showed different distributions over the coast-offshore transect. *Synechococcus* and pigmented nanoflagellates had higher biomass on the shelf, while *Prochlorococcus* dominated the entire region and picoeukaryotes had higher biomass offshore. Overall, our results pinpoint the importance of heterotrophic biomass in the plankton microbial community, providing novel clues for understanding the carbon transport in oligotrophic marine ecosystems.

Key Words: Trophic pathways, heterotrophic bacteria, seamounts, oligotrophic ocean, microbial food webs.

Introduction

In the oligotrophic ocean, local productivity and microbial food web dynamics are shaped by the interrelationships between pico- and nanoplankton and the predominance of their nutritional modes, i.e., autotrophy, heterotrophy, and mixotrophy (Hartmann et al., 2012; Duarte et al., 2013). These small plankton groups are ecologically predominant in phosphorus- and nitrogen-limited oligotrophic regions (Flombaum et al., 2013; Šantić et al., 2021), where the amount of organic matter decomposed by heterotrophic bacteria account for 20-60% of the total primary production, and by times may surpass the phytoplankton biomass (Fuhrman, 1992; del Giorgio et al., 1996; Christaki et al., 1999). In these ecosystems, low nutrient availability promotes alternative trophic strategies among plankton microbial groups, with a prominent role of heterotrophy and mixotrophy. Indeed, these nutritional modes may increase carbon fixation, the transfer of organic matter to higher trophic levels, and nutrient retention in ecosystems (Edwards, 2019; Livanou et al., 2019). Hence, the architecture of microbial food webs shapes not only the number of trophic levels (Loick-Wilde et al., 2019), but also the available organic matter for mesozooplankton and larger consumers (Fenchel, 1988; Karus et al., 2014; Traboni et al., 2021), and the overall productivity of plankton microbial groups.

The contribution of plankton microbial groups to carbon export in oligotrophic systems is likely higher than previously estimated, as shown by recent reports (Guidi et al., 2016; Lomas et al., 2022). In line with this, numerical forecasts predict an increase of small-size plankton biomass, thus suggesting a prominent role of these groups in plankton food webs and carbon transport under future warming scenarios (Flombaum et al., 2020). Despite the central role of plankton microbial groups in marine ecosystems, most of the available literature is focused on temperate regions (Buitenhuis et al., 2012a, 2012b; Visintini et al., 2021), while less efforts have been made in oligotrophic regions from the Global South, such as the Southwestern Tropical Atlantic (SWTA). Therefore, there is a critical need to understand the environmental conditions that control the coexistence of microbial functional groups and nutritional modes that shape trophic transfer. This will provide essential data for modeling and eventually forecasting the responses of microbial plankton communities and the efficiency of trophic transfer in oligotrophic pelagic food webs.

The SWTA is an oligotrophic western boundary system under the influence of the North Brazil Undercurrent – North Brazil Current system (Stramma & England, 1999; Assunção et al., 2020; Dossa et al., 2021). The vertical structure of the SWTA is characterized by different regions portrayed by specific thermocline structures and stratification strength (Araujo et al.,

2011; Assunção et al., 2020). This area further has a large chain of seamounts that modify regional dynamics and water column stability, influencing the depth of the nutricline (Tchamabi et al., 2017; Costa da Silva et al., 2021). The complex hydrogeographic dynamics favour a shallower nutricline offshore that slightly enhances nutrient concentration during austral autumn. The SWTA, however, shows a nitrogen-limited environment where phytoplankton biomass and size structure are dominated by pico- and nanophytoplankton that contribute up to 80% of the total phytoplankton biomass (Farias et al., 2022). Such configuration is expected to shift metabolic pathways towards a more heterotrophic ecosystem, as heterotrophic bacteria might outcompete autotrophic cells in nutrient-poor regions (Calfee et al., 2022; Rahav et al., 2022). These dynamics may change in the coast-offshore gradient shaped by the depth of nutricline.

Deciphering how this environmental configuration structure spatial patterns of plankton microbes and their coexistence is therefore a necessary step to understand trophic transfer and productivity in oligotrophic systems. In this context, we test the hypothesis that changes in thermohaline structure (i.e., stratification and nutricline depth) shift biomass ratios of plankton microbial groups from the dominance of autotrophic to heterotrophic biomass in the coast-offshore gradient. We further examine spatial patterns of pico- and nanoplankton biomass ratios and depict environmental and biotic drivers of their distribution.

Materials and methods

Study area

This study was conducted along the Northeast Brazilian continental shelf and slope between 5ºS and 9ºS, and around oceanic seamounts and islands of the Fernando de Noronha Chain, including the Fernando de Noronha Archipelago itself and the Rocas Atoll up to 3ºS, 38ºW (Fig 1a, b). The region has a narrow continental shelf, with an average depth of 40 m, not exceeding 40 km with an average shelf-break of 80 meters, and a continental slope between 1600 and 3600 m (Knoppers et al., 1999). Coastal waters are governed by a western boundary current system, formed by tropical oligotrophic waters from the North Brazilian undercurrent and the North Brazilian current (Fig. 1c). This current system is further characterized by low thermal stratification and the presence of a frequent and thick barrier layer, which represents the difference between the mixed layer calculated by the temperature and the mixed layer calculated by the water density, and represents an additional barrier to the well-mixed upper

layer and the thermocline (Assunção et al., 2020; Dossa et al., 2021). Offshore, the geomorphology is characterized by a chain of seamounts along the 4ºS latitude, the Fernando de Noronha ridge, that extends for almost 500 km and includes the Rocas Atoll and Fernando de Noronha Island (Kikuchi & Schobbenhaus, 2002). The Fernando de Noronha ridge represents an enhancement in the overall SWTA productivity, due to its topography-induced island wakes (Costa da Silva et al., 2021), serving as a region of feeding and reproduction for several marine species, including sea turtles, dolphins, and several shark and stingray species (Serafini et al., 2010; Salvetat et al., 2022). This area is further influenced by the central and southern branches of the South Equatorial current and the South Equatorial Under current (Fig. 1c), which form the South Equatorial Current System, characterized by a deeper mixed layer, a sharp thermocline, strong static stability (Supplementary Figure 1), and weak surface current (Assunção et al., 2020).

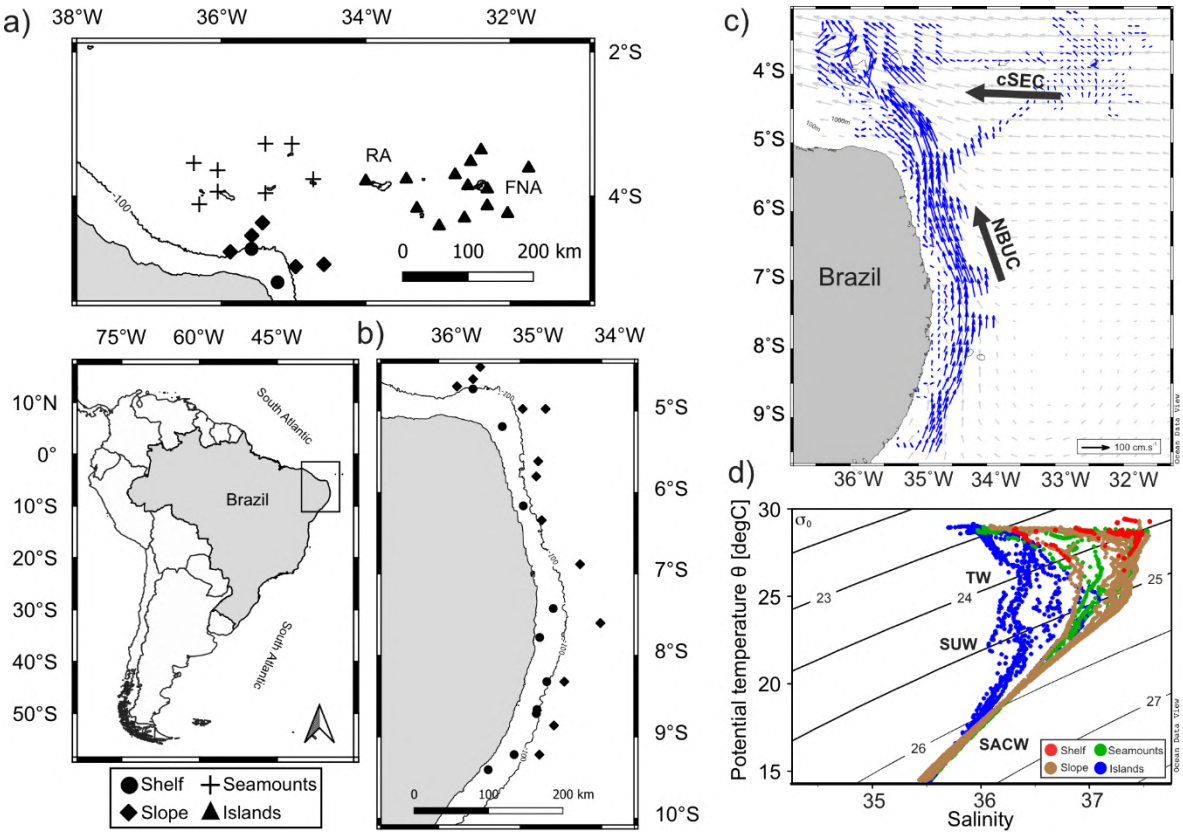

Fig. 1 Description of the study area and sampling stations surveyed during austral autumn in the southwestern tropical Atlantic. RA: Rocas Atoll; FNA: Fernando de Noronha Archipelago; a) Oceanic stations; b) Shelf and Slope stations; c) Surface currents vectors of ADCP data and indicators of the predominant current in the area; NBUC: North Brazil Undercurrent; cSEC: Central branch of the South Equatorial Current; d) Temperature-salinity (T-S) diagram of water masses for the study area during austral autumn, isolines indicate potential density; TW: Tropical Water SUW: Subtropical Under Water; SACW: South Atlantic Central Water

Field Collection

Samples were collected during the Acoustics along the BRAzilian COaSt 2 oceanographic cruise (ABRACOS 2 - Bertrand, 2017), carried out on board the French R/V ANTEA, between April 9th and May 9th of 2017. The ABRACOS 2 comprehended 42 stations encompassing the Fernando de Noronha ridge, including the chain of seamounts (8) and islands (13) (Fig. 1a), the SWTA shelf (11) and continental slope (13) (Fig. 1b) (Supplementary Table 1). At all stations, vertical profiles of temperature (◦C) and salinity were obtained with a CTD profiler Seabird SBE911+. The CTD data were used to calculate physical variables that describe the water column, such as mixed layer depth, barrier layer thickness, and the Brunt–Väisälä frequency (N2). Brunt–Väisälä frequency was calculated according to the following formula: $N^2 = \frac{g}{\theta_{va}} \frac{\partial \theta_{va}}{\partial z}$, where g = 9.8 m s^{-1} is gravitational acceleration, θυa is the ambient virtual potential temperature, and ∂θυa/∂z is the vertical gradient of the ambient virtual potential temperature. Barrier layer thickness was defined as the difference between mixed layer depth (MLD) calculated from temperature minus the mixed layer depth calculated using a density. A detailed description of the physical structure is given in Assunção et al. (2020).

Water sampling for picoplankton and nanophytoplankton was carried out using a rosette at three depths defined by the CTD profiles: mixed layer, deep chlorophyll maximum, and 200 m. In shallow stations, where no peak of fluorescence was observed, deep chlorophyll maximum and 200 m samples were replaced by a shallow bottom sampling at ~10 m above the bottom. For each station and sampled depth, 1.6 mL of water was fixed with 80 µL of formalin with a final concentration of 2% in cryogenic tubes, with one sample per station. Samples were rapidly frozen in liquid nitrogen and then kept in an ultrafreezer (-80ºC) for subsequent laboratory analysis. Details of sampling stations and metadata (date, time, depth, and variables measures) are shown in Supplementary Table 1.

Water samples for nutrients concentration estimation (NOx [NO_{2-} + NO_3^-], PO_4^{3-} and SiO_4^{4-}) were collected in 30 ml falcon tubes, pasteurized (heated at 80°C for 2.5 hours in an oven), and frozen to ensure stability until the laboratory analysis. Nutrient analyses were achieved using classical colorimetric methods (Grasshoff et al., 1983), between two and three sampling depths were realized in the shallow stations (<50m) and between 5 and 6 sampling depths were realized in the deep stations (>50m). For a complete description of the nutrient data, see Farias et al. (2022).

Dominant surface currents and water masses

Surface dominant currents (Fig. 1c) were recorded with an 'Ocean Surveyor' ship-mounted acoustic Doppler current profiler (SADCP) operating at a frequency of 75 kHz with a depth range of 15–700 m. SADCP data were processed and edited using the Common Ocean Data Access System (CODAS) *software*. Relative velocities were rotated from the transducer to the Earth reference frame using the ship gyrocompass. The global positioning system (GPS) was used to retrieve the absolute current velocities. The orientation of the transducer relative to the gyroscopic compass and the amplitude correction factor for the SADCP were determined by standard calibration procedures. Finally, velocity profiles were averaged hourly, providing profiles in the 19–600 m range. SADCP data located over the shelf (bathymetry shallower than 70 m) however, were often affected by spurious reflections on the bottom, so the data coverage was only partial in such shallow areas. To describe current patterns, data from the upper layer (0–200 m depth) were integrated every 0.1 square degree. SADCP data showed two main surface currents. Offshore, flowed the central branch of the South Equatorial Current, an offshore current flowing westward. Along the coast and over the slope flowed the North Brazilian Under Current, an alongshore current flowing north/northeastward.

In the sampled depth range, with exception of the shelf, characterized by Tropical Water only, all sampled regions (seamounts, slope, and islands) shared the same water masses (Fig. 1d). At the surface the warm Tropical Water dominates, being characterized by temperatures >25 ◦C and σθ between 23 and 24.5 kg m^{-3}. Below, in the upper part of the thermocline, lies the Subtropical Underwater formed by the excess of evaporation over precipitation in the subtropics. This current is advected westward within the subtropical gyre and is characterized by salinity higher than 36.5 and densities slightly below 25 kg m^{-3} (Dossa et al., 2021). Finally, in the subsurface, in the lower part and below the thermocline, the South Atlantic Central Water is characterized by σθ up to 27kg m^{-3}.

Flow Cytometry

The abundance of picoplankton and nanophytoplankton was obtained using a FACSCalibur flow cytometer (Becton Dickinson) equipped with a HeNe air-cooled laser (633 nm, 20 mW), following the protocol of (Marie et al., 1997). Samples were analyzed with a mixture of fluorescent beads ('Fluorebrite' YG, Polysciences) of various nominal sizes. Autotrophic cells excited at 633 nm were detected and enumerated according to their forward-angle light scatter (FALS) and right-angle light scatter (RALS) properties, and their orange (576/26 nm) and red fluorescence (660/20 nm and 675/20 nm) from phycoerythrin, phycocyanin and chlorophyll

pigments, respectively. Fluorescent beads (1-2 μm for picophytoplankton and 3, 6, and 10 μm for nanophytoplankton) were added to each sample. True count beads (Becton Dickinson) were added to determine the volume analyzed. This method discriminates various autotrophic and mixotrophic groups such as picoeukaryotes, picocyanobacteria (*Prochlorococcus* and *Synechococcus*), and pigmented nanoflagellates. For heterotrophic bacteria, cell DNA was stained with SYBRGreen I and counted under the emission of green fluorescence, a description of the abundance data can be found in Supplementary Material I. After the quantification of abundances, the biomass of picoplankton and nanophytoplankton was obtained from conversion factors reported in the literature as follows: *Prochlorococcus* (29 fgC $cell^{-1}$), *Synechococcus* (100 fgC $cell^{-1}$), picoeukaryotes (1500 fgC $cell^{-1}$) (Zubkov et al., 2000), pigmented nanoflagellates (3140 fgC $cell^{-1}$) (Pelegrí et al., 1999) and heterotrophic bacteria (12 fgC $cell^{-1}$) (Fukuda et al., 1998).

Data analysis

Characterization of the nutritional environment

The picoplankton and nanophytoplankton biomass and community structure are shaped by the nutritional environment they inhabit (i.e., temperature and nutrient availability). To assess the nutritional environment, first, we characterized dominant water masses according to their temperature, salinity, and nutrients. To do so, we applied a non-parametric Multi-Dimensional Scaling (MDS) using the R-package *vegan* (Dixon, 2003) (Fig. 2a). The technique was based on a similarity matrix using the Euclidian distance index (Clarke & Warwick, 1994). In addition, we computed the relative concentration of nutrients to compare nutrient ratios between water masses with the Redfield ratio (Redfield, 1963) in order to identify areas of nutrient limitation (Fig. 2b).

Structural patterns of the picoplankton and nanophytoplankton communities

Picoplankton and nanophytoplankton biomass data were compared among water masses (Tropical Water, Subtropical Underwater, and South Atlantic Central Water), depth (mixed layer, shallow bottom, deep chlorophyll maximum, and 200 m), and region (shelf, slope, seamounts, and islands) using parametric (one-way ANOVA) or non-parametric (Kruskal-

Wallis) analyses of variance, and between diel periods (day and night) using t-test or Mann-Whitney, depending on the normality of the data.

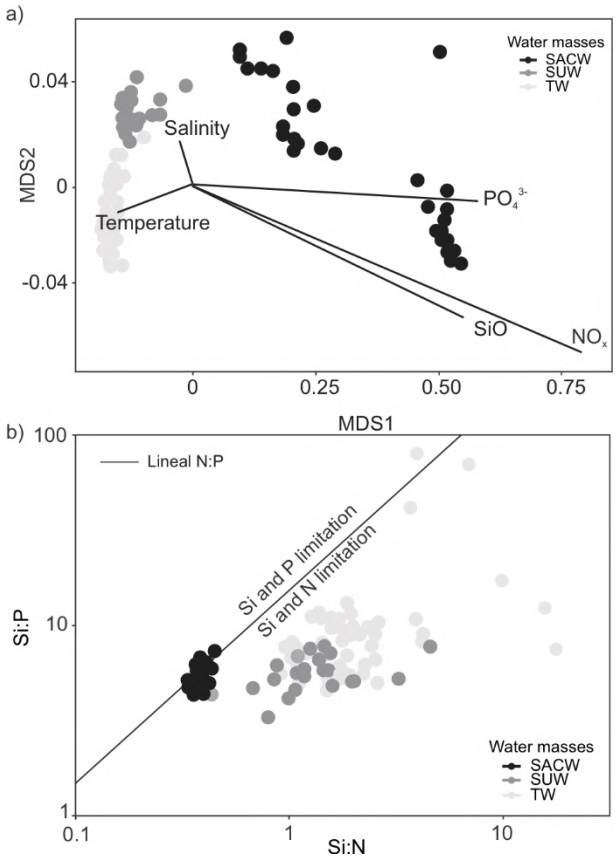

Fig. 2 Relationships between water masses and environmental variables. a) Water masses segregation by MDS showing variables that contributed significantly to their ordination; b) Nutrient ratios of total Si:N vs. Si:P for each water mass. The solid line indicates the ideal N:P in the Redfield Ratio. Values on the right side of the line indicate N and Si limitation, while values on the left side of the line indicate P and Si limitation. SACW: South Atlantic Central Water; SUW: Subtropical Under Water; TW: Tropical Water

Factors controlling the picoplankton and nanophytoplankton distribution

To identify dominant drivers of the spatial distribution of picoplankton and nanophytoplankton biomass, we used Random Forest regression models, a method based on non-parametric regressions. The method randomly splits the dataset and fits regression trees that are confronted with the remaining data. The process is subsequently repeated with every bootstrapped dataset and the resultant trees are combined into a final model. The recursive split of trees at threshold predictor values allows handling non-linear interactions among predictors and the response variable and as well as the identification of relationships with categorical variables (i.e., water masses and region). We used the function *rfsrc* from the R-package *randomForestSRC* (Ishwaran et al., 2022) to set the models with each plankton group as

response variables (heterotrophic bacteria, pigmented nanoflagellates, *Prochlorococcus*, *Synechococcus*, picoeukaryotes), and to identify the hierarchy of their predictors (Feld et al., 2016).

Predictors to be fitted in Random Forest regression trees were selected through correlation plots (Supplementary Figure 2). Only variables showing a correlation >.76 were retained for the analysis. In addition, variables showing multicollinearity were discarded from the analysis (layers and nutrients). Accordingly, predictors were set as water mass, region, and plankton groups other than the one selected as a response variable in each model. Top predictor variables were selected by exploring variable maximal subtree (Ishwaran et al., 2022). We used the *max.subtree* function to select the top predictors for each plankton group. Finally, to visualize the hierarchy of top predictors for each variable we used a circos plot with the R package *circlize* (Gu et al., 2014). circos ideograms are tools for circular layout visualization of positional relationships in datasets (Krzywinski et al., 2009). The building of circos diagrams first converts the table of original data, i.e. the correlation coefficient between two variables, in a polar coordinate system that is mapped. Here, circos plots are shown as circular diagrams where coefficient's weight of each predictor was defined as sectors of the circle in which the width of each sector denotes the hierarchical importance of predictors regarding spatial patterns of picoplankton and nanophytoplankton taxa biomass. The partial response of the selected predictors was plotted using the function *gg_partial*.

The picoplankton and nanophytoplankton biomass proportion between autotrophy (hereafter including also mixotrophic taxa) and heterotrophy can change with horizontal and vertical gradients of stratification and nutrient availability (Susini-Ribeiro, 1999; Gérikas Ribeiro et al., 2016). To identify variables responsible for changes in autotrophic and heterotrophic biomass we used principal component analysis (PCA). The PCA is a tool for identifying the main axes of variance within a dataset (Abdi & Williams, 2010). The matrix used was composed of standardized nutrient (NOx, PO_4^{3-} and SiO_4^{4-}) and physical (mixed layer depth, barrier layer thickness, and stratification [N^2]) data, with the biological data (autotrophic and heterotrophic biomass) as supplementary variables. PCA analysis was performed using the R with the R-packages "*FactoMineR*" (Husson et al., 2016) and "*factoextra*" (Kassambara & Mundt, 2017).

Results

Hydrographic conditions

The water column showed marked stratification and nutrient ratios (Supplementary Figures 1 and 3). Additionally, the shallowing of the South Atlantic Central Water close to the oceanic islands and seamounts promoted stronger stratification, lower temperature, salinity, and higher nutrient concentrations in the deep-sampled depths (deep chlorophyll maximum and 200 m) (Supplementary Figure 1). Nutrient concentrations were overall low on the euphotic layer, the surface layers displayed an average NOX of 0.32 ± 0.17 µmol L^{-1} in the shelf and slope, and offshore around 0.2 ± 0.10 µmol L^{-1}, contrasting the 0.7 ± 1 on the DCM offshore and over 10 µmol L^{-1} below the euphotic zone. PO_4^{3-} and SiO followed similar patterns with averages of 0.12 ± 0.04 and 0.87 ± 0.26 µmol L^{-1} respectively on the shelf and slope surface, versus 0.09 ± 0.05 and 0.89 ± 0.13 µmol L^{-1} respectively offshore. On the DCM PO_4^{3-} and SiO had an average of 0.24 ± 0.13 and 1.26 ± 0.45 respectively on the DCM, surpassing an average of 1 and 4 µmol l^{-1} respectively below the euphotic layer. Temperature and salinity profiles allowed identifying three main water masses: Tropical Water, Subtropical Underwater, and South Atlantic Central Water (Fig. 1d). Tropical Water and Subtropical Underwater, had a high association with temperature and salinity in the MDS, respectively (Fig. 2a). Tropical Water was characterized by the highest temperature (27-28°C), while Subtropical Underwater showed the highest salinity (36.9). Both water masses evidenced low nutrient concentration, with Si and N limitations (Fig. 2b). In contrast, South Atlantic Central Water displayed the highest nutrient content and the lowest temperature (13.8°C) and salinity (35.4).

Autotrophic and heterotrophic picoplankton and nanophytoplankton biomass

Biomass of autotrophic cells ranged from undetected at 200 m depth to 93.83 µgC L^{-1} in the mixed layer, while heterotrophic bacteria biomass ranged from 1.38 µgC L^{-1} at 200 m depth to 50.82 µgC L^{-1} in the mixed layer (Tropical Water). Pigmented nanoflagellates displayed higher biomass over the shelf shallow bottom (Fig. 3a), with an average of 2.41 µgC L^{-1} (Table 1). Picoeukaryotes were associated with the DCM, especially around seamounts and islands (Fig 3b; 22.85 and 17.12 µgC L^{-1}, respectively). *Prochlorococcus* showed higher biomass at the seamounts mixed layer (5.33 µgC L^{-1}; Fig 3c), whereas *Synechococcus* displayed a different pattern, peaking over the shelf shallow bottom (6.37 µgC L^{-1}) and considerably decreasing offshore, with a higher average on the slope mixed layer (1.94 µgC L^{-1}; Fig 3d). The average total biomass showed higher values at the deep chlorophyll maximum due to the accumulation of Picoeukaryotes cells, and over the seamounts in all depths (41.93, 71.56, and

44.95 µgC L^{-1} on the seamounts mixed layer, deep chlorophyll maximum, and 200 m depth respectively).

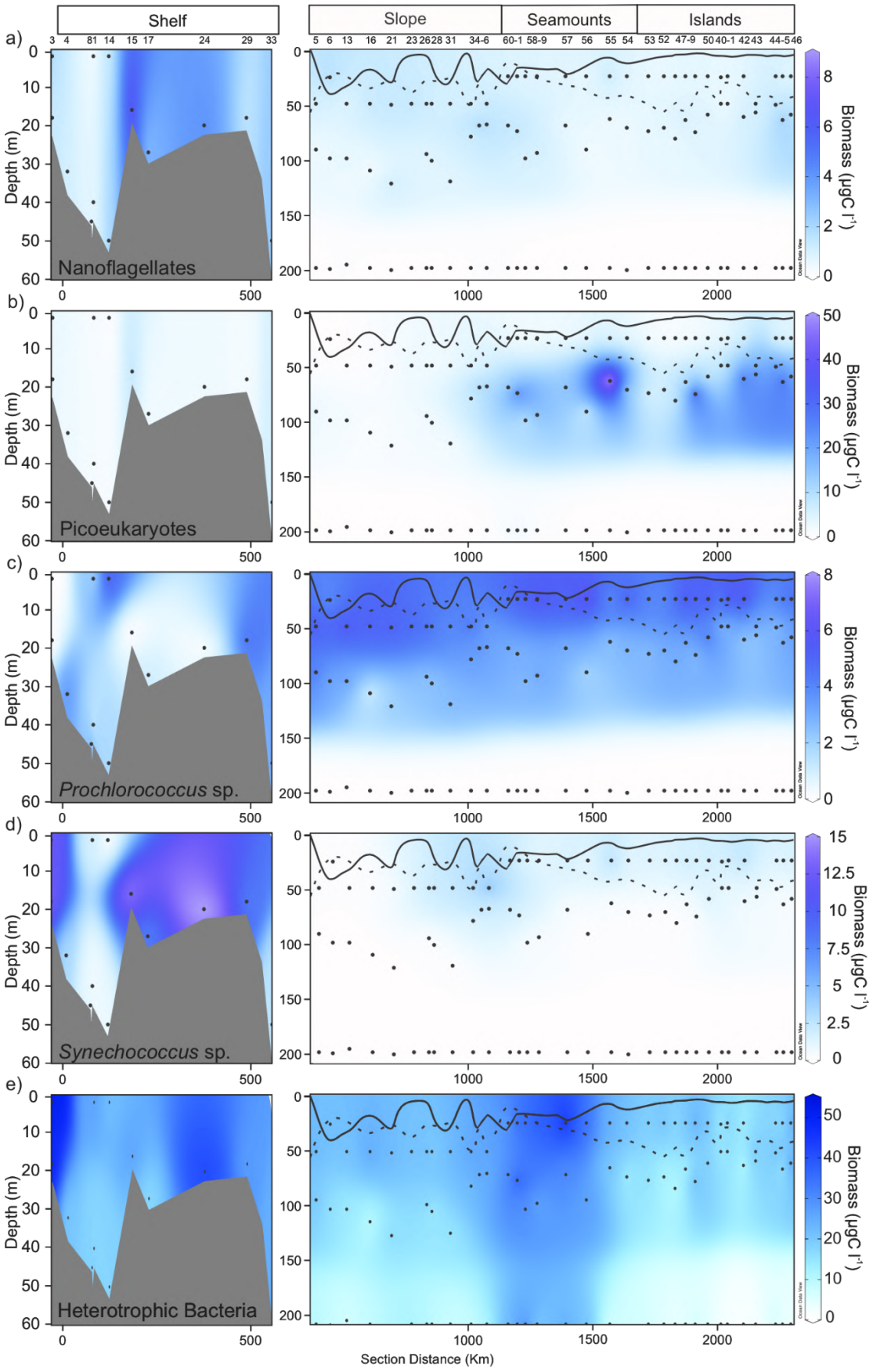

Fig. 3 Vertical profiles of biomass (µg C L^{-1}) of pigmented nanoflagellates (a), picoeukaryotes (b), *Prochlorococcus* sp. (c), *Synechococcus* sp. (d) and HB (e) in the SWTA. The bar over biomass profiles indicates the different regions, station numbers are indicated over the plots, black dots in the vertical profiles represent the sampling depths. The dashed line indicates the ML depth and the whole line indicates BLT. Notice the different depths and scales between plots. Biomass profiles in the shelf section represent a south-north transect, while the offshore section is a west-east transect

Table 1. Average biomass (AB, µg C L^{-1}) of autotrophic groups and heterotrophic bacteria (HB) in the SWTA. The sum of all autotrophic groups biomass is also shown (AB). S: Shelf; SL: Slope; I: Islands; SM: Seamounts; UN: Undetected. PNF: Pigmented nanoflagellates; PEUK: picoeucaryotes.

		PNF	PEUK	*Prochlorococcus* sp.	*Synechococcus* sp.	AB	HB	Total Biomass
Mixed Layer	S	1.31	2.14	2.82	4.45	10.72	30.88	41.6
	SL	1.08	1.09	4.61	1.94	8.72	23.07	31.79
	SM	0.85	1.19	5.33	1.73	9.1	32.83	41.93
	I	0.71	1.6	4.94	1.91	9.16	19.31	28.47
Shallow Bottom	S	2.41	3.26	1.93	6.37	13.97	25.82	39.79
Deep Chlorophyl Maximum	SL	0.99	5.7	2.85	0.41	9.95	17.07	27.02
	SM	0.81	22.85	2.51	0.44	26.61	26.97	53.58
	I	0.98	17.12	2.34	0.33	20.77	14.98	35.75
200 m	SL	0.06	0.05	0.02	>0.01	0.13	8.29	8.43
	SM	0.1	0.71	0.44	0.19	1.44	19.6	21.03
	I	0.02	0.17	0.01	>0.01	0.2	4.17	4.38

Community composition

Overall, the community composition did not show significative diel changes (Supplementary Figure 4). We found however exceptions in the distribution of *Synechococcus* and *Prochlorococcus*, which in the mixed layer of seamounts region were significantly more abundant during the night and day, respectively (*t-test,* $p < 0.05$; *t-test*, $p = 0.01$, respectively), whereas *Synechococcus* and heterotrophic bacteria appeared more abundant around the Islands at 200 m day samples (*MW*, $p < 0.05$; *MW*, $p = 0.01$; respectively) (Supplementary Figure 4).

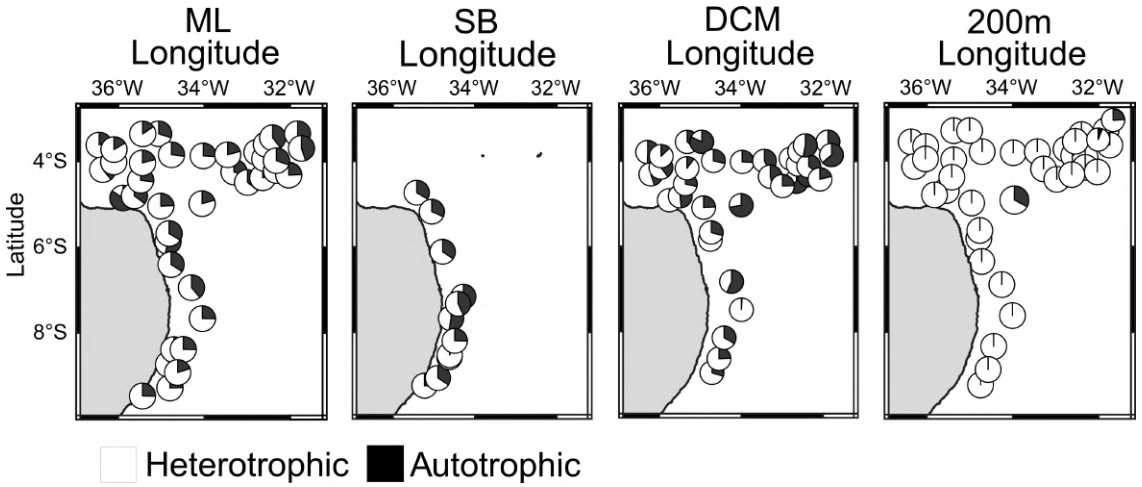

Fig. 4 Proportions between autotrophic and heterotrophic biomass of picoplankton and nanophytoplankton in the SWTA; ML: Mixed Layer; SB: Shallow Bottom; DCM: Deep Chlorophyll Maximum

The autotrophic community showed a clear coast-offshore pattern, with *Synechococcus* showing higher biomass in shelf stations, representing up to 98% of the community (Supplementary Figure 5a, b), although *Prochlorococcus* usually displayed higher biomass, especially offshore (Supplementary Figure 5a, b). Although picoeukaryotes and pigmented nanoflagellates represented a low portion of the community abundance in all regions (Supplementary Material 1), they have a prominent contribution to total biomass (Supplementary Figure 5b), especially picoeukaryotes which contributet with up to 90% of the total autotrophic carbon biomass.

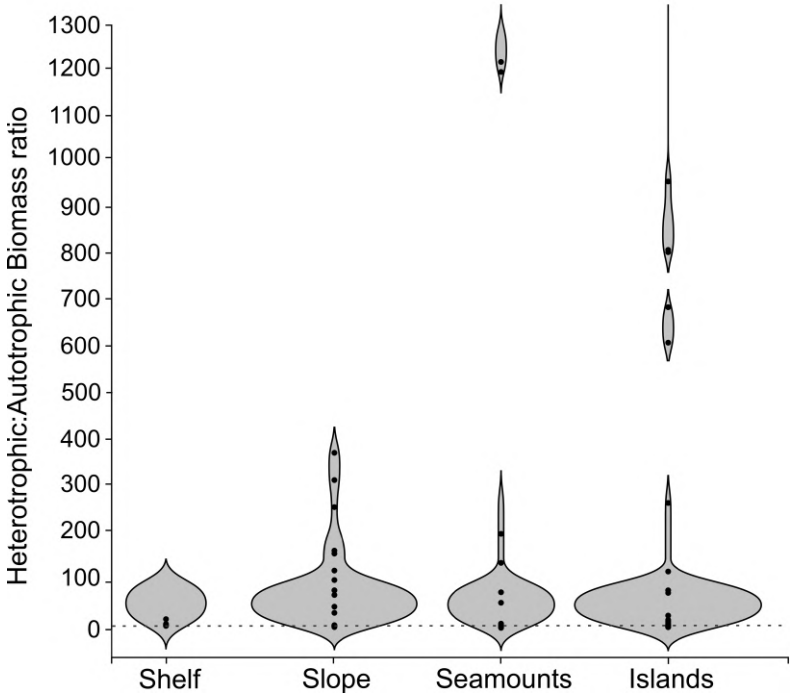

Fig. 5 Heterotrophic:autotrophic biomass ratio in the SWTA. Dashed line indicates 50% proportion, data above this line denotes dominance of heterotrophic over autotrophic biomass. One seamount 200 m depth outlier with a value over 30000 is omitted from the plot.

Overall, heterotrophic bacteria dominated the picoplankton and nanophytoplankton of the SWTA biomass (Fig. 4), although in some DCM (SUW) stations the autotrophic cells biomass (mostly composed of picoeukaryotes) accounted for more than 50% of the total community (Fig. 4b). Between regions the relative heterotrophic biomass did not display significative differences, although lower averages were recorded around the islands and higher over the seamounts at all sampled depths, ranging from 68.12 to 76.93% in the mixed layer, 51.97 to 68.35% in the DCM and shallow bottom, and from 95.17 to 97.34% in the 200 m depth, from the islands and seamounts respectively. The dominance of the heterotrophic over the autotrophic biomass can also be observed in the heterotrophic:autotrophic biomass ratio, where only a few DCM stations displayed values lower than one, especially around the islands (Fig. 5). In most stations the ratio ranged between 1.15 and 15 in the euphotic layer (ML, SB, DCM). Biomass ratios over 50 were recorded in the 200 m, with 30000 times more heterotrophic than autotrophic biomass over one seamounts station.

Drivers of picoplankton and nanophytoplankton spatial patterns and nutrition modes

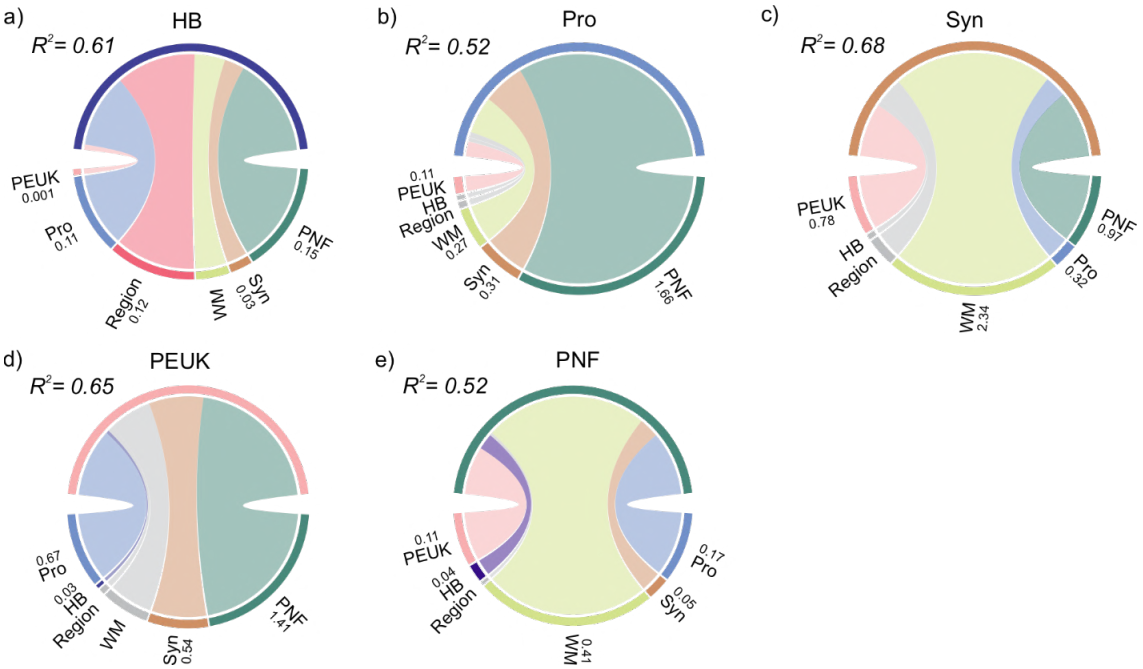

Fig. 6 Circos plots displaying the relative importance of environmental and biotic predictors (width of each sector on the plot) for each group of picoplankton and nanophytoplankton. Each

variable is represented by a different color in the diagram, variables not selected as top predictors (p>.76) are in light grey. The explained variance of each model (R^2) is shown at the top of each diagram. Dependence curves to predictors are shown in Supplementary Figure 6. HB: Heterotrophic bacteria; Pro: *Prochlorococcus*; Syn: *Synechococcus*; PEUK: Picoeukaryotes; PNF: pigmented Nanoflagellates; WM: Water masses; Region denotes the coast-offshore gradient (shelf, slope, islands and seamounts).

Random forest models revealed varied driver importance and partial responses in each plankton group (Fig. 6 and Supplementary Figure 6). Some predictors, however, were identified as dominant drivers (identified as their final position in the tree) of several groups. For instance, water masses were closely associated with the distribution of pigmented nanoflagellates, *Prochlorococcus*, *Synechococcus* and heterotrophic bacteria, with *Synechococcus* showing a higher association with the Tropical Water and the other groups with both Tropical Water and Subtropical Underwater (Supplementary Figure 6). Pigmented nanoflagellates also presented a strong link with the heterotrophic bacteria, *Prochlorococcus*, *Synechococcus*, and picoeukaryotes. The coast-offshore gradient was also an important driver for the heterotrophic bacteria distribution (Fig. 6), with a higher association with the seamounts (Supplementary Figure 6)

PCA results showed that the first two axes explained 79.1% of the variability (Fig. 7). The first axis was associated with nutrient concentrations in opposition to temperature and salinity (Supplementary Table 2). The second axis was defined by the mixed layer depth and the barrier layer thickness. Both autotrophic and heterotrophic biomasses were highly associated with the nutrient-poor TW and SUW and the first axis of the PCA (Fig. 7), with the autotrophic biomass linked to the water column stratification and the heterotrophic biomass with salinity.

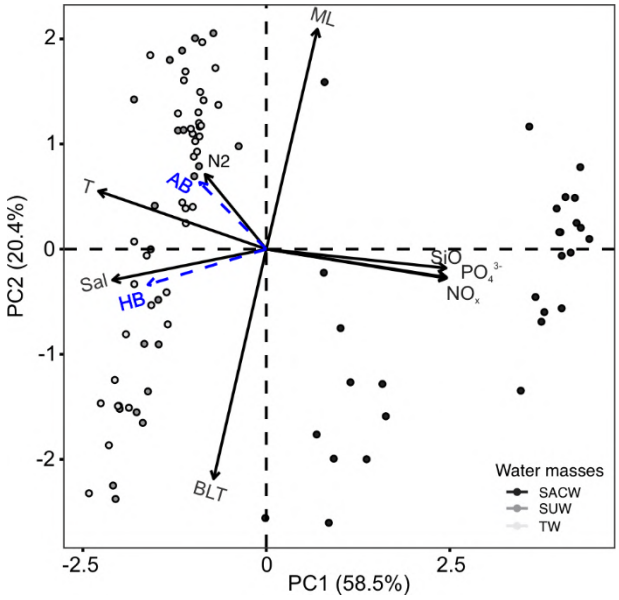

Fig. 7 First two components of the Principal Component Analysis (PCA). Autotrophic biomass (AB) and Heterotrophic bacteria (HB) are plotted as supplementary variables. TW: Tropical Water; SUW: Subtropical Underwater Mass; SACW: South Atlantic Central Water; BLT: Barrier layer thickness; ML: Mixed layer; T: Temperature; Sal: Salinity; N2: Water column stratification

Discussion

Picoplankton and nanophytoplankton community structure and microbial groups interactions

We have characterized mesoscale spatial distribution of picoplankton and nanophytoplankton communities that result from the influence of the nutritional environment and ecological interactions among the microbial network. Perhaps the most evident pattern was the close association of heterotrophic bacteria biomass with the seamounts. Heterotrophic bacteria hotspots have been reported near Vitória-Trindade ridge, in the Atlantic Ocean, and in other seamounts in oligotrophic regions (Mendonça et al., 2012; Dai et al., 2020), as a result of organic matter retention by hydrographic processes (Andrade et al., 2004). Follett et al. (2022) suggested that at least part of such enhancement in heterotrophic bacteria biomass might also occur in response to an increase of organic and inorganic matter released by larger cells. In line with this, higher biomass of large Cyanophyceae was observed in the field survey over the seamounts (Carré et al., unpublished). This nitrogen-fixer Cyanophyceae can form an intrinsic association with heterotrophic bacteria communities for the exchange of nutrients and organic compounds (Lee et al., 2017; Frischkorn et al., 2018), which could also influence the observed increment of bacterial biomass. An alternative, non-exclusive, hypothesis is the resuspension of heterotrophic bacteria communities from the mesopelagic zone through the interactions

between the South Equatorial current and seamounts, an effect that has been previously observed in the zooplankton community around the Saint Peter Saint Paul archipelago on the tropical Atlantic (Melo et al., 2012, 2015).

The autotrophic community showed a clear contrasting pattern, with the biomass of *Synechococcus* and pigmented nanoflagellates decreasing from shelf to oceanic regions, whereas the picoeukaryotes displayed an opposite distribution and *Prochlorococcus* was present in the whole region. Such contrasting pattern of *Synechococcus* and *Prochlorococcus* has been noticed at global (Larkin et al., 2019), and regional scales in oligotrophic regions (Moreira, 2017) (Šantić et al., 2021; Visintini et al., 2021). In coastal oligotrophic waters, high biomass of *Synechococcus* is associated with mesotrophic runoff inputs and upwelling events, gradually being replaced offshore by *Prochlorococcus* (DuRand et al., 2001; Brandini, 2018; Wang et al., 2021). Although the SWTA shelf has weak runoff inputs (Tosetto et al., 2021), uplifts of organic matter have been reported as a result of the physical interaction between North Brazilian Undercurrent water masses and the coastline (Silva et al., 2022). Such phenomenon likely explains the deep maximum of *Synechococcus* we observed.

Picoeukaryote phytoplankton usually aggregates in tropical and subtropical oligotrophic waters at the upper base of the thermocline, where deeper nutrient-rich waters penetrate into the euphotic layers (Jiao et al., 2002; Calvo-Díaz & Morán, 2006). In the SWTA, the uplift of the South Atlantic Central Water promotes slightly euphotic layer fertilization (Brandini, 1990), thereby enhancing phytoplankton production (Farias et al., 2022). However, as previously observed in the South Atlantic Tropical Gyre (Marañón et al., 2003), this uplift does not break the thermocline and does not prevent from nitrogen limitation in the euphotic layer, which promotes the dominance of small cells among primary producers (Farias et al., 2022). In agreement to the aforementioned studies, here, the nutrient imbalance promotes the dominance of pico- and nanophytoplankton such as the picoeukaryotes found here.

Pigmented nanoflagellates were closely associated with heterotrophic bacteria and picophytoplankton taxa, which may indicate their ecological role as both producers and consumers. Although our dataset does not allow us to assess the importance of heterotrophy in nanoflagellates, which are usually the main grazers of heterotrophic bacteria (Livanou et al., 2019), a significant amount of carbon in oligotrophic waters is channeled through mixotrophy. This trophic pathway represents an essential link between autotrophic and heterotrophic bacteria biomass and protist grazers (Fenchel, 2008). In such ecosystems, pigmented nanoflagellates may act either as main bacterivores (Hartmann et al., 2012; Livanou et al.,

2019), grazers of picoeukaryotes (Tsai et al., 2018) and picocyanobacteria (Livanou et al., 2019), thus constituting the most relevant nanoplankton grazers. Therefore, we hypothesize that the results we observed are indicative of mixotrophy as an alternative nutritional mode of pigmented nanoflagellates in this nutrient-limited environment.

We observed that the microbial community was negatively related to nutrient-rich SACW bottom waters, due to the strong light limitation of deep layers. This highlights the capacity of this community to thrive under oligotrophic conditions supported by favorable light conditions and biotic links (i.e., nutrient regenerations by mutualistic interactions). For instance, *Synechococcus* and *Prochlorococcus* in subtropical waters have shown intrinsic mutualist relationships with heterotrophic bacteria through nitrogen remineralization (Nair et al., 2022; Roth-Rosenberg et al., 2020; Zhang et al., 2021). Grazing by nanoflagellates is an additional factor shaping the distribution of Cyanobacteria (Christaki et al., 2002). The latitudinal decline of *Prochlorococcus* has been ascribed to shared predation with similar-sized heterotrophic bacteria. Indeed, it has been observed that a shifting resource ratio favorable to bacteria promote their progressive biomass build-up and leads to an increase of shared grazers and the subsequent decrease of *Prochlorococcus* (Follett et al., 2022). This ecological interaction may influence vertical and horizontal distribution patterns, such as that observed here. In addition, it is worth noticing that while most potential pigmented nanoflagellates prey showed a positive relationship only when grazers reached a threshold biomass, *Prochlorococcus* was the only group that evidenced a bell-like relationship with both pigmented nanoflagellates and heterotrophic bacteria (Supplementary Figure 6). Our assessment of partial response plots suggests that mutualistic relationships between *Prochlorococcus* and heterotrophic bacteria may cease under more favorable nutrient concentrations, such as in seamounts and islands. This may occur, due to the prey preference of nanoflagellates (Christaki et al., 2005; Li et al., 2021; Follett et al., 2022) or caused by outcompeting of other picophytoplankton (Chen et al., 2009).

Heterotrophic:autotrophic biomass ratios

A clear dominance of the heterotrophic bacteria was observed in the biomass of picoplankton and nanophytoplankton. The epipelagic heterotrophic:autotrophic biomass ratios recorded here remained >1, which is consistent with similar surveys in other oligotrophic environments (Gasol et al., 1997; Duarte et al., 2013; Šantić et al., 2021), although these ratios can vary depending on coast-offshore gradients or seasonal variability in nutrient concentrations, stratification, and other environmental variables (Gasol et al., 1997; Šantić et al., 2021). Under

a configuration of high nutrient concentrations and well-mixed water, the ratio heterotrophic:autotrophic biomass may be balanced or dominated by autotrophic cells, while heterotrophic cells might prevail under low nutrient concentrations and stratified water. In contrast, our results showed a persistent dominance of heterotrophic biomass in most of the area, with biomass ratios <1 observed only in the deep chlorophyll maximum of Island stations, which showed higher nitrogen concentrations. However, in this region, the autotrophic biomass rarely reached 60% of the total picoplankton and nanophytoplankton biomass. In fact, the heterotrophic bacteria biomass surpassed the total phytoplankton biomass, even when microphytoplankton carbon biomass (> 20µm) was also considered (Farias et al., 2022) (Supplementary Figure 7). This is partially explained by the previously suggested uncoupled relationship between the increase of nutrients offshore during fall and microphytoplankton (Farias et al., 2022), denoting that nitrogen pulses are not significant enough to nurse high microphytoplankton biomass. Farias et al. (2022) found a dominance of small phytoplankton cells under nitrogen limitation (≅ 0.3 µmol l^{-1} in the euphotic layer) and linked to the maintaining of the stratification by a strong thermocline (Assunção et al., 2020). Our results suggest that nutrient limitation and nutrient ratios in the SWTA prevents the triggering of phytoplankton biomass build-up. Released from phytoplankton competition, oligotrophic conditions promotes the growth of higher nutrient-affinity cells such as bacteria.

Additionally, under the euphotic layer the observed ratios greatly increased (surpassing 200) likely as a result of phytoplankton light-limitation (Yingling et al., 2022), and the enhancement of heterotrophic bacteria, which usually thrives in the DOC-rich mesopelagic realm (Calleja et al., 2018). Although the heterotrophic biomass in the epipelagic and mesopelagic realms can contribute to vertical fluxes of carbon by the formation of colloids and aggregates (Guidi et al., 2016; Zhang et al., 2021), a large proportion of heterotrophic carbon may be redirected toward microzooplankton through the microbial food web. The heterotrophic carbon biomass recorded in our study is similar to previous reports from oligotrophic oceans, varying between 8-26 µg C L^{-1} (Mena et al., 2019; Marañón et al., 2021), and constitute a non-negligible source of carbon to the food web. Indeed, the carbon biomass derived from heterotrophic bacteria has been revealed by isotope analysis as part of the diet of mesopelagic fishes in the SWTA (Eduardo et al., 2023).

While our results showed a clear dominance of heterotrophic bacteria, we have used a conversion factor developed for open ocean communities (Fukuda et al., 1998), which likely underestimates bacteria biomass in a mosaic of hydrogeographic environments, such as the case of the investigated area. Indeed, it has been shown that slight changes in conversion factors to

assess heterotrophic bacteria biomass can duplicate (Lee & Fuhrman, 1987) or triplicate (Fukuda et al., 1998) biomass values. We anticipate that under intensified lower nutrient concentrations, the uncoupling between total biomass and the autotrophic biomass might increase, as well as the role of these organisms in the trophic web.

Conclusion

The observed contrasting patterns in the distribution of picoplankton and nanophytoplankton groups result from the water masses configuration and inter-taxa relationships. These results support our hypothesis, a nitrogen-limited nutritional environment impairs primary productivity while promoting the dominance of heterotrophic bacteria biomass. These observations provide a baseline to understand the microbial food web configuration and trophic pathways in the SWTA. We stress the need for a thorough understanding of microbial interactions to decipher vertical fluxes, metabolic pathways and the fate of the heterotrophic biomass in tropical ocean regions.

Acknowledgments

We wish to express our thanks to the Coordenação de Aperfeiçoamento de Pessoal de Nível Superior – Brasil (CAPES) for the concession of the first author's scholarship (88882.379302/2019-01), and the IMAGO lab who realized the HPLC and nutrients analysis. We acknowledge the French oceanographic fleet for funding the survey ABRACOS and the officers, crew, and scientific team of the R/V Antea for their contribution to the success of the operations. This work is a contribution to the LMI TAPIOCA (www.tapioca.ird.fr), CAPES/COFECUB program (88881.142689/2017-01), the European Union's Horizon 2020 projects PADDLE (grant agreement No. 73427) and TRIATLAS (grant agreement No. 817578).

4 BOTTOM-UP AND TOP-DOWN CONTROLS ON MICROPLANKTON COMMUNITIES UNDER VARIES OLIGOTROPHIC ENVIRONMENTAL SETTINGS

To be submitted – Journal of Plankton Research

Abstract

Deciphering leading drivers of food webs dynamics is crucial to understand productivity patterns and population changes in microbial networks. Here we assessed the influence of bottom-up and top-down mechanisms on the spatial structure of microplankton. To do this, biomass data from a coast-offshore oceanic cruise (ABRACOS 2) were used to depict significative bottom-up and top-down drivers using Random Forest, which were subsequently assessed by means of Generalized Additive Models. Our findings indicate that microphytoplankton biomass was driven by a bottom-up control promoted by the availability of prey. While nitrogen drives microphytoplankton biomass in oligotrophic systems, our results showed that silicate availability play a major role, particularly for diatoms. Mixotrophic and autotrophic microphytoplankton displayed contrasting relationships with silicate, with the former thrived under low concentrations, the latter dominated under a higher nutrient availability. Additionally, we identified the influence of Tintinnina playing a prominent role in the top-down control on the distribution of autotrophic microphytoplankton. We further observed that the microzooplankton was influenced by a variety of drivers, primarily bottom-up control. Our results highlight wide trophic links of Tintinnina acting as a main control of microphytoplankton distribution and *Prochlorococcus* and heterotrophic bacteria, while being prey by Copepoda, thus suggesting a prominent role in both the traditional food web and the microbial food web. Furthermore, the absence of bottom-up control of microphytoplankton on microzooplankton suggests that the microbial community represents a major carbon pathway in the carbon transfer. These results provide a baseline toward modeling microbial networks by identifying linear and nonlinear relationships within the microbial trophic web.

Key Words: microzooplankton, southwestern tropical Atlantic, trophic pathways, GAMs, Random Forest

Introduction

Resolving whether marine populations' structure and carbon fluxes are primarily driven by resource availability (bottom-up) or predation and grazing (top-down) pressures, and how they change under different environmental settings is central in ecological theory, as these processes control not only stability and dynamics in food webs, but also carbon pathways (Power, 1992; Boyce *et al.*, 2015). In oligotrophic systems, food web structure and productivity are mainly addressed through the resource-based hypothesis, which states that organisms are resources limited, e.g., bottom-up nutrient limitation driven by changes in environmental variables (Rissik *et al.*, 2009). In contrast, in environmental settings where resource limitations are less likely to occur, the consumer-based hypothesis, e.g., top-down control, is usually used to address the dynamics of the food web structure. This hypothesis states that organisms are consumer-regulated, and therefore high-level consumers determine biomass pyramids. (Halpern *et al.*, 2006; Baum and Worm, 2009). It is worth noticing however that bottom-up and top-down controls are not mutually exclusive mechanisms, as empirical studies have shown that consumers play a prominent role in storing, recycling, and redistributing nutrients in ecosystems (Loreau, 1995), thus providing a mechanistic link between bottom-up and top-down forces in ecosystems. In addition, both drivers can contribute to the emergence of complex patterns in the dynamics of marine populations (Lynam *et al.*, 2017; Moyano *et al.*, 2023).

Plankton communities serve as compelling models for studying the influences of top-down, bottom-up, and environmental drivers on the structure of pelagic ecosystems. Due to their short generation cycles, large functional diversity, and quick response to ecosystem variability (Ersoy *et al.*, 2019; Fernandes *et al.*, 2020), changes in predation pressure can rapidly reflect throughout the trophic web, impacting the structure, size, and resilience of plankton communities (Ersoy *et al.*, 2019; Gogoi *et al.*, 2021). In this context, small phytoplankton and bacterioplankton communities play a vital role in bottom-up controls of primary and secondary consumers, while serving as indicators of biogeochemical cycles in the ocean (Grossart, 2010; Ward *et al.*, 2013; Jacox *et al.*, 2016). These communities drive primary production, influence nutrient availability, and significantly impact carbon cycling through photosynthesis and carbon remineralization. Consequently, any changes observed in their community structure might provide valuable insights into the overall functioning of marine pelagic ecosystems and the dynamic of bottom-up and top-down controls, making them an essential component of monitoring and conservation efforts, especially in regions with known environmental constraints (Das *et al.*, 2006; Mélin and Hoepffner, 2011).

In the southwestern tropical Atlantic, strong nitrogen limitation has been suggested as a constraining factor that structures phytoplankton productivity, resulting in the dominance of small-celled photoautotrophs (pico- and nanophytoplankton) (Jales *et al.*, 2015; Farias *et al.*, 2022). Also, recent analysis has shown that this nutrient-limited environment favors heterotrophic bacteria biomass over autotrophic biomass in the microbial food web (Chapter 3). However, little is known on the trophic linkages between microzooplankton and their microbial prey and the forces driving microbial food web structure, i.e., resource-limited vs consumer-regulated.

In oligotrophic plankton food webs, the microzooplankton plays a central role, preying on a wide range of prey sizes, from large diatoms to bacteria (Guenther *et al.*, 2019; Arias *et al.*, 2020; Rose *et al.*, 2021). Furthermore, their community structure may be bottom-up controlled by the relative composition of prey in the water column. For instance, communities dominated by the microbial community may support a larger population of Tintinnina, while the biomass of these primary producers may not be available for other grazers like small Copepoda (D'Alelio *et al.*, 2015; López-Abbate, 2021). On the other hand, top-down control by large carnivores, such as Chaetognatha, may be a strong regulating factor of this community biomass and structure (Menéndez, 2022).

To date, little is known on the role of bottom-up and top-down drivers of the microplankton biomass in the southwestern tropical Atlantic. In this nutrient-limited ocean, recent trophic investigations have predominantly focused on mesozooplankton (Figueiredo *et al*., 2020) and mesopelagic fishes (Eduardo *et al*., 2023). These studies highlighted the significance of heterotrophic bacteria as a carbon source for mesopelagic fishes (Eduardo *et al*., 2023) while emphasizing the role of microphytoplankton productivity as the primary organic carbon source for mesozooplankton (Figueiredo *et al*., 2020). In this context, drivers of microzooplankton biomass remain elusive, although their understanding is essential to comprehend the pelagic food web dynamics in this oligotrophic ocean.

In this study, we analyzed the influence of bottom-up and top-down mechanisms on the spatial distribution and structure of microplankton communities. To address these objectives, we use data from a coast-offshore oceanic cruise to identify significant drivers through Random Forest and quantify their impact using Generalized Additive Models.

Material and Methods

Study Area

The research was carried out on the southwestern tropical Atlantic in a coast-offshore sampling comprising two current systems, the Northeast Brazilian continental shelf, slope, and seamounts under the influence of the western boundary current system (WBCS) from 4ºS to 9ºS, and the oceanic seamounts and islands of the Fernando de Noronha chain under the influence of the south equatorial current system (SECS) from 32ºW to 36ºW (Figure 1a). The chain includes both the Rocas Atoll and Fernando de Noronha Island (Kikuchi and Schobbenhaus, 2002). The presence of the Fernando de Noronha Ridge results in increased productivity in the SWTA, as the island wakes created by the ridge's topography provides a favorable environment for feeding and reproduction for varied marine vertebrates (Costa da Silva et al., 2021), including turtles, dolphins, and several species of sharks and stingrays (Serafini *et al.*, 2010; Salvetat *et al.*, 2022). The WBCS area is formed by tropical oligotrophic waters from the North Brazilian undercurrent and the North Brazilian current (Fig. 1b, c). The SECS area is influenced by the central and southern branches of the South Equatorial current and the South Equatorial Under current (Fig. 1b, c) (Assunção *et al.*, 2020). The WBCS and SECS are further distinguished by contrasting thermohaline structures. The WBCS is characterized by low thermal stratification, the presence of frequent and thick barrier layers, and an average mixed layer depth of 39 m during our sampling period, whereas the SECS has a deeper mixed layer (~46 m), a sharp thermocline, strong static stability, and weak surface current (~0.34 m.s 1).

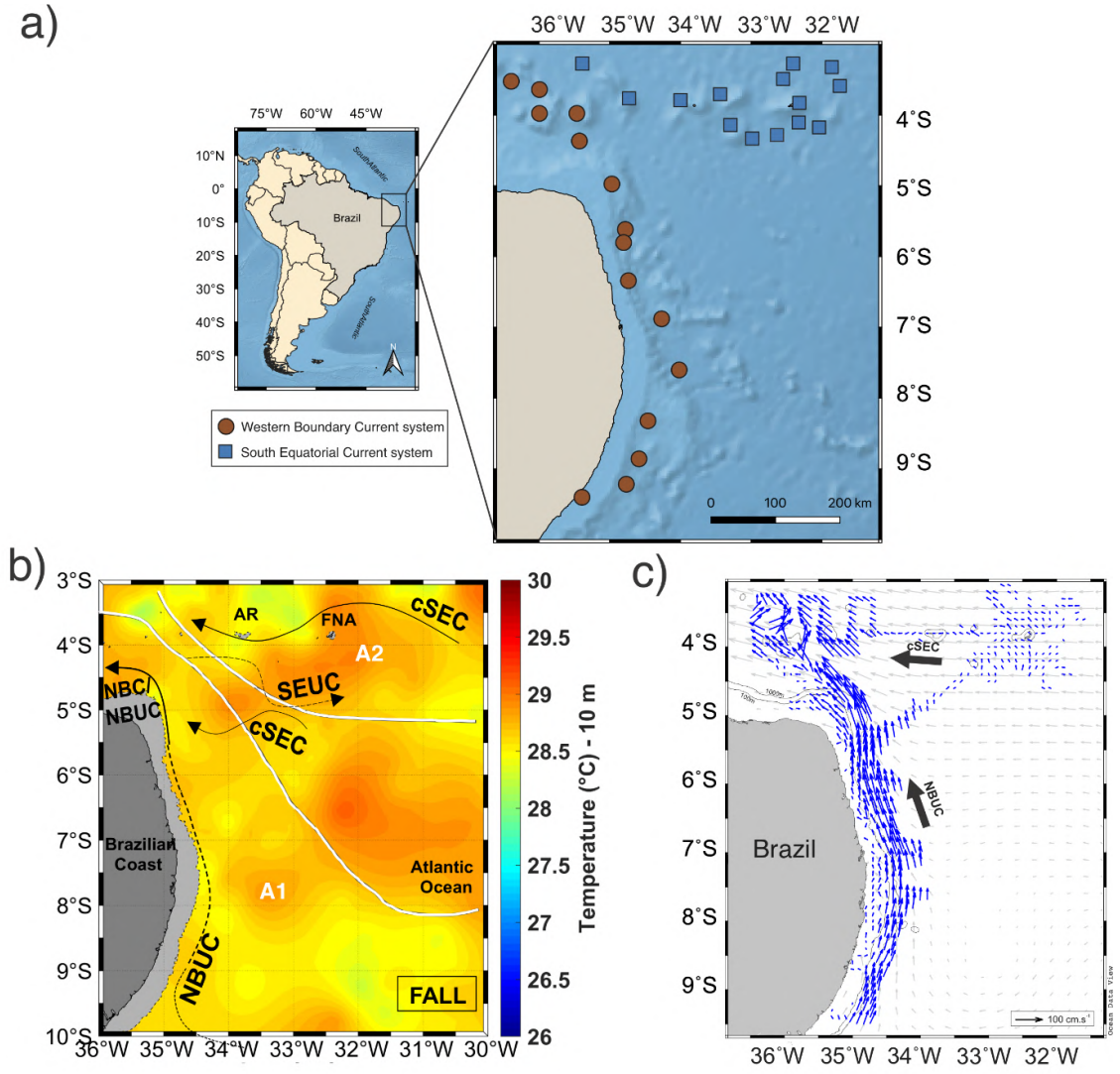

Fig. 1 a) Description of the sampling stations on the western Boundary Current System (WBCS) and offshore on the South Equatorial Current system (SECS) b) 10 m depth temperature field during austral autumn in the southwestern tropical Atlantic, defining different thermohaline areas on the WBCS (A1) and SECS (A2), Redrawn from Assunção et al. (2020); c) Surface currents vectors of ADCP data and indicators of the predominant current in the area; NBUC: North Brazil Undercurrent; cSEC: Central branch of the South Equatorial Current; SEUC: South Equatorial Undercurrent; NBC: North Brazil Current. RA: Rocas Atoll; FNA: Fernando de Noronha Archipelago;

Field Collection and environmental sampling

Samples were collected during ABRACOS 2 cruise (Acoustics along the BRAzilian COaSt 2 oceanographic, Bertrand, 2017), carried out on board the French R/V ANTEA, between April 9th and May 9th of 2017. Our dataset comprehended 29 stations on the WBCS (15) and SECS (14) areas (Fig. 1a). At all stations, vertical profiles of temperature (◦C) and

salinity were obtained with a CTD profiler Seabird SBE911+. CTD data were further used to calculate the vertical stratification of the water column (Brunt–Väisälä frequency, N2).

Samples for estimation of nutrients concentration (NOx [NO2- + NO3-], PO_4^{3-} and SiO_4^{4-}) were collected in 30 ml falcon tubes, pasteurized (heated at 80°C for 2.5 hours in an oven), and frozen to ensure stability until the laboratory analysis. Nutrient analyses were achieved using classical colorimetric methods (Grasshoff *et al.*, 1983), between two and three sampling depths were realized in the shallow stations (<50m), and between 5 and 6 sampling depths were realized in the deep stations (>50m). For a complete description of the nutrient data, see Farias *et al.* (2022).

Plankton sampling methods and analysis

Pico-, nanoplankton, and microphytoplankton samples were collected using a rosette at three depths defined by the CTD profiles: mixed layer, deep chlorophyll maximum, and 200 m. In shallow coast stations, where no peak of fluorescence was observed, deep chlorophyll maximum and 200 m samples were replaced by a shallow bottom sampling at ~10 m above the bottom (usually around 50 and 60 m). For the pico- and nanoplankton, in each station and sampled depth, 1.6 mL of water was fixed with 80 µL of formalin with a final concentration of 2% in cryogenic tubes. Samples were rapidly frozen in liquid nitrogen and then kept in an ultrafreezer (-80ºC) for subsequent laboratory analysis. For the microphytoplankton 2 L of water was concentrated with filtration by gravity on a 5 µm 47 mm PC filter, and resuspended in 30 mL of 0,2 µm filtered seawater, fixed with lugol at 4% final concentration and stored at room temperature in the dark until analysis.

The abundance of pico- and nanoplankton was obtained using a FACSCalibur flow cytometer (Becton Dickinson) equipped with a HeNe air-cooled laser (633 nm, 20 mW), following the protocol of (Marie et al., 1997). Samples were analyzed with a mixture of fluorescent beds (‘Fluorebrite’ YG, Polysciences) of various nominal sizes. Autotrophic cells excited at 633 nm were detected and enumerated according to their forward-angle light scatter (FALS) and right-angle light scatter (RALS) properties, and their orange (576/26 nm) and red fluorescence (660/20 nm and 675/20 nm) from phycoerythrin, phycocyanin and chlorophyll pigments, respectively. Fluorescent beads (1-2 µm for picophytoplankton and 3, 6, and 10 µm for nanophytoplankton) were added to each sample. True count beads (Becton Dickinson) were added to determine the volume analyzed. This method discriminates various autotrophic and mixotrophic groups such as picoeukaryotes, picocyanobacteria (*Prochlorococcus* and

Synechococcus), and pigmented Nanoflagellates. For heterotrophic bacteria, cell DNA was stained with SYBRGreen I and counted under the emission of green fluorescence. After the quantification of abundances, the biomass of pico- and nanoplankton was obtained from conversion factors reported in the literature as follows: *Prochlorococcus* (29 fgC $cell^{-1}$), *Synechococcus* (100 fgC $cell^{-1}$), picoeukaryotes (1500 fgC $cell^{-1}$) (Zubkov et al., 2000), pigmented nanoflagellates (3140 fgC $cell^{-1}$) (Pelegrí et al., 1999) and heterotrophic bacteria (12 fgC $cell^{-1}$) (Fukuda et al., 1998).

Microphytoplankton was counted using an inverted microscope (TCM 400 Labomed) under a Utermöhl chamber. The identification process followed established protocols outlined in publications by Taylor (1976), Balech (1988), Licea et al. (1995), Tomas et al. (1997), Tenenbaum (2006), Gomez et al. (2008), Hoppenrath et al. (2009), and was cross-verified using WorMs (http://www.marinespecies.org). The microphytoplankton diversity was then distinguished into four functional groups depending on their nutritional mode, autotrophic, mixotrophic microphytoplankton, and heterotrophic dinoflagellates. Biovolumes of microphytoplankton functional groups were calculated based on similar geometric models of their general structure (Sun and Liu, 2003). Biovolumes values were then used to assess carbon biomass based on conversion factors available in the literature (Verity *et al.*, 1992; Menden-Deuer and Lessard, 2000).

Microzooplankton sampling was conducted using a bongo net (64 µm mesh size and 30 cm mouth opening diameter). At each station, oblique hauls between 200 m and the surface were conducted. Samples were preserved with 4% formaldehyde buffered with sodium tetraborate (Harris et al., 2000). A minimum of 300 individuals of the microzooplankton samples were analyzed in a Sedgewick-rafter counting chamber under a primo star Zeiss microscope. Microzooplankton taxa (Copepoda, Tintinnina and Chaetognatha), and copepoda functional groups (carnivorous, omnivorous and herbivorous) were identified using specific literature (Boltovskoy 1999; Boxshall and Halsey 2004; Dahms et al. 2006). Biomass (B, mgC m^{-3}) quantification was based on taxa abundance (A, ind. m^{-2}) and individual carbon weight (CW, mgC): $B = A * CW$, defined using length-weight regressions available in the literature (Supplementary Table 1).

Data analysis

We constructed a conceptual model for the microplankton, considering bottom-up, top-down, and environmental drivers. This model was based on previous observations of microbial

community structure in the SWTA (Farias et al., 2022; Chapter 3) (Fig. 2), along with extant published research on the functional groups of microplankton and Copepoda taxa (Supplementary Table 2), including their main nutritional modes. Microphytoplankton and heterotrophic dinoflagellates species (216) were pooled in three compartments, autotrophic and mixotrophic microphytoplankton, and heterotrophic species that included heterotrophic dinoflagellates. For microzooplankton, due to their dominant abundance we used Tintinnina as representative of ciliates (Tosetto et al., 2023), as well as by their known pivotal role linking the microbial food web with metazoans (Pierce and Turner, 1992; Munawar *et al.*, 2020). Copepods (54 species) were pooled into three compartments: herbivorous, carnivorous, and omnivorous. As top predator in our analysis, we used Chaetognatha, which is a main predator of copepods (Fig. 2). Initial model equations (Supplementary Table 3) included the environmental effect of sea surface temperature (SST), salinity (SSS), and water column stratification, and the coast-offshore variability (variable areas, comprising the WBCS and the SECS) on all compartments. For the autotrophic and mixotrophic microphytoplankton we further considered the bottom-up effect of nutrient concentration. Biologic links between compartments were selected based on the feeding preference of each compartment (Supplementary Table 2). Due to the difference in the sampling method used, the nutrients and pico- and nanoplankton data were depth integrated (m^2) on the first 200 m to be used in the further analysis with the zooplankton data

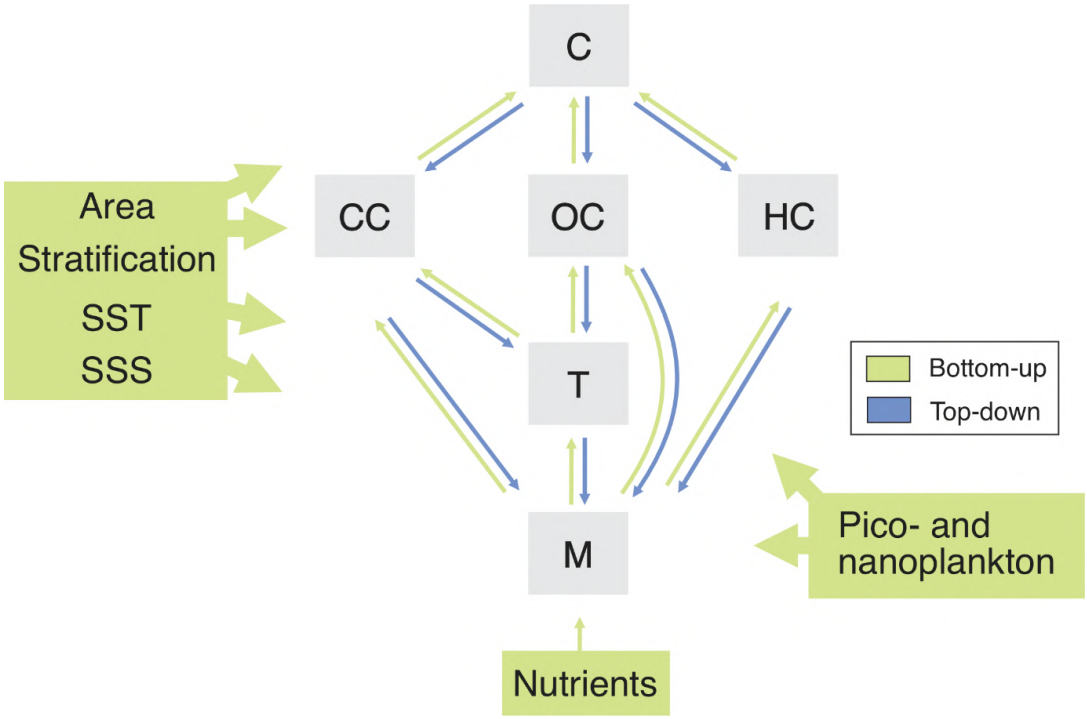

Fig. 2 Proposed relationships tested for bottom-up (in green) and top-down (in blue) controls on the microplankton community. Specific variables fed in the random forest models are described in Supplementary Table 3. SST: sea surface temperature; SSS: sea surface salinity; Areas: WBCS and SECS; pico- and nanoplankton (*Prochlorococcus*, *Synechococcus*, heterotrophic bacteria, picoeukaryotes, and pigmented Nanoflagellates); M: autotrophic and mixotrophic microphytoplankton, and heterotrophic Dinoflagellates. T: Tintinnina; CC: carnivorous Copepoda; OC: omnivorous Copepoda; HC: herbivorous Copepoda; C: Chaetognatha. The left green panel is proposed variables (Area, Stratification, SST, and SSS) that exert bottom-up control on all four compartments. The right green panel is proposed variables (pico- and nanoplankton) that exert bottom-up control on M and T.

To assess bottom-up and top-down mechanisms acting on microplankton biomass we used Random Forest and Generalized Additive Models (GAMs). In the first step leading drivers were detected using Random Forest regression models, a method based on non-parametric regressions. The method randomly splits the dataset and fits regression trees that are confronted with the remaining data. The process is subsequently repeated with every bootstrapped dataset and the resultant trees are combined into a final model. In the second step, we utilized GAMs to assess whether the relationships between the selected variables and microplankton groups are linear or nonlinear. Additionally, we determined potential threshold values that influence these relationships. (Hastie and Tibshirani 1986; Wood 2006; R 2015).

We used the function *rfsrc* from the R-package *randomForestSRC* (Ishwaran *et al.*, 2022) to set the models displayed in Supplementary Table 3. Random forest models were run and predictors with null importance on the regression tree were removed from the final models. Top predictor variables were selected from the final random forest models by exploring variable maximal subtree, using the function *max.subtree* (Ishwaran *et al.*, 2022). GAMs with the top predictors were realized using the function ‘gam’ in the R package ‘mgcv’ (Wood, 2011). The models were selected by p-value and the Generalized cross-validation (GCV) score. GAM plots were constructed using the R package ‘mgcv’ (Wood 2011).

Results

Identification and hierarchy of bottom-up and top-down drivers

The main drivers of the microplankton biomass distribution were determined from Random Forest analysis and highlighted mainly bottom-up and environmental control. Mixotrophic microphytoplankton biomass was influenced by bottom-up control from nutrient concentrations (SiO and NOX) (Fig. 3a). Autotrophic microphytoplankton also displayed an association with SiO and was further linked with Tintinnina, as a secondary driver (Fig. 3b). Furthermore, the heterotrophic Dinoflagellates had their coast-offshore patterns as a main driver together with

the bottom-up effect of the picoeukaryotes biomass, with a lower impact on the top-down control by carnivorous Copepoda.

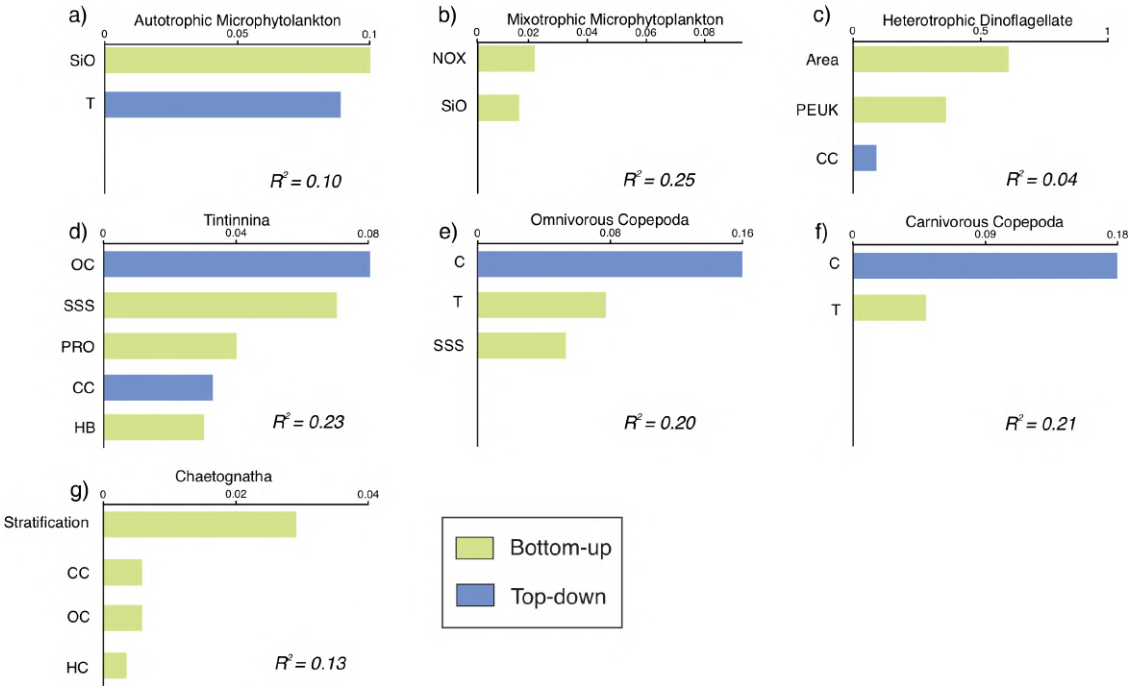

Fig. 3 Bar plot displaying the hierarchical importance of environmental and biotic top drivers depicted by Random Forest max subtrees for each group of microplankton. Bottom-up variables are in green and top-down variables are in blue. The explained variance of each model (R^2) is shown at the top of each diagram. SSS: sea surface salinity; Areas: WBCS and SECS; PRO: *Prochlorococcus*; HB: heterotrophic bacteria; PEUK: picoeukaryotes; T: Tintinnina; HC: herbivorous Copepoda; CC: carnivorous Copepoda carnivorous; OC: omnivorous Copepoda; C: Chaetognatha.

Tintinnina experienced top-down control of omnivorous Copepoda, which was their main driver, and carnivorous Copepoda, followed by the influence of bottom-up drivers as sea surface salinity and Prochlorococcus and heterotrophic bacteria biomass. In the case of Copepoda, the herbivorous taxa displayed no significant link with any of the explanatory variables. Carnivorous and omnivorous Copepoda were top-down controlled by Chaetogatha and bottom-up controlled by Tintinnina as the main drivers of their biomasses, respectively. In addition, Omnivorous Copepoda was further linked with the sea surface salinity. Lastly, Chaetognatha distribution and biomass were mostly influenced by the water column stratification, followed by the effect of the biomass of all three Copepoda functional groups. All selected drivers are bottom-up since no top-down drivers were tested for this group.

The Random Forest results allowed the update of the modeled equations proposed (Supplementary Table 3). These simplified final equations can represent the general patterns of our sampled microplankton community. Modeled patterns of mixotrophic microphytoplankton

and heterotrophic dinoflagellates were the only groups that significantly diverged from observations.

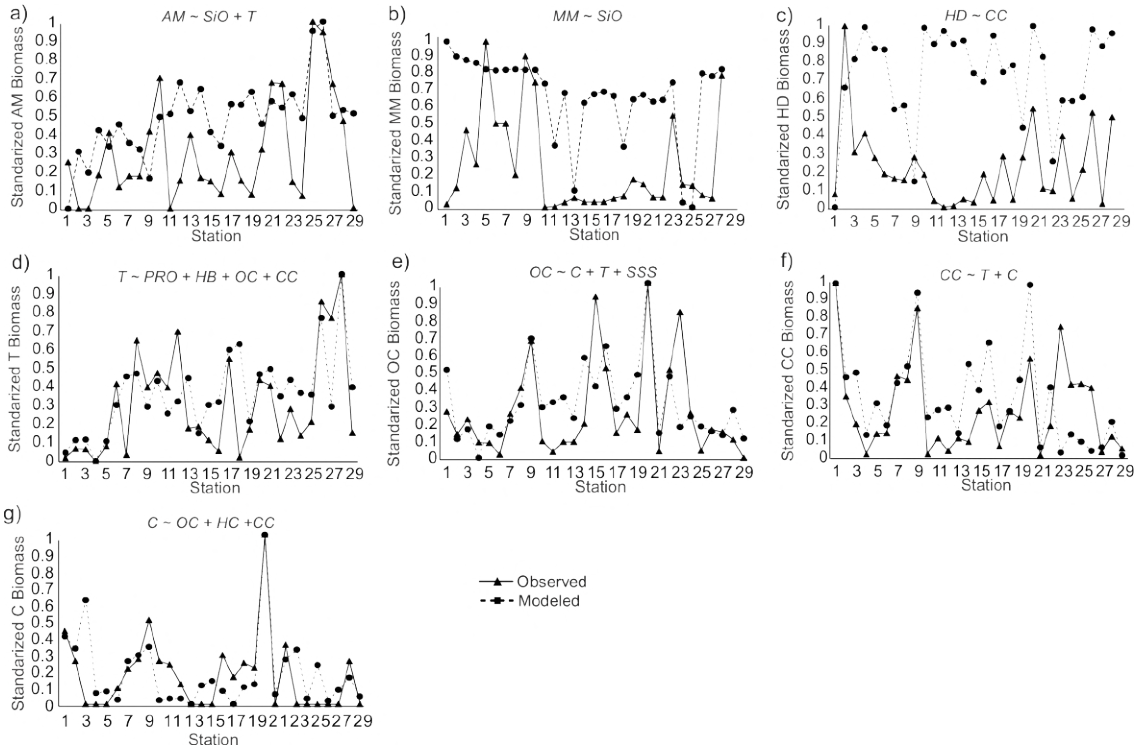

Fig 4. Multiple linear regression reconstructed values of microplankton biomass based on the final models. a) Autotrophic microphytoplankton; b) Mixotrophic microphytoplankton; c) Heterotrophic dinoflagellates; d) Tintinnina; e) Omnivorous Copepoda; f) Carnivorous Copepoda; g) Chaetognatha The solid line represents the observed values and the dashed line represents the modeled values. PRO: *Prochlorococcus*; HB: heterotrophic bacteria; T: Tintinnina; HC: herbivorous Copepoda; CC: carnivorous Copepoda carnivorous; OC: omnivorous Copepoda; C: Chaetognatha.

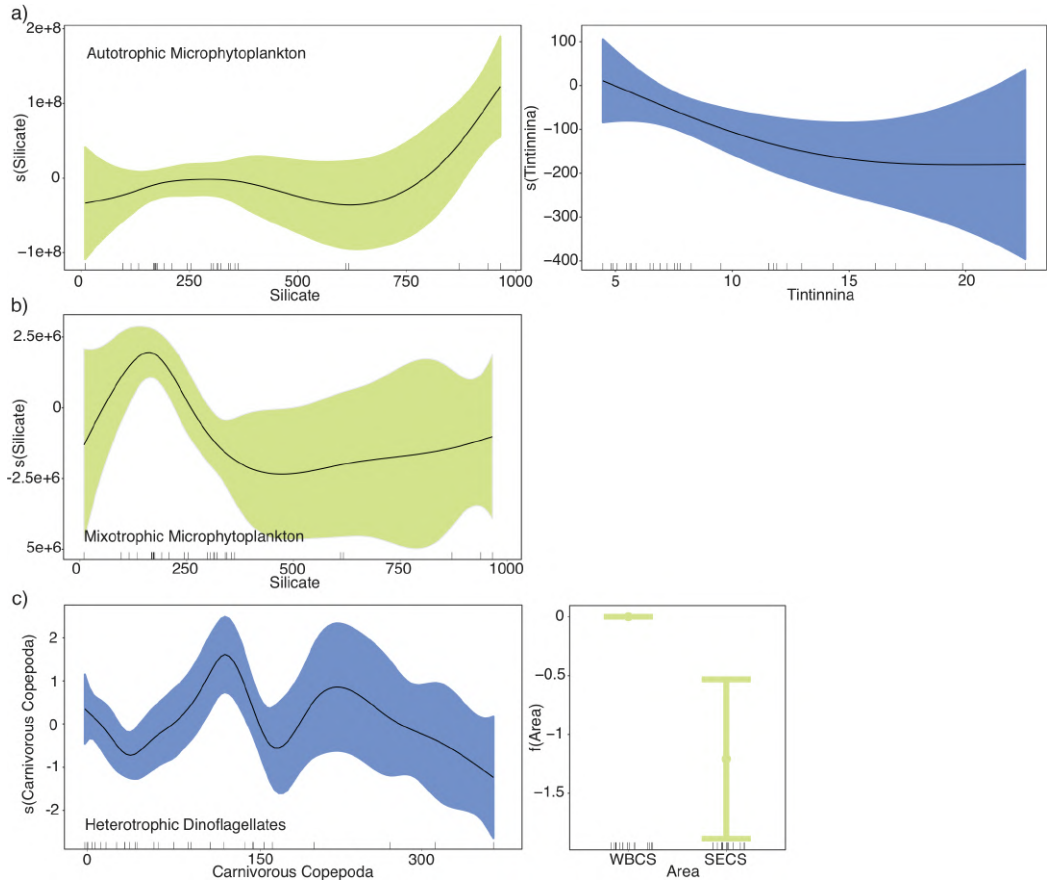

Fig 5. Generalized Additive Models (GAMs) results describe the main bottom-up and top-down factors influencing the microphytoplankton biomass distribution. a) autotrophic microphytoplankton; b) mixotrophic microphytoplankton; c) heterotrophic Dinoflagellates. Solid lines represent smoothed mean relationships from GAM's and shaded areas are 95% confidence intervals.

GAM analysis

GAM models assessing the influence of selected factors on the microplankton compartments explained at least 41% of the total variance (Table 1). Autotrophic microphytoplankton showed a strong increase with vertically integrated silicate values higher than 750 µmol m^{-2} and a slightly almost linear decrease with the Tintinnina (Fig. 5a). Although the random forest indicated nitrogen and silicate as top drivers of the mixotrophic microphytoplankton biomass, only silicate presented a significative relationship with the mixotrophic microphytoplankton on GAM (Fig. 5b), with a biomass threshold increase up to 200 µmol m^{-2} and further decrease to initial values of biomass. Lastly, the heterotrophic Dinoflagellates showed clear association with the WBCS area presenting two peaks of biomass with the carnivorous Copepoda, with no clear threshold between these two compartments' biomass (Fig. 5c), however no significative link was observed with PEUK, which was also selected in the random forest.

Model	R^2	GCV

AM = s(T) + s(SiO)	0.41	3.08×10^{-15}
MM = s(SiO)	0.48	5.19×10^{-12}
HD = s(CC) + Area	0.67	3.56×10^{-12}
T = s(PRO) + s(HB) + s(CC) + s(OC)	0.51	1.4×10^{-3}
OC = s(C) + s(T) + s(SSS)	0.99	2.9×10^{-2}
CC = s(C) + s(T)	0.47	1.37×10^{-2}
C = s(HC) + s(CC) + s(OC)	0.95	1.6×10^{-1}

Table 1. Statistical summary of final generalized additive models between the biomass of microplankton and their top drivers as described by Random Forest. R^2 is the adjusted proportion of total variability explained by the model. GCV: generalized cross-validation score; SSS: sea surface salinity; Areas: WBCS and SECS; AM: autotrophic microphytoplankton; MM: mixotrophic microphytoplankton; HM: heterotrophic Dinoflagellate; PRO: *Prochlorococcus*; HB: heterotrophic bacteria; T: Tintinnina; OC: omnivorous Copepoda; CC: carnivorous Copepoda; C: Chaetognatha.

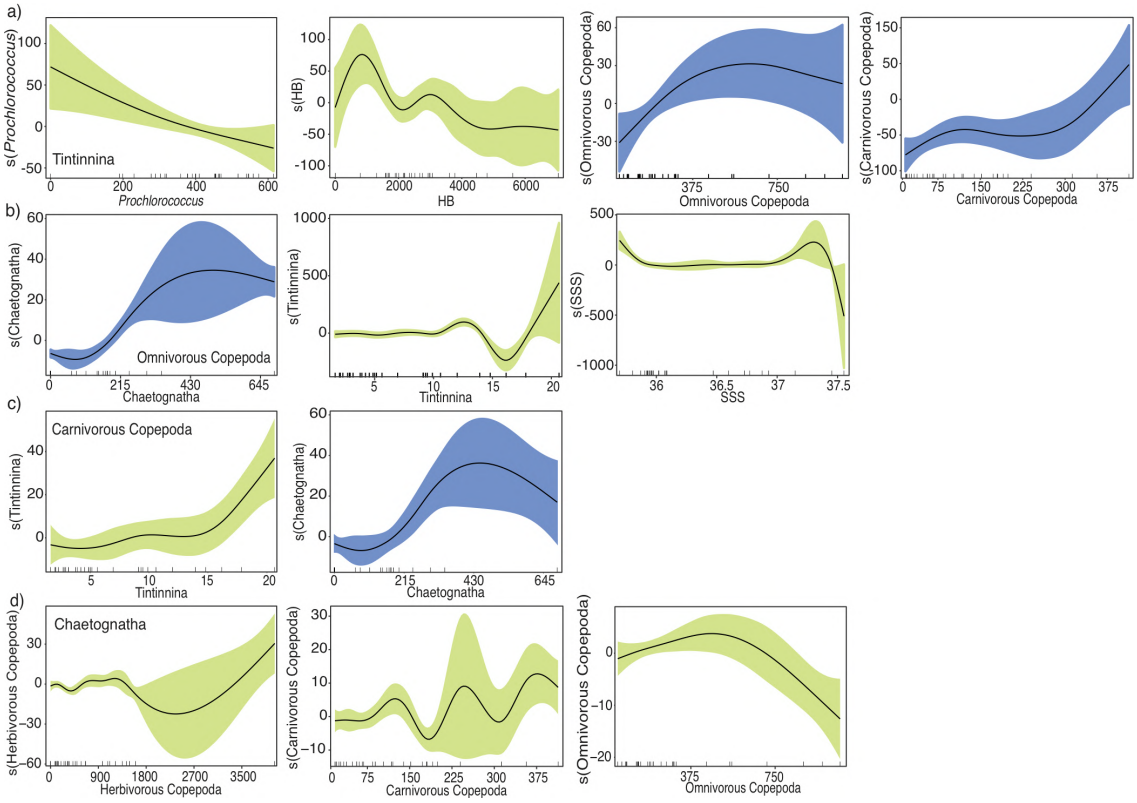

Fig 6. Generalized Additive Models (GAMs) results describe the main Bottom-up and Top-down factors influencing the microzooplankton biomass distribution. a) Tintinnina; b) omnivorous Copepoda; c) carnivorous Copepoda; d) Chaetognatha. Solid lines represent smoothed mean relationships from GAM's and shaded areas are 95% confidence intervals.

Tintinnina displayed a linear negative relationship with *Prochlorococcus*, however, the relationship found with the heterotrophic bacteria displayed a non-linear pattern driven by an initial increase in Tintinnina biomass under low heterotrophic bacteria biomass, which was followed by a decrease under heterotrophic bacteria biomass higher than 1000 µgC m^{-2} (Fig.

6a). Tintinnina had an increase in biomass with Omnivorous Copepoda until biomass of around 400 µg C m^{-3}, and an increase with the Carnivorous Copepoda only with biomass higher than 300 µg C m^{-3}. Both the carnivorous and omnivorous Copepoda showed a similar relationship with Tintinnina and Chaetognatha (Fig 6 b,c), where an increase in Copepoda carbon biomass was observed with Tintinnina biomasses higher than 15 µg C m^{-3} and a decrease with Chaetognatha biomasses higher than 215 µg C m^{-3}. Furthermore, a threshold for Omnivorous Copepoda biomass was observed with SSS higher than 37. Lastly, Chaetognatha showed a biomass increase with herbivorous and carnivorous Copepoda, while with omnivorous Copepoda a decrease was noted with biomasses higher than 500 µg C m^{-3} (Fig. 6d).

Discussion

We have assessed the relative effects of top-down and bottom-up drivers on microplankton biomass in an oligotrophic system. The quantification of bottom-up and top-down drivers on plankton communities has considerable methodological challenges since they are not directly estimated. Studies usually use isotopes (and other biochemical tracers) and gut content to estimate the biological control over plankton communities (Guo *et al.*, 2023; Presta *et al.*, 2023). Abundance and biomass from *in situ* data are also widely used to hypothesize links (i.e. correlation and structural equation modeling) between taxa and environmental variables as inference of trophic relationships and bottom-up vs. top-down control (Duffy *et al.*, 2015; Wollrab *et al.*, 2019; Murphy *et al.*, 2020). However, although these are widely used tools to model community drivers, they still overlook non-linear relationships and changes in the magnitude of the correlation between variables (Sugihara et al., 2012). Non-linear methods such as those used here are alternatives to the observation of small changes in the interactions between variables (Zhang et al., 2021) and help to depict the mosaic nature of bottom-up and top-down drivers on pelagic microbial food webs.

Microphytoplankton and heterotrophic dinoflagellates drivers

In oligotrophic systems, although a combination of factors drives microphytoplankton biomass, usually this compartment is resource-driven (Landry *et al.*, 2009). In the studied area, recent efforts have indicated that nitrogen limitation hinder microphytoplankton biomass (Farias *et al.*, 2022). Therefore, we expected nitrogen to be the main bottom-up controlling factor on microphytoplankton. However, our results showed a leading role of silicate concentrations as the main driving variable of microphytoplankton functional groups (autotrophic and mixotrophic). Silicate is a major limiting factor for microphytoplankton growth, especially diatoms (Wei *et al.*, 2020; Xu *et al.*, 2022), which dominated the autotrophic compartment during our study period (Supplementary Table 2). Silicate can be found as a primary limiting nutrient for diatoms, with nitrogen having a secondary role (Pilkaitytė and Razinkovas, 2007), in fact, our results suggest that even under nitrogen limitation this relationship may remain. It is worth noticing that although nitrogen was a selected driver for the mixotrophic microphytoplankton in the Random Forest, no significative relationship was seen on the GAMs, which may indicate that a larger dataset may be needed to allow this relationship to emerge among models .

Our GAM analysis further allowed the identification of contrasting relationships with the silicate concentration between the autotrophic and mixotrophic microphytoplankton. Mixotrophic dinoflagellates may thrive under low nutrient concentrations (Litchman and Klausmeier, 2008; Leles *et al.*, 2018; Dao, 2021), particularly, under low silicate concentration, mixotrophic microphytoplankton outcompeted diatoms in the present study, as they do not rely on this nutrient to growth (Gettings et al., 2014). However, this advantage diminishes rapidly as silicate concentrations grow, favoring autotrophic microphytoplankton (Egge and Aksnes, 1992; Hansen and Visser, 2019; Okcu et al., 2021).

Research on phytoplankton dynamics has mainly focused on how environmental factors such as temperature, light, and nutrients affect their growth and diversity (Lima *et al.*, 2019; Ajani *et al.*, 2020). However, this approach is limited because it does not consider important biotic interactions like predator-prey relationships, which are crucial for understanding phytoplankton community structure (Mutshinda *et al.*, 2013; Lima-Mendez *et al.*, 2015). In our analysis we identified the role of Tintinnina as an important driver of microphytoplankton biomass, suggesting top-down control as an additional force controlling autotrophic microphytoplankton distribution. This predator-prey relationship is in line with former reports that showed a close correlation between the abundance of Tintinnina and diatoms (Kumar *et al*., 2021; Trifoglio *et al.,* 2023), with diatoms serving as sources of biogenic silica for the construction of the lorica of Tintinnina (Armbrecht et al., 2017), and their community composition directly structuring Tintinnina's assemblages (Van Dinh et al., 2021).

Heterotrophic and mixotrophic dinoflagellates can represent important grazers of the picoplankton (Tsai et al., 2018; Livanou *et al.,* 2019). Conversely to our expectations, no relationship was observed between this small picoplankton and the heterotrophic and mixotrophic dinoflagellates. Heterotrophic dinoflagellates displayed significant association only with the coast-offshore gradient as an identified environmental driver, possibly due to a higher concentration of organic matter over the shelf, which represents an important nutritional source for these organisms (Purina *et al.,* 2004). On the other hand, this group was top-down regulated by the carnivorous Copepoda, which usually are found in oligotrophic regions heavily preying on them, as they are the prevailing food (Benedetti *et al.,* 2015; Joo Lee *et al.,* 2023).

Microzooplankton and mesozooplankton drivers

In contrast to the microphytoplankton, microzooplankton is usually under the effect of many drivers, with the dominance of bottom-up control especially when the classic food web prevails (Mozetič *et al.*, 2012). The influence of Tintinnina on the distribution of

microphytoplankton and the role of *Prochlorococcus* and HB in shaping Tintinnina biomass suggest their potential grazing impact on both the traditional and microbial food webs. The absence of microphytoplankton in the bottom-up control of Tintinnina biomass may further indicate that although these ciliates have an important role in driving the microphytoplankton distribution, their small biomass is not enough to sustain the Tintinnina community, which in turn is regulated by the abundant picoplankton. Additionally, the grazing activity of Tintinnina on phytoplankton may reinforce the predation of Copepoda on them. Herbivore grazing on primary producers has the potential to trigger the release of chemicals that can affect the foraging behavior of higher-order predators, thereby facilitating multitrophic interactions in ecosystems (Harvey, 2013). Specifically, chemicals released during microzooplankton grazing, including Tintinnina on phytoplankton can serve as infochemical cues that induce foraging responses and enhance search efficiency in carnivorous copepods (Walker et al., 2019).

In our results, both the non-herbivorous Copepoda functional groups showed Tintinnina as a main source of bottom-up control, with the absence of a link with both microphytoplankton and the heterotrophic dinoflagellates. This fits with the results observed in Tintinnina, which rely on the picoplankton as a carbon source, suggesting that the microphytoplankton and heterotrophic dinoflagellates biomass, are not enough to sustain the Copepoda community. The preying of Copepoda on Tintinnina reinforces the link between the microbial and classical food webs. Tintinnina may further serve as a bridge for the bacteria biomass to the crustacean zooplankton since these organisms are inefficient grazers on small particles, such as bacteria (Zöllner *et al.*, 2009).

Chaetognatha and Copepoda relationship was clearly identified in our results, indicating their trophic relationship. Chaetognatha is a major predator in pelagic plankton, consuming up to 12 prey day^{-1} (Kehayias, 2003), with Copepoda usually representing their preferred prey (Karati *et al.,* 2019). However, different nonlinear relationships were observed with the distinct Copepoda functional groups, we suggest that this may be related to size selectivity on Chaetognatha. Size selectivity may cause an asymmetry in predation pressure, although Chaetognatha may represent important predators of the microzooplankton (Patuła *et al.,* 2023), they could shift their predation pressure in the presence of larger prey, which seems to be the case with the herbivorous Copepoda. This compartment is composed of larger Copepoda, such as *Acrocalanus* and *Rhincalanus* and an increase in their abundance may represent a reduction in predation pressure on the omnivorous and carnivorous Copepoda. Contrasting with what was expected, no link between herbivorous Copepoda and the microphytoplankton was identified. It was shown that changes in phytoplankton growth rates can lead to temporal decoupling

between primary producers and consumers. This results in modified feeding relationships and can have dramatic consequences on the highest trophic levels populations and ecosystem functioning (Atkinson *et al.*, 2015). Additionally, a large portion of the herbivorous Copepoda identified here are also particle-feeders, feeding on the organic matter available in the water column, suggesting that in the study area, with low microphytoplankton biomass, this may be the main source of organic carbon for this plankton compartment. In fact, under oligotrophic conditions, the food chain based on heterotrophic plankton such as heterotrophic bacteria, ciliates, and dinoflagellates as well as detritivores and carnivore copepods should be established (Menezes *et al.,* 2019), as observed here.

Our results point out the coexistence of bottom-up and top-down control in the microplankton community, and the importance of the picoplankton in the structuring of the food web. As previously suggested, the nutrient limitation in this oligotrophic ocean leads to the predominance of regenerated production and heterotrophic bacteria biomass. Here, the driving role of the picoplankton as a bottom-up driver of Tintinina, and the absence of bottom-up control of the microphytoplankton and heterotrophic dinoflagellates on the microzooplankton suggests that the microbial food web may be the main carbon pathway on this plankton food web (Fig. 7). As climate change scenarios pinpoint a size reduction in the pelagic organisms following ocean warming, these results may be indicative of the structure of plankton food webs in the near future.

Data constrains and future directions

In general, there is increasing recognition of the intricate nature of data and models needed to measure the impact of top-down and bottom-up mechanisms, as well as environmental factors driving food webs. (Rogers *et al.*, 2022). Data availability is often constrained on time or spatial scales, and as a result, inferences based on such studies are limited, especially in highly variable systems (Miller-Rushing et al. 2010). Our conclusions are limited by the absence of data on additional food web components i.e., heterotrophic Nanoflagellates, and the concentrations of particulate organic matter, which seems to be an important source of organic carbon for many compartments in our study area. This lack of data and the low number of observations used may also explain why no drivers were selected for the herbivorous Copepoda community. Thus, non-significant result does not mean the relationship is absent. However, this does not dimmish the results presented here, our modeled results captured the main pattern in the distribution of the groups (Fig. 4), showing that although we are far from having a full picture, in the current state of the art in the microbial plankton of the region, this study represents a first piece in the

complex puzzle and a stepstone on the study of the microplankton community drivers and trophic links in the SWTA.

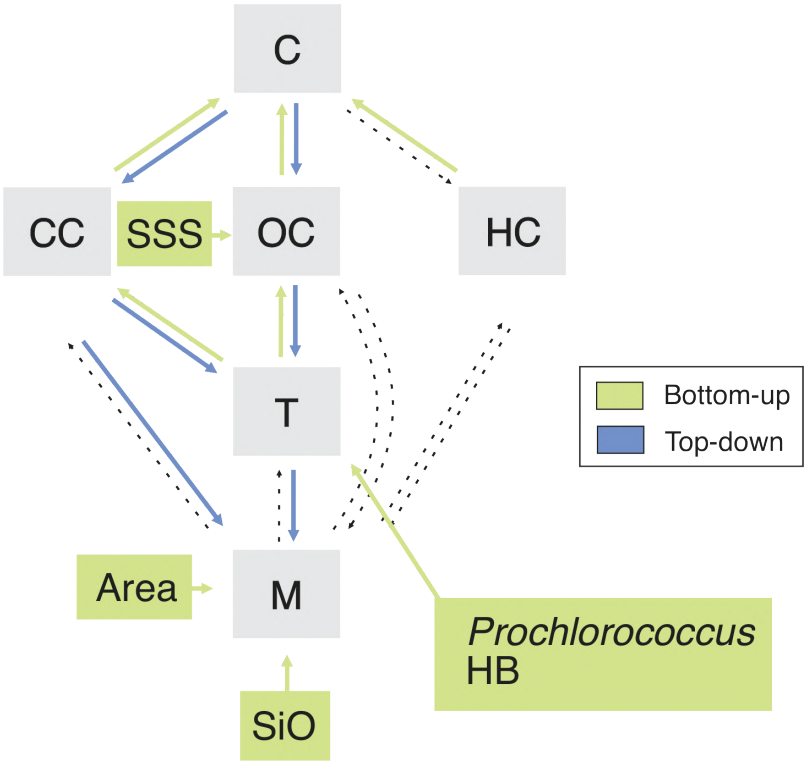

Fig. 7 Updated relationships of bottom-up (in green) and top-down (in blue) controls on the microplankton community. SSS: sea surface salinity; Areas: WBCS and SECS; HB: heterotrophic bacteria; M: autotrophic and mixotrophic microphytoplankton, and heterotrophic Dinoflagellates. T: Tintinnina; CC: carnivorous Copepoda; OC: omnivorous Copepoda; HC: herbivorous Copepoda. Dashed lines indicate non significative relationships.

Acknowledgments

We wish to express our thanks to the Coordenação de Aperfeiçoamento de Pessoal de Nível Superior – Brasil (CAPES) for the concession of the first author's scholarship (88882.379302/2019-01), and the colleagues from the Phytoplankton and Zooplankton labs in the Federal University of Pernambuco for the help in the identification of the samples. We acknowledge the French oceanographic fleet for funding the survey ABRACOS and the officers, crew, and scientific team of the R/V Antea for their contribution to the success of the operations. This work is a contribution to the LMI TAPIOCA (www.tapioca.ird.fr), CAPES/COFECUB program (88881.142689/2017-01), the European Union's Horizon 2020 projects PADDLE (grant agreement No. 73427) and TRIATLAS (grant agreement No. 817578).

5 GENERAL DISCUSSION AND CONCLUSIONS

Small plankton (pico- and nanoplankton) are vital to marine ecosystems as they play crucial roles in carbon fixation, nutrient cycling, and serve as the base of the marine food web, thus supporting biomass production and diversity of marine life (Menéndez, 2022). With global ocean changes, including rising sea temperatures, ocean acidification, and altered nutrient distributions, there is a growing concern about the decrease in the average cell size of plankton communities (Henson et al., 2021). Research suggests that global anthropogenic changes, such as increasing temperatures and altered nutrient availability, favor smaller-sized plankton species, especially pico- and nanoplankton, over larger ones (Morán et al., 2010). These smaller plankton benefit from the novel environmental settings caused by ocean global changes in both direct and indirect ways, their growth rate may be enhanced, as well as their bloom periods extended (due to changes in the global thermohaline stratification), they also can expand to northermost latitudes benefiting from rising temperatures (Winder and Sommer, 2012). Additionally, they can become more competitive in scenarios of higher nutrient limitation and intensified grazing on phytoplankton (Peter and Sommer, 2013; Sommer et al., 2017). To fully comprehend the ramifications of the decrease in plankton size, ongoing research is necessary, especially considering that this portion of the plankton community has been poorly explored in the southwestern tropical Atlantic. Regarding the picophytoplankton, in the offshore area, only general biomass assessments were previously done, using chlorophyll-a as a proxy, and with coarse space and time resolution (Aquino, 2016; Chaves et al., 2006; Cordeiro et al., 2018; Ekau and Knoppers, 1999; Jales et al., 2015; Kikuchi and Schobbenhaus, 2002), with this size class being better explored in continental waters and estuaries (De Aquino et al., 2014; Farrapeira et al., 2009; Feitosa; Nascimento; Muniz, 1999; Feitosa; Passavante, 1990; Nascimento et al., 2003; Otsuka et al., 2018). Likewise, bacterioplankton has been less explored (Moreira, 2017). To fill this gap, we used data from two oceanic cruises in contrasting seasonal periods to provide a baseline to understand picoplankton and nanophytoplankton dynamics in a scenario of contrasting environmental settings and their role in the carbon pathways.

The primary producers and the physical structure of the southwestern tropical Atlantic

The confluence of varied water masses driven by mesoscale currents, e.g., WBCS and SECS, favored hydrographic provinces that promote a mosaic-like spatial distribution of phytoplankton communities. In this region, the thermohaline circulation plays a crucial role in

inter-hemispheric heat, nutrients, and salt transport (Assunção et al., 2020). Moreover, the variability of thermohaline conditions is a driving factor shaping the vertical structure of pelagic habitats (Assunção et al., 2020; de Souza et al., 2013). Data from the same research project (ABRACOS 1 and 2) were used to uncover significant bottom-up control and structural relationships in the entire food web, from primary productivity to fish populations (Eduardo et al., 2021; Figueiredo et al., 2020; Tosetto et al., 2022; Tosetto et al., 2021). These results suggest that the environmental seascape in the SWTA is structuring not only the small plankton communities but all the pelagic food web. According to Figueiredo et al. (2020) and Tosetto et al. (2021), zooplankton exhibited variations in community composition, abundance, and body size (measured by isotopic composition) based on the location (coast-offshore) and season (spring and fall). Figueiredo et al. (2020) found that zooplankton in the WBCS was significantly smaller, but more abundant than in the SECS, suggesting a higher grazing effect on phytoplankton in the WBCS. Tosetto et al. (2021) also observed significant variations in planktonic cnidarian communities among different areas.

Regarding diversity, our results were able only to assess general patterns. However, we observed a clear dominance of Cyanophyceae (mainly composed by *Trichodesmium* spp.) in surface waters (Carré et al., unpublished). Cyanophyceae usually thrive in oligotrophic environments and contribute significantly to the phytoplankton biomass (Lima et al., 2019). With increasing depth, a different Cyanophyceae flourished, *Prochlorococcus*, highlighting different ecotypes and possibly vertical niche partitioning in the SWTA, with taxa adapted to low-light conditions. Such spatial patterns have been previously associated with contrasting conditions of vertical mixing and stratification (Johnson et al., 2006; Zinster et al, 2007). However, in the SWTA This hypothesis needs to be confirmed by an appropriate sampling resolution. Chlorophyceae and Bacillariophyceae showed higher biomass near the shelf, potentially influenced by riverine discharges and silicate concentrations, although overall representing a small portion of the total phytoplankton biomass, the Bacillariophyceae community that belongs to microphytoplankton, displayed a high diversity (Carré et al., unpublished; see Chapter 3 supplementary materials) in line with previous reports in the coastal zone of our study area (Silva-Cunha et al., 1990). Lastly Dinophyceae biomass was considerably low, although this is likely underestimated due to their diverse trophic strategies, different pigments (Hansen, 2011; Jeong et al., 2010; Sherr and Sherr, 2007) and their higher diversity observed in the microscope (Carré et al., unpublished; see Chapter 3 supplementary materials).

Cell size is a critical ecological trait affecting various aspects of phytoplankton ecology, including diversity, production, nutrient assimilation, competition, and biomass transfer to higher trophic levels (Marañón et al., 2015). Our observations in the tropical Atlantic demonstrated a predominance of small pico- and nanophytoplankton communities, indicative of a recycling trophic web. The Fp index revealed a dominance of recycled production, with higher new production, particularly in coastal areas promoted by riverine runoffs. However, it is worth noticing that despite increased nutrient concentrations, large phytoplankton cells were not favored, instead small cells continued to dominate, possibly due to the increase in nutrients, especially nitrogen, not being enough to trigger microphytoplankton production. These smaller cells may play a significant role in the carbon pump, which is usually dominated in middle and high latitudes by large cells such as diatoms (Basu and Mackey, 2018), especially in carbon sequestration, and understanding their role is crucial to assess changes in biogeochemical cycling and food quality for pelagic food webs in a global change scenario (Basu and Mackey, 2018; Guidi et al., 2016; Weinbauer, 2004). Important to note that, the seasonal uncoupling observed here, indirectly assessed through chl-a, may not always indicate trends in phytoplankton productivity, but could rather result from cell photoacclimation (Rodríguez et al., 2006). However, the significant biomass of heterotrophic bacteria in Chapter 3 and the relationships discussed in Chapter 4 support these patterns and emphasize the importance of small plankton in the pelagic food web.

The heterotrophic biomass, an unexplored carbon pathway on the southwestern tropical Atlantic plankton food web

Our results suggest that HB biomass is important for the microbial plankton community and the overall pelagic community, as seen by Eduardo et al. (2023). The bacterioplankton usually is sustained by diverse sources of detritus and exogenous dissolved carbon, which play a crucial role in their functioning within marine ecosystems (Jordan et al., 2021). In oligotrophic systems, where phytoplankton growth is nutrient-limited, bacterioplankton can outcompete phytoplankton for resources due to their higher affinity for phosphorus (Jansson 1998, Vadstein 2000). This is due to among other factors their smaller size, and as a consequence higher surface-to-volume ratios, lower overall grazing pressure compared to phytoplankton, the recycling of organic matter, and allelopathy from bacteria (Kirchman, 1994; Hullot and Huisman, 2004; Zimmerman; Allison and Martin, 2013). Therefore, even in conditions of low nutrient concentrations bacterioplankton can still find a sufficient supply of resources to sustain

their metabolism and growth. The data used do not allow us to quantify the inputs of exogenous dissolved and particulate carbon, however, we hypothesize that organic matter from allochthonous sources, such as the Amazon River plume and the African coast upwelling reaching the southwestern tropical atlantic (Medeiros et al., 2015; Siegfried et al., 2019; Tosetto et al. unpublished) might be a major nurturing source for the plankton food web in this region.

In oligotrophic oceans, the availability of exogenous dissolved organic carbon (DOC) and particulate organic carbon (POC) have significant implications for the pelagic plankton trophic web. For example, the bacterial carbon can act as a subsidy for the food web by increasing bacterial production, thereby boosting basal energy production and the pool of carbon available for the pelagic food web. However, the input of resources may not necessarily lead to a significant increase in phytoplankton productivity, as observed by Faithful et al. (2011) in a mesocosm experiment where phytoplankton production remained similar regardless of the increase in organic carbon.

The observed increase in nutrient ratios under the euphotic layer did not show any effect on autotrophic biomass likely due to light limitation for phytoplankton (Yingling et al. 2022). Instead, it was accompanied by the enhancement of heterotrophic bacteria, which thrive in the DOC-rich mesopelagic realm (Calleja et al. 2018). Although the heterotrophic biomass in both the epipelagic and mesopelagic realms can contribute to carbon vertical fluxes through the formation of colloids and aggregates (Guidi et al. 2016; Zhang, Tang, et al. 2021), we hypothesized that a large portion of the heterotrophic carbon is redirected towards the microbial food web, specifically through mixotrophic pico- and nanoflagellates (PNF) and ciliates (especially Tintinnina).

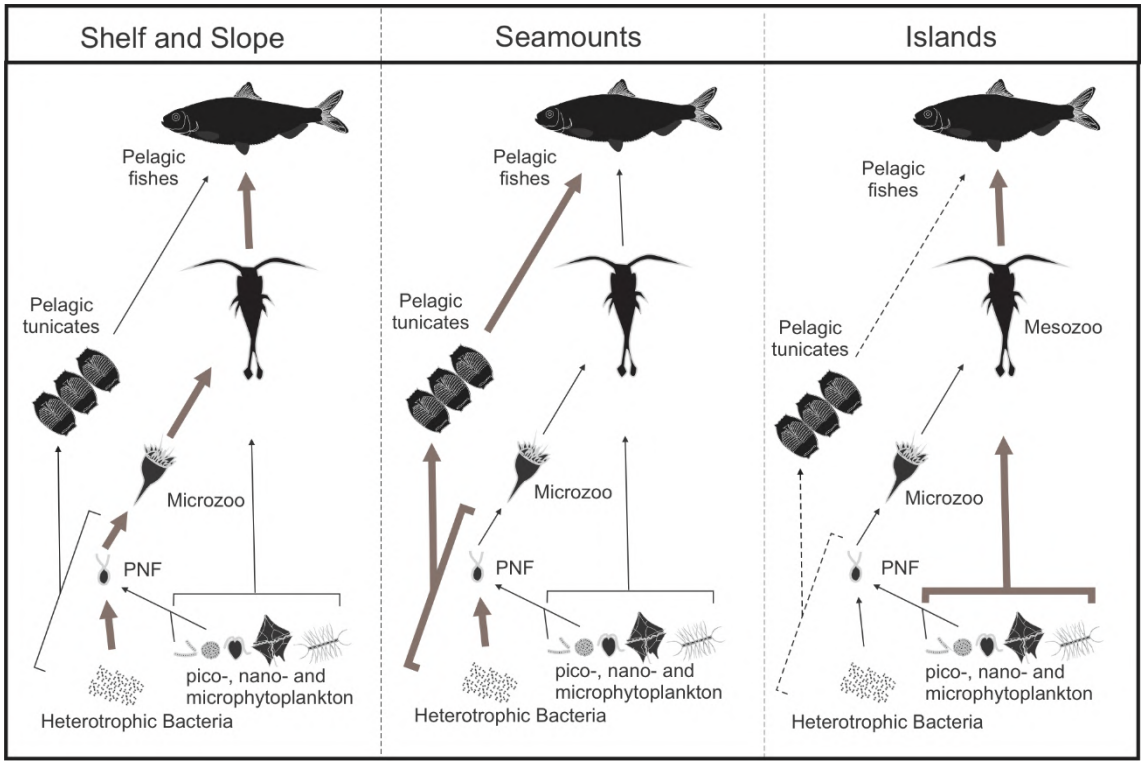

Fig. 1 Conceptual model of the hypothetical trophic pathways in the SWTA from the shelf to the oceanic islands. Brown thick lines indicate the most important hypothetical pathway of the carbon fluxes, and dashed lines indicate an irrelevant hypothetical pathway. Given the absence of direct analysis, this model does not intend to define trophic pathways in the SWTA but suggests hypothetical pathways to be tested. PNF: Pigmented nanoflagellates.

The observed values of autotrophic carbon biomass we found are of similar magnitude to previous reports from other oligotrophic oceans, ranging from 8-26 µg C L^{-1} (Mena et al. 2019; Marañón et al. 2021). However, we hypothesize that the transfer of HB biomass could enhance overall productivity and provide available carbon to other trophic compartments. The interaction observed between PNF and most microbial taxa highlight the relevance of the microbial food web in regional productivity. In line with this, recent reports on the diet of mesopelagic fishes in the SWTA support this hypothesis, indicating that they primarily consume carbon derived from HB (Eduardo et al., 2023). Furthermore, the HB biomass can be further redirected through the grazing of gelatinous zooplankton, such as Tunicates, which are abundant in the SWTA, particularly on the continental seamounts (Tosetto et al. 2022). These gelatinous micro-filter feeders play a significant role by grazing on pico- and nanoplankton, thus mediating the carbon flux towards higher trophic levels (Sutherland and Thompson 2021).

Overall, the results suggest that in the SWTA, the pelagic plankton trophic web relies on HB biomass and the microbial network (Farias et al. 2022). The distribution patterns of pico- and nanoplankton taxa, as well as other pelagic plankton organisms such as tunicates, indicate

different metabolic pathways along the coast-offshore gradient (Figure 1). Mixotrophic PNF-mediated carbon transfer appears more relevant near the shelf, where this group exhibits higher biomass. Conversely, in areas with high abundance of gelatinous tunicates, e.g., *Pyrosoma*, such as in the western seamounts, the plankton trophic web may be shortened. Additionally, the lowest heterotrophic to autotrophic biomass ratios near the islands stress the importance of autotrophic biomass as a primary energy source for epipelagic fishes (Eduardo *et al.,* 2023). In this region of the SWTA, small picoeukaryotes and microphytoplankton likely sustain biological productivity and shape trophic pathways.

The hypothetical metabolic pathways depicted in Figure 1 shape the length, energy transfer efficiency, and overall productivity of the trophic web in the SWTA (Legendre and Rassoulzadegan 1995). Consequently, there is a need for a detailed assessment of the impact of PNF grazing on pico- and nanoplankton and its effects on the microbial food web. Additionally, the proposed pathways should be tested to better understand the contribution of heterotrophic biomass to higher trophic levels and the biological carbon pump through vertical fluxes.

Open questions and future directions

These results shed light on the ecology of pico- and nanoplankton and the functioning of the Southwestern Tropical Atlantic pelagic ecosystems. They also highlight a mosaic of physical variables and ecological interactions shaping their structure. However, still, there are open questions to be contemplated. Firstly, considering the observed dominance of small-sized phytoplankton, what ecological mechanisms underlie their resilience in oligotrophic regions, and how will they respond to ongoing global ocean changes? Secondly, what are the specific environmental factors influencing the distribution and dynamics of bacterioplankton in the SWTA, and what is the extent of their contribution to carbon pathways and microbial food webs? Additionally, how do the metabolic pathways involving mixotrophic pico- and nanoflagellates and ciliates impact the transfer of heterotrophic biomass to higher trophic levels? Furthermore, understanding the interplay between pico- and nanoplankton communities and their predators, i.e. gelatinous taxa, such as tunicates, is crucial for deciphering the length and energy transfer efficiency of the trophic web. Moreover, how the thermohaline structure in the SWTA and its influence in the pelagic communities might be affected by continued climate change? resolving these questions will provide a thorough comprehension of the dynamics and ecological significance of pico- and nanoplankton in the SWTA in the face of global change.

Conclusions

In our study was possible observe that in these mesoscale current systems (WBCS and SECS) the thermohaline structures variability is one of the main features shaping spatial phytoplankton distribution and biomass.

Cell size is a critical ecological trait affecting various aspects of ecology, including diversity, production, nutrient assimilation, competition, and biomass transfer to higher trophic levels. Our observations in the tropical Atlantic demonstrated a predominance of small pico- and nanophytoplankton and heterotrophic bacteria communities, indicating a recycling trophic web. These results also point-out the importance of investigating the smallest compartments of the food web.

The results suggest that the recycling production is partially transferred to higher trophic levels through the microbial food web. However due to the mosaic in the community structure this can be variable, with different trophic structures from the shelf to the islands.

These results highlight the role of thermohaline structure controlling the structure (i.e., size, richness) and productivity of microbial communities. Finally, this thesis represents an important initial step toward modeling microbial networks in the Southwestern Tropical Atlantic.

REFERENCES

Abdi, H., & L. J. Williams. Principal component analysis. WIREs Computational Statistics 2: 433–459, 2010.

Agusti, S., Martinez-Ayala J., Regaudie-de-Gioux, A., Duarte, C.M. Oligotrophication And Metabolic Slowing-Down Of A Nw Mediterranean Coastal Ecosystem. Frontiers In Marine Science, V. 4, 2017. https://doi.org/10.3389/fmars.2017.00432.

Ajani, P. A., C. H. Davies, R. S. Eriksen, & A. J. Richardson. Global Warming Impacts Micro-Phytoplankton at a Long-Term Pacific Ocean Coastal Station. Frontiers in Marine Science 7. 2020. https://doi.org/10.3389/fmars.2020.576011.

Al-Qutob, M., Häse, C., Tilzer, M.M., Lazar, B. Phytoplankton drives nitrite dynamics in the Gulf of Aqaba, Red Sea. Mar. Ecol. Prog. Ser. 239, 233–239. 2002. https://doi.org/10/bz4r7c.

Allen, A. P., Gillooly, J. F.; Brown, J. H. Linking The Global Carbon Cycle To Individual Metabolism. Functional Ecology, V. 19, N. 2, P. 202–213, 2005. https://doi.org/10.1111/j.1365-2435.2005.00952.x.

Alma, L., K. E. Kram, G. W. Holtgrieve, A. Barbarino, C. J. Fiamengo, & J. L. Padilla-Gamiño. Ocean acidification and warming effects on the physiology, skeletal properties, and microbiome of the purple-hinge rock scallop. Comparative Biochemistry and Physiology Part A: Molecular & Integrative Physiology 240: 110579. 2020. 10.1016/j.cbpa.2019.110579.

Andersen, R.A. Biology and systematics of heterokont and haptophyte algae. Am. J. Bot. 91, 1508–1522. 2004. https://doi.org/10.3732/ajb.91.10.1508.

Andrade, L., A. M. Gonzalez, J. L. Valentin, & R. Paranhos. Bacterial Abundance and Production in the Southwest Atlantic Ocean. Hydrobiologia 511: 103–111. 2004. https://doi.org/10.1023/B:HYDR.0000014033.81848.48.

Araujo, M., Limongi, C., Servain, J., Silva, M., Leite, F.S., Veleda, D., Lentini, C.A.D. Salinity-induced mixed and barrier layers in the southwestern tropical Atlantic Ocean off the northeast of Brazil. Ocean Sci. 7, 63–73. 2011. https://doi.org/10/b3fhtj.

Araujo, M.L.V., Mendes, C.R.B., Tavano, V.M., Garcia, C.A.E., Baringer, M.O. Contrasting patterns of phytoplankton pigments and chemotaxonomic groups along 30°S in the subtropical South Atlantic Ocean. Deep Sea Res. Part Oceanogr. Res. Pap. 120, 112–121. 2017. https://doi.org/10/gf7kmx.

Arias, A., Saiz, E., Tiselius, P., and Calbet, A. Trophic interactions and diel feeding rhythms of microzooplankton in a productive Swedish Fjord. ICES Journal of Marine Science, 77, 2718–2728. 2020. https://doi.org/10.1093/icesjms/fsaa137.

Armbrecht, L. H., R. Eriksen, A. Leventer, & L. K. Armand. First observations of living sea-ice diatom agglomeration to tintinnid loricae in East Antarctica. Journal of Plankton Research 39: 795–802. 2017. https://doi.org/10.1093/plankt/fbx036.

Armengol, L., A. Calbet, G. Franchy, A. Rodríguez-Santos, & S. Hernández-León. Planktonic food web structure and trophic transfer efficiency along a productivity gradient in the tropical and subtropical Atlantic Ocean. Scientific Reports Nature Publishing Group 9: 2044. 2019. https://doi.org/10.1038/s41598-019-38507-9.

Assunção, R.V., Silva, A.C., Roy, A., Bourlès, B., Silva, C.H.S., Ternon, J.-F., Araujo, M., Bertrand, A., 3D characterisation of the thermohaline structure in the southwestern tropical Atlantic derived from functional data analysis of in situ profiles. Prog. Oceanogr. 187, 102399. 2020. https://doi.org/10.1016/j.pocean.2020.102399.

Atkinson, D.; Ciotti, B. J.; Montagnes, D. J. S. Protists Decrease In Size Linearly With Temperature: Ca. 2.5% °C−1. Proceedings Of The Royal Society Of London. Series B: Biological Sciences, V. 270, N. 1533, P. 2605–2611, 22 Dez. 2003. https://doi.org/10.1098/rspb.2003.2538.

Atkinson, A., R. A. Harmer, C. E. Widdicombe, A. J. McEvoy, T. J. Smyth, D. G. Cummings, P. J. Somerfield, J. L. Maud, & K. McConville. Questioning the role of phenology shifts and trophic mismatching in a planktonic food web. Progress in Oceanography 137: 498–512. 2015. https://doi.org/10.1016/j.pocean.2015.04.023.

Azam, F.; Malfatti, F. Microbial Structuring Of Marine Ecosystems. Nature Reviews Microbiology, V. 5, N. 10, P. 782, 2007. https://doi.org/10.1038/nrmicro1747.

Bachiller, E., M. Albo-Puigserver, J. Giménez, M. G. Pennino, N. Marí-Mena, A. Esteban, E. Lloret-Lloret, A. Jadaud, B. Carro, J. M. Bellido, & M. Coll. A trophic latitudinal gradient revealed in anchovy and sardine from the Western Mediterranean Sea using a multi-proxy approach. Scientific Reports Nature Publishing Group 10: 17598. 2020. https://doi.org/10.1038/s41598-020-74602-y.

Barton, A.D., Pershing, A.J., Litchman, E., Record, N.R., Edwards, K.F., Finkel, Z.V., Kiorboe, T., Ward, B.A. The biogeography of marine plankton traits. Ecol Lett 16, 522–534. https://doi.org/10/f4sqgs. 2013

Basu, S., & Mackey, K. R. M. Phytoplankton as key mediators of the biological carbon pump: their responses to a changing climate. Sustainability 10: 869. 2018. https://doi.org/10.3390/su10030869.

Batten, S. D. et al. A Global Plankton Diversity Monitoring Program. Frontiers In Marine Science, V. 6, 2019. https://doi.org/10.3389/fmars.2019.00321.

Baum, J. K. and Worm, B. Cascading top-down effects of changing oceanic predator abundances. Journal of Animal Ecology, 78, 699–714. 2009. https://doi.org/10.1111/j.1365-2656.2009.01531.x.

Beaugrand, G. Toward A Better Understanding Of The Influence Of Marine Biodiversity On Ecosystem Functioning. 2013.

Behrenfeld, M. J. et al. Climate-Driven Trends In Contemporary Ocean Productivity. Nature, V. 444, N. 7120, P. 752–755, Dez. 2006. https://doi.org/10.1038/nature05317.

Bell, T., Kalff, J. The contribution of picophytoplankton in marine and freshwater systems of different trophic status and depth. Limnol. Oceanogr. 46, 1243–1248. https://doi.org/10.4319/lo.2001.46.5.1243. 2001.

Benedetti, F., S. Gasparini, & S. D. Ayata. Identifying copepod functional groups from species functional traits. Journal of Plankton Research 38: 159–166. 2016. https://doi.org/10.1093/plankt/fbv096.

Berglund, J. Et Al. Efficiency Of A Phytoplankton-Based And A Bacterial-Based Food Web In A Pelagic Marine System. Limnology And Oceanography, V. 52, N. 1, P. 121–131, Jan. 2007. https://doi.org/10.4319/lo.2007.52.1.0121.

Bertrand, A. ABRACOS cruise, Antea R/V. 2015. https://doi.org/10.17600/15005600.

Bertrand, A. ABRACOS 2 cruise, Antea R/V. 2017. https://doi.org/10.17600/17004100.

Berube, P.M., Coe, A., Roggensack, S.E., Chisholm, S.W. Temporal dynamics of *Prochlorococcus* cells with the potential for nitrate assimilation in the subtropical Atlantic and Pacific oceans. Limnol. Oceanogr. 61, 482–495. 2016. https://doi.org/10.1002/lno.10226.

Boden, B.P. Observations of the island mass effect in the Prince Edward archipelago. Polar Biol. 9, 61–68. https://doi.org/10.1007/BF00441765. 1988

Bonecker, A. C. T.; Bonecker, S. L.; Bassani, C. Plâncton Marinho. Em: Pereira, R. C.; Soares-Gomes, A. (Eds.). Biologia Marinha. [S.L.] Interciência, 2002. https://doi.org/10.1038/330035a0.

Boyce, D. G., Frank, K. T., Worm, B., and Leggett, W. C. Spatial patterns and predictors of trophic control in marine ecosystems. Ecology Letters, 18, 1001–1011. 2015. https://doi.org/10.1111/ele.12481.

Boyle, E. A.; Keigwin, L. North Atlantic Thermohaline Circulation During The Past 20,000 Years Linked To High-Latitude Surface Temperature. Nature, V. 330, N. 6143, P. 35–40, Nov. 1987. https://doi.org/10.1038/330035a.

Brandini, F. P. Produção primária e características fotossintéticas do fitoplâncton na região sueste do Brasil. Bol.Inst.Oceanogr.Sao Paulo 38: 147–159. 1990. https://doi.org/10.1590/S0373-55241990000200004.

Brandini, F. P. Phytoplankton Assemblages of the Subtropical South West Atlantic: Composition and Dynamics in Relation to Physical and Chemical Processes In Hoffmeyer, M. S., M. E. Sabatini, F. P. Brandini, D. L. Calliari, & N. H. Santinelli (eds), Plankton Ecology of the Southwestern Atlantic: From the Subtropical to the Subantarctic Realm. Springer International Publishing, Cham: 129–148. 2018. https://doi.org/10.1007/978-3-319-77869-3_7.

Brierley, A. S.; Kingsford, M. J. Impacts Of Climate Change On Marine Organisms And Ecosystems. Current Biology, V. 19, N. 14, P. R602–R614, 28 Jul. 2009. 10.1016/j.cub.2009.05.046.

Buitenhuis, E. T., W. K. W. Li, M. W. Lomas, D. M. Karl, M. R. Landry, & S. Jacquet. Picoheterotroph (Bacteria and Archaea) biomass distribution in the global ocean. Earth System Science Data 4: 101–106. 2012a. https://doi.org/10.5194/essd-4-101-2012.

Buitenhuis, E. T., W. K. W. Li, D. Vaulot, M. W. Lomas, M. R. Landry, F. Partensky, D. M. Karl, O. Ulloa, L. Campbell, S. Jacquet, F. Lantoine, F. Chavez, D. Macias, M. Gosselin, & G. B. McManus. Picophytoplankton biomass distribution in the global ocean. Earth System Science Data Copernicus GmbH 4: 37–46. 2012b. https://doi.org/10.5194/essd-4-37-2012.

Bullock, H. A.; Luo, H.; Whitman, W. B. Evolution of Dimethylsulfoniopropionate Metabolism In Marine Phytoplankton And Bacteria. Frontiers In Microbiology, V. 8, 19 Abr. 2017. https://doi.org/10.3389/fmicb.2017.00637.

Burson, A., Stomp, M., Greenwell, E., Grosse, J., Huisman, J. Competition for nutrients and light: testing advances in resource competition with a natural phytoplankton community. Ecology 99, 1108–1118. 2018. https://doi.org/10.1002/ecy.2187.

Cabral, A. De S.; Andrade, L.; Paranhos, R. Virioplâncton E Bacterioplâncton: Descritores Espaciais E Temporais. Em: Falcão, A. P. C.; Moreira, D. L. (Eds.). Ambiente Pelágico: Caracterização Ambiental Regional Da Bacia De Campos, Atlântico Sudoeste. Rio De Janeiro: Elsevier. V. 5p. 29–42. 2017. https://doi.org/10.1016/B978-85-352-7276-5.50010-5.

Cabrera, O., Villanoy, C., David, L., Gordon, A. Barrier Layer Control of Entrainment and Upwelling in the Bohol Sea, Philippines. Oceanography 24, 130–141. 2011. https://doi.org/10/cvppt7.

Calfee, B. C., L. D. Glasgo, & E. R. Zinser. *Prochlorococcus* Exudate Stimulates Heterotrophic Bacterial Competition with Rival Phytoplankton for Available Nitrogen. mBio American Society for Microbiology 13: e02571-21. 2022. https://doi.org/10.3389/fmicb.2017.00637.

Calleja, M. L., M. I. Ansari, A. Røstad, L. Silva, S. Kaartvedt, X. Irigoien, & X. A. G. Morán. The Mesopelagic Scattering Layer: A Hotspot for Heterotrophic Prokaryotes in the Red Sea Twilight Zone. Frontiers in Marine Science 5:, 2018. https://www.frontiersin.org/articles/10.3389/fmars.2018.00259.

Calvo-Díaz, A., & X. A. G. Morán. Seasonal dynamics of picoplankton in shelf waters of the southern Bay of Biscay. Aquatic Microbial Ecology 42: 159–174. 2006. doi:10.3354/ame042159.

Capone, D. G. Et Al. Nitrogen Fixation By Trichodesmium Spp.: An Important Source Of New Nitrogen To The Tropical And Subtropical North Atlantic Ocean. Global Biogeochemical Cycles, V. 19, N. 2, 2005. https://doi.org/10.1029/2004GB002331.

Castello, J.P. O futuro da pesca da aquicultura marinha no Brasil: a pesca costeira. Ciênc. E Cult. 62, 32–35. 2010.

Castro, P.; Huber, M. E. Biologia Marinha - 8ed. [S.L.] Amgh Editora, 2012.

Chaves, T., Mafalda, J., Santos, C., Souza, C., Moura, G., Sampaio, J., Melo, G., Passavante, J., Feitosa, F. Planktonic biomass and hydrography in the Exclusive Economic Zone of Brazilian Northeast. Trop. Oceanogr. Online 34, 12–30. 2006.

Chen, B., H. Liu, M. R. Landry, M. DaI, B. Huang, & J. Sune. Close coupling between phytoplankton growth and microzooplankton grazing in the western South China Sea. Limnology and Oceanography 54: 1084–1097. 2009. https://doi.org/10.4319/lo.2009.54.4.1084.

Chen, X. et al. Eddy-Induced Pycnocline Depth Displacement Over The Global Ocean. Journal Of Marine Systems, V. 221, P. 103577, 1 Set. 2021. https://doi.org/10.1016/j.jmarsys.2021.103577.

Cheng, C. et al. Modeling The Thermal Processes Within The Ice Shelf–Ocean Boundary Current Underlain By Strong Pycnocline Underneath A Cold-Water Ice Shelf Using A 2.5-Dimensional Vertical Slice Model. Ocean Modelling, V. 177, P. 102079, 1 Set. 2022. https://doi.org/10.1016/j.ocemod.2022.102079.

Chisholm, S.W. Phytoplankton Size, in: Falkowski, P.G., Woodhead, A.D., Vivirito, K. (Eds.), Primary Productivity and Biogeochemical Cycles in the Sea, Environmental Science Research. Springer US, Boston, MA, pp. 213–237. 1992. https://doi.org/10.1007/978-1-4899-0762-2_12.

Christaki, U., E. Vázquez-Domínguez, C. Courties, & P. Lebaron. Grazing impact of different heterotrophic nanoflagellates on eukaryotic (*Ostreococcus tauri*) and prokaryotic picoautotrophs (*Prochlorococcus* and *Synechococcus*). Environmental Microbiology 7: 1200–1210. 2005. https://doi.org/10.1111/j.1462-2920.2005.00800.x.

Christaki, U., F. Van Wambeke, & J. Dolan. Nanoflagellates (mixotrophs, heterotrophs and autotrophs) in the oligotrophic eastern Mediterranean:standing stocks, bacterivory and relationships with bacterial production. Marine Ecology Progress Series 181: 297–307. 1999. doi:10.3354/meps181297.

Churilova, T. Et Al. Phytoplankton Light Absorption In The Deep Chlorophyll Maximum Layer Of The Black Sea. European Journal Of Remote Sensing, V. 52, N. Sup1, P. 123–136, 28 Mar. 2019. https://doi.org/10.1080/22797254.2018.1533389.

Clarke, K. R., & R. M. Warwick. Similarity-based testing for community pattern: the two-way layout with no replication. Marine Biology 118: 167–176. 1994. https://doi.org/10.1007/BF00699231.

Clarke, K.R., Gorley, R.N. PRIMER V6: user manual-tutorial. Plymouth Marine Laboratory. 2006.

Claustre, H. The trophic status of various oceanic provinces as revealed by phytoplankton pigment signatures. Limnol. Oceanogr. 39, 1206–1210. 1994. https://doi.org/10/fj9bb6.

Costa da Silva, A., A. Chaigneau, A. N. Dossa, G. Eldin, M. Araujo, & A. Bertrand. Surface Circulation and Vertical Structure of Upper Ocean Variability Around Fernando de Noronha Archipelago and Rocas Atoll During Spring 2015 and Fall 2017. Frontiers in Marine Science 8:, https://www.frontiersin.org/article/10.3389/fmars.2021.598101. 2021

D'Alelio, D., Mazzocchi, M. G., Montresor, M., Sarno, D., Zingone, A., Di Capua, I., Franzè, G., Margiotta, F., et al. The green–blue swing: plasticity of plankton food-webs in response to coastal oceanographic dynamics. Marine Ecology, 36, 1155–1170. 2015. https://doi.org/10.1111/maec.12211.

da Silveira, I.C.A., Schmidt, A.C.K., Campos, E.J.D., de Godoi, S.S., Ikeda, Y. A corrente do Brasil ao largo da costa leste brasileira. Rev Bras Ocean 48, 171–183. 2000. https://doi.org/10/gf4mq3.

Dai, S., Zhao, Y., Li, X., Wang, Z., Zhu, M., Liang, J., Liu, H., Tian, Z., Sun, X. The seamount effect on phytoplankton in the tropical western Pacific. Mar. Environ. Res. 105094. 2020. https://doi.org/10/gg72jv

Dandonneau, Y., Deschamps, P.Y., Nicolas, J.M., Loisel, H., Blanchot, J., Montel, Y., Thieuleux, F., Bécu, G. Seasonal and interannual variability of ocean color and composition of phytoplankton communities in the North Atlantic, equatorial Pacific and South Pacific. Deep Sea Res. Part II Top. Stud. Oceanogr., Views of Ocean Processes from the Sea-viewing Wide Field-of-view Sensor (SeaWiFS) Mission: Volume 1 51, 303–318. 2004. https://doi.org/10.1016/j.dsr2.2003.07.018.

Danovaro, R. et al. Marine Viruses And Global Climate Change. Fems Microbiology Reviews, V. 35, N. 6, P. 993–1034, 1 Nov. 2011. https://doi.org/10.1111/j.1574-6976.2010.00258.x.

Dao, M. H. Trait-based numerical model for mixotrophic phytoplankton and application in Singapore water. arXiv:2106.08227 [physics]. 2021. https://doi.org/10.48550/arXiv.2106.08227.

Das, S., Lyla, P. S., and Khan, S. A. Marine microbial diversity and ecology: importance and future perspectives. Current Science, 90, 1325–1335. 2006.

del Giorgio, P. A., D. F. Bird, Y. T. Prairie, & D. Planas. Flow cytometric determination of bacterial abundance in lake plankton with the green nucleic acid stain SYTO 13. Limnology and Oceanography 41: 783–789. 1996. https://doi.org/10.4319/lo.1996.41.4.0783.

Dixon, P. VEGAN, a package of R functions for community ecology. Journal of Vegetation Science Wiley Online Library 14: 927–930. 2003.

Dinh, N. V., B. E. Casareto, M. P. Niraula, K. Toyoda, A. Meekaew, & Y. Suzuki;mEffect of diatom abundance and biogenic silica availability on the population growth of tintinnid ciliates at Suruga Bay. Journal of Oceanography 77: 307–321. 2021. https://doi.org/10.1007/s10872-020-00569-z.

Dossa, A. N., A. C. Silva, A. Chaigneau, G. Eldin, M. Araujo, & A. Bertrand. Near-surface western boundary circulation off Northeast Brazil. Progress in Oceanography 190: 102475. 2021. https://doi.org/10.1016/j.pocean.2020.102475.

Doty, M.S., Oguri, M. The island mass effect. ICES J. Mar. Sci. 22, 33–37. 1956 https://doi.org/10.1093/icesjms/22.1.33.

Duarte, C. M., A. Regaudie-de-Gioux, J. M. Arrieta, A. Delgado-Huertas, & S. Agustí. The oligotrophic ocean is heterotrophic. Annual Review of Marine Science Annual Reviews 5: 551–569. 2013. https://doi.org/10.1146/annurev-marine-121211-172337.

Ducklow, H. W.; Steinberg, D. K.; Buesseler, K. O. Upper Ocean Carbon Export And The Biological Pump. Oceanography, V. 14, 2001.

Duffy, J. E., Reynolds, P. L., Boström, C., Coyer, J. A., Cusson, M., Donadi, S., Douglass, J. G., Eklöf, J. S., et al. Biodiversity mediates top–down control in eelgrass ecosystems: a global comparative-experimental approach. Ecology Letters, 18, 696–705. 2015. https://doi.org/10.1111/ele.12448.

DuRand, M. D., R. J. Olson, & S. W. Chisholm. Phytoplankton population dynamics at the Bermuda Atlantic Time-series station in the Sargasso Sea. Deep Sea Research Part II: Topical Studies in Oceanography 48: 1983–2003. 2001. https://doi.org/10.1016/S0967-0645(00)00166-1.

Eddy, T. D. et al. Energy Flow Through Marine Ecosystems: Confronting Transfer Efficiency. Trends In Ecology & Evolution, V. 36, N. 1, P. 76–86, 1 Jan. 2021. https://doi.org/10.1016/j.tree.2020.09.006.

Edwards, K. F. Mixotrophy in Nanoflagellates Across Environmental Gradients In The Ocean. Proceedings of the National Academy Of Sciences, V. 116, N. 13, P. 6211–6220, 26 Mar. 2019. https://doi.org/10.1073/pnas.181486011.

Edwards, M. Plankton And Global Change. Marine Plankton: A Practical Guide To Ecology, Methodology, And Taxonomy. Oxford University Press, Oxford, P. 67–80, 2017.

Egge, J.K. Are diatoms poor competitors at low phosphate concentrations? J. Mar. Syst. 16, 191–198. 1998. https://doi.org/10/d3747t.

Ekau, W., Knoppers, B. An introduction to the pelagic system of the North-East and East Brazilian shelf. Arch. Fish. Mar. Res. 47, 113–132. 1999.

Ersoy, Z., Brucet, S., Bartrons, M., and Mehner, T. Short-term fish predation destroys resilience of zooplankton communities and prevents recovery of phytoplankton control by zooplankton grazing. PLOS ONE, 14, e0212351. 2019. https://doi.org/10.1371/journal.pone.0212351.

Falkowski, P.G., Oliver, M.J. Mix and match: how climate selects phytoplankton. Nat. Rev. Microbiol. 5, 813–819. 2007. https://doi.org/10/chrd2m.

Farias, G. B., Molinero, J.-C., Carré, C., Bertrand, A., Bec, B., and Melo, P. A. M. de C. Uncoupled changes in phytoplankton biomass and size structure in the western tropical Atlantic. Journal of Marine Systems, 227, 103696. 2022. https://doi.org/10.1016/j.jmarsys.2021.103696.

Feld, C. K., P. Segurado, & C. Gutiérrez-Cánovas. Analysing the impact of multiple stressors in aquatic biomonitoring data: A 'cookbook' with applications in R. Science of The Total Environment 573: 1320–1339. 2016. https://doi.org/10.1016/j.scitotenv.2016.06.243.

Fenchel, T. The Microbial food web – 25 Years Later. Journal Of Experimental Marine Biology And Ecology, Marine Ecology: A Tribute To The Life And Work Of John S. Gray. V. 366, N. 1, P. 99–103, 15 Nov. 2008. https://doi.org/10.1016/j.jembe.2008.07.013.

Fernandes, L. F. L., Paiva, T. R. M., Longhini, C. M., Pereira, J. B., Ghisolfi, R. D., Lázaro, G. C. S., Demoner, L. E., Laino, P. de S., et al. Marine zooplankton dynamics after a major mining dam rupture in the Doce River, southeastern Brazil: Rapid response to a changing environment.

Science of The Total Environment, 736, 139621. 2020. https://doi.org/10.1016/j.scitotenv.2020.139621.

Feucher, C.; Maze, G.; Mercier, H. Subtropical Mode Water and Permanent Pycnocline Properties In The World Ocean. Journal Of Geophysical Research: Oceans, V. 124, N. 2, P. 1139–1154, 2019. https://doi.org/10.1029/2018JC014526.

Field, C. B. Et Al. Primary Production of The Biosphere: Integrating Terrestrial And Oceanic Components. Science, V. 281, N. 5374, P. 237–240, 1998. 10.1126/science.281.5374.237.

Figueiredo, G.G.A.A. de, Schwamborn, R., Bertrand, A., Munaron, J.M., Le Loc'h, F. Body size and stable isotope composition of zooplankton in the western tropical Atlantic. J. Mar. Syst. 212, 103449. 2020. https://doi.org/10.1016/j.jmarsys.2020.103449.

Finkel, Z.V., Beardall, J., Flynn, K.J., Quigg, A., Rees, T.A.V., Raven, J.A. Phytoplankton in a changing world: cell size and elemental stoichiometry. J. Plankton Res. 32, 119–137. 2010. https://doi.org/10/bb25d7.

Fitzer, S. C. et al. Ocean Acidification Alters tyhe Material Properties Of Mytilus Edulis Shells. Journal Of The Royal Society Interface, V. 12, N. 103, P. 20141227, 6 Fev. 2015. https://doi.org/10.1098/rsif.2014.1227.

Flombaum, P., Gallegos, J.L., Gordillo, R.A., Rincón, J., Zabala, L.L., Jiao, N., Karl, D.M., Li, W.K.W., Lomas, M.W., Veneziano, D., Vera, C.S., Vrugt, J.A., Martiny, A.C. Present and future global distributions of the marine Cyanobacteria *Prochlorococcus* and *Synechococcus.* Proc. Natl. Acad. Sci. 110, 9824–9829. 2013. https://doi.org/10/f436jc.

Flombaum, P., W.-L. Wang, F. W. Primeau, & A. C. Martiny. Global picophytoplankton niche partitioning predicts overall positive response to ocean warming. Nature Geoscience Nature Publishing Group 13: 116–120. 2020. https://doi.org/10.1038/s41561-019-0524-2.

Flynn, K. J. et al. Misuse Of The Phytoplankton–Zooplankton Dichotomy: The Need To Assign Organisms As Mixotrophs Within Plankton Functional Types. Journal Of Plankton Research, V. 35, N. 1, P. 3–11, 1 Jan. 2013. https://doi.org/10.1093/plankt/fbs062.

Follett, C. L., S. Dutkiewicz, F. Ribalet, E. Zakem, D. Caron, E. V. Armbrust, & M. J. Follows. Trophic interactions with heterotrophic bacteria limit the range of Prochlorococcus. Proceedings of the National Academy of Sciences National Academy of Sciences 119:, 2022. https://www.pnas.org/content/119/2/e2110993118.

Frischkorn, K. R., S. T. Haley, & S. T. Dyhrman. Coordinated gene expression between Trichodesmium and its microbiome over day–night cycles in the North Pacific Subtropical Gyre. The ISME Journal Nature Publishing Group 12: 997–1007. 2018. https://doi.org/10.1038/s41396-017-0041-5.

Fuentes, M. S., Meseck, S. L., Wikfors, G. H., and Khan-Bureau, D. Silicon limitation induces colony formation in the benthic diatom Nitzschia cf. pusilla (Bacillariales, Bacillariophyceae). Diatom Research, 30, 87–92. 2015. https://doi.org/10.1080/0269249X.2014.960006.

Fuhrman, J. Bacterioplankton Roles in Cycling of Organic Matter: The Microbial Food Web In Falkowski, P. G., A. D. Woodhead, & K. Vivirito (eds), Primary Productivity and Biogeochemical Cycles in the Sea. Springer US, Boston, MA: 361–383. 1992. https://doi.org/10.1007/978-1-4899-0762-2_20.

Fukuda, R., H. Ogawa, T. Nagata, & I. Koike. Direct Determination of Carbon and Nitrogen Contents of Natural Bacterial Assemblages in Marine Environments. Applied and Environmental Microbiology 64: 3352–3358. 1998. https://doi.org/10.1128/AEM.64.9.3352-3358.1998.

Gasol, J. M., P. A. del Giorgio, & C. M. Duarte. Biomass distribution in marine planktonic communities. Limnology and Oceanography 42: 1353–1363. 1997. https://doi.org/10.4319/lo.1997.42.6.1353.

Gérikas Ribeiro, C., D. Marie, A. Lopes dos Santos, F. Pereira Brandini, & D. Vaulot. Estimating microbial populations by flow cytometry: Comparison between instruments: Estimating microbial populations by FCM. Limnology and Oceanography: Methods 14: 750–758. 2016. https://doi.org/10.1002/lom3.10135.

Giorgio, P. Del; Williams, P. Respiration in Aquatic Ecosystems. [S.L.] Oup Oxford, 2005.

Gissi, E. et al. A Review of The Combined Effects Of Climate Change And Other Local Human Stressors On The Marine Environment. Science Of The Total Environment, V. 755, P. 142564, 10 Fev. 2021. https://doi.org/10.1016/j.scitotenv.2020.142564.

Glibert, P. M. Margalef Revisited: A New Phytoplankton Mandala Incorporating Twelve Dimensions, Including Nutritional Physiology. Harmful Algae, V. 55, P. 25–30, 1 Maio 2016. https://doi.org/10.1016/j.hal.2016.01.008.

Gogoi, P., Das, S. K., Das Sarkar, S., Chanu, T. N., Manna, R. K., Sengupta, A., Raman, R. K., Samanta, S., et al. Environmental factors driving phytoplankton assemblage pattern and diversity: insights from Sundarban eco-region, India. Ecohydrology & Hydrobiology, 21, 354–367. 2021. https://doi.org/10.1016/j.ecohyd.2020.09.005.

Grasshoff, Klaus, M. Ehrhardt, e K. Kremling. Methods of seawater analysis. Weinheim: Verlag Chemie, 1983.

Grattan, L. M.; Holobaugh, S.; Morris, J. G. Harmful Algal Blooms And Public Health. Harmful Algae, Harmful Algal Blooms And Public Health. V. 57, P. 2–8, 1 Jul. 2016. https://doi.org/10.1016/j.hal.2016.05.003.

Gregg, W.W., Casey, N.W. Modeling coccolithophores in the global oceans. Deep Sea Res. Part II Top. Stud. Oceanogr., The Role of Marine Organic Carbon and Calcite Fluxes in Driving Global Climate Change, Past and Future 54, 447–477. 2007. https://doi.org/10/fxbzsg.

Grimaud, G. M. Et Al. Modeling The Temperature Effect On The Specific Growth Rate Of Phytoplankton: A Review. Reviews In Environmental Science And Bio/Technology, V. 16, N. 4, P. 625–645, 1 Dez. 2017. https://doi.org/10.1007/s11157-017-9443-0.

Grossart, H.-P. Ecological consequences of bacterioplankton lifestyles: changes in concepts are needed. Environmental Microbiology Reports, 2, 706–714. 2010. https://doi.org/10.1111/j.1758-2229.2010.00179.x.

Gu, Z., L. Gu, R. Eils, M. Schlesner, & B. Brors, 2014. Circlize implements and enhances circular visualization in R. Bioinformatics Oxford University Press 30: 2811–2812. 2014.

Guenther, M., Costa, A. E. S. F., Pessoa-Fidelis, V. T., Neumann-Leitão, S., Guenther, M., Costa, A. E. S. F., Pessoa-Fidelis, V. T., and Neumann-Leitão, S. Seasonal variations in plankton trophic structure under highly eutrophic conditions. Mar. Freshwater Res., 71, 641–652. 2019. https://doi.org/10.1071/MF18449.

Guidi, L., S. Chaffron, L. Bittner, D. Eveillard, A. Larhlimi, S. Roux, Y. Darzi, S. Audic, L. Berline, J. Brum, L. P. Coelho, J. C. I. Espinoza, S. Malviya, S. Sunagawa, C. Dimier, S. Kandels-Lewis, M. Picheral, J. Poulain, S. Searson, coordinators Tara Oceans, L. Stemmann, F. Not, P. Hingamp, S. Speich, M. Follows, L. Karp-Boss, E. Boss, H. Ogata, S. Pesant, J. Weissenbach, P. Wincker, S. G. Acinas, P. Bork, C. de Vargas, D. Iudicone, M. B. Sullivan, J. Raes, E. Karsenti, C. Bowler, & G. Gorsky, Plankton networks driving carbon export in the oligotrophic ocean. Nature 532: 465–470. 2016. https://doi.org/10.1038/nature16942.

Guo, C., Li, S., Ke, J., Liao, C., Hansen, A. G., Jeppesen, E., Zhang, T., Li, W., et al. The feeding habits of small-bodied fishes mediate the strength of top-down effects on plankton and water quality in shallow subtropical lakes. Water Research, 233, 119705. 2023. https://doi.org/10.1016/j.watres.2023.119705.

Halpern, B. S., Cottenie, K., and Broitman, B. R. Strong Top-Down Control in Southern California Kelp Forest Ecosystems. Science, 312, 1230–1232. 2006. DOI: 10.1126/science.1128613.

Hanley, T. C.; Pierre, K. J. L. Trophic Ecology. [S.L.] Cambridge University Press, 2015.

Hansen, P.J. The Role of Photosynthesis and Food Uptake for the Growth of Marine Mixotrophic Dinoflagellates1. J. Eukaryot. Microbiol. 58, 203–214. 2011. https://doi.org/10/d9czss.

Harris, R. et Aa. Ices Zooplankton Methodology Manual. Academic Press, 2000.

Harvey, E. L.,.The impact of predator-prey relationships on the formation of harmful algal blooms in Heterosigma akashiwo. University of Rhode Island. 2013.

Hartmann, M., C. Grob, G. A. Tarran, A. P. Martin, P. H. Burkill, D. J. Scanlan, & M. V. Zubkov, Mixotrophic basis of Atlantic oligotrophic ecosystems. Proceedings of the National Academy of Sciences Proceedings of the National Academy of Sciences 109: 5756–5760. 2012. https://doi.org/10.1073/pnas.1118179109.

Hasegawa, D., Yamazaki, H., Ishimaru, T., Nagashima, H., Koike, Y. Apparent phytoplankton bloom due to island mass effect. J. Mar. Syst., Physical-Biological Interactions in the Upper Ocean 69, 238–246. 2008. https://doi.org/10.1016/j.jmarsys.2006.04.019.

Hastie, T., Tibshirani, R. Generalized Additive Models: Some Applications. Journal of the American Statistical Association 82, 371–386. 1987. https://doi.org/10.1080/01621459.1987.10478440.

Hawco, N.J., Fu, F., Yang, N., Hutchins, D.A., John, S.G. Independent iron and light limitation in a low-light-adapted Prochlorococcus from the deep chlorophyll maximum. ISME J. 15, 359–362. 2021. https://doi.org/10.1038/s41396-020-00776-y.

Hazin, F.H.V. Coleção Programa REVIZEE Score Nordeste. Martins & Cordeiro. 2009.

Henson, S. A. et al. Future Phytoplankton Diversity In A Changing Climate. Nature Communications, V. 12, N. 1, P. 5372, 10 Set. 2021. https://doi.org/10.1038/s41467-021-25699-w.

Hickman, A. et al. Primary Production and Nitrate Uptake Within The Seasonal Thermocline Of A Stratified Shelf Sea. Marine Ecology Progress Series, V. 463, P. 39–57, 30 Ago. 2012.

Hillebrand, H. et al. Cell Size as Driver And Sentinel Of Phytoplankton Community Structure And Functioning. Functional Ecology, V. 36, N. 2, P. 276–293, 2022.

Höfer, J. et al. The Role of Water Column Stability And Wind Mixing In The Production/Export Dynamics Of Two Bays In The Western Antarctic Peninsula. Progress In Oceanography, Subantarctic and Antarctic Marine Ecosystems: Outlining Patterns And Processes In A Changing Ocean. V. 174, P. 105–116, 1 Maio 2019.

Hooker, S.B., Rees, N.W., Aiken, J. An objective methodology for identifying oceanic provinces. Prog. Oceanogr. 45, 313–338. 2000. https://doi.org/10/fns4hr.

Hulot, F. D., & Huisman, J. Allelopathic interactions between phytoplankton species: the roles of heterotrophic bacteria and mixing intensity. Limnology and Oceanography, 49(4part2), 1424-1434. 2004. https://doi.org/10.4319/lo.2004.49.4_part_2.1424.

Hunt, G. L. and McKinnell, S. Interplay between top-down, bottom-up, and wasp-waist control in marine ecosystems. Progress in Oceanography, 68, 115–124. 2006. https://doi.org/10.1016/j.pocean.2006.02.008.

Husson, F., J. Josse, S. Le, J. Mazet, & M. F. Husson. Package 'factominer.' An R package 96: 698. 2016.

Hutchinson, G. E. The Paradox of The Plankton. The American Naturalist, V. 95, N. 882, P. 137–145, 1961.

Ishwaran, H., U. B. Kogalur, & M. U. B. Kogalur. Package 'randomForestSRC.' breast 6: 1. 2022.

Islabão, C.A., Mendes, C.R.B., Detoni, A.M.S., Odebrecht, C. Phytoplankton community structure in relation to hydrographic features along a coast-to-offshore transect on the SW Atlantic Continental Shelf. Cont. Shelf Res. 151, 30–39. 2017. https://doi.org/10/ggs2dn.

Jacox, M. G., Hazen, E. L., and Bograd, S. J. Optimal Environmental Conditions and Anomalous Ecosystem Responses: Constraining Bottom-up Controls of Phytoplankton Biomass in the California Current System. Sci Rep, 6, 27612. 2016. https://doi.org/10.1038/srep27612.

Jales, M. C., Feitosa, F. A. do N., Koening, M. L., Montes, M. de J. F., Araújo, M. C. de, and Silva, R. A. da Phytoplankton biomass dynamics and environmental variables around the Rocas Atoll Biological Reserve, South Atlantic. Braz. j. oceanogr., 63, 443–454. 2015. https://doi.org/10.1590/S1679-87592015093906304.

Jardine, J., Palmer, M., Mahaffey, C., Holt, J., Mellor, A., Wakelin, S. Rainfall as a trigger for stratification and winter phytoplankton growth in temperate shelf seas 19, 6828. 2017.

Jeong, H.J., Yoo, Y.D., Kim, J.S., Seong, K.A., Kang, N.S., Kim, T.H. Growth, feeding and ecological roles of the mixotrophic and heterotrophic dinoflagellates in marine planktonic food webs. Ocean Sci. J. 45, 65–91. 2010. https://doi.org/10/c7sjzw.

Jiang, Z. et al. Phytoplankton Biomass and Size Structure in Xiangshan Bay, China: Current State And Historical Comparison Under Accelerated Eutrophication And Warming. Marine Pollution Bulletin, V. 142, P. 119–128, 1 Maio 2019. https://doi.org/10.1016/j.marpolbul.2019.03.013.

Jiao, N., Y. Yang, H. Koshikawa, & M. Watanabe. Influence of hydrographic conditions on picoplankton distribution in the East China Sea. Aquatic Microbial Ecology 30: 37–48. 2002. doi:10.3354/ame030037.

Jonkers, L.; Hillebrand, H.; Kucera, M. Global Change Drives Modern Plankton Communities Away From The Pre-Industrial State. Nature, V. 570, N. 7761, P. 372–375, Jun. 2019. https://doi.org/10.1038/s41586-019-1230-3.

Johnson, Z. I., Zinser, E. R., Coe, A., McNulty, N. P., Woodward, E. M. S., & Chisholm, S. W. Niche partitioning among *Prochlorococcus* ecotypes along ocean-scale environmental gradients. Science, 311(5768), 1737-1740. 2006. doi: 10.1126/science.1118052.

Jordan, C. F., & Jordan, C. F. Ecosystem Control: A Top-Down View. Evolution from a Thermodynamic Perspective: Implications for Species Conservation and Agricultural Sustainability, 47-62. 2022.

Karlusich, J. J. P.; Ibarbalz, F. M.; Bowler, C. Phytoplankton In The Tara Ocean. Annual Review Of Marine Science, V. 12, N. 1, P. 233–265, 3 Jan. 2020.

Karus, K., T. Paaver, H. Agasild, & P. Zingel. The effects of predation by planktivorous juvenile fish on the microbial food web. European Journal of Protistology 50: 109–121. 2014.

Kassambara, A., & F. Mundt. Package 'factoextra.' Extract and visualize the results of multivariate data analyses 76:. 2017.

Katechakis, A.; Stibor, H. The Mixotroph Ochromonas Tuberculata May Invade And Suppress Specialist Phago- And Phototroph Plankton Communities Depending On Nutrient Conditions. Oecologia, V. 148, N. 4, P. 692–701, Jul. 2006.

Katz, M. E.; Fennel, K.; Falkowski, P. G. Chapter 18 - Geochemical And Biological Consequences Of Phytoplankton Evolution. Em: Falkowski, P. G.; Knoll, A. H. (Eds.). Evolution Of Primary Producers In The Sea. Burlington: Academic Press, 2007.

Karati, K. K., A. M. Al-Aidaroos, R. P. Devassy, M. M. El-Sherbiny, B. H. Jones, U. Sommer, & B. Kürten. Ecohydrographic control on the community structure and vertical distribution of pelagic Chaetognatha in the Red Sea. Marine Biology 166: 30. 2019.

Kehayias, G. Quantitative aspects of feeding of chaetognaths in the eastern Mediterranean pelagic waters. Journal of the Marine Biological Association of the United Kingdom Cambridge University Press 83: 559–569. 2003.

Kumar, U., A. H. M. Kamal, N. U. Karim, N. W. Rasdi, J. Das, M. H. Idris, M. H. Abualreesh, & J. Ismail. Spatiotemporal variation of tintinnid microzooplankton (Ciliophora: tintinnina) from Sarawak inshore water, South China Sea. Community Ecology 22: 351–365. 2021.

Kikuchi, R. K. P., & C. Schobbenhaus. Atol das Rocas, Litoral do Nordeste do Brasil-Único atol do Atlântico Sul Equatorial Ocidental. Sítios geológicos e paleontológicos do Brasil Comissão Brasileira de Sítios Geológicos e Paleobiológicos 1: 379–390. 2002.

Kirchman, D.L. The uptake of inorganic nutrients by heterotrophic bacteria. Microb Ecol 28, 255–271. 1994. https://doi.org/10.1007/BF00166816.

Knauss, J. A.; Garfield, N. Introduction To Physical Oceanography: Third Edition. [S.L.] Waveland Press, 2016.

Knoppers, B., Ekau, W., Figueiredo, A.G. The coast and shelf of east and northeast Brazil and material transport. Geo-Mar. Lett. 19, 171–178. 1999. https://doi.org/10/cxdvxw..

Kroeker, K.J., Kordas, R.L., Crim, R., Hendriks, I.E., Ramajo, L., Singh, G.S., Duarte, C.M., Gattuso, J.-P. Impacts of ocean acidification on marine organisms: quantifying sensitivities and interaction with warming. Global Change Biology 19, 1884–1896. 2013. https://doi.org/10.1111/gcb.12179.

Krzywinski, M., J. Schein, İ. Birol, J. Connors, R. Gascoyne, D. Horsman, S. J. Jones, & M. A. Marra. Circos: An information aesthetic for comparative genomics. Genome Research 19: 1639–1645. 2009.

Landry, M. R., Ohman, M. D., Goericke, R., Stukel, M. R., and Tsyrklevich, K. Lagrangian studies of phytoplankton growth and grazing relationships in a coastal upwelling ecosystem off Southern California. Progress in Oceanography, 83, 208–216. 2009.

Landry, M.R. Integrating classical and microbial food web concepts: evolving views from the open-ocean tropical Pacific. Hydrobiologia 480, 29–39. 2002. https://doi.org/10/cv8mnr.

Lange, P.K., Brewin, R.J.W., Dall'Olmo, G., Tarran, G.A., Sathyendranath, S., Zubkov, M., Bouman, H.A. Scratching Beneath the Surface: A Model to Predict the Vertical Distribution of *Prochlorococcus* Using Remote Sensing. Remote Sens. 10, 847. 2018. https://doi.org/10/gdv5dk.

Larkin, A. A.; Mackey, K. R. M.; Martiny, A. C. Marine Cyanobacteria: *Prochlorococcus* And *Synechococcus.* Em: Encyclopedia Of Ocean Sciences. [S.L.] Elsevier, 2019.

LaRoche, J., Breitbarth, E. Importance of the diazotrophs as a source of new nitrogen in the ocean. Journal of Sea Research, Iron Resources and Oceanic Nutrients - Advancement of Global Environmental Simulations 53, 67–91. 2005. https://doi.org/10.1016/j.seares.2004.05.005.

Lee, M. D., N. G. Walworth, E. L. McParland, F.-X. Fu, T. J. Mincer, N. M. Levine, D. A. Hutchins, & E. A. Webb. The Trichodesmium consortium: conserved heterotrophic co-occurrence and genomic signatures of potential interactions. The ISME Journal Nature Publishing Group 11: 1813–1824. 2017.

Lee, S., & J. A. Fuhrman. Relationships between Biovolume and Biomass of Naturally Derived Marine Bacterioplanktont. APPL. ENVIRON. MICROBIOL. 53: 6. 1987.

Lee, M. J., H. J. Jeong, Y. D. Yoo, S. A. Park, & H. C. Kang. Feeding by the calanoid copepods Acartia spp. on the heterotrophic dinoflagellates Gyrodinium jinhaense, G. dominans, and G. moestrupii. Marine Biology 170: 37. 2023.

Leles, S. G., Moser, G. A. O., Valentin, J. L., and Figueiredo, G. M. A Lagrangian study of plankton trophodynamics over a diel cycle in a eutrophic estuary under upwelling influence. Journal of the Marine Biological Association of the United Kingdom, 98, 1547–1558. 2018.

Lemonnier, H., Lantoine, F., Courties, C., Guillebault, D., Nézan, E., Chomérat, N., Escoubeyrou, K., Galinié, C., Blockmans, B., Laugier, T. Dynamics of phytoplankton communities in eutrophying tropical shrimp ponds affected by vibriosis. Mar. Pollut. Bull. 110, 449–459. 2016. https://doi.org/10.1016/j.marpolbul.2016.06.015.

Lepori-Bui, M. Et Al. Evidence For Evolutionary Adaptation Of Mixotrophic Nanoflagellates To Warmer Temperatures. Biorxiv,,. Disponível Em: <Https://Www.Biorxiv.Org/Content/10.1101/2022.02.03.479051v1>. 2022.

Lewington-Pearce, L., Narwani, A., Thomas, M.K., Kremer, C.T., Vogler, H., Kratina, P. Temperature-dependence of minimum resource requirements alters competitive hierarchies in phytoplankton. Oikos 128, 1194–1205. 2019 https://doi.org/10.1111/oik.06060.

Li, Q., K. F. Edwards, C. R. Schvarcz, K. E. Selph, & G. F. Steward. Plasticity in the grazing ecophysiology of Florenciella (Dichtyochophyceae), a mixotrophic nanoflagellate that consumes *Prochlorococcus* and other bacteria. Limnology and Oceanography 66: 47–60. 2021.

Lima-Mendez, G., Faust, K., Henry, N., Decelle, J., Colin, S., Carcillo, F., Chaffron, S., Ignacio-Espinosa, J. C., et al. Determinants of community structure in the global plankton interactome. Science, 348, 1262073. 2015.

Lima, D. T. de, Moser, G. A. O., Piedras, F. R., Cunha, L. C. da, Tenenbaum, D. R., Tenório, M. M. B., Campos, M. V. P. B. de, Cornejo, T. de O., et al. Abiotic Changes Driving Microphytoplankton Functional Diversity in Admiralty Bay, King George Island (Antarctica). Frontiers in Marine Science, 6. 2019.

Lima-Mendez, G., K. Faust, N. Henry, J. Decelle, S. Colin, F. Carcillo, S. Chaffron, J. C. Ignacio-Espinosa, S. Roux, F. Vincent, L. Bittner, Y. Darzi, J. Wang, S. Audic, L. Berline, G. Bontempi, A. M. Cabello, L. Coppola, F. M. Cornejo-Castillo, F. d'Ovidio, L. De Meester, I. Ferrera, M.-J. Garet-Delmas, L. Guidi, E. Lara, S. Pesant, M. Royo-Llonch, G. Salazar, P. Sánchez, M. Sebastian, C. Souffreau, C. Dimier, M. Picheral, S. Searson, S. Kandels-Lewis, Tara Oceans coordinators, G. Gorsky, F. Not, H. Ogata, S. Speich, L. Stemmann, J. Weissenbach, P. Wincker, S. G. Acinas, S. Sunagawa, P. Bork, M. B. Sullivan, E. Karsenti, C. Bowler, C. de Vargas, & J. Raes. Determinants of community structure in the global plankton interactome. Science American Association for the Advancement of Science 348: 1262073. 2015.

Litchman, E. and Klausmeier, C. A. Trait-Based Community Ecology of Phytoplankton. Annual Review of Ecology, Evolution, and Systematics, 39, 615–639. 2008.

Litchman, E. et al. Global Biogeochemical Impacts Of Phytoplankton: A Trait-Based Perspective. Journal Of Ecology, V. 103, N. 6, P. 1384–1396, Nov. 2015.

Litchman, E., de Tezanos Pinto, P., Edwards, K.F., Klausmeier, C.A., Kremer, C.T., Thomas, M.K., Global biogeochemical impacts of phytoplankton: a trait-based perspective. J. Ecol. 103, 1384–1396. 2015. https://doi.org/10/f7v9v2.

Litchman, E.; Klausmeier, C. A. Trait-Based Community Ecology Of Phytoplankton. Annual Review Of Ecology, Evolution, And Systematics, V. 39, N. 1, P. 615–639, 2008.

Litchman, E.; Ohman, M. D.; Kiorboe, T. Trait-Based Approaches To Zooplankton Communities. Jounal Of Plankton Research, V. 35, N. 3, P. 473–484, 2013.

Livanou, E. Et Al. Role Of Mixotrophic Nanoflagellates In The Eastern Mediterranean Microbial Food Web. Marine Ecology Progress Series, V. 672, P. 15–32, 19 Ago. 2021.

Livanou, E., A. Lagaria, I. Santi, M. Mandalakis, A. Pavlidou, K. Lika, & S. Psarra. Pigmented and heterotrophic nanoflagellates: Abundance and grazing on prokaryotic picoplankton in the ultra-oligotrophic Eastern Mediterranean Sea. Deep Sea Research Part II: Topical Studies in Oceanography 164: 100–111. 2019.

Loick-Wilde, N., I. Fernández-Urruzola, E. Eglite, I. Liskow, M. Nausch, D. Schulz-Bull, D. Wodarg, N. Wasmund, & V. Mohrholz. Stratification, nitrogen fixation, and cyanobacterial bloom stage regulate the planktonic food web structure. Global Change Biology 25: 794–810. 2019.

Lomas, M. W., N. R. Bates, R. J. Johnson, D. K. Steinberg, & T. Tanioka, Adaptive carbon export response to warming in the Sargasso Sea. Nature Communications Nature Publishing Group 13: 1211. 2022.

Lomas, M.W., Lipschultz, F. Forming the primary nitrite maximum: Nitrifiers or phytoplankton? Limnol. Oceanogr. 51, 2453–2467. 2006. https://doi.org/10/dd87bh.

López-Abbate, M. C. Microzooplankton Communities in a Changing Ocean: A Risk Assessment. Diversity, 13, 82. 2021.

Lynam, C. P., Llope, M., Möllmann, C., Helaouët, P., Bayliss-Brown, G. A., and Stenseth, N. C. Interaction between top-down and bottom-up control in marine food webs. Proceedings of the National Academy of Sciences, 114, 1952–1957. 2017.

Mabesoone, J.M., Coutinho, P.N. Litoral and shalow marine geology of Northeastern Brasil. Trop. Oceanogr. 12, 1–214. 1970. https://doi.org/10/ggnmd3.

Macedo, S., Montes, M., Lins, I., Costa, K. Revizee. Programa de Avaliação do Potencial Sustentável dos Recursos Vivos da Zona Econômica Exclusiva, SCORE/NE. 1988.

Mackey, K.R.M., Bristow, L., Parks, D.R., Altabet, M.A., Post, A.F., Paytan, A.. The influence of light on nitrogen cycling and the primary nitrite maximum in a seasonally stratified sea. Prog. Oceanogr. 91, 545–560. 2011. https://doi.org/10.1016/j.pocean.2011.09.001.

Marañón, E. Cell Size as a Key Determinant of Phytoplankton Metabolism and Community Structure. Annu. Rev. Mar. Sci. 7, 241–264. 2015. https://doi.org/10.1146/annurev-marine-010814-015955.

Marañón, E., Behrenfeld, M.J., González, N., Mouriño, B., Zubkov, M.V. High variability of primary production in oligotrophic waters of the Atlantic Ocean: uncoupling from phytoplankton biomass and size structure. Mar. Ecol. Prog. Ser. 257, 1–11. 2003. https://doi.org/10/dqhww3.

Marañón, E., F. Van Wambeke, J. Uitz, E. S. Boss, C. Dimier, J. Dinasquet, A. Engel, N. Haëntjens, M. Pérez-Lorenzo, V. Taillandier, & B. Zäncker, Deep maxima of phytoplankton biomass, primary production and bacterial production in the Mediterranean Sea. Biogeosciences Copernicus GmbH 18: 1749–1767. 2021.

Marañón, E., Holligan, P.M., Varela, M., Mouriño, B., Bale, A.J., Basin-scale variability of phytoplankton biomass, production and growth in the Atlantic Ocean. Deep Sea Res. Part Oceanogr. Res. Pap. 47, 825–857. 2000. https://doi.org/10/fq6vc9.

Marañón, E., M. J. Behrenfeld, N. González, B. Mouriño, & M. V. Zubkov. High variability of primary production in oligotrophic waters of the Atlantic Ocean: uncoupling from phytoplankton biomass and size structure. Marine Ecology Progress Series 257: 1–11. 2003.

Margalef, R. Life-Forms Of Phytoplankton As Survival Alternatives In An Unstable Environment. Oceanologica Acta, V. 1, N. 4, P. 493–509, 1978.

Marie, D., F. Partensky, S. Jacquet, & D. Vaulot, Enumeration and Cell Cycle Analysis of Natural Populations of Marine Picoplankton by Flow Cytometry Using the Nucleic Acid Stain SYBR Green I. Applied and environmental microbiology 63: 186–193. 1997.

Maureaud, A. Et Al. Global Change In The Trophic Functioning Of Marine Food Webs. Plos One, V. 12, N. 8, P. E0182826, 11 Ago. 2017.

Meeder, E., Mackey, K.R.M., Paytan, A., Shaked, Y., Iluz, D., Stambler, N., Rivlin, T., Post, A.F., Lazar, B., Nitrite dynamics in the open ocean—clues from seasonal and diurnal variations. Mar. Ecol. Prog. Ser. 453, 11–26. 2012. https://doi.org/10/df98vc.

Medeiros, P. M., Seidel, M., Ward, N. D., Carpenter, E. J., Gomes, H. R., Niggemann, J., Dittmar, T. Fate of the Amazon River dissolved organic matter in the tropical Atlantic Ocean. Global Biogeochemical Cycles, 29(5), 677-690. 2015.

Meiri, S. Bergmann's Rule – What's In A Name? Global Ecology And Biogeography, V. 20, N. 1, P. 203–207, 2011.

Mélin, F. and Hoepffner, N. Monitoring Phytoplankton Productivity from Satellite–An Aid to Marine Resources Management. Handbook of satellite remote sensing image interpretation: applications for marine living resources conservation and management, edited by: Morales, J., Stuart, V., Platt, T., and Sathyendranath, S., EU PRESPO and IOCCG, 79–93. 2012.

Melo, P. A. M. C., M. Melo Júnior, M. Araujo, & S. Neumann-Leitão. The first occurrence of the Order Mormonilloida (Copepoda) in the Tropical Southwest Atlantic Ocean. Anais da Academia Brasileira de Ciências 87: 233–237. 2015.

Melo, P.A.M.C., Diaz, X.F.G., Macedo, S.J., Neumann-Leitão, S., Diurnal and spatial variation of the mesozooplankton community in the Saint Peter and Saint Paul Archipelago, Equatorial Atlantic. Mar. Biodivers. Rec. 5, 1–14. 2012. https://doi.org/10/ggczfq.

Mena, C., P. Reglero, M. Hidalgo, E. Sintes, R. Santiago, M. Martín, G. Moyà, & R. Balbín. Phytoplankton Community Structure Is Driven by Stratification in the Oligotrophic Mediterranean Sea. Frontiers in Microbiology Frontiers 10:,. 2019. https://www.frontiersin.org/articles/10.3389/fmicb.2019.01698/full.

Menden-Deuer, S. and Lessard, E. J. Carbon to volume relationships for dinoflagellates, diatoms, and other protist plankton. Limnology and Oceanography, 45, 569–579. 2000.

Mendonça, A., J. Arístegui, J. C. Vilas, M. F. Montero, A. Ojeda, M. Espino, & A. Martins. Is There a Seamount Effect on Microbial Community Structure and Biomass? The Case Study of Seine and Sedlo Seamounts (Northeast Atlantic). PLOS ONE Public Library of Science 7: e29526. 2012.

Menéndez, D. L. C. C., Anabela Anahí Berasategui, María Clara. Zooplankton: The Ocean Drifters. Marine Biology. CRC Press. 2022.

Menezes, B. S., L. C. P. de Macedo-Soares, & A. S. Freire, 2019. Changes in the plankton community according to oceanographic variability in a shallow subtropical shelf: SW Atlantic. Hydrobiologia 835: 165–178.

Metzler, P.M., Glibert, P.M., Gaeta, S.A., Ludlam, J.M. New and regenerated production in the South Atlantic off Brazil. Deep Sea Res1 Ocean. 44, 363–384. 1997. https://doi.org/10/d4rpjd.

Mignot, A., Claustre, H., Uitz, J., Poteau, A., D'Ortenzio, F., Xing, X.. Understanding the seasonal dynamics of phytoplankton biomass and the deep chlorophyll maximum in oligotrophic environments: A Bio-Argo float investigation. Glob. Biogeochem. Cycles 28, 856–876. 2014. https://doi.org/10/f6j525.

Mishra, R.K., Senga, Y., Nakata, K., Mishra, S., Sahu, B.K. Spatio-temporal variation of Prochlorococcus and phytoplankton community between Shimizu coast and Suruga bay, Northwest Pacific Ocean. Reg. Stud. Mar. Sci. 33, 100890. 2020. https://doi.org/10/gg3hsj.

Mishra, R.K., Shaw, B.P., Sahu, B.K., Mishra, S., Senga, Y. Seasonal appearance of Chlorophyceae phytoplankton bloom by river discharge off Paradeep at Orissa Coast in the Bay of Bengal. Environ. Monit. Assess. 149, 261–273. 2009. https://doi.org/10/ffvwpq.

Mitra, A. Et Al. Defining Planktonic Protist Functional Groups On Mechanisms For Energy And Nutrient Acquisition: Incorporation Of Diverse Mixotrophic Strategies. Protist, V. 167, N. 2, P. 106–120, 1 Abr. 2016.

Moore, L.R., Rocap, G., Chisholm, S.W. Physiology and molecular phylogeny of coexisting Prochlorococcus ecotypes. Nature 393, 464–467. 1998. https://doi.org/10.1038/30965.

Morán, X. A. G. Et Al. Increasing Importance Of Small Phytoplankton In A Warmer Ocean. Global Change Biology, V. 16, N. 3, P. 1137–1144, 2010.

Moreira, D. L. Ambiente pelágico da bacia de Sergipe-Alagoas. 2017.

Moyano, M., Illing, B., Akimova, A., Alter, K., Bartolino, V., Börner, G., Clemmesen, C., Finke, A., et al. Caught in the middle: bottom-up and top-down processes impacting recruitment in a small pelagic fish. Rev Fish Biol Fisheries, 33, 55–84. 2023.

Mozetič, P., Francé, J., Kogovšek, T., Talaber, I., and Malej, A. Plankton trends and community changes in a coastal sea (northern Adriatic): Bottom-up vs. top-down control in relation to environmental drivers. Estuarine, Coastal and Shelf Science, 115, 138–148. 2012.

Munawar, M., Niblock, H., Fitzpatrick, M., and Lorimer, J. Ciliate ecology in the eutrophic Bay of Quinte, Lake Ontario: Community structure and feeding characteristics. Aquatic Ecosystem Health & Management, 23, 35–44. 2020.

Murphy, G. E. P., Romanuk, T. N., and Worm, B. Cascading effects of climate change on plankton community structure. Ecology and Evolution, 10, 2170–2181. 2020.

Mutshinda, C. M., Finkel, Z. V., and Irwin, A. J. Which environmental factors control phytoplankton populations? A Bayesian variable selection approach. Ecological Modelling, 269, 1–8. 2013. 2013.

Novak, T. et al. Global Warming And Oligotrophication Lead To Increased Lipid Production In Marine Phytoplankton. Science Of The Total Environment, V. 668, P. 171–183, 10 Jun. 2019.

Nunes-Neto, N. F.; Do Carmo, R. S.; El-Hani, C. N. A Link Between Algae And Clouds: Theoretical Grounds Of The Claw Hypothesis And Its Implications To Climate Change. Oecologia Australis, V. 13, N. 4, P. 596–608, 2009.

Otsuka, A.Y., Feitosa, F.A. do N., Montes, M. de J.F., Silva, A.C. da. Influence of fluvial discharge on the dynamics of Chlorophyll-α in the continental shelf adjacent to the Recife Port Basin (Pernambuco-Brazil). Braz. J. Oceanogr. 66, 91–103. 2018. https://doi.org/10.1590/s1679-87592018149106601.

Paczkowska, J. Et Al. Drivers Of Phytoplankton Production And Community Structure In Nutrient-Poor Estuaries Receiving Terrestrial Organic Inflow. Marine Environmental Research, V. 151, P. 104778, 1 Out. 2019.

Pang, N. Et Al. Exploiting Mixotrophy For Improving Productivities Of Biomass And Co-Products Of Microalgae. Renewable And Sustainable Energy Reviews, V. 112, P. 450–460, 1 Set. 2019.

Patuła, W., M. Ronowicz, & A. Weydmann-Zwolicka. The interplay between predatory chaetognaths and zooplankton community in a high Arctic fjord. Estuarine, Coastal and Shelf Science 285: 108295. 2023.

Paulo, J.G. Distribuição vertical dos nutrientes dissolvidos no Nordeste do Brasil entre as latitudes 6° 20'S e 7° 33'S. Universidade Federal de Pernambuco. 2016.

Pelegrí, S., J. Dolan, & F. Rassoulzadegan. Use of high temperature catalytic oxidation (HTCO) to measure carbon content of microorganisms. Aquatic Microbial Ecology 16: 273–280. 1999.

Pérez, V., Fernández, E., Marañón, E., Serret, P., Varela, R., Bode, A., Varela, M., Varela, M.M., Morán, X.A.G., Woodward, E.M.S., Kitidis, V., García-Soto, C., Latitudinal distribution of microbial plankton abundance, production, and respiration in the Equatorial Atlantic in autumn 2000. Deep Sea Res. Part Oceanogr. Res. Pap. 52, 861–880. 2005. https://doi.org/10/cp6csx.

Peter, K. H., & Sommer, U. (2013). Phytoplankton cell size reduction in response to warming mediated by nutrient limitation. PloS one, 8(9), e71528.

Pierce, R. W. and Turner, J. T. Ecology of Planktonic Ciliates in Marine Food Webs. Reviews in Aquatic Sciences, 6, 139–181. 1992.

Pilkaitytė, R. and Razinkovas, A. Seasonal changes in phytoplankton composition and nutrient limitation in a shallow Baltic lagoon. 2007.

Power, M. E. Top-Down and Bottom-Up Forces in Food Webs: Do Plants Have Primacy. Ecology, 73, 733–746. 1992.

Presta, M. L., Riccialdelli, L., Bruno, D. O., Castro, L. R., Fioramonti, N. E., Florentín, O. V., Berghoff, C. F., Capitanio, F. L., et al. Mesozooplankton community structure and trophic relationships in an austral high-latitude ecosystem (Beagle Channel): The role of bottom-up and top-down forces during springtime. Journal of Marine Systems, 240, 103881. 2023.

Ptacnik, R. Et Al. A Light-Induced Shortcut In The Planktonic Microbial food web. Scientific Reports, V. 6, N. 1, P. 29286, 11 Jul. 2016.

Ptacnik, R. Et Al. Effects Of Microzooplankton And Mixotrophy In An Experimental Planktonic Food Web. Limnology And Oceanography, V. 49, N. 4part2, P. 1435–1445, 2004.

Purina, I., M. Balode, C. Béchemin, T. Põder, C. Vérité, & S. Maestrini. Influence of dissolved organic matter from terrestrial origin on the changes of dinoflagellate species composition in the Gulf of Riga, Baltic Sea. Hydrobiologia 514: 127–137. 2004.

Qu, T., Meyers, G. Seasonal variation of barrier layer in the southeastern tropical Indian Ocean. J. Geophys. Res. Oceans 110. 2005. https://doi.org/10/cbcw8p.

Queiroz, A.R., Flores Montes, M., Melo, P.A.M.C., Silva, R.A., Koening, M.L., 2015. Vertical and horizontal distribution of phytoplankton around an oceanic archipelago of the Equatorial Atlantic. Mar. Biodivers. Rec. 8, 1–13. 2015. https://doi.org/10/gf7kmv.

Rahav, E., B. Herut, D. Spungin, A. Levi, M. R. Mulholland, & I. Berman-Frank. Heterotrophic bacteria outcompete diazotrophs for orthophosphate in the Mediterranean Sea. Limnology and Oceanography 67: 159–171. 2022.

Raven, J. A.; Beardall, J. Influence Of Global Environmental Change On Plankton. Journal Of Plankton Research, V. 43, N. 6, P. 779–800, 1 Nov. 2021.

Raven, J.; Beardall, J. Evolution Of Phytoplankton In Relation To Their Physiological Traits. Journal Of Marine Science And Engineering, V. 10, N. 2, P. 194, Fev. 2022.

Redfield, A. C. The influence of organisms on the composition of seawater. The sea Wiley-Interscience 2: 26–77. 1963.

Reynolds, C. S. The Ecology Of Phytoplankton. [S.L.] Cambridge University Press, 2006.

Richardson, A. J. In Hot Water: Zooplankton And Climate Change. Ices Journal Of Marine Science, V. 65, N. 3, P. 279–295, 2008.

Rii, Y.M., Karl, D.M., Church, M.J. Temporal and vertical variability in picophytoplankton primary productivity in the North Pacific Subtropical Gyre. Mar. Ecol. Prog. Ser. 562, 1–18. 2016. https://doi.org/10.3354/meps11954. 2016.

Rissik, D., Shon, E. H., Newell, B., Baird, M. E., and Suthers, I. M. Plankton dynamics due to rainfall, eutrophication, dilution, grazing and assimilation in an urbanized coastal lagoon. Estuarine, Coastal and Shelf Science, 84, 99–107. 2009.

Rodriguez, F., Chauton, M., Johnsen, G., Andresen, K., Olsen, L. M., & Zapata, M. Photoacclimation in phytoplankton: implications for biomass estimates, pigment functionality and chemotaxonomy. Marine Biology, 148, 963-971. 2006.

Rogers, T. L., Bashevkin, S. M., Burdi, C. E., Colombano, D. D., Dudley, P. N., Mahardja, B., Mitchell, L., Perry, S., et al. Evaluating top-down, bottom-up, and environmental drivers of pelagic food web dynamics along an estuarine gradient. 2022.

Rose, V., Rollwagen-Bollens, G., Bollens, S. M., and Zimmerman, J. Effects of Grazing and Nutrients on Phytoplankton Blooms and Microplankton Assemblage Structure in Four Temperate Lakes Spanning a Eutrophication Gradient. Water, 13, 1085. 2021.

Roy, S., Llewellyn, C.A., Egeland, E.S., Johnsen, G.. Phytoplankton Pigments: Characterization, Chemotaxonomy and Applications in Oceanography. Cambridge University Press. 2011.

Ryabov, A. B.; Rudolf, L.; Blasius, B. Vertical Distribution And Composition Of Phytoplankton Under The Influence Of An Upper Mixed Layer. Journal Of Theoretical Biology, V. 263, N. 1, P. 120–133, Mar. 2010.

Safran, P. Fisheries And Aquaculture - Volume V. [S.L.] Eolss Publications, 2009.

Salvetat, J., Bez, N., Habasque, J., Lebourges-Dhaussy, A., Lopes, C., Roudaut, G., Simier, M., Travassos, P., et al. Comprehensive spatial distribution of tropical fish assemblages from multifrequency acoustics and video fulfils the island mass effect framework. Sci Rep, 12, 8787. 2022.

Šantić, D., A. Vrdoljak Tomaš, & J. Lušić. Spatial and Temporal Patterns of Picoplankton Community in the Central and Southern Adriatic Sea In Joksimović, A., M. Đurović, I. S. Zonn, A. G. Kostianoy, & A. V. Semenov (eds), The Montenegrin Adriatic Coast: Marine Biology. Springer International Publishing, Cham: 29–51. 2021. https://doi.org/10.1007/698_2020_645.

Sardet, C. Plankton: Wonders Of The Drifting World. [S.L.] University Of Chicago Press, 2015.

Schmoker, C.; Hernández-León, S.; Calbet, A. Microzooplankton Grazing In The Oceans: Impacts, Data Variability, Knowledge Gaps And Future Directions. Journal Of Plankton Research, V. 35, N. 4, P. 691–706, 1 Jul. 2013.

Serafini, T. Z., G. B. de França, & J. M. Andriguetto-Filho. Ilhas oceânicas brasileiras: biodiversidade conhecida e sua relação com o histórico de uso e ocupação humana. Revista de Gestão Costeira Integrada-Journal of Integrated Coastal Zone Management Associação Portuguesa dos Recursos Hídricos 10: 281–301. 2010.

Serrano, D.; Valle-Levinson, A. Effects Of River Discharge And The California Current On Pycnocline Depth At The Eastern Entrance To The Gulf Of California. Continental Shelf Research, V. 215, P. 104356, 15 Fev. 2021.

Sherr, E.B., Sherr, B.F. Heterotrophic dinoflagellates: a significant component of microzooplankton biomass and major grazers of diatoms in the sea. Mar. Ecol. Prog. Ser. 352, 187–197. 2007. https://doi.org/10/d8s5p6.

Shi, P., Shen, H., Wang, W., Chen, W., and Xie, P. The relationship between light intensity and nutrient uptake kinetics in six freshwater diatoms. Journal of Environmental Sciences, 34, 28–36. 2015.

Sieburth, J.M., Smetacek, V., Lenz, J. Pelagic ecosystem structure: heterotrophic compartments of the plankton and their relationship to plankton size fractions. Limnology and oceanography 23, 1256–1263. 1978. https://doi.org/10/d4k7wp.

Signorini, S. R.; Franz, B. A.; Mcclain, C. R. Chlorophyll Variability In The Oligotrophic Gyres: Mechanisms, Seasonality And Trends. Frontiers In Marine Science, V. 2, 2015.

Silva, M. V. B., B. Ferreira, M. Maida, S. Queiroz, M. Silva, H. L. Varona, T. C. M. Araújo, & M. Araújo. Flow-topography interactions in the western tropical Atlantic boundary off Northeast Brazil. Journal of Marine Systems 227: 103690. 2022.

Šolić, M. Et Al. Impact Of Water Column Stability Dynamics On The Succession Of Plankton Food Web Types In The Offshore Area Of The Adriatic Sea. Journal Of Sea Research, V. 158, P. 101860, 1 Mar. 2020.

Souza, C.S., Luz, J.A.G., Macedo, S., Montes, M. de J.F., Mafalda, P. Chlorophyll a and nutrient distribution around seamounts and islands of the tropical south-western Atlantic. Mar. Freshw. Res. 64, 168–184. 2013. https://doi.org/10/f4qx95.

Sommer, U., Peter, K. H., Genitsaris, S., & Moustaka-Gouni, M. Do marine phytoplankton follow B ergmann's rule sensu lato?. Biological Reviews, 92(2), 1011-1026. 2017.

Speight, M. R.; Henderson, P. A. Marine Ecology: Concepts And Applications. [S.L.] John Wiley & Sons, 2013.

Staehr, P. A.; Birkeland, M. J. Temperature Acclimation Of Growth, Photosynthesis And Respiration In Two Mesophilic Phytoplankton Species. Phycologia, V. 45, N. 6, P. 648–656, 1 Nov. 2006.

Stoecker, D. K. Et Al. Mixotrophy In The Marine Plankton. Annual Review Of Marine Science, V. 9, N. 1, P. 311–335, 3 Jan. 2017.

Stramma, L., England, M. On the water masses and mean circulation of the South Atlantic Ocean. J. Geophys. Res. Oceans 104, 20863–20883. 1999. https://doi.org/10/bvxhdz.

Sugihara, G., May, R., Ye, H., Hsieh, C., Deyle, E., Fogarty, M., and Munch, S. (2012) Detecting Causality in Complex Ecosystems. Science, 338, 496–500. 2012.

Sun, J. and Liu, D. Geometric models for calculating cell biovolume and surface area for phytoplankton. Journal of Plankton Research, 25, 1331–1346. 2003.

Sunagawa, S. Et Al. Tara Oceans: Towards Global Ocean Ecosystems Biology. Nature Reviews Microbiology, V. 18, N. 8, P. 428–445, Ago. 2020.

Susini-Ribeiro, S. M. M. Biomass distribution of pico-, nano-and microplankton on the continental shelf of Abrolhos, East Brazil. Archive of Fishery and Marine Research GUSTAV FISCHER VERLAG VILLENGANG 2, D-07745 JENA, GERMANY 47: 271–284. 1999.

Suthers, I.; Rissik, D.; Richardson, A. Plankton: A Guide To Their Ecology And Monitoring For Water Quality. [S.L.] Csiro Publishing, 2019.

Tanimoto, Y.; Ouellette, N. T.; Koseff, J. R. Interaction Between An Inclined Gravity Current And A Pycnocline In A Two-Layer Stratification. Journal Of Fluid Mechanics, V. 887, P. A8, Mar. 2020.

Tchamabi, C.C., Araujo, M., Silva, M., Bourlès, B. A study of the Brazilian Fernando de Noronha island and Rocas atoll wakes in the tropical Atlantic. Ocean Model. 111, 9–18. 2017. https://doi.org/10/f92mvn.

Thurman, H. V. Essentials Of Oceanography. Ed 12. 2016

Toseland, A., Daines, S.J., Clark, J.R., Kirkham, A., Strauss, J., Uhlig, C., Lenton, T.M., Valentin, K., Pearson, G.A., Moulton, V., Mock, T. The impact of temperature on marine phytoplankton resource allocation and metabolism. Nat. Clim. Change 3, 979–984. 2013. https://doi.org/10/f5p2g3

Tosetto, E. G., A. Bertrand, S. Neumann-Leitão, A. Costa da Silva, & M. Nogueira Júnior. Spatial patterns in planktonic cnidarian distribution in the western boundary current system of the tropical South Atlantic Ocean. Journal of Plankton Research. 2021. https://doi.org/10.1093/plankt/fbaa066.

Traboni, C., A. Calbet, & E. Saiz. Mixotrophy upgrades food quality for marine calanoid copepods. Limnology and Oceanography 66: 4125–4139. 2021.

Traboni, C., A. Calbet, & E. Saiz. Effects of prey trophic mode on the gross-growth efficiency of marine copepods: the case of mixoplankton. Scientific Reports Nature Publishing Group 10: 12259. 2020.

Travassos, P., Hazin, F., Zagaglia, J., Advíncula, R. Estrutura Termohalina da Zona Econômica Exclusiva (ZEE) do Nordeste brasileiro durante a Expedição Oceanográfica JOPS II, do NOc. Victor Hensen-Influências das Ilhas e Bancos oceânicos. Presented at the Congresso Latino Americano de Ciências Sobre o Mar, p. 502. 1997.

Trifoglio, N. L., H. F. Olguín Salinas, & V. A. Alder. Diatoms, tintinnids, and the protist community of the western Weddell Sea in summer: latitudinal distribution and biogeographic boundaries. Polar Biology 46: 427–444. 2023.

Tsai, A.-Y., G.-C. Gong, C.-C. Chung, & Y.-T. Huang. Different impact of nanoflagellate grazing and viral lysis on Synechococcus spp. and picoeukaryotic mortality in coastal waters. Estuarine, Coastal and Shelf Science 209: 1–6. 2018.

Tsai, A.-Y.; Mukhanov, V. Response Of Growth And Grazing Rate Of Nanoflagellates On Synechococcus Spp. To Experimental Nutrient Enrichment. Water, V. 13, N. 19, P. 2686, Jan. 2021.

Tuerena, R. E. Et Al. Internal Tides Drive Nutrient Fluxes Into The Deep Chlorophyll Maximum Over Mid-Ocean Ridges. Global Biogeochemical Cycles, V. 33, N. 8, P. 995–1009, 2019.

Vargas, C.A., Martínez, R.A., Cuevas, L.A., Pavez, M.A., Cartes, C., GonzÁlez, H.E., Escribano, R., Daneri, G. The relative importance of microbial and classical food webs in a highly productive coastal upwelling area. Limnol. Oceanogr. 52, 1495–1510. 2007. https://doi.org/10/frznhv.

Verberk, W. C. E. P. Et Al. Shrinking Body Sizes In Response To Warming: Explanations For The Temperature–Size Rule With Special Emphasis On The Role Of Oxygen. Biological Reviews, V. 96, N. 1, P. 247–268, 2021.

Verity, P. G., Robertson, C. Y., Tronzo, C. R., Andrews, M. G., Nelson, J. R., and Sieracki, M. E. Relationships between cell volume and the carbon and nitrogen content of marine photosynthetic nanoplankton. Limnology and Oceanography, 37, 1434–1446. 1992.

Vernet, M. Et Al. Influence Of Phytoplankton Advection On The Productivity Along The Atlantic Water Inflow To The Arctic Ocean. Frontiers In Marine Science, V. 6, 2019.

Visintini, N., A. C. Martiny, & P. Flombaum. *Prochlorococcus*, *Synechococcus*, and picoeukaryotic phytoplankton abundances in the global ocean. Limnology and Oceanography Letters n/a:, https://aslopubs.onlinelibrary.wiley.com/doi/abs/10.1002/lol2.10188. 2021.

Vrede, T. Et Al. Effects Of N : P Loading Ratios On Phytoplankton Community Composition, Primary Production And N Fixation In A Eutrophic Lake. Freshwater Biology, V. 54, N. 2, P. 331–344, 2009.

Vrede, T., Ballantyne, A., Mille-Lindblom, C., Algesten, G., Gudasz, C., Lindahl, S., Brunberg, A.K., Effects of N: P loading ratios on phytoplankton community composition, primary production and N fixation in a eutrophic lake. Freshw. Biol. 54, 331–344. 2009.. https://doi.org/10.1111/j.1365-2427.2008.02118.x.

Walker, N., H. Susanto, M. Steinke, & E. A. Codling. Bottom-up and top-down control in a multitrophic system: the role of nutrient limitation and infochemical-mediated predation in a plankton food-web model. Communication in Biomathematical Sciences Indonesian Bio-Mathematical Society 2: 65–84. 2019.

Wang, F., Y. Wei, J. Yue, C. Guo, & J. Sun. Distribution and environmental impact factors of picophytoplankton in the East China Sea during spring. Journal of Oceanology and Limnology . 2021. https://doi.org/10.1007/s00343-020-0230-3.

Ward, B. A., Dutkiewicz, S., and Follows, M. J. Modelling spatial and temporal patterns in size-structured marine plankton communities: top–down and bottom–up controls. Journal of Plankton Research. 2013.

Wei, Y., Sun, J., Zhang, G., Wang, X., and Wang, F. Environmental factors controlling the dynamics of phytoplankton communities during spring and fall seasons in the southern Sunda Shelf. Environ Sci Pollut Res, 27, 23222–23233. 2020.

Weinbauer, M.G. Ecology of prokaryotic viruses. FEMS Microbiol. Rev. 28, 127–181. 2004.https://doi.org/10.1016/j.femsre.2003.08.001.

Wilken, S. Et Al. Mixotrophic Organisms Become More Heterotrophic With Rising Temperature. Ecology Letters, V. 16, N. 2, P. 225–233, 2013.

Winder, M., & Sommer, U. Phytoplankton response to a changing climate. Hydrobiologia, 698, 5-16. 2012.

Wollrab, S., Pondaven, P., Behl, S., Beker, B., and Stibor, H. Differences in size distribution of marine phytoplankton in presence versus absence of jellyfish support theoretical predictions on top-down control patterns along alternative energy pathways. Mar Biol, 167, 9. 2019.

Wood, S.N. On Confidence Intervals for Generalized Additive Models Based on Penalized Regression Splines. Australian & New Zealand Journal of Statistics 48, 445–464. 2006. https://doi.org/10.1111/j.1467-842X.2006.00450.x.

Wood, S.N. Fast stable restricted maximum likelihood and marginal likelihood estimation of semiparametric generalized linear models. J. R. Stat. Soc. Ser. B Stat. Methodol. 73, 3–36. 2011. https://doi.org/10/cbb27p.

Xu, S., Liu, Y., Fan, J., Xiao, Y., Qi, Z., and Lakshmikandan, M. Impact of salinity variation and silicate distribution on phytoplankton community composition in Pearl River estuary, China. Ecohydrology & Hydrobiology, 22, 466–475. 2022.

Yasunaka, S., Kouketsu, S., Strutton, P.G., Sutton, A.J., Murata, A., Nakaoka, S., Nojiri, Y. Spatio-temporal variability of surface water pCO2 and nutrients in the tropical Pacific from 1981 to 2015. Deep Sea Res. Part II Top. Stud. Oceanogr., Understanding changes in transitional areas of the Pacific Ocean 169–170, 104680. 2019.https://doi.org/10.1016/j.dsr2.2019.104680.

Yingling, N., T. B. Kelly, T. A. Shropshire, M. R. Landry, K. E. Selph, A. N. Knapp, S. A. Kranz, & M. R. Stukel, Taxon-specific phytoplankton growth, nutrient utilization and light limitation in the oligotrophic Gulf of Mexico. Journal of Plankton Research 44: 656–676. 2022.

Young, J. W. Et Al. The Trophodynamics Of Marine Top Predators: Current Knowledge, Recent Advances And Challenges. Deep Sea Research Part Ii: Topical Studies In Oceanography, Impacts Of Climate On Marine Top Predators. V. 113, P. 170–187, 1 Mar. 2015.

Zapata, M., Fraga, S., Rodríguez, F., Garrido, J.L. Pigment-based chloroplast types in dinoflagellates. Mar. Ecol. Prog. Ser. 465, 33–52. 2012. https://doi.org/10.3354/meps09879.

Zhang, J., Zhi, M., and Zhang, Y. Combined Generalized Additive model and Random Forest to evaluate the influence of environmental factors on phytoplankton biomass in a large eutrophic lake. Ecological Indicators, 130, 108082. 2021.

Zhang, Z., S. Nair, L. Tang, H. Zhao, Z. Hu, M. Chen, Y. Zhang, S.-J. Kao, N. Jiao, & Y. Zhang. Long-Term Survival of Synechococcus and Heterotrophic Bacteria without External Nutrient Supply after Changes in Their Relationship from Antagonism to Mutualism. mBio American Society for Microbiology 12: e01614-21. 2021.

Zimmerman, A. E., Allison, S. D., & Martiny, A. C. Phylogenetic constraints on elemental stoichiometry and resource allocation in heterotrophic marine bacteria. Environmental microbiology, 16(5), 1398-1410. 2014.

Zinser, E. R., Johnson, Z. I., Coe, A., Karaca, E., Veneziano, D., & Chisholm, S. W. Influence of light and temperature on Prochlorococcus ecotype distributions in the Atlantic Ocean. Limnology and Oceanography, 52(5), 2205-2220. 2007.

Zöllner, E., Hoppe, H.-G., Sommer, U., and Jürgens, K. Effect of zooplankton-mediated trophic cascades on marine microbial food web components (bacteria, nanoflagellates, ciliates). Limnology and Oceanography, 54, 262–275. 2009.

Zubkov, M. V., M. A. Sleigh, P. H. Burkill, & R. J. G. Leakey. Picoplankton community structure on the Atlantic Meridional Transect: a comparison between seasons. Prog.Oceanogr. 45: 369–386. 2000.

APPENDIX A - SUPPLEMENTARY MATERIAL

Chapter 2: Supplementary Material

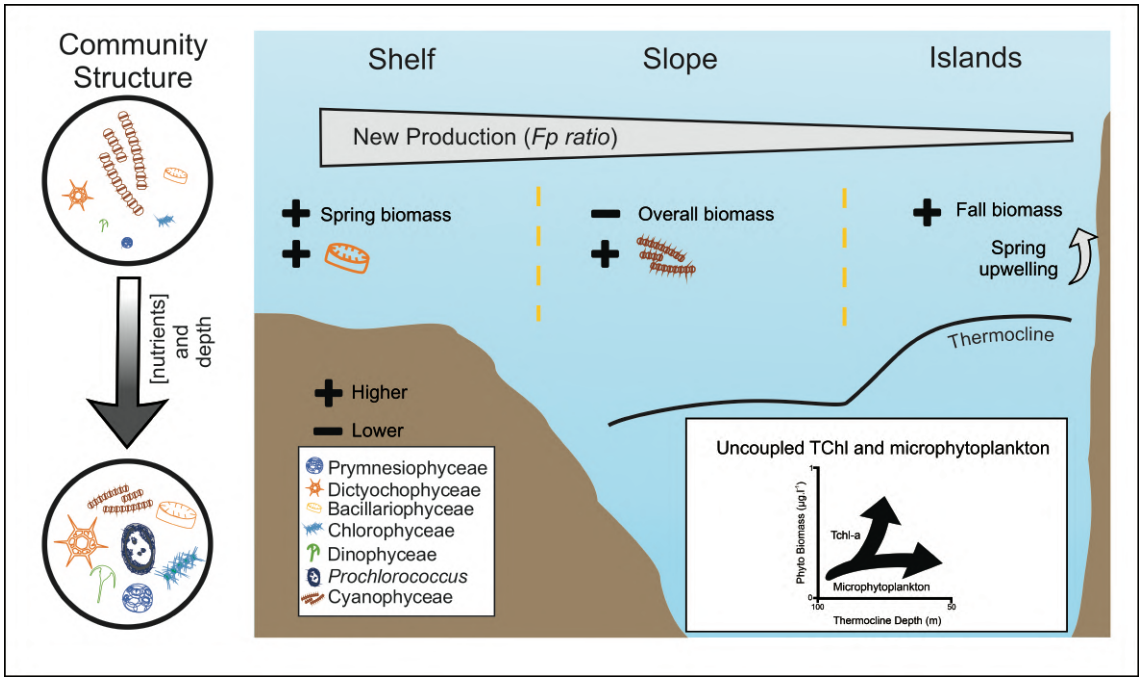

Visual Abstract

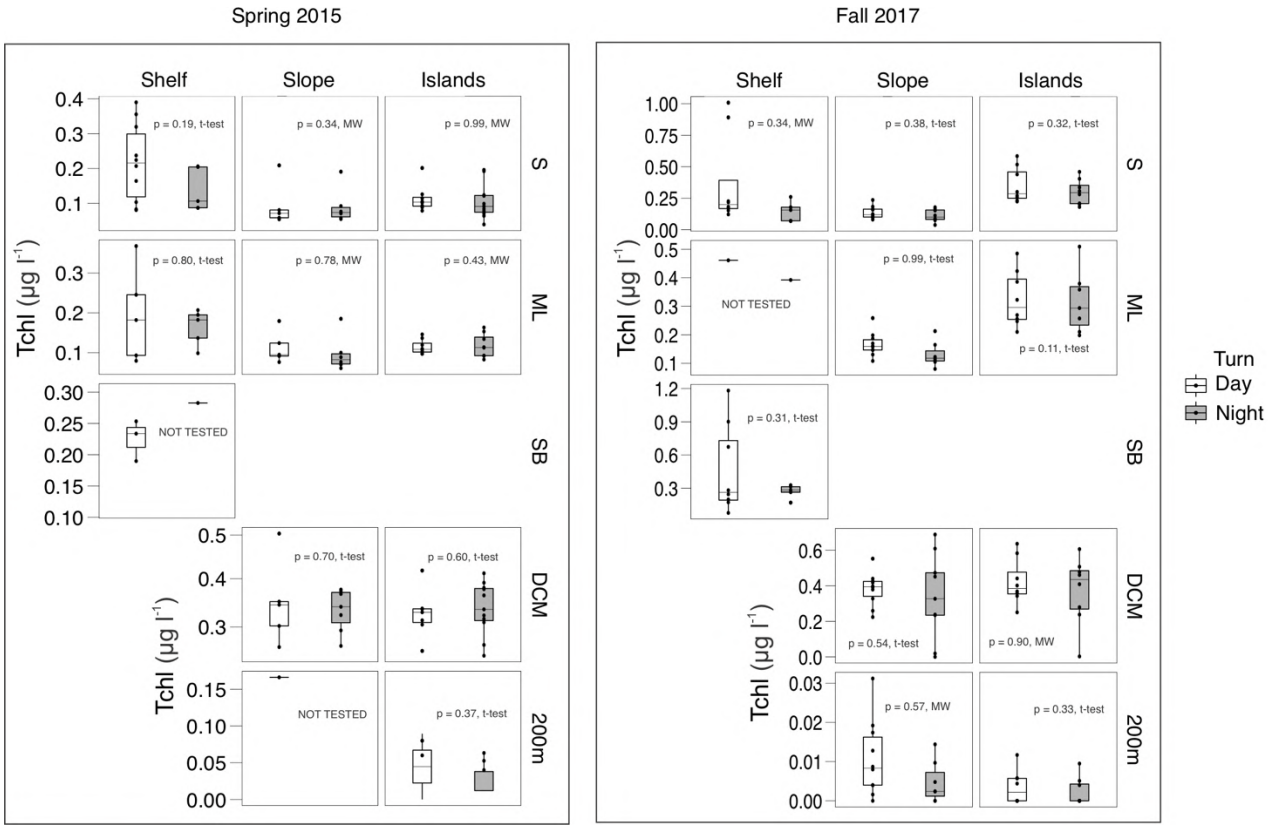

Supplementary Fig. 1. Day vs. night tests with p-values for the total phytoplankton biomass (TChl-a) in the SWTA during spring and fall. S: Surface, ML: Mixed Layer; SB: Shallow Bottom, DCM: Deep Chlorophyl Maximum.

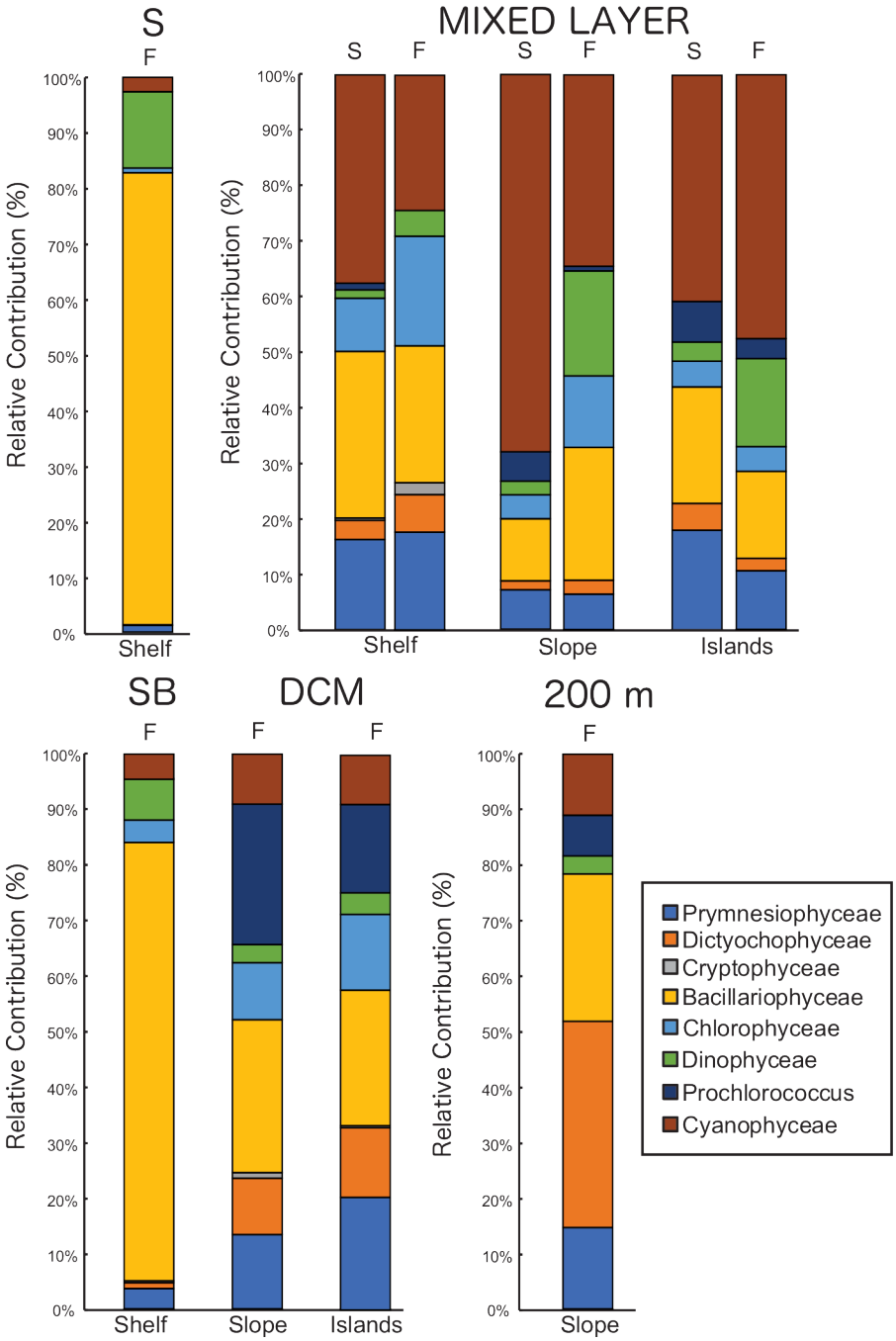

Supplementary Fig. 2. Relative contribution of the microphytoplankton taxa pigment biomarkers (as indicated in Table 1) in the SWTA during spring and fall. S: spring; F: fall.

			Temperature (ºC)	Salinity	NO_2^- (µmol l^{-1})	NO_3^- (µmol l^{-1})	PO_4^{3-} (µmol l^{-1})	SiO (µmol l^{-1})	Tchl-*a* (µg l^{-1})
SPRING	S	Shelf	26.88 ± 0.28	36.62 ± 0.15	0.0008 ± 0.003	0.03 ± 0.05	0.07 ± 0.03	0.84 ± 0.42	0.19 ± 0.10
		Slope	26.70 ± 0.12	36.45 ± 0.17	-	0.07 ± 0.05	0.07 ± 0.023	0.55 ± 0.12	0.09 ± 0.05
		Islands	26.65 ± 0.13	36.23 ± 0.02	0.0037 ± 0.009	0.03 ± 0.04	0.10 + 0.03	0.48 ± 0.10	0.11 ± 0.04
	ML	Shelf	26.74 ± 0.17	36.58 ± 0.13	0.0030 ± 0.003	0.04 ± 0.04	0.05 ± 0.02	0.62 ± 0.17	0.18 ± 0.08
		Slope	26.62 ± 0.10	36.56 ± 0.20	0.0009 ± 0.003	0.10 ± 0.04	0.06 ± 0.03	0.50 ± 0.16	0.10 ± 0.04
		Islands	26.60 ± 0.10	36.24 ± 0.02	0.0028 ± 0.006	0.03 ± 0.05	0.10 ± 0.01	0.47 ± 0.10	0.11 ± 0.02
	DCM	Slope	23.84 ± 0.46	37.02 ± 0.09	0.0244 ± 0.03	0.21 ± 0.20	0.13 ± 0.03	0.51 ± 0.19	0.33 ± 0.06
		Islands	23.11 ± 3.93	36.52 ± 0.47	0.0505 ± 0.05	3.58 ± 6.05	0.13 ± 0.37	1.59 ± 2	0.34 ± 0.05
	SB	Shelf	26.29 ± 0.92	36.80 ± 0.44	0.0060 ± 0.006	0.04 ± 0.05	0.09 ± 0.005	0.98 ± 0.15	0.22 ± 0.07
	200m	Slope	17.90	36.02	0.0500	5.10	0.48	2.05	0.16
		Islands	12.55 ± 0.71	35.23 ± 0.09	0.0083 ± 0.01	14.43 ± 14.43	1.06 ± 0.90	5.95 ± 6.34	0.03 ± 0.04
FALL	S	Shelf	28.87 ± 0.24	37.06 ± 0.38	0.0050 ± 0.009	0.32 ± 0.17	0.12 ± 0.04	0.87 ± 0.26	0.26 ± 0.27
		Slope	28.87 ± 0.19	36.51 ± 0.48	0.0170 ± 0.01	0.34 ± 0.15	0.1 ± 0.04	0.78 ±0.51	0.11 ± 0.04
		Islands	28.88 ± 0.13	35.90 ± 0.07	0.0086 ± 0.19	0.22 ± 0.12	0.09 ± 0.05	0.89 ± 0.13	0.32 ± 0.12
	ML	Shelf	28.39	36.40	0.0020	0.20	0.07	0.82	0.27 ± 0.17
		Slope	28.48 ± 0.42	37 ± 0.48	0.008 ± 0.004	0.33 ± 0.11	0.09 ± 0.36	0.74 ± 0.16	0.14 ± 0.03
		Islands	28.69 ± 0.46	35.97 ± 0.07	0.0043 ± 0.009	0.20 ± 0.10	0.08 ± 0.045	0.87 ± 0.12	0.32 ± 0.10
	DCM	Slope	25.22 ± 0.93	37.17 ± 0.17	0.0833 ± 0.11	0.36 ± 0.17	0.14 ± 0.04	0.83 ± 0.19	0.38 ± 0.16
		Islands	24.98 ± 1.99	36.38 ± 0.26	0.0768 ± 0.10	0.71 ± 1	0.24 ± 0.13	1.26 ± 0.45	0.40 ± 0.16
	SB	Shelf	28.41 ± 0.78	37 ± 0.33	0.0258 ± 0.038	0.35 ± 0.21	0.11 ± 0.05	1.1 ± 0.63	0.39 ± 0.32
	200	Slope	15.15 ± 1.66	35.57 ± 0.24	0.019 ± 0.017	9.36 ± 0.24	0.74 ± 0.24	3.82 ± 1.95	0.008 ± 0.004

		Islands	12.45 ± 0.23	35.22 ± 0.03	0.015 ± 0.02	24.03 ± 1.19	1.51 ± 0.08	9.52 ± 0.5	0.003 ± 0.008

Supplementary Table 1. Average values with standard deviation of the environmental data (Temperature, Salinity and nutrients) and total biomass (TChl-a) in the SWTA during spring and fall. S: Surface; ML: Mixed Layer Depth; DCM: Deep Chlorophyll Depth; SB: Shallow Bottom.

Chapter 3: Supplementary Material

Supplementary Material 1

Autotrophic and heterotrophic picoplankton and nanophytoplankton biomass

Autotrophic cells displayed a wide range of abundance among samples, from undetected at 200 m depth to 3.26 x 10^8 cells L^{-1} in the mixed layer (Tropical Water), whereas heterotrophic bacteria showed higher abundance with a less intense vertical gradient, ranging from 1.1 x 10^8 cells L^{-1} in 200 m to 4.2 x 10^9 cells L^{-1} in the mixed layer (Tropical Water) (Fig. 1e). Overall, autotrophic cells showed an offshore vertical decreasing pattern in abundance with increasing depth (Fig. 1), confirmed by the *KW* results which showed statistically different abundances between water layers (*KW*, $p < 0.001$). Only the distribution of picoeukaryotes contrasted this pattern, showing higher abundances around seamounts and islands deep chlorophyll maximum (0.15 and 0.11 and x 10^9 cells L^{-1}, respectively) (Subtropical Underwater) (*KW*, $p < 0.001$). Over the shelf, both pigmented nanoflagellates and *Synechococcus* (Fig. 1a, d) displayed slightly higher abundances on the shallow bottom (0.0008 and 0.66 x 10^9 cells L^{-1}, respectively), although no statistical differences between depths were found (*KW*, $p > 0.05$). In the coast-offshore gradient, the abundance of *Synechococcus*, *Prochlorococcus,* and heterotrophic bacteria differed among regions (*KW*, $p < 0.001$), with *Synechococcus* more abundant over the shelf area (Fig 1d), while *Prochlorococcus* dominated in the offshore areas (Fig. 1b), and heterotrophic bacteria had higher abundances over the seamounts (Fig. 1e) (Table I). Although picoeukaryotes displayed higher average abundances offshore (Fig. 1c) and pigmented nanoflagellates over the shelf (Fig 1a) this difference was not significative.

Table I. Mean abundance ($\bar{x}$, 10^6 cells L^{-1}) with standard deviation and median (M), of the phytoplankton and bacterioplankton in the south-western tropical Atlantic. SB: Shallow Bottom; ML: Mixed Layer; DCM: Deep Chlorophyl Maximum; S: Shelf; SL: Slope; I: Islands; SM: Seamounts.

			Nanoflagellates	Picoeukaryotes	*Prochlorococcus* sp.	*Synechococcus* sp.	Heterotrophic Bacteria
ML	S	$\bar{x}$	0.42 ± 0.28	1.43 ± 1.01	97.17 ± 82.87	44.48 ± 53.43	2573.70 ± 1119.48
		M	0.47	1.46	10.01	27.1	2113.71
	SL	$\bar{x}$	0.34 ± 0.14	0.73 ± 0.64	159.00 ± 467.72	19.41 ± 25.09	1922.25 ± 2804.97
		M	0.31	0.52	170	12.22	1892.75
	I	$\bar{x}$	3.21 ± 1.16	1.35 ± 2.11	159.11 x ± 734.74	17.88 ± 85.13	1608.79 ± 4174.38
		M	0.22	0.54	151	16.4	1662.98
	SM	$\bar{x}$	0.27 ± 0.12	0.79 ± 0.63	183.73 ± 58.08	17.27 ± 16.99	2735.30 ± 855.11
		M	0.25	0.57	187.5	80.41	2899.28
SB	S	$\bar{x}$	0.77 ± 0.70	2.17 ± 1.48	66.44 ± 67.01	63.67 ± 57.95	2152.02 ± 890.51
		M	0.54	1.6	51.7	40.5	1910.29
DCM	SL	$\bar{x}$	0.31 ± 0.27	3.80 ± 4.90	98.39 ± 46.19	4.14 ± 1.02	1422.64 ± 465.65
		M	0.22	1.72	92.7	0	1398.58
	I	$\bar{x}$	0.31 ± 0.25	11.41 ± 11.78	80.85 ± 44.12	3.28 ± 5.80	1248.60 ± 571.60
		M	0.24	6.51	78.55	0.95	1216.82
	SM	$\bar{x}$	0.26 ± 0.15	15.23 ± 21.30	86.40 ± 22.03	4.43 ± 7.44	2247.66 ± 799.69
		M	0.19	6.35	85.45	0.81	2218.79
200m	SL	$\bar{x}$	0.02 ± 0.02	0.03 ± 0.12	0.67 ± 0.66	0.15 ± 0.04	691.58 ± 264.59
		M	0.02	0	0.47	0	688.8
	I	$\bar{x}$	0.27 ± 1.02	0.10 ± 0.19	0.19 ± 0.14	0.02 ± 0.03	330.56 ± 167.76
		M	0	0	0.17	4.23	299.43
	SM	$\bar{x}$	0.01 ± 0.02	0.44 ± 1.26	0.55 ± 0.63	17 ± 33	1523.81 ± 861.95
		M	0.005	0	0.25	0	1679.66

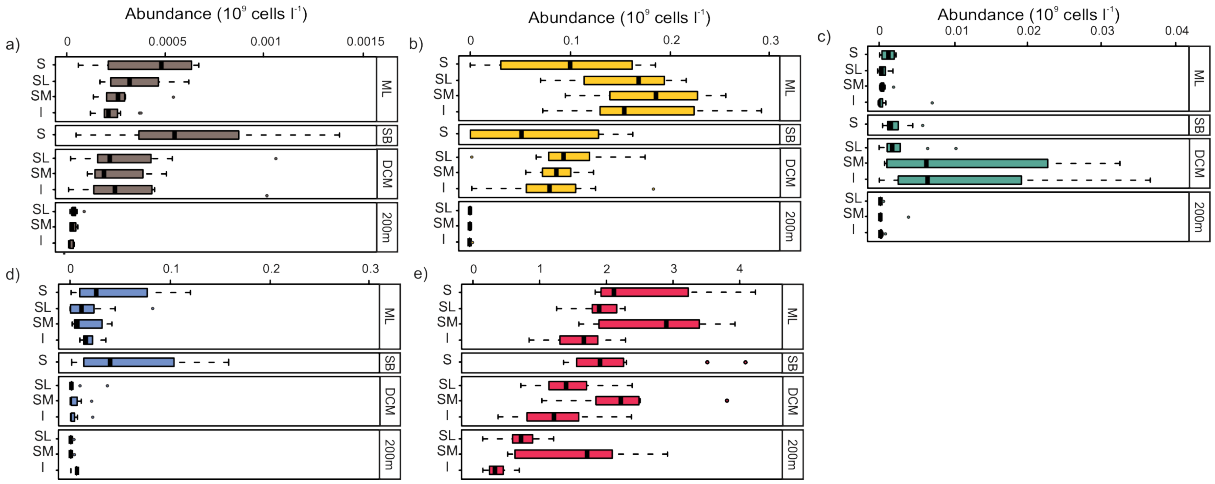

Fig. 1 Total abundance (10^9 cells L^{-1}) of pigmented Nanoflagellates (a), *Prochlorococcus* (b), Picoeukaryotes (c), *Synechococcus* sp. (d) and HB (e) in the SWTA. ML: Mixed Layer; SB:

Shallow Bottom; DCM: Deep Chlorophyll Maximum; S: Shelf; SL: Slope; SM: Seamounts; I: Islands.

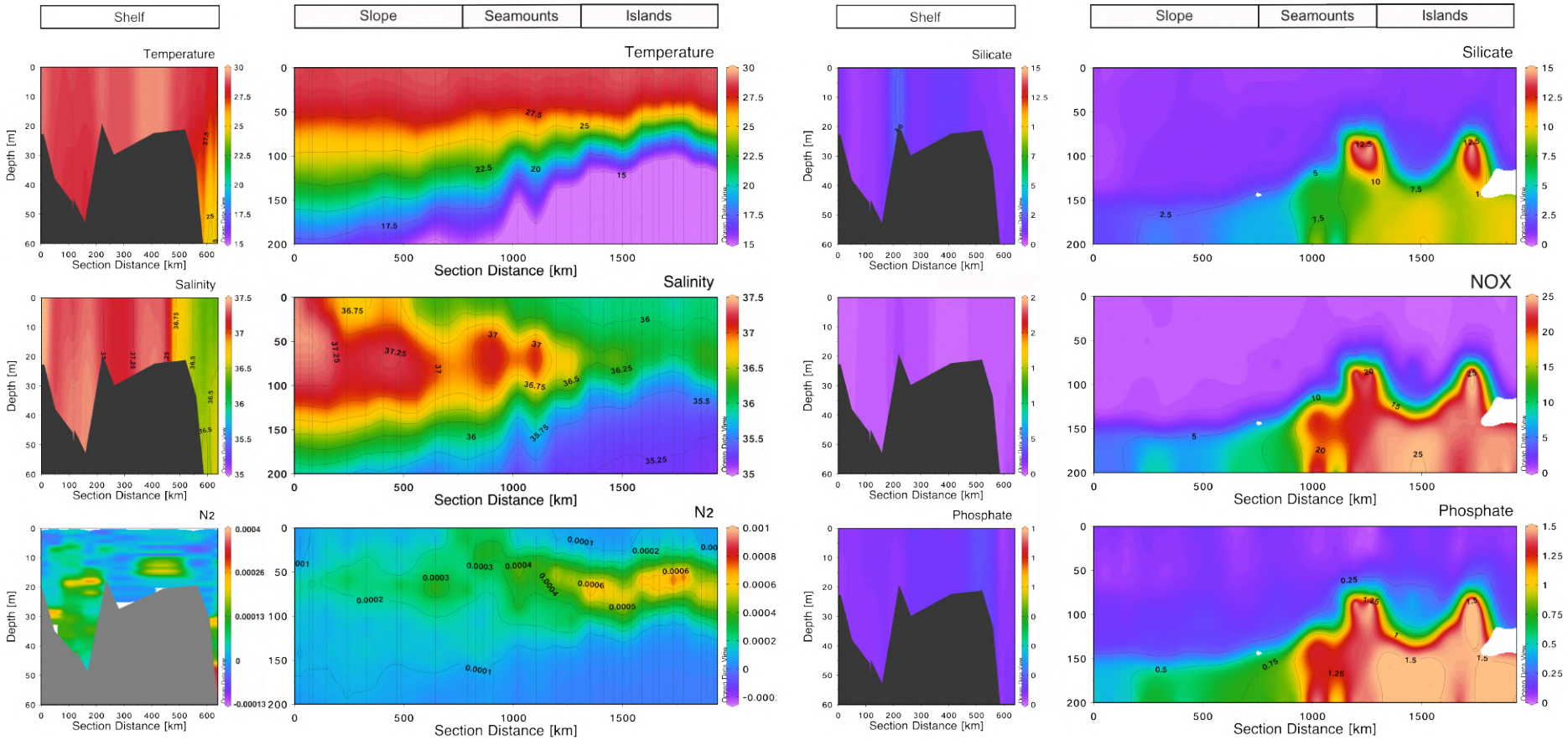

SF1. Vertical and coast-offshore profiles of temperature (°C), salinity, stratification (N2) and nutrient concentrations (µmol l^{-1}). The bar over profiles indicates the different regions, station numbers are indicated over the plots. Notice the different depths and scales between plots. On the profiles, the shelf section represents a south-north transect, while the offshore section is a west-east transect.

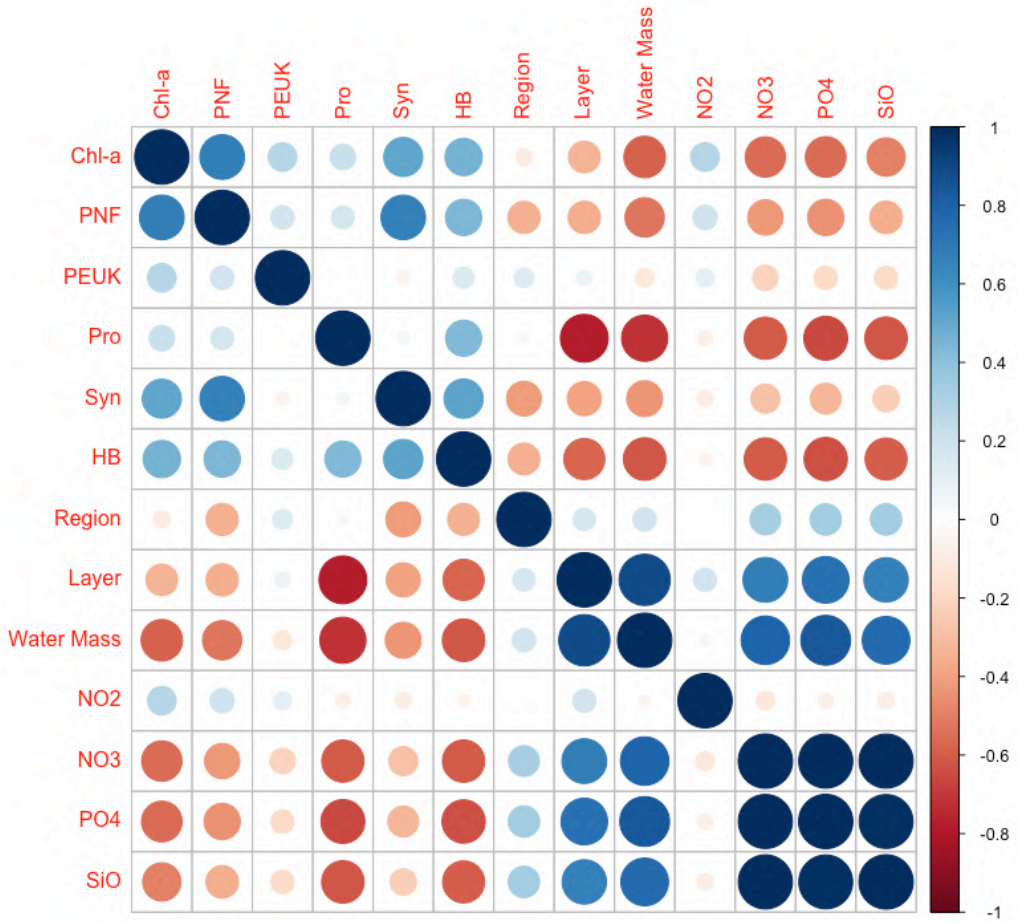

SF2. Correlation plot between biological (taxa biomass) and environmental variables in the SWTA. Chl-a: total phytoplankton community chlorophyll-a biomass; PNF: Pigmented Nanoflagellates; PEUK: Picoeukaryotes; Pro: *Prochlorococcus*; Syn: *Synechococcus*; HB: Heterotrophic Bacteria

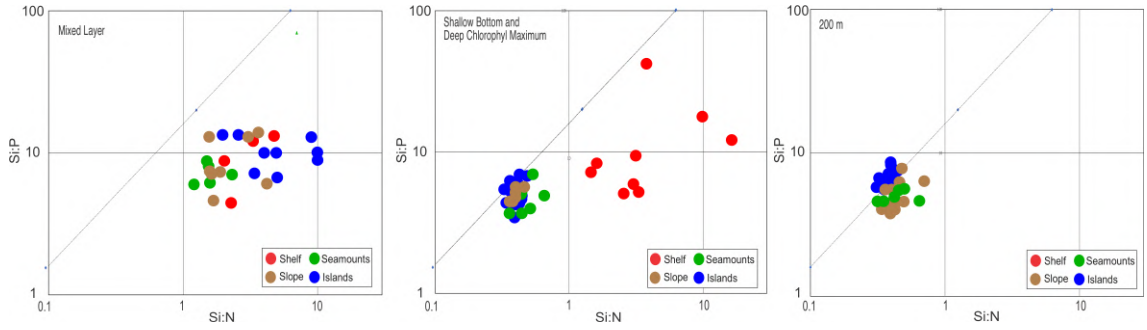

SF3. Si:N and Si:P diagram between regions and depths showing the logarithm ratio of nutrients relative to each water mass. The solid line indicates the ideal P:N in the Redfield Ratio. Values on the right side of the line indicate N and Si limitation, while values on the left side of the line indicate P and Si limitation.

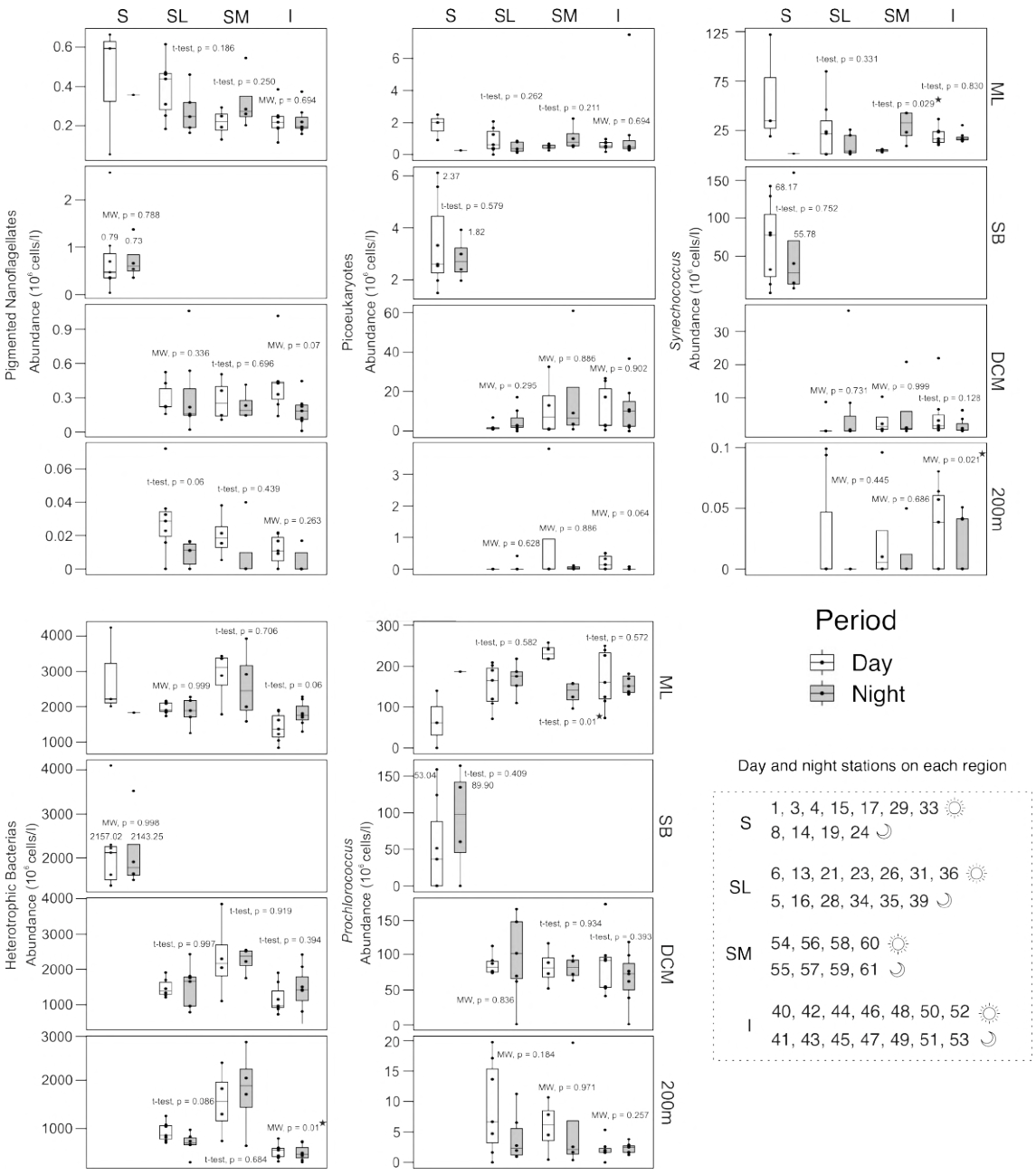

SF4. Abundance (10^6 cells l^{-1}) of the different microbial groups between day and night in the different regions and depths; S: Shelf; SL: Slope; SM:Seamounts; I: Islands; ML: Mixed layer; SB: Shallow Bottom; DCM: Deep Chlorophyll Maximum; Stars indicate significative differences. Day-night differences on the shelf were not tested in most of the depths because there were fewer than three samples during the night.

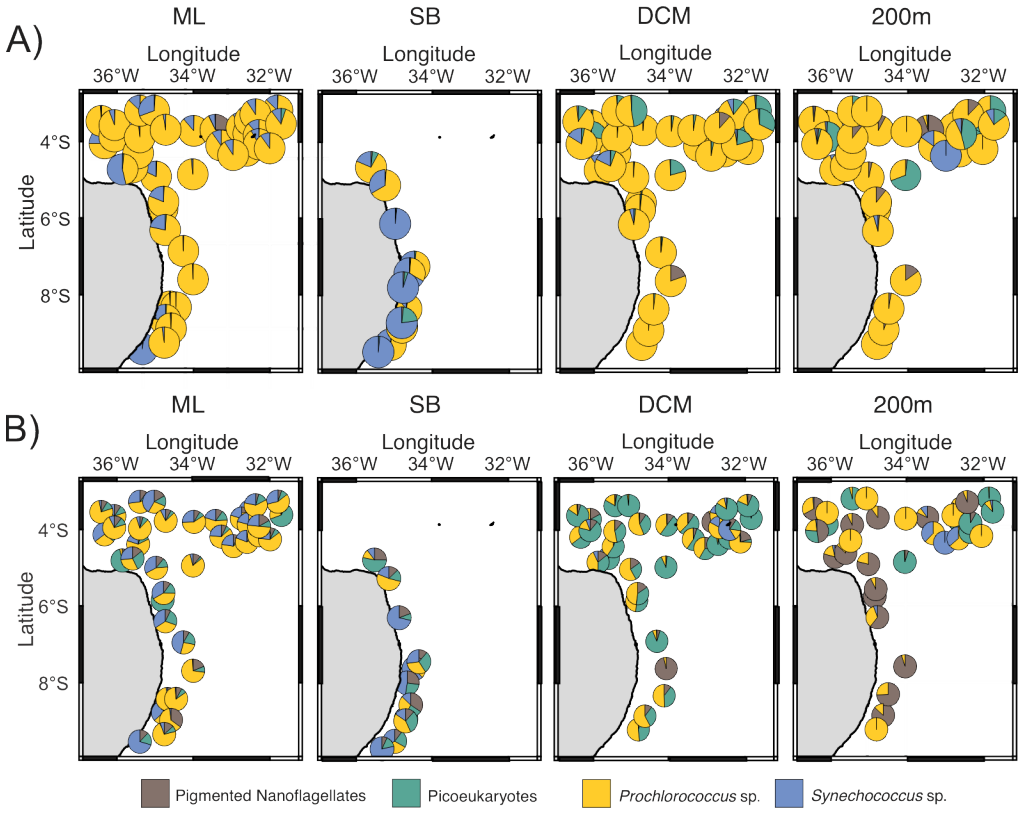

SF5. Relative abundance (A) and biomass (B) of autotrophic pico- and nanophytoplankton in the southwestern tropical Atlantic. ML: Mixed Layer; SB: Shallow Bottom; DCM: Deep Chlorophyll Maximum.

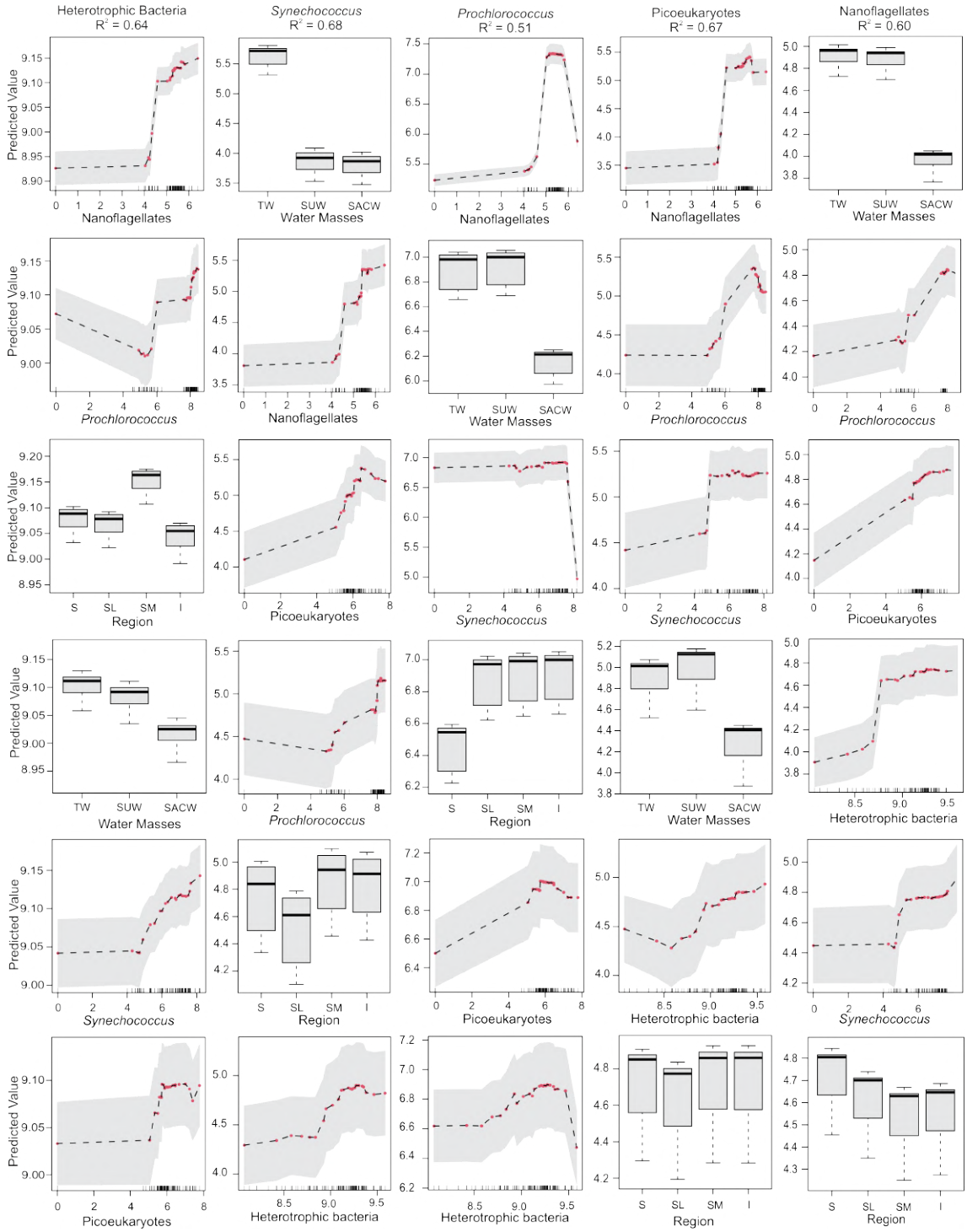

SF6. Partial responses of plankton groups (rows) to top predictor variables as depicted by Random Forest (from left to right according to their hierarchical order of importance). In plots showing dependence curves to continuous predictors (abundance of plankton groups), solid lines represent the mean partial dependence of the response variables, and shaded areas are the 95% confidence intervals. Box plots denote the mean dependence and error intervals for each level of categorical variables (water mass and regions). The percentage of explained variance of each model is shown in parentheses.

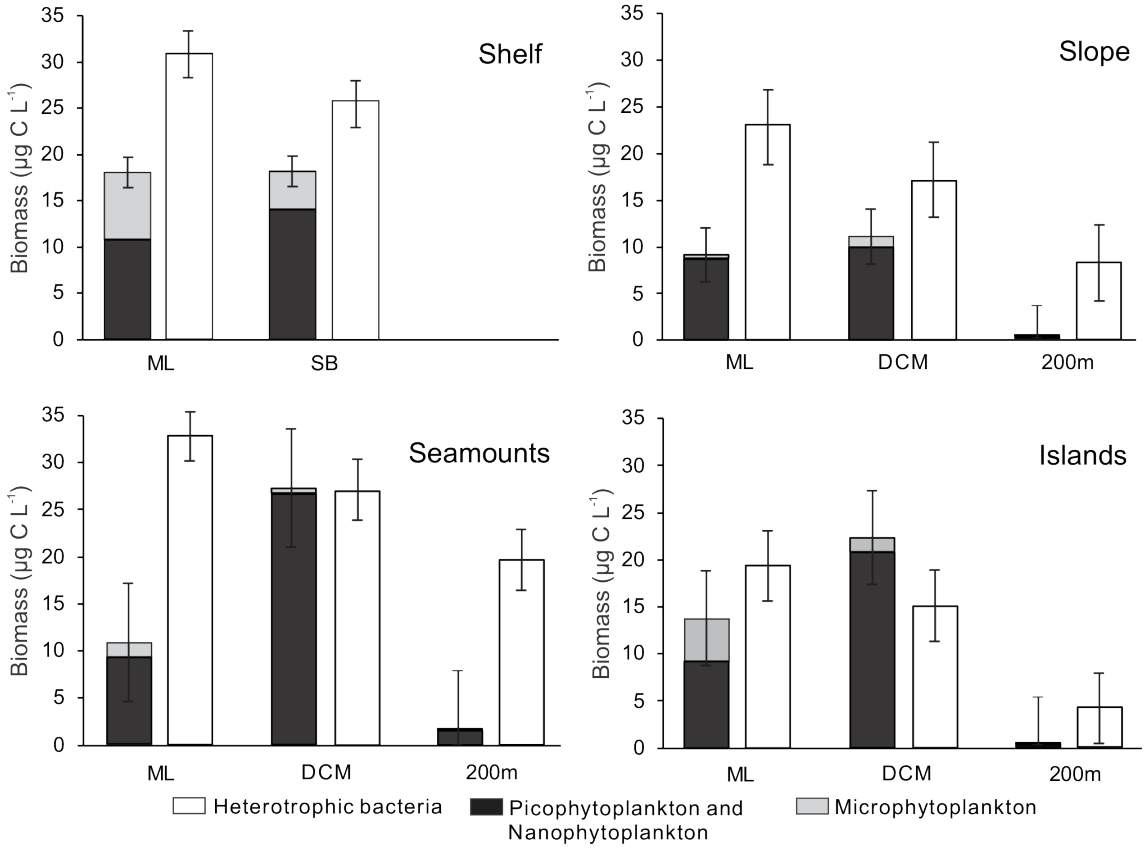

SF7. Total autotrophic (pico- nano- and microphytoplankton) and heterotrophic carbon biomass (µg C l^{-1}) in the SWTA. ML: Mixed Layer; SB: Shallow Bottom; DCM: Deep Chlorophyll Maximum.

Supplementary Table I. Sampled stations with associated metadata

Station	Date	Latitude	Longitude	Region	Layer	Water Mass	Turn	Sampled
1	2017-04-09T19:20:00	-8.6668667	-34.7962	Shelf	ML	TSW	Day	CTD; Nutrients; Cytometry
1	2017-04-09T19:20:00	-8.6668667	-34.7962	Shelf	SB	TSW	Day	CTD; Nutrients; Cytometry
3	2017-04-10T12:54:00	-9.4027203	-35.393964	Shelf	ML	TSW	Day	CTD; Nutrients; Cytometry
3	2017-04-10T12:54:00	-9.4027203	-35.393964	Shelf	SB	TSW	Day	CTD; Nutrients; Cytometry
4	2017-04-10T19:22:00	-9.2170272	-35.076225	Shelf	SB	TSW	Day	CTD; Nutrients; Cytometry
5	2017-04-10T23:12:00	-9.2139792	-34.765635	Slope	DCM	SUW	Night	CTD; Nutrients; Cytometry
5	2017-04-10T23:12:00	-9.2139792	-34.765635	Slope	ML	TSW	Night	CTD; Nutrients; Cytometry
5	2017-04-10T23:12:00	-9.2139792	-34.765635	Slope	200m	SACW	Night	CTD; Nutrients; Cytometry
6	2017-04-11T13:18:00	-8.8556427	-34.588563	Slope	DCM	SUW	Day	CTD; Nutrients; Cytometry
6	2017-04-11T13:18:00	-8.8556427	-34.588563	Slope	ML	TSW	Day	CTD; Nutrients; Cytometry
6	2017-04-11T13:18:00	-8.8556427	-34.588563	Slope	200m	SACW	Day	CTD; Nutrients; Cytometry
8	2017-04-11T21:46:00	-8.7131378	-34.803591	Shelf	SB	TSW	Night	CTD; Nutrients; Cytometry
13	2017-04-13T20:19:00	-8.3174062	-34.459037	Slope	DCM	SUW	Day	CTD; Nutrients; Cytometry
13	2017-04-13T20:19:00	-8.3174062	-34.459037	Slope	ML	TSW	Day	CTD; Nutrients; Cytometry
13	2017-04-13T20:19:00	-8.3174062	-34.459037	Slope	200m	SACW	Day	CTD; Nutrients; Cytometry
14	2017-04-14T01:26:00	-8.321901	-34.67566	Shelf	SB	TSW	Night	CTD; Nutrients; Cytometry
14	2017-04-14T01:26:00	-8.321901	-34.67566	Shelf	ML	TSW	Night	CTD; Nutrients; Cytometry
15	2017-04-14T15:23:00	-7.7786417	-34.762533	Shelf	SB	TSW	Day	CTD; Nutrients; Cytometry
16	2017-04-14T23:34:02	-7.59948	-34.020804	Slope	ML	TSW	Night	CTD; Nutrients; Cytometry
16	2017-04-14T23:34:02	-7.59948	-34.020804	Slope	DCM	SUW	Night	CTD; Nutrients; Cytometry
16	2017-04-14T23:34:02	-7.59948	-34.020804	Slope	200m	SACW	Night	CTD; Nutrients; Cytometry
17	2017-04-15T12:48:00	-7.530556	-34.80833	Shelf	SB	TSW	Day	CTD; Nutrients; Cytometry
19	2017-04-15T21:05:00	-7.2519473	-34.471376	Shelf	SB	TSW	Night	CTD; Nutrients; Cytometry
21	2017-04-16T13:16:02	-6.8761558	-34.269928	Slope	ML	TSW	Day	CTD; Nutrients; Cytometry
21	2017-04-16T13:16:03	-6.8761558	-34.269928	Slope	DCM	SUW	Day	CTD; Nutrients; Cytometry
21	2017-04-16T13:16:04	-6.8761558	-34.269928	Slope	200m	SACW	Day	CTD; Nutrients; Cytometry
23	2017-04-17T12:28:02	-6.3364257	-34.738421	Slope	DCM	SUW	Night	CTD; Nutrients; Cytometry
23	2017-04-17T12:28:03	-6.3364257	-34.738421	Slope	ML	TSW	Day	CTD; Nutrients; Cytometry
23	2017-04-17T12:28:04	-6.3364257	-34.738421	Slope	200m	SACW	Day	CTD; Nutrients; Cytometry
24	2017-04-17T23:18:00	-6.163746	-34.963501	Shelf	SB	TSW	Night	CTD; Nutrients; Cytometry
26	2017-04-18T12:52:01	-5.7951543	-34.806481	Slope	ML	TSW	Day	CTD; Nutrients; Cytometry
26	2017-04-18T12:52:02	-5.7951543	-34.806481	Slope	DCM	SUW	Day	CTD; Nutrients; Cytometry
26	2017-04-18T12:52:03	-5.7951543	-34.806481	Slope	200m	SACW	Day	CTD; Nutrients; Cytometry
28	2017-04-19T00:29:01	-5.6101953	-34.783051	Slope	ML	TSW	Night	CTD; Nutrients; Cytometry
28	2017-04-19T00:29:02	-5.6101953	-34.783051	Slope	DCM	SUW	Night	CTD; Nutrients; Cytometry
28	2017-04-19T00:29:03	-5.6101953	-34.783051	Slope	200m	SACW	Night	CTD; Nutrients; Cytometry
29	2017-04-19T12:24:00	-5.1901342	-35.221118	Shelf	SB	TSW	Day	CTD; Nutrients; Cytometry
31	2017-04-19T18:22:01	-4.9665128	-34.974074	Slope	ML	TSW	Day	CTD; Nutrients; Cytometry
31	2017-04-19T18:22:02	-4.9665128	-34.974074	Slope	DCM	SUW	Day	CTD; Nutrients; Cytometry
31	2017-04-19T18:22:03	-4.9665128	-34.974074	Slope	200m	SACW	Day	CTD; Nutrients; Cytometry
33	2017-04-20T17:37:00	-4.7279665	-35.58116	Shelf	ML	TSW	Day	CTD; Nutrients; Cytometry

33	2017-04-20T17:37:01	-4.7279665	-35.58116	Shelf	SB	TSW	Day	CTD; Nutrients; Cytometry
34	2017-04-20T21:16:01	-4.6760618	-35.565917	Slope	DCM	TSW	Night	CTD; Nutrients; Cytometry
34	2017-04-20T21:16:02	-4.6760618	-35.565917	Slope	200m	SACW	Night	CTD; Nutrients; Cytometry
35	2017-04-21T00:23:02	-4.3609118	-35.436655	Slope	DCM	SUW	Night	CTD; Nutrients; Cytometry
35	2017-04-21T00:23:03	-4.3609118	-35.436655	Slope	ML	TSW	Night	CTD; Nutrients; Cytometry
35	2017-04-21T00:23:04	-4.3609118	-35.436655	Slope	200m	SACW	Night	CTD; Nutrients; Cytometry
36	2017-04-21T12:26:02	-4.7773767	-35.841996	Slope	DCM	TSW	Day	CTD; Nutrients; Cytometry
36	2017-04-21T12:26:03	-4.7773767	-35.841996	Slope	ML	TSW	Day	CTD; Nutrients; Cytometry
36	2017-04-21T12:26:04	-4.7773767	-35.841996	Slope	200m	SACW	Day	CTD; Nutrients; Cytometry
39	2017-04-24T23:40:02	-4.9078495	-34.026656	Slope	DCM	SUW	Night	CTD; Nutrients; Cytometry
39	2017-04-24T23:40:03	-4.9078495	-34.026656	Slope	200m	SACW	Night	CTD; Nutrients; Cytometry
39	2017-04-24T23:40:04	-4.9078495	-34.026656	Slope	ML	TSW	Night	CTD; Nutrients; Cytometry
40	2017-04-26T12:31:02	-3.519792	-32.551878	Islands	ML	TSW	Day	CTD; Nutrients; Cytometry
40	2017-04-26T12:31:03	-3.519792	-32.551878	Islands	DCM	TSW	Day	CTD; Nutrients; Cytometry
40	2017-04-26T12:31:04	-3.519792	-32.551878	Islands	200m	SACW	Day	CTD; Nutrients; Cytometry
41	2017-04-26T23:46:02	-3.3608402	-32.408411	Islands	DCM	TSW	Night	CTD; Nutrients; Cytometry
41	2017-04-26T23:46:03	-3.3608402	-32.408411	Islands	ML	TSW	Night	CTD; Nutrients; Cytometry
41	2017-04-26T23:46:04	-3.3608402	-32.408411	Islands	200m	SACW	Night	CTD; Nutrients; Cytometry
42	2017-04-27T15:01:02	-3.2667177	-31.837298	Islands	DCM	SUW	Day	CTD; Nutrients; Cytometry
42	2017-04-27T15:01:03	-3.2667177	-31.837298	Islands	ML	TSW	Day	CTD; Nutrients; Cytometry
42	2017-04-27T15:01:04	-3.2667177	-31.837298	Islands	200m	SACW	Day	CTD; Nutrients; Cytometry
43	2017-04-28T00:30:02	-3.6102723	-31.747895	Islands	DCM	SUW	Night	CTD; Nutrients; Cytometry
43	2017-04-28T00:30:03	-3.6102723	-31.747895	Islands	ML	TSW	Night	CTD; Nutrients; Cytometry
43	2017-04-28T00:30:04	-3.6102723	-31.747895	Islands	200m	SACW	Night	CTD; Nutrients; Cytometry
44	2017-04-28T14:25:02	-3.9002778	-32.322995	Islands	DCM	TSW	Day	CTD; Nutrients; Cytometry
44	2017-04-28T14:25:02	-3.9002778	-32.322995	Islands	ML	TSW	Day	CTD; Nutrients; Cytometry
44	2017-04-28T14:25:02	-3.9002778	-32.322995	Islands	200m	SACW	Day	CTD; Nutrients; Cytometry
45	2017-04-29T00:03:02	-4.2383205	-32.039352	Islands	DCM	TSW	Night	CTD; Nutrients; Cytometry
45	2017-04-29T00:03:02	-4.2383205	-32.039352	Islands	ML	TSW	Night	CTD; Nutrients; Cytometry
45	2017-04-29T00:03:02	-4.2383205	-32.039352	Islands	200m	SACW	Night	CTD; Nutrients; Cytometry
46	2017-04-29T13:00:02	-4.132613	-32.321553	Islands	DCM	TSW	Day	CTD; Nutrients; Cytometry
46	2017-04-29T13:00:02	-4.132613	-32.321553	Islands	ML	TSW	Day	CTD; Nutrients; Cytometry
46	2017-04-29T13:00:02	-4.132613	-32.321553	Islands	200m	SACW	Day	CTD; Nutrients; Cytometry
47	2017-04-29T01:33:02	-4.3010848	-32.636047	Islands	DCM	TSW	Night	CTD; Nutrients; Cytometry
47	2017-04-29T01:33:03	-4.3010848	-32.636047	Islands	ML	TSW	Night	CTD; Nutrients; Cytometry
47	2017-04-29T01:33:04	-4.3010848	-32.636047	Islands	200m	SACW	Night	CTD; Nutrients; Cytometry
48	2017-04-30T12:30:02	-4.4114628	-32.985719	Islands	DCM	TSW	Day	CTD; Nutrients; Cytometry
48	2017-04-30T12:30:03	-4.4114628	-32.985719	Islands	ML	TSW	Day	CTD; Nutrients; Cytometry
48	2017-04-30T12:30:04	-4.4114628	-32.985719	Islands	200m	SACW	Day	CTD; Nutrients; Cytometry
49	2017-04-30T23:15:02	-4.1671812	-33.294324	Islands	DCM	SUW	Night	CTD; Nutrients; Cytometry
49	2017-04-30T23:15:03	-4.1671812	-33.294324	Islands	ML	TSW	Night	CTD; Nutrients; Cytometry
49	2017-04-30T23:15:04	-4.1671812	-33.294324	Islands	200m	SACW	Night	CTD; Nutrients; Cytometry
50	2017-05-01T12:48:02	-3.8540693	-32.589739	Islands	DCM	SUW	Day	CTD; Nutrients; Cytometry

50	2017-05-01T12:48:03	-3.8540693	-32.589739	Islands	ML	TSW	Day	CTD; Nutrients; Cytometry
50	2017-05-01T12:48:04	-3.8540693	-32.589739	Islands	200m	SACW	Day	CTD; Nutrients; Cytometry
51	2017-05-01T23:11:02	-3.7037482	-32.768347	Islands	ML	TSW	Night	CTD; Nutrients; Cytometry
51	2017-05-01T23:11:03	-3.7037482	-32.768347	Islands	DCM	SUW	Night	CTD; Nutrients; Cytometry
51	2017-05-01T23:11:04	-3.7037482	-32.768347	Islands	200m	SACW	Night	CTD; Nutrients; Cytometry
52	2017-05-02T13:34:00	-3.7617878	-33.440053	Islands	DCM	SUW	Day	CTD; Nutrients; Cytometry
52	2017-05-02T13:34:00	-3.7617878	-33.440053	Islands	ML	TSW	Day	CTD; Nutrients; Cytometry
52	2017-05-02T13:34:00	-3.7617878	-33.440053	Islands	200m	SACW	Day	CTD; Nutrients; Cytometry
53	2017-05-03T00:07:02	-3.7881942	-34.001317	Islands	ML	TSW	Night	CTD; Nutrients; Cytometry
53	2017-05-03T00:07:03	-3.7881942	-34.001317	Islands	DCM	SUW	Night	CTD; Nutrients; Cytometry
53	2017-05-03T00:07:04	-3.7881942	-34.001317	Islands	200m	SACW	Night	CTD; Nutrients; Cytometry
54	2017-05-03T13:02:02	-3.7616155	-34.728971	Seamounts	DCM	SUW	Day	CTD; Nutrients; Cytometry
54	2017-05-03T13:02:03	-3.7616155	-34.728971	Seamounts	ML	TSW	Day	CTD; Nutrients; Cytometry
54	2017-05-03T13:02:04	-3.7616155	-34.728971	Seamounts	200m	SACW	Day	CTD; Nutrients; Cytometry
55	2017-05-04T00:15:02	-3.2689148	-35.022454	Seamounts	DCM	SUW	Night	CTD; Nutrients; Cytometry
55	2017-05-04T00:15:03	-3.2689148	-35.022454	Seamounts	ML	TSW	Night	CTD; Nutrients; Cytometry
55	2017-05-04T00:15:04	-3.2689148	-35.022454	Seamounts	200m	SACW	Night	CTD; Nutrients; Cytometry
56	2017-05-04T12:34:02	-3.9525453	-35.394365	Seamounts	ML	TSW	Day	CTD; Nutrients; Cytometry
56	2017-05-04T12:34:03	-3.9525453	-35.394365	Seamounts	DCM	SUW	Day	CTD; Nutrients; Cytometry
56	2017-05-04T12:34:04	-3.9525453	-35.394365	Seamounts	200m	SACW	Day	CTD; Nutrients; Cytometry
57	2017-05-05T00:44:02	-3.2701682	-35.391654	Seamounts	DCM	SUW	Night	CTD; Nutrients; Cytometry
57	2017-05-05T00:44:03	-3.2701682	-35.391654	Seamounts	ML	TSW	Night	CTD; Nutrients; Cytometry
57	2017-05-05T00:44:04	-3.2701682	-35.391654	Seamounts	200m	SACW	Night	CTD; Nutrients; Cytometry
58	2017-05-05T13:44:02	-3.9335167	-36.053157	Seamounts	DCM	SUW	Day	CTD; Nutrients; Cytometry
58	2017-05-05T13:44:03	-3.9335167	-36.053157	Seamounts	ML	TSW	Day	CTD; Nutrients; Cytometry
58	2017-05-05T13:44:04	-3.9335167	-36.053157	Seamounts	200m	SACW	Day	CTD; Nutrients; Cytometry
59	2017-05-05T23:30:02	-3.6389753	-36.047721	Seamounts	ML	TSW	Night	CTD; Nutrients; Cytometry
59	2017-05-05T23:30:03	-3.6389753	-36.047721	Seamounts	DCM	SUW	Night	CTD; Nutrients; Cytometry
59	2017-05-05T23:30:04	-3.6389753	-36.047721	Seamounts	200m	SACW	Night	CTD; Nutrients; Cytometry
60	2017-05-06T12:30:02	-3.5327528	-36.388422	Seamounts	DCM	SUW	Day	CTD; Nutrients; Cytometry
60	2017-05-06T12:30:03	-3.5327528	-36.388422	Seamounts	ML	TSW	Day	CTD; Nutrients; Cytometry
60	2017-05-06T12:30:04	-3.5327528	-36.388422	Seamounts	200m	SACW	Day	CTD; Nutrients; Cytometry
61	2017-05-06T23:58:00	-4.1097105	-36.306802	Seamounts	ML	TSW	Night	CTD; Nutrients; Cytometry
61	2017-05-06T23:58:01	-4.1097105	-36.306802	Seamounts	DCM	TSW	Night	CTD; Nutrients; Cytometry
61	2017-05-06T23:58:02	-4.1097105	-36.306802	Seamounts	200m	SACW	Night	CTD; Nutrients; Cytometry

Supplementary Table II. PCA cumulative variance percentage and variables axis correlation. NOX: NO2 + NO3; ML: mixed layer; BLT: barrier layer thickness; N2: stratification.

	PC1	PC2	PC3	PC4	PC5
Cummulative Variance Percentage	58.54	78.94	90.27	94.92	98.55
Temperature	-0.9132431	0.22068592	-0.18853159	-0.08445459	0.01001508
Salinity	-0.8365030	-0.11750595	-0.01800384	0.43877962	-0.30551738
NOX	0.9804011	-0.11072349	0.03433945	0.08679841	-0.07067151
PO_4	0.9806872	-0.10708270	0.09265181	0.10636194	-0.04691599
SiO	0.9781172	-0.07199295	0.05203147	0.09586182	-0.07898046
ML	0.2776828	0.83559620	-0.25052165	0.31239176	0.25300670
BLT	-0.2865303	-0.87249900	-0.01437080	0.20699347	0.33481642
N2	-0.3332107	0.28449453	0.89195607	0.06209931	0.08460737

Chapter 4: Supplementary Material

Supplementary Table I. Average sizes, biovolumes (Tintinnina), and associated length-weight equations of the zooplankton.

	Average size/biovolume (µm/µm3)	Equation	Equation Reference	Average size/biovolume reference
Tintinnina				
Codonella acuta	240000	pgC = LV * 0.553 + 444.5	Verity et al., (1984)	Cunha et al., (2009)
Codonella amphorella	240000	pgC = LV * 0.553 + 444.5	Verity et al., (1984)	Cunha et al., (2009)
Codonella apicata	240000	pgC = LV * 0.553 + 444.5	Verity et al., (1984)	Cunha et al., (2009)
Codonella sp.	240000	pgC = LV * 0.553 + 444.5	Verity et al., (1984)	Cunha et al., (2009)
Tintinnopsis tocantinensis	130000	pgC = LV * 0.553 + 444.5	Verity et al., (1984)	Verity (1987)
Tintinnopsis spp.	130000	pgC = LV * 0.553 + 444.5	Verity et al., (1984)	Verity (1987)
Codonellopsis ostenfeldi	40000	pgC = LV * 0.553 + 444.5	Verity et al., (1984)	Buck et al., (1992)
Codonellopsis sp.	40000	pgC = LV * 0.553 + 444.5	Verity et al., (1984)	Buck et al., (1992)
Coxliella sp.	46000	pgC = LV * 0.553 + 444.5	Verity et al., (1984)	Cunha et al., (2009)
Dadayiella sp.	49142	pgC = LV * 0.553 + 444.5	Verity et al., (1984)	Cunha et al., (2009)
Dictyocysta spp.	118826	pgC = LV * 0.553 + 444.5	Verity et al., (1984)	Cunha et al., (2009)
Epiplocylis undella	381605	pgC = LV * 0.553 + 444.5	Verity et al., (1984)	Cunha et al., (2009)
Epiplocylis sp.	381605	pgC = LV * 0.553 + 444.5	Verity et al., (1984)	Cunha et al., (2009)
Favella enrenbergii	460000	pgC = LV * 0.553 + 444.5	Verity et al., (1984)	Verity (1987)
Eutintinnus spp.	27000	pgC = LV * 0.553 + 444.5	Verity et al., (1984)	Verity (1987)
Amphorellopsis spp.	46652	pgC = LV * 0.553 + 444.5	Verity et al., (1984)	Cunha et al., (2009)
Rabdonella elegans	244290	pgC = LV * 0.553 + 444.5	Verity et al., (1984)	Cunha et al., (2009)
Rabdonella brandti	244290	pgC = LV * 0.553 + 444.5	Verity et al., (1984)	Cunha et al., (2009)
Rabdonellopsis spp.	481342	pgC = LV * 0.553 + 444.5	Verity et al., (1984)	Cunha et al., (2009)
Undella claparedei	495064	pgC = LV * 0.553 + 444.5	Verity et al., (1984)	Cunha et al., (2009)
Undella sp.	495064	pgC = LV * 0.553 + 444.5	Verity et al., (1984)	Cunha et al., (2009)
Tintinnina (others)	47000	pgC = LV * 0.553 + 444.5	Verity et al., (1984)	Cunha et al., (2009)
Copepoda				
Nannocalanus minor	1800	log WW[ug] = (3.121 * log(TL[mm])) -7.796	Shmeleva et al., (1965)	Brun et al., (2017)
Nannocalanus sp.	1800	log WW[ug] = (3.121 * log(TL[mm])) -7.796	Shmeleva et al., (1965)	Brun et al., (2017)
Neocalanus robustior	3400	log WW[ug] = (3.086 * log(TL[mm])) -7.73	Gruzov et al. (1970)	Brun et al., (2017)
Undinula vulgaris	2500	log WW[ug] = (3.177 * log(TL[mm])) -7.974	Gruzov et al. (1970)	Brun et al., (2017)
Acrocalanus longicornis	1100	Ln OS = 2,78 ln P – 16,52	Webber and Roff (1995)	Brun et al., (2017)
Acrocalanus sp. (copepodite)	1100	Ln OS = 2,78 ln P – 16,52	Webber and Roff (1995)	Brun et al., (2017)
Calocalanos pavo	800	Ln OS = 2,78 ln P – 16,52	Webber and Roff (1995)	Brun et al., (2017)
Calocalanus sp.	800	Ln OS = 2,78 ln P – 16,52	Webber and Roff (1995)	Brun et al., (2017)
Delibus sewelli	500	Ln OS = 2,78 ln P – 16,52	Webber and Roff (1995)	Brun et al., (2017)
Delibus sp. (copepodite)	500	Ln OS = 2,78 ln P – 16,52	Webber and Roff (1995)	Brun et al., (2017)
Mecynocera sp. (copepodite)	*1000*	Ln OS = 2,78 ln P – 16,52	Webber and Roff (1995)	Brun et al., (2017)
Paracalanus aculeatus	1100	ln DW = 3.25 ln P 19.65	Chisholm et al., (1990)	Brun et al., (2017)
Paracalanus spp.	1100	ln DW = 3.25 ln P 19.65	Chisholm et al., (1990)	Brun et al., (2017)
Rhincalanus cornutus	3140	Ln OS = 2,78 ln P – 16,52	Webber and Roff (1995)	Brun et al., (2017)
Subeucalanus sp. (copepodite)	2280	Ln OS = 2,73 ln P – 15,93	Webber and Roff (1995)	Brun et al., (2017)
Clausocalanus furcatus	830	log WW[ug] = (2.489 * log(PL[um])) -5.638	Shmeleva et al., (1965)	Brun et al., (2017)
Clausocalanus mastigophorus	1410	log WW[ug] = (2.489 * log(PL[um])) -5.638	Shmeleva et al., (1965)	Brun et al., (2017)
Clausocalanus spp.	1310	log WW[ug] = (2.489 * log(PL[um])) -5.638	Shmeleva et al., (1965)	Brun et al., (2017)
Euchaeta spp.	2090	ln C[ug] = (3.82 * ln(L[um])) -25.19	Stapomin (1999)	Brun et al., (2017)
Scolecithrix danae	2100	log WW[ug] = (2.46 * log(TL[mm])) -5.352	Gruzov et al. (1970)	Brun et al., (2017)
Scolecithrix sp. (copepodite)	2500	log WW[ug] = (2.46 * log(TL[mm])) -5.352	Gruzov et al. (1970)	Brun et al., (2017)
Lucicutia flavicornis	1400	log WW[ug] = (3.327 * log(PL[um])) -8.007	Shmeleva et al., (1965)	Brun et al., (2017)
Lucicutia sp.	1400	log WW[ug] = (3.327 * log(PL[um])) -8.007	Shmeleva et al., (1965)	Brun et al., (2017)
Pleuromamma sp. (copepodite)	1760	log WW[ug] = (2.977 * log(TL[mm])) -7.438	Gruzov et al. (1970)	Brun et al., (2017)
Temora stylifera	950	log WW[ug] = (2.057 * log(PL[um])) -4.042	Shmeleva et al., (1965)	Brun et al., (2017)
Temora turbinata	1350	Ln OS = 3,34 ln P – 19,59	Chisholm et al., (1990)	Brun et al., (2017)
Candacia spp.	1850	log WW[ug] = (3.012 * log(TL[mm])) -7.506	Gruzov et al. (1970)	Brun et al., (2017)
Candacia sp. (copepodite)	1850	log WW[ug] = (3.012 * log(TL[mm])) -7.506	Gruzov et al. (1970)	Brun et al., (2017)
Calanopia americana	1500	Ln OS = 2,67 ln P – 15,47	Chisholm et al., (1990)	Brun et al., (2017)
Acartia danae	1000	Ln OS = 3,09 ln P – 19,19	Chisholm et al., (1990)	Brun et al., (2017)
Acartia lilljeborgii	1250	Ln OS = 3,09 ln P – 19,19	Chisholm et al., (1990)	Brun et al., (2017)
Calanoida (others copepodite)	2000	Ln OS = 2,73 ln P – 15,93	Webber and Roff (1995)	Brun et al., (2017)
Oithona atlantica	850	Ln OS = 1,68 ln P – 10,20	Ara (2001)	Brun et al., (2017)
Oithona plumifera	850	Ln OS = 1,68 ln P – 10,20	Webber and Roff (1995)	Brun et al., (2017)
Oithona setigera	850	Ln OS = 1,10 ln P – 7,07	Chisholm et al., (1990)	Brun et al., (2017)
Oithona hebes	850	Ln OS = 1,10 ln P – 7,07	Chisholm et al., (1990)	Brun et al., (2017)
Oithona spp.	850	Ln OS = 1,10 ln P – 7,07	Chisholm et al., (1990)	Brun et al., (2017)
Microsetella norvegica	620	Ln OS = 3,25 ln P – 19,65	Webber and Roff (1995)	Brun et al., (2017)
Microsetella rosea	620	Ln OS = 3,25 ln P – 19,65	Webber and Roff (1995)	Brun et al., (2017)
Microsetella spp.	620	Ln OS = 3,25 ln P – 19,65	Webber and Roff (1995)	Brun et al., (2017)

Macrosetella gracilis	1280	ln DW = 2.52 ln P 16.03	Webber and Roff (1995)	Brun et al., (2017)
Miracia efferata	1640	Ln OS = 1,53 ln P – 8,7	Webber and Roff (1995)	Brun et al., (2017)
Oncaea media	440	ln C[ug] = (2.9 * ln(L[um])) -17.5	Stapomin (1999)	Brun et al., (2017)
Oncaea venusta	440	ln C[ug] = (2.9 * ln(L[um])) -17.5	Stapomin (1999)	Brun et al., (2017)
Oncaea mediterranea	440	ln C[ug] = (2.9 * ln(L[um])) -17.5	Stapomin (1999)	Brun et al., (2017)
Oncaea scottodicarloi	440	ln C[ug] = (2.9 * ln(L[um])) -17.5	Stapomin (1999)	Brun et al., (2017)
Oncaea spp.	440	ln C[ug] = (2.9 * ln(L[um])) -17.5	Stapomin (1999)	Brun et al., (2017)
Hemicyclops thallassius	850	Ln OS = 1,53 ln P – 8,7	Webber and Roff (1995)	Brun et al., (2017)
Copilia spp.	3240	Ln OS = 1,53 ln P – 8,7	Webber and Roff (1995)	Brun et al., (2017)
Agetus flaccus	1470	Ln OS = 1,53 ln P – 8,7	Webber and Roff (1995)	Brun et al., (2017)
Corycaeus speciosus	1570	ln C[ug] = (1.99 * ln(L[um])) -12.21	Stapomin (1999)	Brun et al., (2017)
Corycaeus spp.	1570	ln C[ug] = (1.99 * ln(L[um])) -12.21	Stapomin (1999)	Brun et al., (2017)
Farranula gracilis	810	Ln OS = 2,52 ln P – 16,03	Webber and Roff (1995)	Brun et al., (2017)
Farranula spp.	810	Ln OS = 2,52 ln P – 16,03	Webber and Roff (1995)	Brun et al., (2017)
Chaetognatha				
Sagitta friedreich	4900	Log = 2,8 Log L – 0,6	Imao et al., (2005)	Boltovoskoy et al., (2002)
Sagitta spp.	4900	Log = 2,8 Log L – 0,6	Imao et al., (2005)	Boltovoskoy et al., (2002)
Chaetognatha (others)	4900	Log = 2,8 Log L – 0,6	Imao et al., (2005)	Boltovoskoy et al., (2002)

Supplementary Table II. Trophic mode of the identified taxa

Taxa	Trophic Mode	References
Bacillariophyceae		
Grammatophora sp.	Autotrophic	Kraberg et al., (2010)
Planktoniella sol	Autotrophic	Kraberg et al., (2010)
Pleuro/gyrosigma sp.	Autotrophic	Kraberg et al., (2010)
Podocystis adriatica	Autotrophic	Kraberg et al., (2010)
Podocystis sp.	Autotrophic	Kraberg et al., (2010)
Proboscia alata	Autotrophic	Bachimanchi et al. (2022)
Proboscia sp.	Autotrophic	Bachimanchi et al. (2022)
Pseudo-nitzschia pungens	Autotrophic	Kraberg et al., (2010)
Pseudo-nitzschia spp.	Autotrophic	Kraberg et al., (2010)
Thalassionema nitzschioides	Autotrophic	Bachimanchi et al. (2022)
Thalassiosira sp.	Autotrophic	Bachimanchi et al. (2022)
Actinoptychus sp.	Autotrophic	Hällfors (2004)
Amphiprora sp.	Autotrophic	Hällfors (2004)
Amphora spp.	Autotrophic	Kraberg et al., (2010)
Amphora turgida var. turgida	Autotrophic	Kraberg et al., (2010)
Asterionella bleakeleyi var. notata	Autotrophic	Hällfors (2004)
Asterionella sp. 2	Autotrophic	Hällfors (2004)
Asteromphalus flabellatus	Autotrophic	Coroppo et al., (1999)
Campyloneis sp.	Autotrophic	Kraberg et al., (2010)
Campylosira sp.	Autotrophic	Kraberg et al., (2010)
Centrics spp.	Autotrophic	Kraberg et al., (2010)
Chaetoceros spp.	Autotrophic	Coroppo et al., (1999)
Cocconeis spp.	Autotrophic	Kraberg et al., (2010)
Coscinodiscus spp.	Autotrophic	Kraberg et al., (2010)
Cyclotella sp. 2	Autotrophic	Villanova et al., (2021)
Cylindrotheca closterium	Autotrophic	Coroppo et al., (1999)
Cylindrotheca sp.	Autotrophic	Coroppo et al., (1999)
Dimeregramma dubium	Autotrophic	Kraberg et al., (2010)
Diploneis sp.	Autotrophic	Kraberg et al., (2010)
Entomoneis alata	Autotrophic	Kraberg et al., (2010)
Fragilaria unipunctata	Autotrophic	Hällfors (2004)
Gossleriella tropica	Autotrophic	Kraberg et al., (2010)
Helicotheca tamesis	Autotrophic	Hällfors (2004)
Hemiaulus membranaceus	Autotrophic	Hällfors (2004)
Isthmia enervis	Autotrophic	Kraberg et al., (2010)
Lampriscus shadboldtianum	Autotrophic	Politis (1960)
Lyrella lyra	Autotrophic	Kraberg et al., (2010)
Mastogloia sp. 2	Autotrophic	Dey et al., (2022)
Melchersiela hexagonalis	Autotrophic	Cavalvanci et al., (2018)
Melosira sp.	Autotrophic	Hällfors (2004)
Navicula membranacea	Autotrophic	Kraberg et al., (2010)
Navicula spp.	Autotrophic	Kraberg et al., (2010)
Nitzschia longissima	Mixotrophic	Villanova et al., (2021)
Nitzschia spp.	Mixotrophic	Villanova et al., (2021)
Paralia sulcata	Autotrophic	Kraberg et al., (2010)
Pennate cf. Bacillariophycidae spp.	Autotrophic	Kraberg et al., (2010)
Pennate cf. Fragilariophycidae spp.	Autotrophic	Kraberg et al., (2010)
Plagiogramma sp.	Autotrophic	Hällfors (2004)
Plagiotropis sp. 6	Autotrophic	Hällfors (2004)

Rhabdonema adriaticum	Autotrophic	Kraberg et al., (2010)
Rhabdonema sp.	Autotrophic	Kraberg et al., (2010)
Rhizosolenia hebetata	Autotrophic	Bachimanchi et al. (2022)
Rhizosolenia spp.	Autotrophic	Bachimanchi et al. (2022)
Skeletonema costatum	Autotrophic	Hällfors (2004)
Spatangidium arachne	Autotrophic	Kraberg et al., (2010)
Striatella sp.	Autotrophic	Dey et al., (2022)
Synedra crystallina	Autotrophic	Kraberg et al., (2010)
Synedra sp. 5	Autotrophic	Kraberg et al., (2010)
Tabularia fasciculata	Autotrophic	Hällfors (2004)
Thalassiothrix 146ênue146rrânea var. pacifica	Autotrophic	Bachimanchi et al. (2022)
Thalassiothrix sp. 1	Autotrophic	Bachimanchi et al. (2022)
Triceratium pentacrinus	Autotrophic	Kraberg et al., (2010)
Triceratium sp.	Autotrophic	Kraberg et al., (2010)
Trieres mobiliensis	Autotrophic	Lavigne et al., (2015)
Chlorophyceae		
Chlorophyceae 1	Autotrophic	Kraberg et al., (2010)
Chlorophyceae 2	Autotrophic	Kraberg et al., (2010)
Chlorophyceae 3	Autotrophic	Kraberg et al., (2010)
Chlorophyceae 4	Autotrophic	Kraberg et al., (2010)
Chlorophyceae 5	Autotrophic	Kraberg et al., (2010)
Korshikoviella sp.	Autotrophic	Kraberg et al., (2010)
Oscillatoriales spp.	Autotrophic	Kraberg et al., (2010)
Spirulina sp.	Autotrophic	Kraberg et al., (2010)
Trichodesmium thiebautii	Autotrophic	Kraberg et al., (2010)
Dictyochophyceae		
Dictyocha fibula	Autotrophic	Kraberg et al., (2010)
Dictyocha sp.	Autotrophic	Kraberg et al., (2010)
Dictyochophyceae sp.	Autotrophic	Kraberg et al., (2010)
Octactis speculum	Autotrophic	Bachimanchi et al. (2022)
Dinophyceae		
Alexandrium sp. 15	Autotrophic	Kraberg et al., (2010)
Amphidoma nucula	Autotrophic	Kraberg et al., (2010)
Amphisolenia globifera	Mixotrophic	Hansen et al., (2011)
Amphisolenia schroederi	Mixotrophic	Hansen et al., (2011)
Ceratium platycorne	Mixotrophic	Barton et al., (2013)
Ceratium spp.	Autotrophic	Kraberg et al., (2010)
Ceratium tenue	Autotrophic	Kraberg et al., (2010)
Ceratium 146ênue var. buceros	Autotrophic	Kraberg et al., (2010)
Ceratium tripos var. atlanticum	Mixotrophic	Barton et al., (2013)
Ceratocorys horrida	Autotrophic	Coroppo et al., (1999)
Ceratocorys sp.	Autotrophic	Coroppo et al., (1999)
Cladopyxis brachiolata	Heterotrophic	Barton et al., (2013)
Cladopyxis hemibrachiata	Heterotrophic	Barton et al., (2013)
Cladopyxis sp.	Heterotrophic	Barton et al., (2013)
Corythodinium constrictum	Autotrophic	Kraberg et al., (2010)
Corythodinium curvicaudatum	Autotrophic	Kraberg et al., (2010)
Corythodinium diploconus	Autotrophic	Kraberg et al., (2010)
Corythodinium elegans	Autotrophic	Kraberg et al., (2010)
Corythodinium frenguellii	Autotrophic	Kraberg et al., (2010)
Corythodinium milneri	Autotrophic	Kraberg et al., (2010)
Corythodinium sp.	Autotrophic	Kraberg et al., (2010)
Corythodinium tesselatum	Autotrophic	Kraberg et al., (2010)
Coscinodiscus centralis	Autotrophic	Kraberg et al., (2010)
Coscinodiscus lineatus	Autotrophic	Kraberg et al., (2010)
Dinophyceae Athecate spp.	Autotrophic	Kraberg et al., (2010)
Dinophyceae Thecate spp.	Autotrophic	Kraberg et al., (2010)
Dinophysis argus	Mixotrophic	Kraberg et al., (2010)
Dinophysis hastata	Mixotrophic	Kraberg et al., (2010)
Dinophysis sp.	Mixotrophic	Kraberg et al., (2010)
Diplopsalid	Heterotrophic	Coroppo et al., (1999)
Gonyaulax birostris	Mixotrophic	Coroppo et al., (1999)
Gonyaulax fusiformis	Mixotrophic	Coroppo et al., (1999)
Gonyaulax polygramma	Mixotrophic	Coroppo et al., (1999)
Gonyaulax spinifera	Mixotrophic	Coroppo et al., (1999)
Gonyaulax spp.	Mixotrophic	Coroppo et al., (1999)
Gymnodinium spp.	Mixotrophic	Linacre et al., (2021)
Gyrodinium sp.	Heterotrophic	Kraberg et al., (2010)
Heterocapsa minima	Autotrophic	Kraberg et al., (2010)
Heterocapsa niei	Autotrophic	Kraberg et al., (2010)
Heterocapsa spp.	Autotrophic	Kraberg et al., (2010)
Histioneis cymbalaria	Heterotrophic	Kraberg et al., (2010)
Histioneis hyalina	Heterotrophic	Kraberg et al., (2010)
Histioneis milneri	Heterotrophic	Kraberg et al., (2010)
Histioneis spp.	Heterotrophic	Kraberg et al., (2010)

Kryptoperidinium triquetrum	Heterotrophic	Bachimanchi et al. (2022)
Lessardia elongata	Heterotrophic	Saldarriaga et al., (2003)
Lingulodinium polyedra	Autotrophic	Kraberg et al., (2010)
Metaphalacroma skogsbergii	Autotrophic	Kraberg et al., (2010)
Ornithocercus magnificus	Heterotrophic	Bachimanchi et al. (2022)
Ornithocercus quadratus	Heterotrophic	Kraberg et al., (2010)
Ornithocercus sp.	Heterotrophic	Kraberg et al., (2010)
Ornithocercus steinii	Heterotrophic	Kraberg et al., (2010)
Oxytoxum caudatum	Autotrophic	Kraberg et al., (2010)
Oxytoxum cf. sphaeroideum	Autotrophic	Kraberg et al., (2010)
Oxytoxum crassum	Autotrophic	Kraberg et al., (2010)
Oxytoxum curvatum	Autotrophic	Kraberg et al., (2010)
Oxytoxum elegans	Autotrophic	Kraberg et al., (2010)
Oxytoxum globosum	Autotrophic	Kraberg et al., (2010)
Oxytoxum laticeps	Autotrophic	Bachimanchi et al. (2022)
Oxytoxum longiceps	Autotrophic	Kraberg et al., (2010)
Oxytoxum mediterraneum	Autotrophic	Kraberg et al., (2010)
Oxytoxum obliquum	Autotrophic	Kraberg et al., (2010)
Oxytoxum parvum	Autotrophic	Kraberg et al., (2010)
Oxytoxum scolopax	Autotrophic	Kraberg et al., (2010)
Oxytoxum challengeroides	Autotrophic	Kraberg et al., (2010)
Oxytoxum spp.	Autotrophic	Kraberg et al., (2010)
Oxytoxum tesselatum	Autotrophic	Kraberg et al., (2010)
Oxytoxum turbo	Autotrophic	Kraberg et al., (2010)
Oxytoxum variabile	Heterotrophic	Coroppo et al., (1999)
Phalacroma doryphorum	Heterotrophic	Kraberg et al., (2010)
Phalacroma mitra	Heterotrophic	Kraberg et al., (2010)
Phalacroma rotundatum	Heterotrophic	Kraberg et al., (2010)
Phalacroma sp.	Heterotrophic	Kraberg et al., (2010)
Podolampas elegans	Heterotrophic	Kraberg et al., (2010)
Podolampas palmipes	Heterotrophic	Kraberg et al., (2010)
Podolampas sp.	Heterotrophic	Kraberg et al., (2010)
Podolampas spinifera	Heterotrophic	Kraberg et al., (2010)
Pronoctiluca rostrata	Heterotrophic	Coroppo et al., (1999)
Pronoctiluca spinifera	Heterotrophic	Coroppo et al., (1999)
Prorocentrum balticum	Autotrophic	Kraberg et al., (2010)
Prorocentrum cordatum	Mixotrophic	Kraberg et al., (2010)
Prorocentrum dactylus	Autotrophic	Kraberg et al., (2010)
Prorocentrum emarginatum	Autotrophic	Kraberg et al., (2010)
Prorocentrum gracile	Autotrophic	Kraberg et al., (2010)
Prorocentrum lenticulatum	Autotrophic	Kraberg et al., (2010)
Prorocentrum lima	Autotrophic	Kraberg et al., (2010)
Prorocentrum mexicanum	Autotrophic	Kraberg et al., (2010)
Prorocentrum micans	Mixotrophic	Coroppo et al., (1999)
Prorocentrum rostratum	Autotrophic	Kraberg et al., (2010)
Prorocentrum shikokuense	Autotrophic	Kraberg et al., (2010)
Prorocentrum sp. 2	Autotrophic	Kraberg et al., (2010)
Prorocentrum spp.	Autotrophic	Kraberg et al., (2010)
Prorocentrum triestinum	Mixotrophic	Kraberg et al., (2010)
Prorocentrum vaginula	Autotrophic	Kraberg et al., (2010)
Protoceratium reticulatum	Heterotrophic	Kraberg et al., (2010)
Protoceratium sp.	Heterotrophic	Kraberg et al., (2010)
Protoceratium spinulosum	Heterotrophic	Kraberg et al., (2010)
Protoperidinium cassum	Heterotrophic	Coroppo et al., (1999)
Protoperidinium deficiens	Heterotrophic	Coroppo et al., (1999)
Protoperidinium divergens	Heterotrophic	Coroppo et al., (1999)
Protoperidinium pyriforme	Heterotrophic	Coroppo et al., (1999)
Protoperidinium spp.	Heterotrophic	Coroppo et al., (1999)
Pyrocystis lunula	Heterotrophic	Coroppo et al., (1999)
Pyrocystis robusta	Heterotrophic	Coroppo et al., (1999)
Pyrocystis sp.	Heterotrophic	Coroppo et al., (1999)
Pyrophacus sp.	Autotrophic	Coroppo et al., (1999)
Schuettiella mitra	Autotrophic	Kraberg et al., (2010)
Scrippsiella acuminata	Mixotrophic	Kraberg et al., (2010)
Scrippsiella spinifera	Autotrophic	Kraberg et al., (2010)
Scrippsiella spp.	Autotrophic	Kraberg et al., (2010)
Spatulodinium pseudonoctiluca	Heterotrophic	Tarenko (2010)
Triadinium polyedricum	Autotrophic	Kraberg et al., (2010)
Tripos arietinus	Mixotrophic	Kraberg et al., (2010)
Tripos azoricus	Mixotrophic	Kraberg et al., (2010)
Tripos belone	Mixotrophic	Kraberg et al., (2010)
Tripos candelabrum	Mixotrophic	Kraberg et al., (2010)
Tripos declinatus	Mixotrophic	Kraberg et al., (2010)
Tripos extensum	Mixotrophic	Kraberg et al., (2010)
Tripos falcatus	Autotrophic	Kraberg et al., (2010)
Tripos furca	Mixotrophic	Kraberg et al., (2010)

Tripos fusus	Mixotrophic	Kraberg et al., (2010)
Tripos geniculatus	Mixotrophic	Kraberg et al., (2010)
Tripos gibberus	Autotrophic	Kraberg et al., (2010)
Tripos horridus	Mixotrophic	Kraberg et al., (2010)
Tripos incisus	Autotrophic	Kraberg et al., (2010)
Tripos kofoidii	Mixotrophic	Kraberg et al., (2010)
Tripos limulus	Autotrophic	Kraberg et al., (2010)
Tripos lineatus	Mixotrophic	Kraberg et al., (2010)
Tripos macroceros	Autotrophic	Kraberg et al., (2010)
Tripos muelleri	Mixotrophic	Kraberg et al., (2010)
Tripos pentagonus	Mixotrophic	Kraberg et al., (2010)
Tripos pulchellus	Autotrophic	Kraberg et al., (2010)
Tripos seta	Mixotrophic	Kraberg et al., (2010)
Tripos teres	Mixotrophic	Kraberg et al., (2010)
Tripos trichoceros	Autotrophic	Kraberg et al., (2010)
Triposolenia depressa	Mixotrophic	Tarangkoon (2010)
Euglenophyceae sp.	Autotrophic	Kraberg et al., (2010)
Prymnesiophyceae		
Coccolithophorid spp.	Autotrophic	Kraberg et al., (2010)
Pontosphaera sp.	Autotrophic	Hällfors (2004)
Tintinnina		
Codonella acuta	Omnivorous Filter-Feeder	Bernard and Rassoulzadegan (1993); Kim and Moon (2003); Balazi and Matis (2002)
Codonella amphorella	Omnivorous Filter-Feeder	Bernard and Rassoulzadegan (1993); Kim and Moon (2003); Balazi and Matis (2002)
Codonella apicata	Omnivorous Filter-Feeder	Bernard and Rassoulzadegan (1993); Kim and Moon (2003); Balazi and Matis (2002)
Codonella sp.	Omnivorous Filter-Feeder	Bernard and Rassoulzadegan (1993); Kim and Moon (2003); Balazi and Matis (2002)
Tintinnopsis tocantinensis	Omnivorous Filter-Feeder	Bernard and Rassoulzadegan (1993); Horsted et al (1998)
Tintinnopsis spp.	Omnivorous Filter-Feeder	Bernard and Rassoulzadegan (1993); Horsted et al (1998)
Codonellopsis ostenfeldi	Omnivorous Filter-Feeder	Bernard and Rassoulzadegan (1993); Kim et al., 2013
Codonellopsis sp.	Omnivorous Filter-Feeder	Bernard and Rassoulzadegan (1993); Kim et al., 2013
Coxliella sp.	Omnivorous Filter-Feeder	Strom (2001); Strom (2007)
Dadayiella sp.	Omnivorous Filter-Feeder	Rakshit et al (2017); Bernard and Rassoulzadegan (1993)
Dictyocysta spp.	Omnivorous Filter-Feeder	Bernard and Rassoulzadegan (1993)
Epiplocylis undella	Omnivorous Filter-Feeder	Burns (1982)
Epiplocylis sp.	Omnivorous Filter-Feeder	Burns (1982)
Favella enrenbergii	Omnivorous Filter-Feeder	Bernard and Rassoulzadegan (1993)
Eutintinnus spp.	Omnivorous Filter-Feeder	Verity (1987); Bernard and Rassoulzadegan (1993)
Amphorellopsis spp.	Omnivorous Filter-Feeder	Kamiyama and Matsuyama (2005)
Rabdonella elegans	Omnivorous Filter-Feeder	Bernard and Rassoulzadegan (1993)
Rabdonella brandti	Omnivorous Filter-Feeder	Bernard and Rassoulzadegan (1993)
Rabdonellopsis spp.	Omnivorous Filter-Feeder	
Undella claparedei	Omnivorous Filter-Feeder	Fernandes (2004)
Undella sp.	Omnivorous Filter-Feeder	Fernandes (2004)
Xystonellopsis heros	Omnivorous Filter-Feeder	Li et al (2021)
Copepoda		
Nannocalanus minor	Omnivore-Herbivore (Herbivore)	Benedetti et al., 2015; Boltovoskoy, 1999
Nannocalanus sp.	Omnivore-Herbivore (Herbivore)	Benedetti et al., 2015; Boltovoskoy, 1999
Neocalanus robustior	Carnivore	Benedetti et al., 2015; Boltovoskoy, 1999
Undinula vulgaris	Omnivore-Herbivore (Herbivore)	Wickramasinghe et al., 1982; Boltovoskoy, 1999
Acrocalanus longicornis	Herbivore	Mulyadi et al., 2018; Boltovoskoy, 1999
Acrocalanus sp. (copepodite)	Herbivore	Mulyadi et al., 2018; Boltovoskoy, 1999
Calocalanos pavo	Omnivore-Herbivore (Herbivore)	Boltovoskoy, 1999; Benedetti et al., 2015
Calocalanus sp.	Omnivore-Herbivore (Herbivore)	Boltovoskoy, 1999; Benedetti et al., 2015
Mecynocera sp. (copepodite)	Omnivore-Herbivore (Herbivore)	Brun et al., 2016; Boltovoskoy, 1999
Paracalanus aculeatus	Omnivore-Herbivore (Herbivore)	Benedetti et al., 2015; Boltovoskoy, 1999
Paracalanus spp.	Omnivore-Herbivore (Herbivore)	Benedetti et al., 2015; Boltovoskoy, 1999
Rhincalanus cornutus	Omnivore-Herbivore (Herbivore)	Benedetti et al., 2015; Boltovoskoy, 1999
Subeucalanus sp. (copepodite)	Omnivore-Herbivore (Herbivore)	Benedetti et al., 2015; Boltovoskoy, 1999
Clausocalanus furcatus	Omnivore-Herbivore (Herbivore)	Benedetti et al., 2015; Boltovoskoy, 1999
Clausocalanus mastigophorus	Omnivore-Herbivore (Herbivore)	Benedetti et al., 2015; Boltovoskoy, 1999
Clausocalanus spp.	Omnivore-Herbivore (Herbivore)	Benedetti et al., 2015; Boltovoskoy, 1999
Euchaeta spp.	Carnivore	Benedetti et al., 2015; Boltovoskoy, 1999
Scolecithrix danae	Omnivore-Detritivore	Benedetti et al., 2015; Boltovoskoy, 1999
Scolecithrix sp. (copepodite)	Omnivore-Detritivore	Benedetti et al., 2015; Boltovoskoy, 1999
Lucicutia flavicornis	Omnivore-Herbivore (Herbivore)	Benedetti et al., 2015; Boltovoskoy, 1999
Lucicutia sp.	Omnivore-Herbivore (Herbivore)	Benedetti et al., 2015; Boltovoskoy, 1999
Pleuromamma sp. (copepodite)	Omnivore	Benedetti et al., 2015; Boltovoskoy, 1999
Temora stylifera	Omnivore-Herbivore (Herbivore)	Benedetti et al., 2015; Boltovoskoy, 1999
Temora turbinata	Omnivore-Herbivore (Herbivore)	Benedetti et al., 2015; Brun et al., 2016; Boltovoskoy, 1999
Candacia spp.	Carnivore	Benedetti et al., 2015; Brun et al., 2016; Boltovoskoy, 1999
Candacia sp. (copepodite)	Carnivore	Benedetti et al., 2015; Brun et al., 2016; Boltovoskoy, 1999
Calanopia americana	Omnivore	Benedetti et al., 2015; Brun et al., 2016; Boltovoskoy, 1999
Acartia danae	Omnivore-Herbivore (Herbivore)	Benedetti et al., 2015; Brun et al., 2016; Boltovoskoy, 1999

Acartia lilljeborgii	Omnivore-Herbivore (Herbivore)	Benedetti et al., 2015; Brun et al., 2016; Boltovoskoy, 1999
Oithona atlantica	Omnivore	Benedetti et al., 2015; Boltovoskoy, 1999
Oithona plumifera	Omnivore	Benedetti et al., 2015; Boltovoskoy, 1999
Oithona setigera	Omnivore	Benedetti et al., 2015; Boltovoskoy, 1999
Oithona hebes	Omnivore	Benedetti et al., 2015; Boltovoskoy, 1999
Oithona spp.	Omnivore	Benedetti et al., 2015; Boltovoskoy, 1999
Microsetella norvegica	Omnivore-Detritivore	Benedetti et al., 2015; Boltovoskoy, 1999
Microsetella rosea	Omnivore-Detritivore	Benedetti et al., 2015; Boltovoskoy, 1999
Microsetella spp.	Omnivore-Detritivore	Benedetti et al., 2015; Boltovoskoy, 1999
Macrosetella gracilis	Omnivore-Herbivore (Herbivore)	Benedetti et al., 2015; Brun et al., 2016; Boltovoskoy, 1999
Miracia efferata	Omnivore-Herbivore (Herbivore)	O'Neil and Roman 1994; Boltovoskoy, 1999
Oncaea media	Omnivore-Detritivore	Benedetti et al., 2015; Boltovoskoy, 1999
Oncaea venusta	Omnivore-Detritivore	Benedetti et al., 2015; Boltovoskoy, 1999
Oncaea mediterranea	Omnivore-Detritivore	Benedetti et al., 2015; Boltovoskoy, 1999
Oncaea scottodicarloi	Omnivore-Detritivore	Benedetti et al., 2015; Boltovoskoy, 1999
Oncaea spp.	Omnivore-Detritivore	Benedetti et al., 2015; Boltovoskoy, 1999
Copilia spp.	Omnivore	Conceição et al., 2021; Boltovoskoy, 1999
Agetus flaccus	Omnivore-Herbivore (Herbivore)	Benedetti et al., 2015; Brun et al., 2016; Boltovoskoy, 1999
Corycaeus speciosus	Carnivore	Benedetti et al., 2015; Boltovoskoy, 1999
Corycaeus spp.	Carnivore	Benedetti et al., 2015; Boltovoskoy, 1999
Farranula gracilis	Carnivore	Benedetti et al., 2015; Brun et al., 2016; Boltovoskoy, 1999
Farranula spp.	Carnivore	Benedetti et al., 2015; Brun et al., 2016; Boltovoskoy, 1999
Chaetognatha		
Sagitta friedreich	Carnivore	Boltovoskoy, 1999
Sagitta spp.	Carnivore	Boltovoskoy, 1999
Chaetognatha (others)	Carnivore	Boltovoskoy, 1999

Supplementary Table III. Proposed conceptual models fed on the random forest analysis. SST: sea surface temperature; SSS: sea surface salinity; Areas: WBCS and SECS; PRO: *Prochlorococcus*; SYN: *Synechococcus*; HB: heterotrophic bacteria; PEUK: picoeukaryotes; PNF: pigmented nanoflagellates; AM: autotrophic microphytoplankton; MM: mixotrophic microphytoplankton; HD: heterotrophic Dinoflagellates; T: Tintinnina; HC: herbivorous Copepoda; CC: carnivorous Copepoda carnivorous; OC: omnivorous Copepoda; C: Chaetognatha.

AM = SiO + PO4 + NOX + Stratification + SST + SSS + Area + T + HC + OC
MM = SiO + PO4 + NOX + Stratification + SST + SSS + Area + PRO + PNF + SYN + HB + PEUK + T + HC + OC
HM = Stratification + SST + SSS + Area + PRO + PNF + SYN + HB + PEUK + T + OC + CC
T = Stratification + SST + SSS + Area + PRO + PNF + SYN + HB + PEUK + AM + MM + HM + HC + CC
CC = Stratification + SST + SSS + Area + MH + T + C
OC = Stratification + SST + SSS + Area + AM + MM + HM + T + C
HC = Stratification + SST + SSS + Area + AM + MM + C
C = Stratification + SST + SSS + Area + HC + CC + OC

APPENDIX B – METHODOLOGICAL APPENDIX

Laboratory Methods

The identification and quantification of plankton communities can be accomplished through various methods, including direct observation through microscopy and the use of imaging plankton counters, such as FlowCam and Zooscan. However, these methods can be time-consuming and often rely on strong taxonomic knowledge. They are also not well suited for the analysis of small-celled plankton, such as the pico- and nanoplankton communities, i.e. optical microscopy is able to distinguish microplankton (> 20 µm) at the species level, however, identifies with limitations nanoplankton (fraction between 2 and 20 µm). In such cases, techniques such as high-performance liquid chromatography (HPLC) and flow cytometry emerge as good alternatives to quickly obtain not only the identification but the quantification of the abundance and biomass of these small plankton communities.

1) High-performance liquid chromatography (HPLC)

Basis

High-Performance Liquid Chromatography (HPLC) is a widely used analytical technique in chemistry, biochemistry, and ecology. It is a type of column chromatography that separates components in a mixture based on their chemical and physical properties, such as size, charge, and affinity for the stationary phase. HPLC utilizes a high-pressure pump to force a sample mixture through a column packed with a stationary phase, which can either be a solid, or a liquid supported on a solid. The components in the mixture are then separated as they pass through the column and are detected by a detector, such as a UV-visible spectrophotometer.

In the study of plankton, the HPLC is used to identify and quantify phytoplankton communities providing information on their pigment composition, distribution, and abundance. The determination of phytoplankton composition from pigments does not depend on cell size, encompassing micro-, nano- and picoplankton, including fragile cells that may have their identifications hindered due to limitations imposed by other techniques. HPLC is capable of resolving and quantifying individual pigment compounds with high sensitivity and specificity, allowing for the determination of the relative proportions of different pigment types within a phytoplankton sample. The ratios of different pigments, such as chlorophylls and carotenoids for example, can be indicative not only of the physiological state of the phytoplankton but also used to identify taxonomic groups.

Phytoplankton and pigments

The phytoplankton photosynthesis process, responsible for half of the global organic carbon assimilation is carried out through a series of specialized pigments responsible for absorbing energy from sunlight. Chlorophyll-a and b are the most abundant of these pigments found in phytoplankton cells, as is the case of terrestrial plants. However, the phytoplankton that dominates today's oceans mostly come from secondary pigments? or later endosymbiotic events, where eukaryotic algae were taken in by a eukaryotic cell, particularly those involving the incorporation of algal red-derived chloroplasts. This means that while terrestrial plants evolved around 450 million years ago and occupy a small corner of the tree of life, the marine photosynthetic community consists of organisms with deeply rooted branches throughout the eukaryotic evolutionary tree, leading to a high diversity of pigments.

Therefore, in addition to chlorophyll a and b, the primary pigments responsible for absorbing light energy in the process of photosynthesis, cells also contain many other "photocolector pigments" such as chlorophylls c, and various carotenoids, such as peridinin, fucoxanthin, 19'hexanoyloxy-fucoxanthin, 19'butanoyloxy-fucoxanthin, and prasinoxanthin. These pigments serve to expand the light spectrum absorption range, maximizing the collection of light energy. Some carotenoids, known as "photoprotective pigments," like violaxanthin, diadinoxanthin, diatoxanthin, zeaxanthin, and lutein, protect the cells from high levels of irradiance that can harm the photosynthetic apparatus. The accessory pigments present in cells can vary among different taxonomic groups, with some specific to a particular class (such as alloxanthine in Cryptophyceae and peridinin in Dinophyceae) and others occurring in multiple groups (β-carotene, diadinoxanthine, chlorophylls-c) (Figure 1). Due to this taxa specificity, the different pigments present in a sample can be used to identify and classify the taxonomic diversity of phytoplankton. The presence and abundance of specific pigments can provide insight into the dominant groups of phytoplankton present in a particular aquatic environment. For example, the presence of chlorophyll-a and b, along with the presence of carotenoids, can indicate the dominance of green algae, while high concentrations of xanthophylls can indicate the presence of diatoms.

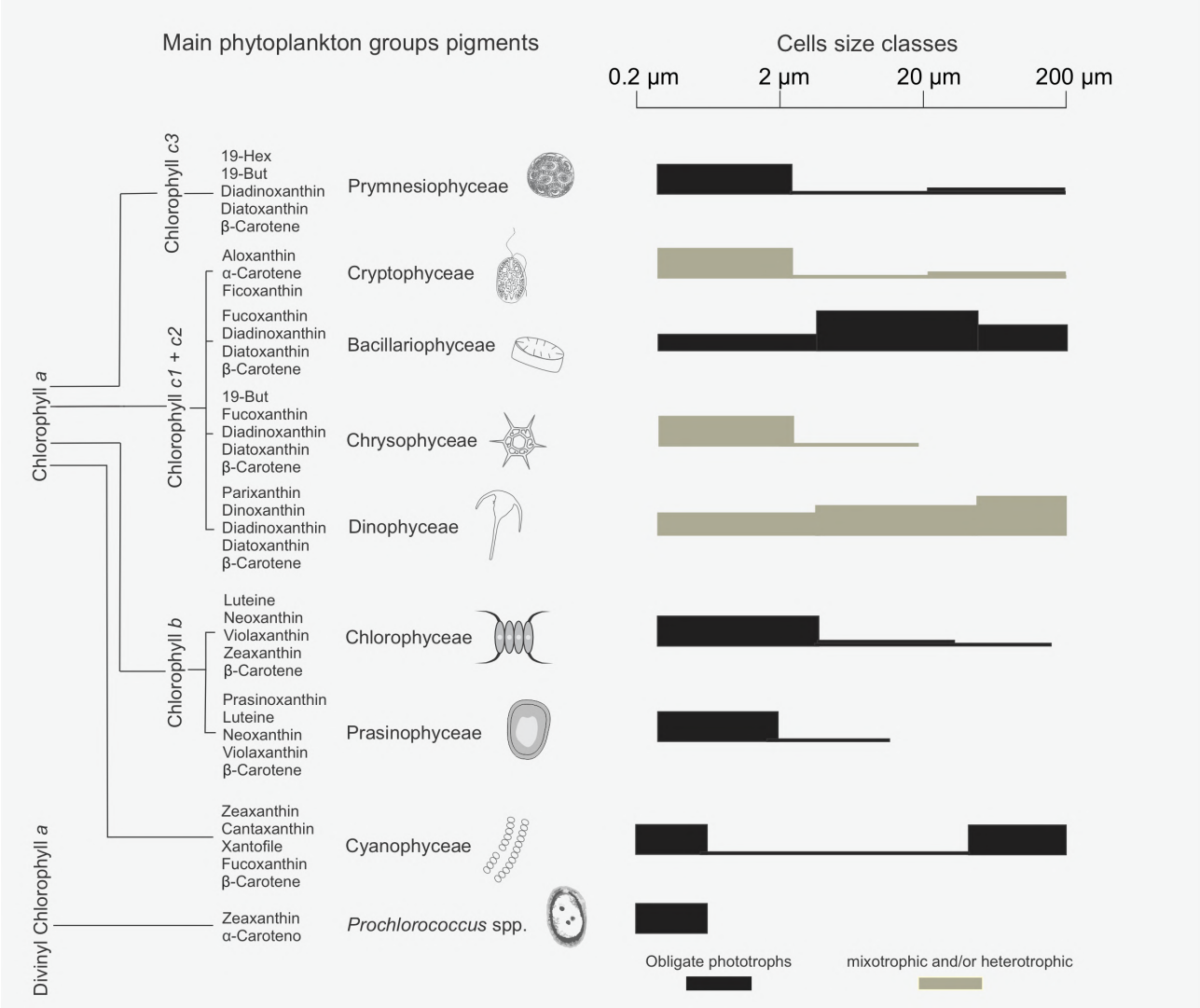

Figure 1. Illustrates the characterization of phytoplankton groups, including their main pigments, cell size, and trophic modes. The left panel shows the identification of phytoplankton groups through HPLC, depicting their main and accessory pigments. The right panel represents the cell size distribution (bars) and trophic modes (color) of different phytoplankton groups.

Assessment of pigments concentrations

To analyze a sample through HPLC the sample is first filtered to remove larger particles, and then the pigments are extracted from the filtered sample (usually with acetone) and run through the columns for separation, based on their differential interactions with the stationary phase. The separated pigments are then detected by a photodiode array detector, which measures the absorption of light at different wavelengths. The absorption spectra of the pigments are then used to calculate the concentration of each pigment in the sample. Once the concentration of pigments is determined, the proportion of the different taxonomic groups can be estimated by the concentration of their diagnostic pigments (Figure 2). Further analysis is possible to estimate

biomass concentrations in the sample using conversion factors that take into account the specific pigment content of each phytoplankton species (CHEMTAX). This conversion factor can be determined through laboratory experiments or published literature. For a better description of the identification of biomass and the analysis through CHEMTAX please refer to Mackey et al. (1996).

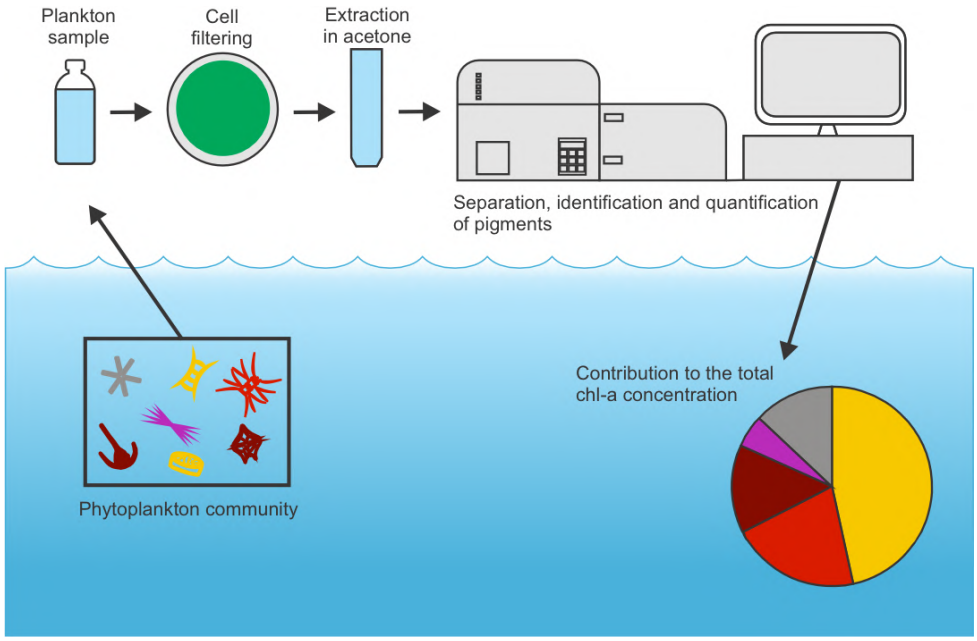

Figure 2. Description of the steps in the phytoplankton sample analysis through HPLC

Basic literature for the analysis

[Wright, S., S. Jeffrey, R. Mantoura, C. Llewellyn, T. Bjørnland, D. Repeta, & N. Welschmeyer, 1991. Improved HPLC method for the analysis of chlorophylls and carotenoids from marine phytoplankton. Marine ecology progress series JSTOR 183–196. https://www.jstor.org/stable/24826571]

[Zapata, M., S. Jeffrey, S. Wright, F. Rodríguez, J. Garrido, & L. Clementson, 2004. Photosynthetic pigments in 37 species (65 strains) of Haptophyta: implications for oceanography and chemotaxonomy. Marine Ecology Progress Series 270: 83–102. https://www.int-res.com/abstracts/meps/v270/p83-102/]

[Mackey, M., D. Mackey, H. Higgins, & S. Wright, 1996. CHEMTAX - a program for estimating class abundances from chemical markers: application to HPLC measurements of phytoplankton. Marine Ecology Progress Series 144: 265–283. https://www.int-res.com/abstracts/meps/v144/p265-283]

[Roy, S., C. A. Llewellyn, E. S. Egeland, & G. Johnsen, 2011. Phytoplankton Pigments: Characterization, Chemotaxonomy and Applications in Oceanography. Cambridge University Press. https://bityli.com/Er52l]

Other useful links

Chemtax software version 1.95

Application of HPLC

2) Flow Cytometry

Basis

Flow cytometry is a powerful tool that enables the simultaneous measurement of multiple physical and chemical characteristics of particles between 0.5 and 1000 μm, predominantly cells, in a fluid stream. The basic principle of flow cytometry involves the interaction of cells with lasers, which excites fluorescent dyes that have been attached to specific cellular components, or natural fluorescent pigment, as in the case of phytoplankton cells (Figure 3). This interaction leads to the emission of light that is detected and measured by specialized sensors. This measurement allows for the rapid and simultaneous analysis of multiple parameters, such as cell size, granularity, and fluorescence intensity, providing a comprehensive and multi-dimensional characterization of individual cells.

Flow cytometry has a wide range of applications in the field of biology, including the study of cellular function, the identification and quantification of rare cells, and the characterization of populations as in the case of plankton studies. This technology is also commonly used in clinical diagnosis, where it is employed to analyze blood samples for the presence of abnormal cells. Furthermore, flow cytometry has proven to be a valuable tool in drug discovery, where it is used to monitor the effects of drug treatments on cellular behavior and to identify the mechanism of action of new therapeutic agents.

The use in plankton samples

Flow cytometry has become an indispensable tool for the identification and characterization of marine pico- and nanoplankton communities. Flow cytometry offers a solution to these challenges by providing a rapid, high-throughput, and quantitative approach to the analysis of marine plankton. One of the key advantages of flow cytometry in the study of marine plankton is the ability to distinguish between different types of cells by their pigments, even those with similar morphological characteristics. This ability is particularly useful in the identification of phytoplankton taxa. Further differentiation can also be obtained by cell size, with communities of picoeukaryotes, Nanoflagellates and small Cyanobacteria such as *Prochlorococcus* and *Synechococcus* being easily distinguished by the analysis of cytograms.

Assessment of pico- and nanoplankton communities

To analyze a plankton sample using flow cytometry, the sample is first prepared by suspending it in a buffer solution and filtering it to remove any particulate matter. If necessary, a fluorescent stain is added to label specific cellular components (needed for the analysis of non-photosynthetic organisms such as heterotrophic bacteria). The sample is then loaded into a flow cytometer, which passes the cells one by one through a laser beam and detects the fluorescence signals emitted. The flow cytometer records the fluorescence signals and generates cytograms for analysis (Figure 3). The data can then be analyzed using specialized software to generate plots, histograms, and other graphical representations of the data. The data is used to determine the composition and abundance of the plankton sample. The total biomass of the sample can be calculated by multiplying the cell size or volume by the cell count. This information can be obtained by integrating the fluorescence intensity histogram over a suitable range of cell sizes or volumes. Additionally, if data on cell volume is not available, the biomass can be obtained through specific cell x carbon biomass ratios available in the literature.

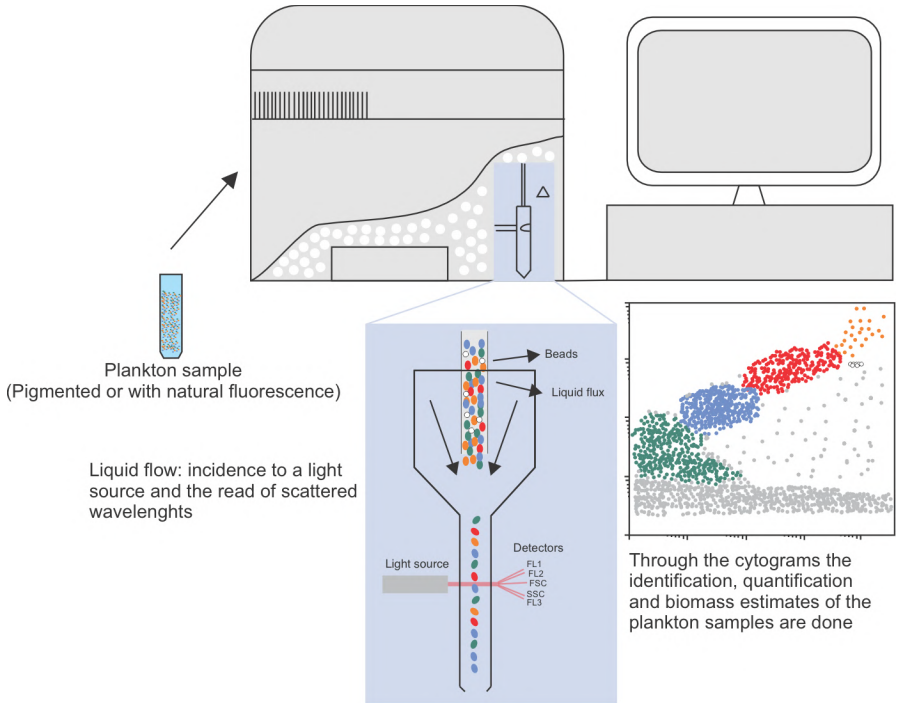

Figure 3. Description of the analysis of a plankton sample through flow cytometry

Basic literature for the analysis

[Marie, D., F. Rigaut-Jalabert, & D. Vaulot, 2014. An improved protocol for flow cytometry analysis of phytoplankton cultures and natural samples. Cytometry Part A 85: 962–968. https://onlinelibrary.wiley.com/doi/full/10.1002/cyto.a.22517]

[Marie, D., F. Partensky, D. Vaulot, & C. Brussaard, 1999. Enumeration of Phytoplankton, Bacteria, and Viruses in Marine Samples. Current Protocols in Cytometry 10: 11.11.1-11.11.15. https://currentprotocols.onlinelibrary.wiley.com/doi/abs/10.1002/0471142956.cy1111s10]

[Marie, D., N. Simon, & D. Vaulot, 2005. Phytoplankton cell counting by flow cytometry. Algal culturing techniques Elsevier Academic Press Burlington, MA 1: 253–267. https://bityli.com/aXJ1O]

Other useful links

Cytoflex Manual

Flow cytometry basic principles

Statistical Methods

1) PERMANOVA

Basis

The PERMANOVA, (permutational multivariate analysis of variance), is a non-parametric alternative to MANOVA, or multivariate ANOVA test. It is appropriate to be used with multiple sets of variables that do not meet the assumptions of MANOVA, i.e. multivariate normality, equal variance and absence of outliers, with the main assumptions of the PERMANOVA being the exchangeability of observations under the null hypothesis and the independence of samples. PERMANOVA is usually used with ecological data, which rarely presents normal distribution, to discriminate contrasting conditions/areas.

This analysis is conducted based on a resemblance matrix (usually Bray-Curtis for biotic and Euclidean distance for abiotic data) testing the null hypothesis that there is no difference in the centroids (the geometric center of all data points) and dispersion of the set of variables between groups defined *a priori* (Figure 1). The PERMANOVA calculates the p-value through random permutations of observations among groups, if the null hypothesis is rejected it means that either the centroid or the dispersion of observations differs between groups. PERMANOVA results are usually presented with ordination plots, such as MDS and PCoA, which helps visually represent the distance between groups.

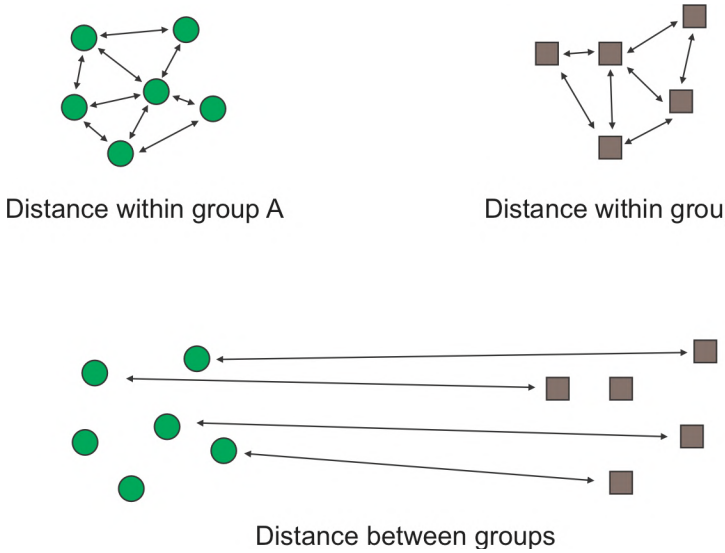

Figure 4. The PERMANOVA tests the distance between observations within the defined groups and the distance between groups.

The PERMANOVA statistics are calculated as an F-ratio similar to the ANOVA, or pseudo-F, which compares the total sum of squared dissimilarities among the objects belonging to different groups to that of objects from the same group, represented by the formula:

$$F = \frac{SS_A \div (a-1)}{SS_W \div (N-a)}$$

Where SS_W is the sum of squared dissimilarities within groups, SS_A is the sum of squared dissimilarities between groups, a is the number of groups and N is the total number of observations. In the PERMANOVA statistics larger F-ratios represent a higher separation between groups.

Limitations

I. PERMANOVA does not take into account correlations between variables and any hypothesis that depends on detecting such relationships.
II. Nested or hierarchical designs require an appropriate permutational scheme, carefully understanding which objects are truly exchangeable under null hypothesis.
III. Groups of objects with different dispersions, but no significant differences in centroids, may result in misleadingly low p-values. It is thus recommended that the dispersion be evaluated and considered when interpreting the results.

Papers that applied this methodology

[Santos, M., A. Amorim, V. Brotas, J. P. C. Cruz, C. Palma, C. Borges, L. R. Favareto, V. Veloso, M. L. Dâmaso-Rodrigues, P. Chainho, P. M. Félix, & A. C. Brito, 2022. Spatio-temporal dynamics of phytoplankton community in a well-mixed temperate estuary (Sado Estuary, Portugal). Scientific Reports Nature Publishing Group 12: 16423. https://www.nature.com/articles/s41598-022-20792-6]

[Menezes, B. S., L. C. P. de Macedo-Soares, & A. S. Freire, 2019. Changes in the plankton community according to oceanographic variability in a shallow subtropical shelf: SW Atlantic. Hydrobiologia 835: 165–178.
https://link.springer.com/article/10.1007/s10750-019-3936-5]

[Pinto, M., P. Polania Zenner, T. M. Langer, J. Harrison, M. Simon, M. M. Varela, & G. J. Herndl, 2020. Putative degraders of low-density polyethylene-derived compounds are ubiquitous members of plastic-associated bacterial communities in the marine environment. Environmental Microbiology 22: 4779–4793.
https://sfamjournals.onlinelibrary.wiley.com/doi/full/10.1111/1462-2920.15232]

Code for R

```
data <- read.csv (file = “” sep = ";")
library(vegan)
library(phyloseq)

#### PERMANOVA #####
set.seed(1)

# Calculate bray curtis distance matrix
GPfr_phylum_bray <- phyloseq::distance(data, method = "bray")

# make a data frame from the sample_data
sampledf <- data.frame(sample_data(data))

# Adonis test
adonis(GPfr_phylum_bray ~ SampleType, data = sampledf)
adonis(GPfr_phylum_bray ~ Description, data = sampledf)
adonis(GPfr_phylum_bray ~ SampleType + Description, data = sampledf)
```

Other useful links

Permutational Multivariate Analysis of Variance (PERMANOVA) in R

2) Generalized Additive Models (GAMs)

Basis

Although linear models such as linear regression are widespread and easy to use and understand, the world rarely is linear, therefore such models may miss important patterns of our dataset. Generalized Additive Models (GAMs) represent an advance in complexity when compared with regular linear regression by allowing us to model *non-linear* relationships while keeping it explainable and understandable. In Figure 2 we have a scatter plot of two variables, X and Y with a clear relationship between the two. However, by fitting a linear model (Figure 2a) we lose too much information and oversimplify the patterns. In contrast, by using non-GAMs a closer representation of reality can be obtained (Figure 2b). This is possible because instead of fitting a linear function among the data, the GAMs use a flexible function that can take a wide variety of shapes, including linear, known as smooths or splines to fit the data. This smooth function in GAMs is constructed by many smaller functions, called basis functions (Figure 2b, light-green lines). Each smooth line is the sum of a large number of basis functions that are multiplied by the parameters in the model.

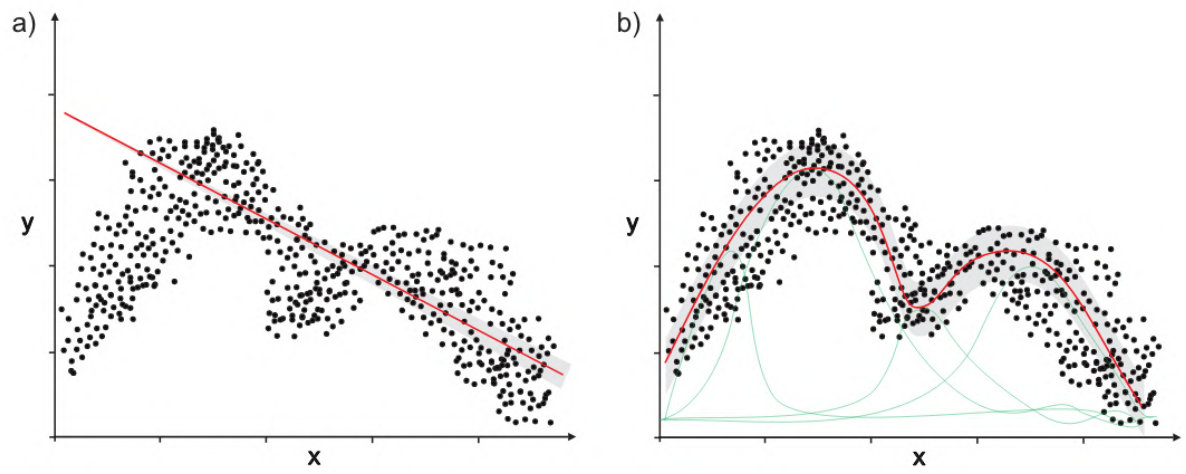

Figure 5. Models applied to a hypothetical dataset of variables x and y. (a) linear models oversimplify the relationships and miss the main patterns while the use of flexible models such as (b) GAMs allows us to get a closer look at natural patterns, by using several smooth functions to build a smooth model.

Mathematically the key difference between GAMs and linear models is that the linear predictor in GAMs incorporates a smooth function (*s*) of at least one (possibly all) variable, represented by the following equation:

$$Z = s_o x_o + s_1 x_1 + ... + s_n x_n$$

s, in turn, is represented by the sum of each polynomial basis function:

$$s(x) = \sum_{k=1}^{k} \beta_k b_k(x)$$

With k being the number of basis functions or knots in your smooth.

Limitations

I. As GAMs work with many bases function, overfitting may happen in the model output, with too much complexity that prevents the prediction of additional data. However, this can be solved by changing the number of bases functions (k) in the model, or by choosing a simpler model such as GLM.

Papers that applied this methodology

[Cavalcanti, L. F., F. A. do N Feitosa, M. V. J. Cutrim, M. de J. F. Montes, C. B. Lourenço, J. A. Furtado, & A. K. D. dos S Sá, 2022. Drivers of phytoplankton biomass and diversity in a

macrotidal bay of the Amazon Mangrove Coast, a Ramsar site. Ecohydrology & Hydrobiology 22: 435–453.
https://bityli.com/tZicxjrdF]

[Zhang, J., M. Zhi, & Y. Zhang, 2021. Combined Generalized Additive model and Random Forest to evaluate the influence of environmental factors on phytoplankton biomass in a large eutrophic lake. Ecological Indicators 130: 108082.
https://www.sciencedirect.com/science/article/pii/S1470160X21007470]

[Fugère, V., M.-P. Hébert, N. B. da Costa, C. C. Y. Xu, R. D. H. Barrett, B. E. Beisner, G. Bell, G. F. Fussmann, B. J. Shapiro, V. Yargeau, & A. Gonzalez, 2020. Community rescue in experimental phytoplankton communities facing severe herbicide pollution. Nature Ecology & Evolution Nature Publishing Group 4: 578–588.
https://www.nature.com/articles/s41559-020-1134-5]

Code for R

```
dados <- read.csv(file = "", sep =";")

library(psych)
library(mgcv)

#Remove all NA lines from the data
Dados$X.1 <- NULL
Dados$X.2 <- NULL

#Standarize the biomass data
Dados$Prymnesiophyceae = scale(Dados$Prymnesiophyceae, center = TRUE, scale = TRUE)
Dados$Dictyochophyceae = scale(Dados$Dictyochophyceae, center = TRUE, scale = TRUE)
Dados$Cryptophyta = scale(Dados$Cryptophyta, center = TRUE, scale = TRUE)
Dados$Bacillariophyceae = scale(Dados$Bacillariophyceae, center = TRUE, scale = TRUE)
Dados$Chlorophyta = scale(Dados$Chlorophyta, center = TRUE, scale = TRUE)
Dados$Dinophyceae = scale(Dados$Dinophyceae, center = TRUE, scale = TRUE)
Dados$Prochlorococcus = scale(Dados$Prochlorococcus, center = TRUE, scale = TRUE)
Dados$Cyanophyceae = scale(Dados$Cyanophyceae, center = TRUE, scale = TRUE)

#Standarize the environmental data
Dados$Temperature = scale(Dados$Temperature, center = TRUE, scale = TRUE)
Dados$Salinity = scale(Dados$Salinity, center = TRUE, scale = TRUE)
Dados$NO2 = scale(Dados$NO2, center = TRUE, scale = TRUE)
Dados$NO3 = scale(Dados$NO3, center = TRUE, scale = TRUE)
Dados$Phosphate = scale(Dados$Phosphate, center = TRUE, scale = TRUE)
Dados$Silicate = scale(Dados$Silicate, center = TRUE, scale = TRUE)
Dados$MLD = scale(Dados$MLD, center = TRUE, scale = TRUE)
Dados$BLT = scale(Dados$BLT, center = TRUE, scale = TRUE)

####Find Covariances####
Var = data.frame(Dados$Temperature, Dados$Salinity, Dados$NO2, Dados$NO3,
Dados$Phosphate, Dados$Silicate, Dados$MLD, Dados$BLT)
pairs.panels(Var[1:8])

####Run the GAMs#####
# Example

prymneGAM_c1 <-
gam(Dados_C1$Prymnesiophyceae~s(Dados_C1$Temperature)+s(Dados_C1$Salinity)+s(Da
dos_C1$NO2)+ Dados_C1$Spatial.Variability)

summary(gam1) #See GAM output
gam.check (gam1)#Run diagnostic tests of the fitted gam models

plot(gam1, shift= 10.9, residuals=F, se=TRUE,pch=19, cex=0.75, scheme=1,
      shade=T,shade.col='grey')
```

Other useful links:

GAMs in R
Generalized Additive Models | R bloggers

3) PCA

Basis

Principal Component Analysis (PCA) is a technique that finds the major patterns in data for dimensionality reduction. It arises from a main problem when working with a large volume of variables allowing to cut down the number of variables and still explain the same proportion of the reality. To do this, the PCA finds new variables in the data that are linear combinations of the original variables but also are uncorrelated with the original ones. These new variables define "new directions" in the data, which are principal components representing the maximal variation inside the dataset. One of the main assumptions of the PCA is that there is a correlation between variables. If the variables are not correlated, PCA will be unable to determine principal components.

In the PCA, there are as many principal components as there are variables in the data, principal components are constructed in such a manner that the first principal component accounts for the largest possible variance in the data set (Figure 3). The second principal component is calculated in the same way, with the condition that it is uncorrelated with (i.e., perpendicular, or orthogonal) the first principal component and accounts for the next highest variance. This continues until a total of p principal components have been calculated, equal to the original number of variables.

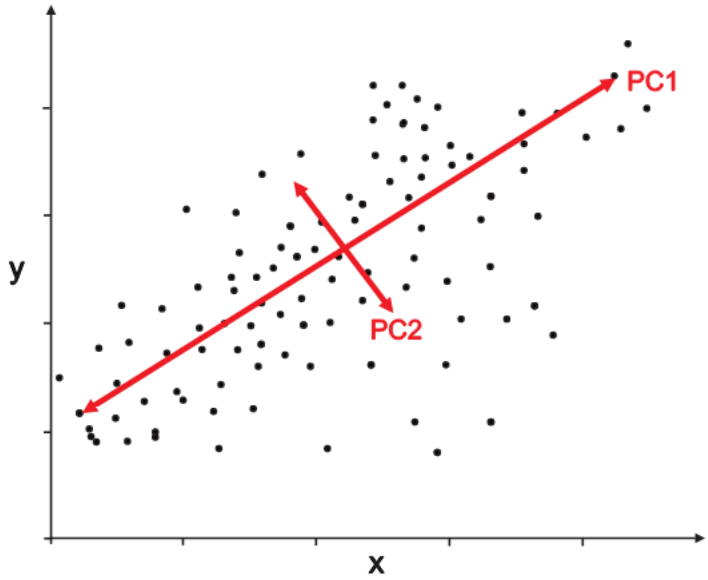

Figure 6 - PCA plot demonstrating the definition of the first two PCs, the first principal component direction (PC1) is the direction along which the measurements vary the most, and the second principal component direction (PC2) represents the second direction which the measurements vary the most of the variability not explained by the first component and is perpendicular to the first component.

PCA associates the existing variables with new ones using covariance matrixes. These matrixes are used to calculate the eigenvalues and eigenvectors. The eigenvectors represent the directions or components of the new variables, whereas the eigenvalues are coefficients given to the eigenvectors and represent their magnitude

Limitations

I. PCA is sensitive to the scale of variables. This is why it's so important to standardize the values first.
II. Its an analysis venerable to rendundant variables.
III. PCA is not robust against outliers. The algorithm will be biased in datasets with strong outliers. This is why it is recommended to remove outliers before performing PCA.
IV. PCA assumes a linear relationship between features. The algorithm is not well suited to capturing non-linear relationships.

Papers that applied this methodology

[Araujo, M., C. Noriega, G. A. Hounsou-gbo, D. Veleda, J. Araujo, L. Bruto, F. Feitosa, M. Flores-Montes, N. Lefèvre, P. Melo, A. Otsuka, K. Travassos, R. Schwamborn, & S. Neumann-Leitão, 2017. A Synoptic Assessment of the Amazon River-Ocean Continuum during Boreal

Autumn: From Physics to Plankton Communities and Carbon Flux. Frontiers in Microbiology 8: 1–8.
https://hal.archives-ouvertes.fr/hal-01684900/document]

[Livanou, E., A. Lagaria, I. Santi, M. Mandalakis, A. Pavlidou, K. Lika, & S. Psarra, 2019. Pigmented and heterotrophic nanoflagellates: Abundance and grazing on prokaryotic picoplankton in the ultra-oligotrophic Eastern Mediterranean Sea. Deep Sea Research Part II: Topical Studies in Oceanography 164: 100–111.
http://bitly.ws/y9Yh]

[Livanou, E., A. Lagaria, I. Santi, M. Mandalakis, A. Pavlidou, K. Lika, & S. Psarra, 2019. Pigmented and heterotrophic nanoflagellates: Abundance and grazing on prokaryotic picoplankton in the ultra-oligotrophic Eastern Mediterranean Sea. Deep Sea Research Part II: Topical Studies in Oceanography 164: 100–111.
https://link.springer.com/article/10.1007/s10661-019-8046-3]

Code for R

```
 #### Principal Component Analysis in R ####
#About PCA
#http://www.sthda.com/english/articles/31-principal-component-methods-in-r-practical-guide/112-pca-principal-component-analysis-essentials/

data <- read.csv (file = “” sep = ";")
library("FactoMineR")
library("factoextra")

d <- na.omit(data)
active_data <- d[,14:23]

#### PCA with Standarized data (n - mean / sd) ####
res.pca <- PCA(active_data, quanti.sup = 1:2, graph = FALSE)
print(res.pca)
eig.val <- get_eigenvalue(res.pca)
eig.val

#Scree Plot, Eigen Values
fviz_eig(res.pca, addlabels = TRUE, ylim = c(0, 50))

#### Results of PCA ####
var <- get_pca_var(res.pca)
var
# Coordinates
head(var$coord)
# Cos2: quality on the factore map
head(var$cos2)
# Contributions to the principal components
head(var$contrib)

#Variables Coorelation plot
fviz_pca_var(res.pca, col.var = "black")

#Quality of representation of variables
library("corrplot")
corrplot(var$cos2, is.corr=FALSE)

#### Plot by variable ####

fviz_pca_biplot(res.pca,
                geom.ind = "point",
                pointshape = 21,
                point.size = 5,
                fill.ind = variable, # color by groups
                col.var = "black", repel = TRUE,
                legend.title = "Groups",
                mean.point = FALSE,)
```

Other useful links:

How exactly does PCA work?

PCA in R

4) Random Forest

Basis

Random forest is an ensemble learning method (methods that use multiple learning algorithms) extension of single classification trees in which multiple decision trees are built with random subsets of the original input dataset. All random subsets have the same number of data points and are selected from the complete dataset in a process called "bagging". A part of the dataset is not used in the bagging to build the trees, being called 'out-of-the-bag' data. This part is later used to evaluate the model. Random forest classification output usually brings a list of the variable selected in most trees for each response variable and can be used to select variables with a higher explanatory power (Figure 4). Therefore, random forests can be used to rank the importance of variables in natural ecosystems. For a description of the formulas involved in the learning process and selection of variables please see Ishwaran et al. (2022), "Package *randomForestSCR"*.

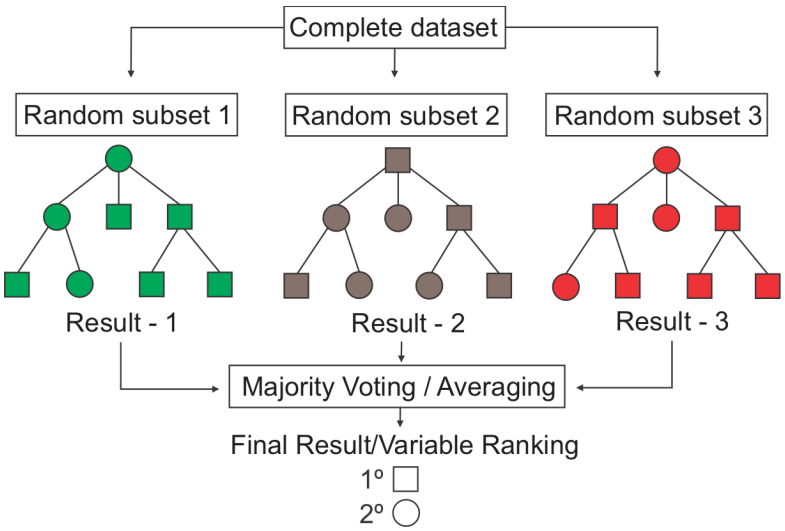

Figure 7 - Demonstration of random forest methodology

The random forest has several advantages, being an accurate learning algorithm, being able to handle several predictor variables, and providing estimates of the importance of each one of them. In addition, being a non-parametric method, no formal distribution assumptions are

required. However, although achieving higher accuracy than single decision trees this had a trade-off with the easy interpretability of the previous method.

Limitations

I. May overfit relationships in datasets with a lot of noise.
II. Random forests may be biased for predictors with more levels. Therefore, when including categorical variables with different numbers of levels, this should be taken into account.

Papers that applied this methodology

[Zhang, J., M. Zhi, & Y. Zhang, 2021. Combined Generalized Additive model and Random Forest to evaluate the influence of environmental factors on phytoplankton biomass in a large eutrophic lake. Ecological Indicators 130: 108082. https://www.sciencedirect.com/science/article/pii/S1470160X21007470]

[Cheng, Y., V. N. Bhoot, K. Kumbier, M. P. Sison-Mangus, J. B. Brown, R. Kudela, & M. E. Newcomer, 2021. A novel random forest approach to revealing interactions and controls on chlorophyll concentration and bacterial communities during coastal phytoplankton blooms. Scientific Reports Nature Publishing Group 11: 19944. https://www.nature.com/articles/s41598-021-98110-9]

[Ellen, J. S., C. A. Graff, & M. D. Ohman, 2019. Improving plankton image classification using context metadata. Limnology and Oceanography: Methods 17: 439–461. https://aslopubs.onlinelibrary.wiley.com/doi/full/10.1002/lom3.10324]

Code for R

```
#Random Forest----
# 1) DETECTION OF OUTLIERS: Outliers can be detected numerically or graphically. The numerical check
# is done with R's summary statistics:

Setwd(“”)

library(usdm) # Collinearity
library(randomForestSRC) # RF
library(ggRandomForests) # RF
library(gbm) # BRT
library(dismo) # BRT
library(MuMIn) # Multi-model inference
library(ggplot2)
library(LaplacesDemon)
```

```
source("simul_functions.R")

my.data <- read.table(file = "",
                      header = TRUE,
                      dec = ".")
my.data <- my.data[1:11]
head(my.data)
my.data <- my.data[complete.cases(my.data), ]

cor (my.data)
pairs (my.data)
# In order to apply the histogram and smoother functions, the following code must be run
before (copy-paste
# the code into the R console and press enter):
panel.hist <- function(x, ...)
{
 usr <- par("usr"); on.exit(par(usr))
 par(usr = c(usr[1:2], 0, 1.5) )
 h <- hist(x, plot = FALSE)
 breaks <- h$breaks; nB <- length(breaks)
 y <- h$counts; y <- y/max(y)
 rect(breaks[-nB], 0, breaks[-1], y, col = "cyan", ...)
}
panel.cor <- function(x, y, digits = 2, prefix = "", cex.cor, ...)
{
 usr <- par("usr"); on.exit(par(usr))
 par(usr = c(0, 1, 0, 1))
 r <- abs(cor(x, y))
 txt <- format(c(r, 0.123456789), digits = digits)[1]
 txt <- paste0(prefix, txt)
 if(missing(cex.cor)) cex.cor <- 0.8/strwidth(txt)
 text(0.5, 0.5, txt, cex = cex.cor * r)
}

pairs (my.data, diag.panel=panel.hist, upper.panel=panel.smooth,
      lower.panel=panel.cor) # calculates Pearson correlation coefficients by default

# VIF account for non-linear relationships between variables which may remain undetected
using correlation
# analysis. The R package usdm contains the function vif():
library (usdm)

vif (my.data)

# A VIF>8 indicates variance-inflated variables (Zuur et al. 2007). If more than one variable
exhibit high
# VIFs, it is recommended to exclude them stepwise, starting with the variable that has the
highest VIF.
# This procedure is repeated until all variable's VIFs>8
```

```
vifstep (my.data, th=7) # threshold set to VIFb7

#RandomForest
library (randomForestSRC)

set.seed (1234) # sets a numerical starting point; will be set randomly, if not set by the user

#RF Nano----
my.rf <- rfsrc (NanoA ~ PicoA+ProA+SynA+BacA+WaterMass+Region,
            mtry=2.5, ntree=2000, importance="random", data=my.data)
my.rf
plot(my.rf)
md.obj <- max.subtree(my.rf)
md.obj$topvars
my.rf.part.plot <- plot.variable(my.rf, partial=TRUE,stored=FALSE,
                           show.plot=TRUE, notch=FALSE)

my.rf.part.plot

gg.part <- gg_partial(my.rf.part.plot)

gg.part

my.rf.part.plot <- plot.variable(my.rf, partial=TRUE,stored=FALSE,
                           show.plot=TRUE, notch=FALSE)
gg.part <- gg_partial(my.rf.part.plot)


df.WM<- gg.part[[1]]
n.wm <- ggplot(data=df.WM,aes(x=WaterMass,y=yhat))+
  geom_boxplot(outlier.shape = NA)+
  labs(x="Water Mass", y="Predicted value") +
  scale_x_discrete(labels=c("1" = "TSW", "2" = "SUW", "3" = "SACW")) +
  ggtitle(expression(paste("Nanoflagellates"~"(",R^2,"=0.62",")"))) +
  theme_bw()
n.wm

df.ProA<- gg.part[[2]]
n.pro <- ggplot(data=df.ProA,aes(x=ProA,y=yhat))+
  geom_line()+
  geom_ribbon(aes(ymin=yhat+se, ymax=yhat-se), alpha=0.1, fill = "blue",
              color = "black", linetype = "dotted")+
  labs(x="Pro", y="") +
  theme_bw()
n.pro

df.PicoA<- gg.part[[4]]
n.pico <- ggplot(data=df.PicoA,aes(x=PicoA,y=yhat))+
  geom_line()+
  geom_ribbon(aes(ymin=yhat+se, ymax=yhat-se), alpha=0.1, fill = "blue",
```

```
            color = "black", linetype = "dotted")+
  labs(x="PicoEuk", y="") +
  theme_bw()
n.pico

df.BacA<- gg.part[[5]]
n.bac <- ggplot(data=df.BacA,aes(x=BacA,y=yhat))+
  geom_line()+
  geom_ribbon(aes(ymin=yhat+se, ymax=yhat-se), alpha=0.1, fill = "blue",
            color = "black", linetype = "dotted")+
  labs(x="Bac", y="") +
  theme_bw()
n.bac

df.SynA<- gg.part[[6]]
n.syn <- ggplot(data=df.SynA,aes(x=SynA,y=yhat))+
  geom_line()+
  geom_ribbon(aes(ymin=yhat+se, ymax=yhat-se), alpha=0.1, fill = "blue",
            color = "black", linetype = "dotted")+
  labs(x="Syn", y="") +
  theme_bw()
n.syn

graphics.off()
tiff("parplt_nano_gabrielBF.tiff", width = 140, height = 100, units="mm", res = 600,
compression=c("lzw"))
plot_grid(n.wm, n.pro, n.pico, n.bac, n.syn, ncol = 3, nrow = 2)
dev.off()
```

Other useful links:

Random Forest Algorithm Clearly Explained!

Visual Guide of Random Forest

A complete guide to Random Forest in R

APPENDIX C - SUPPLEMENTARY MATERIAL

The data generated and used on this thesis are available on the SEANOEA database, at the following links:

Generated data

- Phytoplankton pigment data collected during the ABRACOS 1 and 2 surveys performed along the northeast Brazilian continental shelf, slope and open ocean | Available in: https://www.seanoe.org/data/00840/95171/ | doi: 10.17882/95171

- Nutrient data collected during the ABRACOS 1 and 2 surveys performed along the northeast Brazilian continental shelf, slope and open ocean | Available in: https://www.seanoe.org/data/00840/95172/ | doi: 10.17882/95172

- Picoplankton and nanophytoplankton cytometry data collected during the ABRACOS 2 survey performed along the northeast Brazilian continental shelf, slope and open ocean | Available in: https://www.seanoe.org/data/00840/95241/ | doi: 10.17882/95241

Associated data

- ABRACOS cruise - Physical datasets | Available in: https://www.seanoe.org/data/00655/76696/ | doi: 10.17882/76696

- ABRACOS cruise 2 - Physical datasets | Available in: https://www.seanoe.org/data/00651/76352/ | doi: ABRACOS cruise - Physical datasets | Available in: https://www.seanoe.org/data/00655/76696/ | doi: 10.17882/76696

Figures availability

- All pre- and post- textual figures are available by request on the author's email: bittencourt.bio@gmail.com

APPENDIX D – OTHER ACTIVITIES

Other academic activities

Presentation at congress and conferences

(1) FARIAS, GABRIEL BITENCOURT. Vortices effect in phytoplankton community at the BRAZIL-MALVINAS CONFLUENCE. 2022. SCAR 2022.

(2) FARIAS, G.B.; MOLINERO J.C.; LEITÃO S.N.; JUNIOR M. M.; MELO. P.A.M.C. The demersal copepod community of a Southwestern Tropical Atlantic coastal reef: seasonal variability. e-ICOC 2022.

Talks and presentations

(1) FARIAS, GABRIEL BITENCOURT. Biomassa e Produção do Plâncton Marinho. 2022.

(2) FARIAS, G. B. Métodos de amostragem do fitoplâncton. 2020.

Short Courses Taught

(1) FARIAS, G. B.; DE SANTANA, C. S. Plâncton Marinho: ecologia, diversidade, conservação e papel como indicadores ambientais. 2021.

(2) FARIAS, G. B. Introdução a gestão de bibliografias e citações com Zotero. 2021.

(3) FARIAS, GABRIEL BITENCOURT; DE SANTANA, C. S. Ecologia do Zooplâncton Marinho e o Efeito de Impactos Antrópicos em sua Comunidade. 2020.

Teaching in graduation courses

(1) Graduation course: Oceanography. Discipline: Oceanografia Geral. (Teaching Internship). 2019
(2) Graduation course: Oceanography. Discipline: Ecologia de Ecossistemas Marinhos. (Teaching Internship). 2019

Participation in Monograph Comitee

(1) MELO, P. A. M. C.; FEITOSA, F. A. N.; FARIAS, G. B. Participação em banca de Angélica Viana e Silva. Biomassa Fitoplanctônica em estuários de Pernambuco após derrame de óleo de 2019. 2021. Trabalho de Conclusão de Curso (Graduação em Ciências Biológicas) - Universidade Federal de Pernambuco.

Orientations and Supervisions

(1) Pedro de Amorim Reis. MONITORAMENTO DO DERRAME DE ÓLEO SOBRE A BIOMASSA FITOPLANCTÔNICA EM TAMANDARÉ-PE (COORIENTADOR). 2021. Trabalho de Conclusão de Curso. (Graduação em Ciências Biológicas) - Universidade Federal de Pernambuco.

Book Chapters

(1) MELO, PEDRO AUGUSTO MENDES DE CASTRO ; OTSUKA, A. ; GREGO, C. K. S. ; ESKINAZI-LECA, E. ; AQUINO, E. P. ; FEITOSA, F. A. N. ; FARIAS, G. B. ; BORGES, G. C. P. ; SILVA, K. H. F. ; FERREIRA, L. C. ; OLIVEIRA, M. G. T. ; MULLER, M. N. ; SILVA, N. B. A. ; LACERDA, S. R. ; CUNHA, M. G. G. S. . Fitoplâncton Marinho Tropical. In: Danielle de Lima Viana; Jorge Eduardo Lins Oliveira; Fábio Hissa Vieira Hazin; Marco Antonio Carvalho de Souza.. (Org.). Ciências do mar : dos oceanos do mundo ao nordeste do Brasil : bioecologia, pesca e aquicultura. 1ed.Olinda: Via Design Publicações, 2021, v. 2, p. 1-509.

Cruises

(1) Embarque científico na OPERANTAR XXXVIII a bordo do Navio Polar Almirante Maxiniano entre a área marítima do rio de Janeiro e o continente Antártico, do período de 08 de outubro a 04 de novembro de 2019, totalizando 3798 milhas náuticas e 22 dias de mar.

Manuscripts published or submitted

(1) FARIAS, GABRIEL BITTENCOURT; LEITÃO, SIGRID NEUMANN; MAURO DE MELO JUNIOR; MELO, PEDRO AUGUSTO MENDES DE CASTRO. Exploring the structure, biomass, and functional diversity of demersal mesozooplankton during contrasting seasons on a shallow reef ecosystem. Marine Biology Research. *UNDER REVIEW* (Submission Number: 238142307).

(2) FARIAS, GABRIEL BITTENCOURT, PEDRO AUGUSTO MENDES DE CASTRO MELO, LUCAS GUEDES PEREIRA FIGUEIRÊDO, SIGRID NEUMANN LEITÃO, KAIO HENRIQUE FARIAS. The first record of the calanoid family Pseudocyclopidae Giesbrecht, 1893 in South Atlantic Ocean. Journal of the Marine Biological Association of the United Kingdom. *UNDER REVIEW* (Submission Number: JMBA-04-23-0061)